
# Development of polymeric nanoparticles for intravesical drug delivery to the bladder

Sandra Lazauskaite

Thesis submitted to the School of Pharmacy, University of East Anglia in fulfilment of the requirement for the degree of Doctor of Philosophy

June 2024

# Abstract

Urinary tract infections (UTIs) are one of the most commonly acquired bacterial infections, resulting in frequent hospitalisations and increased economic burden on the healthcare system. Due to the systemic exposure during the treatment, UTIs are often associated with increased risk of side effects, diminished therapeutical effects within the bladder, and increased risk of uropathogenic bacteria acquiring antimicrobial resistance.

Intravesical drug delivery (IDD) to the bladder was proposed as a solution for improved drug delivery. IDD ensures full drug dosage instillation into the infection site, reduces systemic exposure due to poor permeability of the bladder, and minimises the risk of side effects. However, IDD suffers from fast drug dilution and wash-out, due to bladder physiological functions such as urine filling and voiding. Therefore, use of nanotechnology has been proposed, as coupled with mucoadhesive materials, drug nanocarriers would attach to the bladder lining, prolonging drug retention time in the bladder. Additionally, drug entrapment into polymeric nanoparticles could reduce drug associated toxicity and demonstrate sustained drug release.

The aim of this project is to obtain two types of colloidally stable drug loaded polymeric nanoparticles and enhance their mucoadhesive properties for prolonged retention time in the bladder. The work presented herein involves the preparation, optimisation and characterisation of hydrophilic antibiotic loaded and hydrophobic cyclooxygenase-2 inhibitor drug loaded poly(lactic-co-glycolic acid) (PLGA) nanoparticles. Comparison between nanoparticle synthesis methods was performed by utilising Design of Experiments, studying how nanoparticle preparation parameters affect the physicochemical characteristics of drug loaded PLGA nanoparticles. Additionally, chitosan was incorporated into nanoparticle formulations, resulting in particles exhibiting cationic charge, allowing them to form electrostatic interactions with anionic mucin layer of the urothelium. Finally, to improve the entrapment of hydrophilic drugs into PLGA nanoparticles, hydrophobic ion pairing technique was used to increase hydrophobicity of the antibiotic, also sustaining its drug release rate.

## Acknowledgements

I would like to thank my supervisors Professor Sheng Qi and Dr Chris Morris for their invaluable help, support and guidance throughout my PhD. I would also like to express my gratitude to Professor Peter Belton for his generous support and invaluable expertise during my project. I must thank my iCASE industry partners UroPharma and the team: Howard, Lyubov, Scott, Gabriel and Anton, as their unwavering support, encouragement and help has made sure my project was always running smoothly. I would like to extend my thanks to Mr Bertrand Leze and Dr Alex Morritt for their continuous technical support and assistance during the running of this project.

I would like to express my gratitude to my former colleagues Dr Randa Zoqlam and Dr Sherif Hamdallah, who showed me immense support and guidance in finding my way in the nanotechnology and drug delivery field. Thank you to my fellow PhD colleagues, with a special thanks to Dami, who has always listened and offered advice when things were going wrong in the lab. I also would like to thank my best friend Sam, who was always there when I needed a break from the lab, your immense support and encouragement has always lifted me up even on the gloomy days. Also, a special thanks to my friends back home: Emile, Migle, Aurelija and Monika, for always finding time to see me.

To my parents, I cannot thank you enough for your unwavering support, encouragement and belief in me throughout this journey. Words cannot describe how grateful I am for you and for always inspiring me to grow and push myself forwards even when it is incredibly hard. I would like to offer my gratitude to my extended family too, for their continuous love and support.

To my loving partner Tom, who was there with me from start to finish of this project, I offer my endless love and gratitude for your infinite patience and care for me. You were my rock throughout this journey, and I will be forever grateful to you for your understanding, kindness and love. There are no words to describe how much it meant to me having you by my side during this project.

# Table of Contents

# List of Figures

# List of Tables

# Publication

Zoqlam, R., **Lazauskaite, S.**, Glickman, S., Zaitseva, L., Ilie, P. C., Qi, S. Emerging molecular mechanisms and genetic targets for developing novel therapeutic strategies for treating bladder diseases. *European Journal of Pharmaceutical Sciences*. 173 (2022). https://doi.org/10.1016/j.ejps.2022.106167.

# List of abbreviations

| | |
|---|---|
| **ABU** | Asymptomatic bacteriuria |
| **ACNT** | Acetonitrile |
| **AMP** | Ampicillin |
| **AMR** | Antimicrobial resistance |
| **ANOVA** | Analysis of variance |
| **AOT** | Docusate sodium salt |
| **API** | Active pharmaceutical ingredient |
| **ATR-FTIR** | Attenuated total reflectance – Fourier transform infra-red spectroscopy |
| **AU** | Artificial urine |
| **BCG** | Bacille Calmette-Guerin |
| **BCS** | Biopharmaceutics Classification System |
| **C6** | Coumarin-6 |
| **C-CS** | Carboxymethyl chitosan |
| **CFU** | Colony-forming unit |
| **CLSI** | Clinical and Laboratory Standards Institute |
| **CLX** | Celecoxib |
| **CMC** | Critical micelle concentration |
| **COX-2** | Cyclooxygenase 2 |
| **CPP** | Cell-penetrating peptide |
| **CS-H** | High molecular weight chitosan |
| **CS-L** | Low molecular weight chitosan |
| **CS-M** | Medium molecular weight chitosan |
| **Da** | Damkohler number |

| | |
|---|---|
| **DAPI** | (4′,6-diamidino-2-phenylindole) |
| **DCM** | Dichloromethane |
| **DLS** | Dynamic light scattering |
| **DMSO** | Dimethyl sulfoxide |
| **DoE** | Design of Experiments |
| **DOS** | Degree of supersaturation |
| **DS%** | Dissociation efficiency |
| **DSS** | Dextran sulphate sodium salt |
| **EAU** | European Association of Urology |
| **EE%** | Encapsulation efficiency |
| **EMA** | European Medicines Agency |
| **EMDA** | Electromotive drug administration |
| **EO** | Ethylene oxide |
| **EPS** | Extracellular polymeric substances |
| **EtOH** | Ethanol |
| **FDA** | Food and Drug Administration |
| **GA** | Glycolic acid |
| **GAG** | Glycosaminoglycan |
| **GEN** | Gentamicin |
| **GEN:HIP** | Ion paired gentamicin |
| **GP** | General practitioner |
| **H&E** | Haematoxylin and Eosin stain |
| **HIP** | Hydrophobic ion pairing |
| **HIP%** | Hydrophobic ion pairing binding efficiency |

| | |
|---|---|
| **HPLC** | High-performance liquid chromatography |
| **IBC** | Intracellular bacterial community |
| **IDD** | Intravesical drug delivery |
| **IRE** | Internal reflection element |
| **LA** | Lactic acid |
| **LC%** | Loading capacity |
| **LC-MS** | Liquid chromatography – mass spectometry |
| **LOD** | Limit of detection |
| **LOQ** | Limit of quantification |
| **MDR** | Multi-drug resistance |
| **MeOH** | Methanol |
| **MIC** | Minimum inhibitory concentration |
| **MQW** | MilliQ water |
| **MW** | Molecular weight |
| **NHS** | National Health Service |
| **NICE** | National Institute for Health and Care |
| **NPPT** | Nanoprecipitation |
| **NSAID** | Non-steroid anti-inflammatory drug |
| **OA** | Sodium oleate |
| **OPA** | O-phthalaldehyde |
| **P407** | Poloxamer 407 (Pluronic 127) |
| **PBS** | Phosphate buffer saline |
| **PDI** | Polydispersity index |
| **PEG** | Poly(ethylene glycol) |

| | |
|---|---|
| **PLGA** | Poly(lactic-co-glycolic acid) |
| **PO** | Propylene oxide |
| **PS** | Protamine sulphate |
| **PVA** | Poly(vinyl alcohol) |
| **PXRD** | Powder X-ray diffraction |
| **QIR** | Quiescent intracellular reservoir |
| **RCF** | Relative centrifugal force |
| **ROS** | Reactive oxygen species |
| **RPM** | Round per minute |
| **RSM** | Response Surface Methodology |
| **RTC** | Randomised controlled trial |
| **SD** | Standard deviation |
| **SDS** | Sodium dodecyl sulphate |
| **SE** | Single emulsion – solvent evaporation |
| **SEM** | Scanning electron microscopy |
| **TEM** | Transmission electron microscopy |
| **TGA** | Thioglycolic acid |
| **$T_g$** | Glass transition temperature |
| **$T_m$** | Melting temperature |
| **UNP-GEN** | Non-ion paired free gentamicin |
| **UPEC** | Uropathogenic *Escherichia Coli* |
| **UTI** | Urinary tract infection |

# Chapter 1

## Introduction

## 1.1. Human urinary bladder and urinary tract infections

### 1.1.1. Anatomy and physiology of the human urinary bladder

The human urinary bladder is a muscular, tetrahedron shaped organ, that lies within the pelvis and temporary stores urine until its excretion from the body [1,2]. The inner layer of bladder, which is called mucosa, is comprised of transitional epithelium, also often referred to as urothelium, and lamina propria (**Figure 1.1**). Mucosa plays an important role in signalling and sensory transducing of physical and chemical stimuli, but its crucial role is to act as permeability barrier [3]. Urothelium, in combination with junctional proteins and mucin layer comprised of glycosaminoglycans (GAG), functions as a barrier, which prevents pathogens and various molecules from entering deeper tissues in the bladder wall [2–4]. Lamina propria, sometimes also referred to as sub-urothelium or sub-mucosa, is a layer that lies between the basement membrane of the urothelium and detrusor muscularis [5,6]. This layer is comprised of extracellular matrix, which contains interstitial cells, fibroblasts, adipocytes, as well as efferent and afferent nerve endings [5,6].

Mucosa layer is covered by smooth muscle called detrusor, which is protected by adventitia and then external serosa. Detrusor muscle layer consists of interlacing randomly orientated muscle fibres, only organising into distinct layers – longitudinal and circumferential – near the internal urethra [1]. The organised muscle layers help form the bladder sphincter, which facilitates passage of urine through urethra, while maintaining urinary continence and allowing volitional voiding. Smoot muscles located in the bladder provides elasticity to the bladder wall, ensuring that urine can be stored during filling process [7]. Normally, human bladder can store up to 500ml of urine, due to the consistent detrusor muscle cell relaxation and elongation to accommodate storage of urine [1]. Upon receiving appropriate signals from neural control system, the voiding reflex is initiated by coordinated contractions of detrusor muscle. These contractions can be inducted by parasympathetic fibres releasing transmitters that lead to contractions to void urine [8]. By fulfilling the functions of storing and voiding urine that is constantly excreted by kidneys, bladder disposes of substances that are toxic to human organism [1].

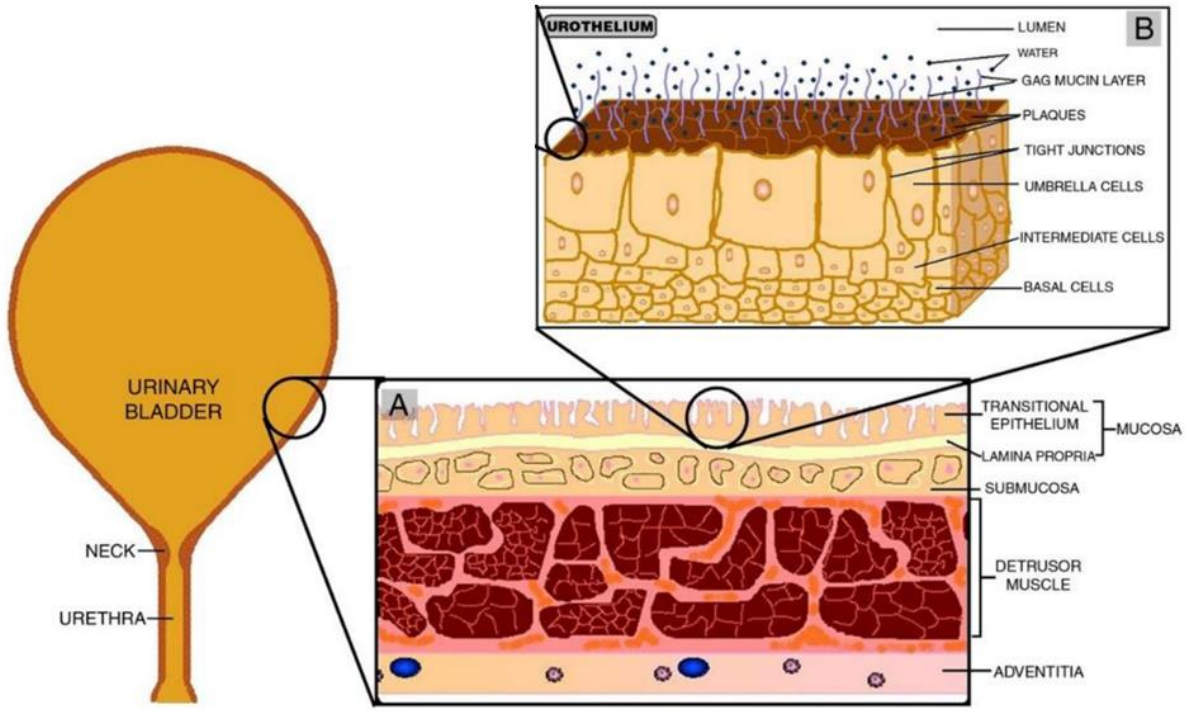


**Figure 1.1:** Schematic representation of structure of the human urinary bladder. Detailed view of the (A) layers of the bladder wall and (B) layers of urothelium. Figure reprinted with permission from GuhaSarkar and Banerjee, 2010 [9].

### 1.1.1.1. Structure and function of the urothelium

The urinal tract is lined with urothelium layer, which is a stratified epithelium tissue comprised of single layer of umbrella cells, one or multiple layers of intermediate cells, and single layer of basal cells (**Figure 1.1B**) [10]. Urothelium is a permeability barrier, that accommodates the urine flow and volume, while controlling metabolic product exchange between urine and blood [11]. In addition to this, it also protects deeper bladder tissues from pathogens. Urothelium has been demonstrated to be the least penetrable epithelium among mammalians, as it prevents permeation of water, ions, solutes and noxious agents back into bloodstream and underlying tissues [12]. The outermost layer of umbrella cells, which forms a barrier comprised of apical membrane, GAG layer and tight junctions of umbrella cells, plays a crucial role in protecting deeper layers of urothelium [10].

Urothelium surface is lined with gel-like mucin layer, which is comprised of sulfonated GAGs and glycoproteins [13,14]. GAGs are long, linear and highly negatively charged polysaccharides, that bind water molecules resulting in well-hydrated and non-adhesive bladder surface (**Figure 1.1B**) [15]. GAG layer is comprised of hyaluronic acid, heparin,

chondroitin sulphate, dermatan sulphate, and keratan sulphate [13,16]. Chondroitin sulphate and hyaluronic acid have been reported to play a significant role in antibacterial defence mechanism [16]. Damiano et al., 2011 reports that intravesical treatment of patients with chondroitin sulphate and hyaluronic acid demonstrated reduced numbers of recurring UTI cases in women [17]. This suggests that repaired GAG layer successfully prevents bacterial adhesion to the bladder wall and protects from further pathogen penetration into the deeper layers [16,17]. If untreated, pathogen access to mucosa can lead to chronic bladder epithelial damage, that could then further escalate into chronic inflammatory bladder diseases, such as recurring UTIs, cystitis or bladder pain syndrome/interstitial cystitis [18].

Apart from GAGs, there are other types of proteins that are important in controlling permeability of the bladder. Uroplakins are small family of transmembrane proteins, suggested to contribute to the apical membrane permeability layer [10]. Uroplakins form a constantly recycled urothelial plaque, which covers the umbrella cells and can modify their surface area to facilitate bladder filling and voiding [4]. This plaque provides transcellular resistance, therefore controlling water and ion absorption from the urine, as well as functioning as a barrier against all substances found in urine to protect the underlying tissues [19]. In addition to the plaque, tight and adherens junctions between umbrella cells also contribute to the low permeability of the bladder [4,20]. If the barrier function of the urothelium is compromised, the normal and abnormal contents of the urine can reach the muscle or neural layers of the bladder, therefore resulting in urgency, frequency and pain during voiding.

Aside from protective function, bladder participates in the maintenance of homeostasis of plasma osmolality, by altering urine osmolality and ensuring the stability of plasma pH, as well as hallmarked nutrient and electrolyte levels [21]. Bladder participates in homeostasis through endocrine and stretch-mediated urine reabsorption, which matches slow and steady urine filling due to kidney excretion [3,21]. Poor permeability of tightly positioned umbrella cell layer, along with asymmetric membrane on the apical side, ensures that urothelium can withstand low pH and three-fold-higher osmotic pressure of urine, compared to the serum [21].

### 1.1.2. Urinary tract infections (UTIs)

Urinary tract infections (UTIs) are one of the most commonly encountered bacterial infections, estimated to be about a quarter of the cases of the healthcare associated infections [22]. In

October 2023, the National Health Service (NHS) and UK Health Security Agency launched a new awareness of UTIs campaign due to estimated 1.8 million hospital admissions involving UTIs between years 2018-19 and 2022-23 [23]. In addition, a population-based household survey revealed that 37% of women over 16 years of age reported at least one episode of UTI over their lifetime, with 29% of women reporting more than one episode of UTI, and 3% of the same group reporting history of recurring UTI in the past year [24]. In the United States of America (USA), the cost of UTI antibiotic treatments reaches over $1 billion annually, making 15% of all antibiotics prescribed in USA to be used for treating UTIs [22]. Based on these numbers, a clear clinical and economic burden on healthcare systems can be observed, including social and psychological pressures that could impact the quality of life of the patient.

Most common bacterial pathogen to cause UTIs is uropathogenic *Escherichia Coli* (UPEC), responsible for more than 80% of the community-acquired infections [25]. This pathogen originates from intestinal microbiome, where it normally exists within symbiotic relationship with intestinal microflora and rarely results in any complications [26]. However, this bacterial strain has adapted to disseminate via oral-faecal routes, as well as through contaminated food products or sexual contact [27]. The mechanism of infection begins with contamination of periurethral or vaginal areas by pathogenic bacteria, leading to its colonisation in the urethra, followed by pathogen migration to the bladder lumen [28,29]. Once there, UPEC can adhere and penetrate the bladder epithelium cells via various virulence factors. These include surface structural components, such as flagella, pili, non-pilus adhesins, lipopolysaccharides, secreted toxins and more [11,29].

After urothelium envelopment, intracellular bacteria enter rapid doubling, thus forming intracellular bacterial communities (IBC) (**Figure 1.2**) [30]. Consequently, within 12 hours of post-infection more than half of the bacteria are intracellular. Promptly, the infection can be sensed by innate host responses, therefore initiating cytokine production, recruitment of inflammatory monocytes and neutrophils, along with exfoliation of dying urothelium cells [11]. Although the latter response is needed to eliminate infected cells from the body, it can also cause the exposure of deeper layers of epithelium to the pathogens, allowing bacteria to invade and persist in small quiescent intracellular reservoirs (QIRs) (**Figure 1.2**) [11]. These QIRs present in urothelium cells do not elicit an immune response and are protected from antibiotic treatment, as well as rinsing flow of urine due to resilient barrier function of urothelium [31]. Through an unknown mechanism, reservoirs of the bacteria can reactivate and release UPEC

back into the bladder lumen, therefore making QIRs a considered mechanism for recurrent UTIs [32].

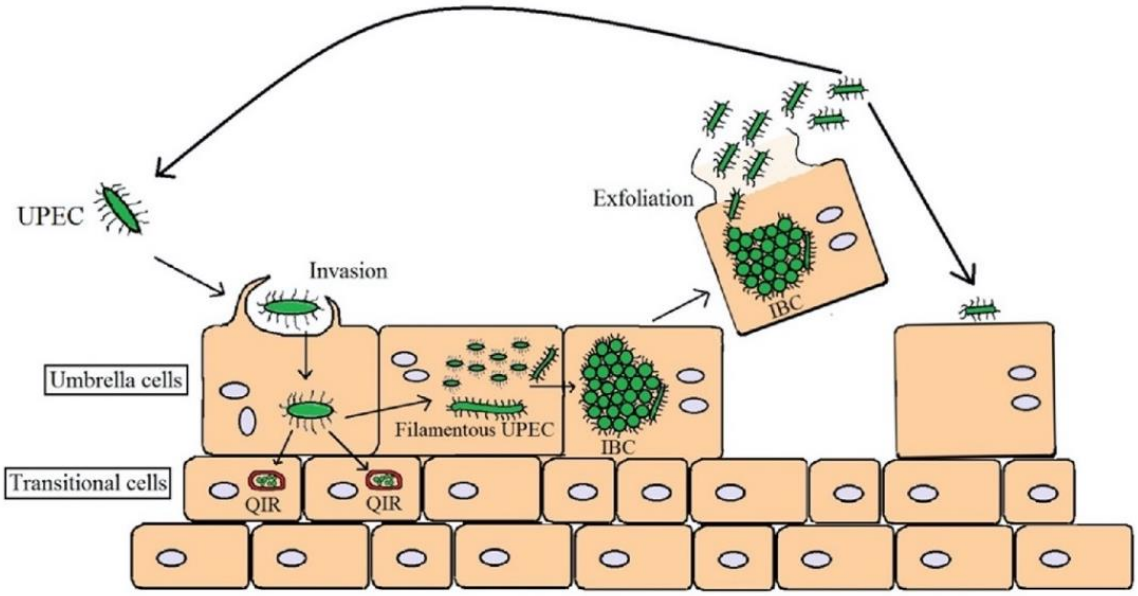


**Figure 1.2:** Schematic representation of underlying mechanism of bacterial invasion and colony establishment resulting in UTIs. Figure reprinted with permission from Kumar and Das, 2017 [22].

Similarly to IBC formation, UPEC can also form multi-cellular communities known as biofilms [33]. These bacterial communities protect UPEC from innate host immunity and antibiotic treatments, while uropathogenic bacteria undergoes maturation and further invasion [34]. Reports in literature indicate that some of the same virulence factors and polysaccharides, which facilitate the formation of IBS, are also important in initiating the formation of biofilms [35]. Biofilms are known for their distinct bacterial colony embedment in matrix, usually produced by microorganism themselves [36]. Therefore, biofilm production is initiated once bacteria adhere to the appropriate surface and change their form from planktonic to sessile, allowing production of extracellular polymeric substances (EPS) [33]. These substances are made of conglomeration of different types of biopolymers and are important for biofilm adhesion to the surfaces and for the cohesion within the biofilm [36]. Produced matrix immobilises the microorganisms and keeps them in close proximity for cell-cell interactions, nutrition source, DNA reservoir important for horizontal gene transfer, as well as protection from antibiotics and host immune defences [36]. Due to biofilm structure, most of the

antimicrobials struggle to penetrate the matrix barrier, therefore resulting in infections that are challenging to treat and could require multi-drug treatment strategies [37].

Apart from UPEC, other pathogens such as *Klebsiella pneumoniae*, *Proteus mirabilis*, *Pseudomonas aeruginosa*, *Enterococcus faecalis*, *Enterobacter cloacae*, *Streptococcus bovis* and fungus *Candida albicans* can also cause UTIs [29].

### 1.1.3. Classification of UTIs and risk factors

UTIs can be classified into different types, depending on clinical symptoms, laboratory data and microbiological findings [38]. Based on this, the most important criteria for patient assessment include clinical specificity and severity of symptoms, pattern of infections, contributing risk factors, pathogen identification and circumstances under which the UTI was acquired. Completed assessment then allows to identify the category of the UTI that the patient is suffering from, such as asymptomatic bacteriuria, uncomplicated UTI, complicated UTI, acute or recurrent UTI [39]:

- **Asymptomatic bacteriuria (ABU)** shows no physical signs or symptoms that could refer to UTI cases, apart from having positive bacterial cultures in the urine [40]. It can be diagnosed only through laboratory tests and urinalysis;
- **Uncomplicated UTIs** usually affect patients that have healthy urinary system with no abnormalities or injuries, therefore infection rarely cause any serious damage to the urothelium and it can be naturally cleared by the immune system [26];
- **Complicated UTI** cases are characterised by infection occurring due to structural or functional anatomical abnormalities, compromised state of the immune system, use of medical devices such as catheters, and/or due to impaired renal function [41]. This kind of infection requires prolonged treatment and is associated with increased risk of complications [26];
- **Acute UTIs** are usually a complication of untreated symptomatic UTI, which can result in cystitis (lower UTI, with bacteria present in the bladder) or pyelonephritis (upper UTI, with infection present in the kidneys) [29];
- **Recurring infection** is identified by at least 2 UTI episodes in 6 months or 3 episodes in 12 months [39]. Treatment of recurrent UTI can result in bacteria developing multidrug resistance, due to repeat treatment courses of antibiotics [42].

The risk factors for acquiring UTIs can be behavioural, anatomical or of genetic nature, with transient or permanent health conditions also having an impact on severity of the infection [43]. The main risk factors of UTI are linked with being a female and include use of spermicides, that might alter vaginal pH, back-to-front wiping after bowel movement, younger age of the first intercourse and increased frequency of sexual intercourse, obstructed urinary flow and lower vitamin D levels [42,44]. Additionally, history of UTI during childhood, along with maternal family history with UTIs can also contribute to elevated risk of contracting bladder infections. Analysis of several studies revealed that child obesity and poor fluid intake increased the risk of recurring UTIs in children, while circumcision and breast-feeding were protective factors for UTI [45].

There are higher risks associated with complicated UTIs in pregnant women, as they are more likely to develop ABU, which during the pregnancy can become symptomatic and evolve into complicated UTI cases [43]. Development of ABU during pregnancy is very common due to predisposing factors, such as changes in hormones, slowed peristalsis, uterine growth, bladder displacement and increased volume of residual urine [43].

According to European Association of Urology (EAU), urological conditions, such as urinary incontinence, urogenital atrophy, renal transplantation and bladder catheterisation in post-menopausal and elderly women also increase the risk of acquiring UTI. In addition, patients suffering from pelvic prolapse are often at risk of developing UTI due to voiding issues [44,45]. If surgical intervention is needed, pre-surgical cases of UTI signify the risk for acquiring the post-surgical UTIs. Increased length of post-surgical stay in the hospital is significantly associated with UTIs, especially if indwelling or intermittent catheterisation is needed [45].

## 1.2. Treatment of UTIs

### 1.2.1. Current treatment options and antimicrobial resistance

UTI method of treatment has not fundamentally changed in over 70 years as to this day bladder infections are treated with antibiotics. After oral administration, traditional drugs are absorbed into the bloodstream, where they circulate until the target site is reached and drug concentration achieved determines the drug efficacy [46]. This can lead to systemic side effects and organ or tissue function disorder, as higher concentrations of drugs are administered to enhance the treatment efficiency. However, orally administrated antibiotics for bladder infections face the

opposite issue, where due to renal clearance of antibiotics into the bladder, a minimum inhibitor concentration (MIC) of the drugs is delayed [21]. MIC is defined as the lowest concentration of the antimicrobial needed to prevent the growth of the bacterial strain after defined incubation period under *in vitro* conditions [21]. As demonstrated in **Figure 1.3**, prolonged drug filtration into the bladder creates a ”window of opportunity”, where in sublethal concentration of the drug bacteria can acquire antimicrobial resistance (AMR).

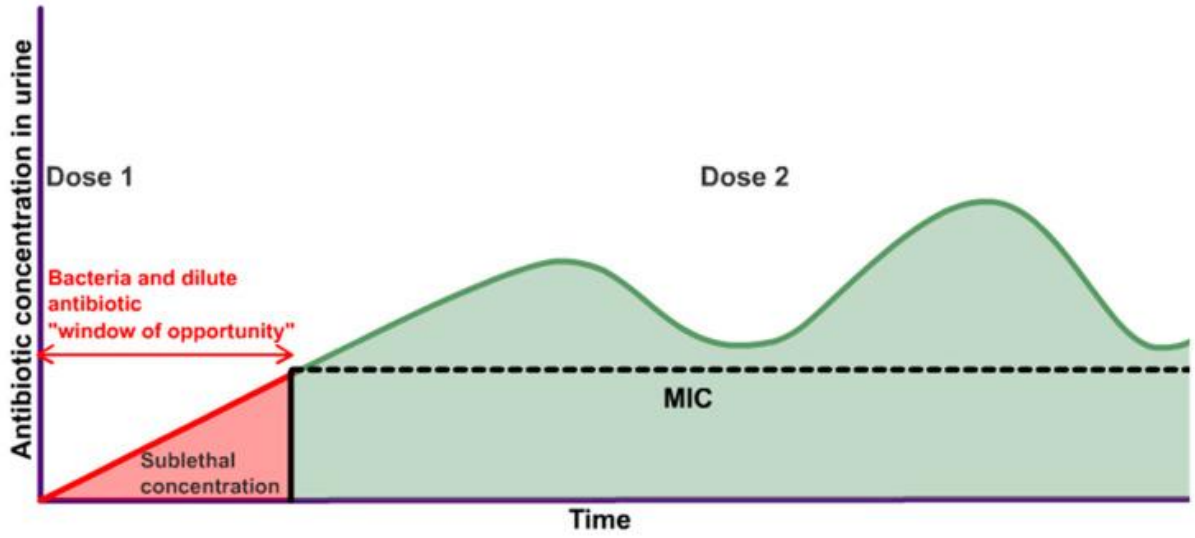


**Figure 1.3:** A schematic representation of repeat oral dosage of antibiotics, where time-dependent variability in antibiotic concentration in urine leaves a window of opportunity for the activation of AMR in bacterial colonies. Figure reprinted with permission from Tyagi et al., 2024 [21].

AMR can be acquired by UPEC strains through different mechanisms, where resistance genes are acquired though mobile genetic elements, such as plasmids, transposons, gene cassettes in the integrons, or changes in regulatory locus on the chromosome of bacteria [27]. With resistance genes acquired, UPEC strains then employ AMR mechanisms that aim to counteract the treatment of UTI with antibiotics [47]. These mechanisms include destroying antimicrobial compound enzymatically by use of β-lactamases, modifying the bacterial targets of the antibiotics, restricting the access of antibiotics by changing the function of outer membrane porins, or removing antimicrobial compounds by expression of efflux pumps [27,47].

AMR has become one of the biggest threats to human health worldwide, as it has elevated morbidity and mortality associated with common bacterial infections [48]. Although AMR can

arise naturally through genetic changes in organisms resulting in acquired resistance, the resistance problem is largely driven by ubiquitous use of antibiotics, especially due to inappropriate and excessive use of them [48,49]. If inappropriate antibiotics are selected for UTI treatment, the antimicrobials are unable to destroy bacterial reservoir, in turn acting like a shelter for bacterial survival in the bladder cells [27]. Additionally, lack of knowledge of antimicrobials also contributes to the problem, where large portions of general public, especially in the developing countries, believe that antibiotics can be used for treating viral infections and common colds (**Figure 1.4**) [48,49]. Recent data estimates that by year 2050 AMR will be responsible for 100 million deaths annually, due to ineffectiveness of the treatments [49].

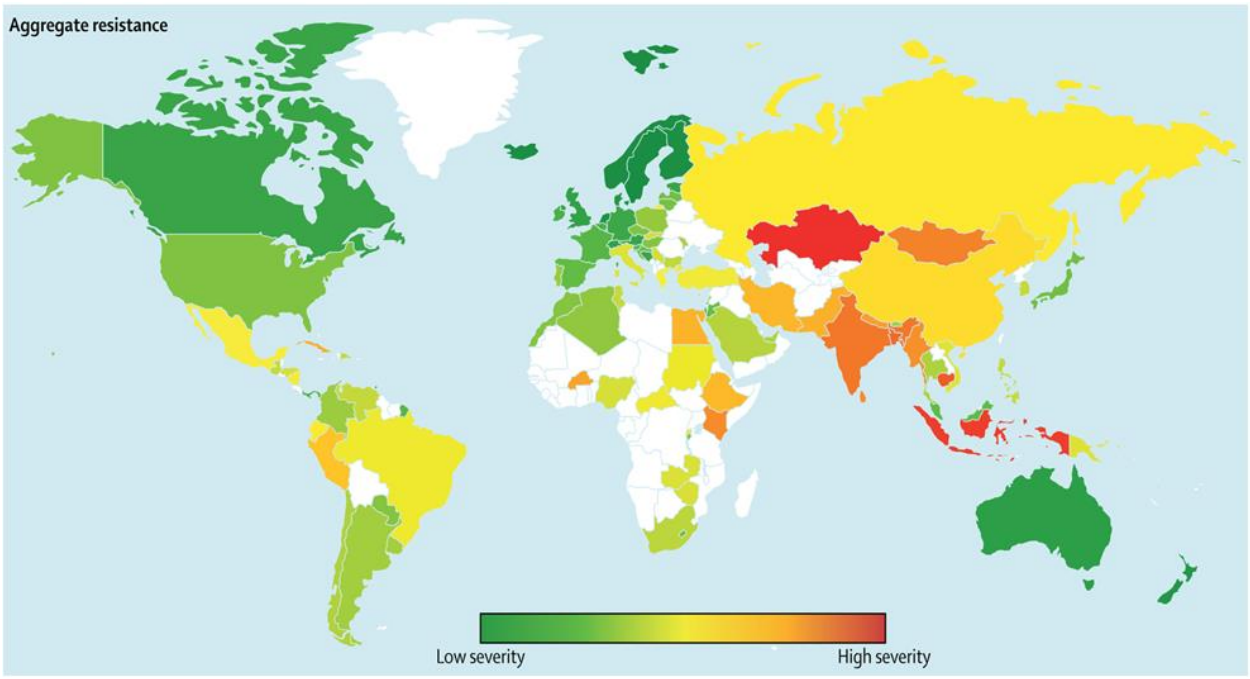


**Figure 1.4:** Figure demonstrates global aggregate resistance (%), defined as average resistance prevalence of *E. Coli*, *Klebsiella* spp., and *Staphylococcus aureus* [49,50]. Figure reprinted with permission from Collignon et al., 2018 [50].

Over the last decades, improper use of antibiotics has resulted in UPEC bacteria acquiring multidrug resistance [51], which in turn significantly decreased the activity of previously used key antibiotics for UTI treatment, such as cefotaxime, amoxicillin, gentamicin (GEN) and co-trimoxazole [52]. Statistically, the resistance rates of antibiotics such as trimethoprim, ampicillin, amoxicillin and sulfonamide in Europe risen up to 20%, with some data suggesting resistance rates of amoxicillin and trimethoprim as high as 50% [53]. Therefore, treatment of

UTIs with antibiotics that have high prevalence of bacterial resistance, such as ampicillin and amoxicillin, are no longer advised.

National Institute for Health and Care Excellence (NICE) guides the general practitioners (GPs) to only use nitrofurantoin as first choice antibiotic for men and non-pregnant women aged 16 and over, due to high effectiveness against UPEC and comparatively low AMR rates [53]. If used in short-term treatment, nitrofurantoin does not exhibit severe adverse reaction and can be an appropriate treatment option for adults [54]. However, extended prophylaxis treatment by this drug have been documented to result in pulmonary fibrosis and hepatoxicity [55]. According to the NICE guidelines, trimethoprim can also be used to treat UTI cases if patient's likelihood of resistance is low. However, due to rising resistance rates, as well as increased risk of acute rise in potassium levels and hyperkalaemia, it is less likely to be prescribed to patients [56,57]. It was also found to have higher risk of more adverse drug event outcomes than treatment with nitrofurantoin [56]. Additionally, no microbiome related adverse effects were observed with nitrofurantoin treatment as therapeutically active concentrations of this drug are possibly achieved only in urine [56].

Numerous studies have reported dysbiosis of the gut microbiome due to systemic exposure of antibiotic treatment [42,56,58,59]. Recent studies have shown increased risk of obesity, types 1 and 2 diabetes, inflammatory bowel disease, asthma, allergies and Chron's disease in patients that were exposed to antibiotic treatment in early childhood, when the adult microbiome was yet to fully establish [58,59]. Healthy microbiome in the gut is responsible for vitamin production, nutrient metabolism, protection against infection and immunomodulation, therefore harm to microbiota can lead to compromised immune system in fighting infections, increased risk in developing Parkinson's disease, Alzheimer's and multiple sclerosis, as well as depression, anxiety and psychosis [58]. Research has proved that antimicrobials alter balance of natural flora that lives within human body and therefore creates an attractive environment for harmful organisms to thrive in [42]. It has been observed that UTI treatment by antibiotics significantly affects the diversity of gut microbiota, leading to its diminished abundance and dysbiosis [58]. Although some evidence has shown resilience and potential recovery of microbiota once the treatment with antibiotics ceased, some drugs had permanently damaging effect on the healthy bacteria [58]. These findings highlight the need of restrictive and well-regulated use of antibiotics in order to prevent potential long-term toxicity.

Proposal from the NICE suggested full clinical assessment for each patient in order to identify the most suitable antibiotic treatment [42]. However, although this suggestion could potentially reduce part of the AMR problem, the delay in drug prescription would put patient at risk for development of UTI related complications and potential hospital admission. In addition, systemic exposure of the drug, as well as sub-lethal antibiotic concentrations in bladder at the beginning of antibiotic treatment would still mean that AMR and adverse toxic effects remain associated with the UTI treatment by antibiotics.

### 1.2.2. Novel treatment methods

Given the challenges of conventional UTI treatment, there is an urgent need for more effective, safe and targeted ways to treat patients suffering from bladder infections. Due to the rising risk of AMR caused by use of current antibiotic treatment, along with their side effects on healthy flora of the human body, scientist have turned to develop novel strategies for UTI treatment: novel antibiotics, vaccines targeting virulence factors of the bacteria, probiotics, bladder instillations and improved drug delivery systems enhanced by nanotechnology [60].

It is important to note, that most of these novel treatment options still need improvements and additional testing in order to be accepted as routine treatment options for UTI. In addition, although these therapies appear like attractive methods that do not involve antibiotics, antimicrobials will remain to be the most effective strategy in fighting bacterial infections. However, alternative methods can be implemented as preventative or prophylaxis methods for UTI management, while use of antibiotics can be reduced or used in an improved safety and efficacy way.

#### 1.2.2.1. Novel antibiotics

A promising novel antibiotic drug cefiderocol (formerly S-649266) was approved for human use by the Food and Drug Administration (FDA) in November of 2019. Due to the unique chemical structure of the drug, where both a cephalosporin core and a catechol siderophore side chain is present, it is more likely to overcome several AMR mechanisms [61]. This drug is known to bind to the iron and take advantage of bacterial iron transport system, therefore achieving periplasmic penetration and binding to penicillin-binding proteins [62]. Additionally, cefiderocol is stable against β-lactamase enzymes and is able to overcome efflux pump overexpression [61]. Pharmacokinetic studies revealed that two thirds of orally administrated

drugs are excreted by kidneys as unchanged parent drug [63]. RCT data demonstrated non-inferiority and superiority of cefiderocol compared to imipenem/cilastatin, however now this antibiotic is administrated only intravenously in the hospital setting to treat complicated UTI cases [62].

Another potentially promising new antibiotic is finafloxacin, a fluoroquinolone that is being developed for intravenous and oral use [62]. This drug was demonstrated to withstand in acidic environments, making it an appealing option for treating infections in urinary tract and vagina [63]. Due to the chemical structure of finafloxacin, it demonstrates enhanced penetration into the bacterial cells, along with strong hydrophobic interactions with the grove of bacterial DNA, which are responsible for large bioavailability of fluoroquinolones [64]. Finafloxacin was reported to be less absorbed at the tubular level in the kidneys, therefore enhancing its availability in the bladder. In the phase II of the clinical trials, finafloxacin was shown to eradicate pathogens and improve clinical outcomes on average about 10% better than ciprofloxacin [60]. Additionally, shorter treatment times were reported, with bacterial eradication achieved within 3 days with no increased rate of relapse recorded [65].

#### 1.2.2.2. Vaccines

A new UTI treatment strategy has emerged, where UPEC genomic components could be used as potential vaccine antigens. The guidelines established by EAU recommend the use of immunoactive strategy for preventing UTIs by priming the immune response to uropathogens [66,67]. Currently, there are several available vaccines that have gone through or are still in progress of RCTs: Uro−Vaxom®, Urovac®, ExPEC4V, MV140 and Uromune® [66]. The vaccines are comprised of bacterial extracts from UPEC strains or several inactivated bacterial pathogens, that help to generate protective antibodies and act as preventative strategy against recurrent UTIs [66]. These vaccines show reduction in UTI occurrences compared to placebo group patients, as well as reduced severity of the UTI symptoms, with documented reduction of antibiotics use during recurring UTI treatment [67,68].

#### 1.2.2.3. Probiotics

In the last couple of decades, several small trials tried to investigate the efficacy of using probiotics in order to treat or prevent recurring UTI in women. Normally, healthy female urogenital flora is comprised of different species of micro-organisms, of which *Lactobacilli* are

dominant within this microbiota [69]. However, alterations in vaginal or periurethral microbiota have been observed in women with recurring UTI [60]. Probiotics were reported to prevent pathogen ascension into the bladder by interfering with pathogen adhesion, preventing biofilm formation, as well as diminishing the growth, invasion and expression of virulence factors of the pathogens [69,70]. In addition, several *Lactobacilli* strains have demonstrated potential in clearing UPEC reservoirs in the bladder, therefore reducing risk of recurring UTIs [29]. A recent trial by Gupta et al., 2024 reports that the number of recurrent and complicated UTI cases were lower in test groups that were treated with oral and vaginal probiotics compared to the placebo test group [70]. However, no statistically significant differences were observed between the groups, indicating that while probiotics could be a good tactic to reduce risk factors of acquiring UTIs, it might not be an effective treatment option. Similarly, some *Lactobacilli* strains have been tested as a prophylactic measure against recurring UTIs, which again showed no significant effect on reducing number of the occurrences [29,70]. Although some great insights were achieved by smaller trials leading to promising effects of probiotic therapy in lowering the risk of recurrent UTIs, however large-scale RCTs are warranted.

### 1.2.2.4. Non-steroid anti-inflammatory drugs (NSAIDs)

Non-steroidal anti-inflammatory drugs (NSAIDs) are a family of drugs that are used to relieve inflammation and pain. During UTI episode, the pain experienced during voiding is caused by an inflammatory reaction, therefore use of NSAIDs could help to reduce the release of pro-inflammatory cytokines and chemokines, as well as lower prostaglandin E2 levels [71]. NSAIDs work by inhibiting the cyclooxygenase (COX) enzymes that normally catalyse the production of prostaglandins, which are responsible for controlling inflammation and pain [72]. NSAIDs usually target COX-1 and COX-2 enzymes non-selectively, however use of non-selective NSAIDs elevate the risk of gastric irritation, due to COX-1 generating prostaglandins mainly in gastrointestinal tract [72,73]. Therefore, some studies choose to investigate COX-2 selective NSAIDs, which are thought to be a safer and more efficient option for symptomatic UTI treatment [73].

A small RTC investigated the use of COX inhibitor drug ibuprofen as alternative treatment for UTI instead of antibiotic ciprofloxacin [74,75]. After 3-day treatment no significant difference between the drugs were observed, suggesting that symptom control by NSAIDs could be

sufficient option for uncomplicated UTI treatment. However, this outcome could have been observed due to uncomplicated UTI being a self-limiting disorder, which usually converts into asymptomatic bacteriuria that is relatively common in healthy women [74]. Some adverse events reported by the patients in both study groups, mostly involving gastrointestinal disorders and headache.

Subsequently, a study by Hannan et al., 2014 demonstrates that COX-2 inhibitors can be used as treatment and prevention option for UTI [76]. This study demonstrates that treatment with COX-2 selective drug celecoxib (CLX) reduced pyuria in mice UTI model, as well as showed no influence on mucosal responses of the urothelium, such as urothelium exfoliation and innate immune system activation [76]. In addition, this study observed that previously UTI affected mice were prone to more severe inflammation and mucosal damage, that could lead to recurrent UTIs. Authors suggest that by inhibiting COX-2, the damage to the urothelium barrier can be prevented, therefore suggesting that CLX can also be used as prophylaxis measure in preventing recurring UTIs [76].

In addition, CLX was shown to increase sensitivity of multi-drug resistant (MDR) bacteria to antibiotics in study done by Kalle and Rizvi, 2011 [77]. Authors demonstrated that by inhibiting the efflux pump of MDR bacteria with CLX, the concentration of intracellular antibiotics can be increased. They demonstrated that combination therapy of CLX with different antibiotics (ampicillin, kanamycin, ciprofloxacin or chloramphenicol) has significantly increased bacterial sensitivity to the treatment [77].

Based on small amount of evidence acquired, COX-2 inhibitor drugs could be a used as an option to reduce antibiotic treatment for UTIs, by increasing bacterial susceptibility to the antimicrobials, as well as providing quicker symptomatic relief to the patients.

### 1.2.2.5. Bladder instillations

In standard clinical practise, pharmaceutical treatments are often dosed systemically, although the target for the treatment might be specific tissue or organ. Additionally, to achieve therapeutic concentrations of the drug in target areas, usually a much larger drug dose is administrated, which increases the likelihood of side effects [60]. Therefore, UTI treatment could be immensely improved if drugs were to be delivered directly to the bladder. This would

reduce antibiotic systemic exposure, reduce the risk of adverse side effects, and most importantly would eliminate the risk of AMR.

Over the last decade, there were a lot of studies and trials testing the efficacy of intravesical GEN instillations as treatment or prophylaxis for lower UTIs [78–85]. In these studies, mainly 80 mg of GEN (in some studies lower dose of 14 to 28 mg were used [80,81]) dissolved in 0.9% sodium chloride or sterile water were administered once daily directly to the bladder, after complete drainage of the urine prior to the treatment. It is important to note that high dose of GEN instilled directly to bladder would eliminate the issue of temporary sublethal antibiotic concentrations in the bladder (discussed in **section 1.2.1.**), observed after oral administration of antibiotic dose [21]. Results of intravesical GEN studies demonstrated significantly reduced number of UTI occurrences, with 90% of the bacteria eliminated within 3 hours of the treatment administration, along with minimal or no contribution to AMR, extremely rare cases of systemic absorption of GEN, and no side effects reported [21,78–82]. Due to low GEN levels in the plasma, significantly higher dose of GEN can be administered, while the same dose delivered orally or intravenously would be toxic [21].

Contrary to positive results reported, intravesical GEN is only offered as off-label alternative UTI treatment, when conventional treatment of oral antibiotics has failed or been ineffective over time [79,81]. In addition, some challenges persist, making this treatment less appealing to the GPs and general public. Firstly, intravesical drug delivery requires catheterisation, which is mostly performed by a trained professional in a hospital setting to ensure safe and effective treatment. Furthermore, the conventional drugs are not licensed for intravesical use by medicines regulatory agencies, making this unregulated off-label treatment. This arises the problem of standard drainage catheters used for intravesical drug delivery, which are not certified for such use and therefore significantly increase infection risks [86]. Based on this, the perception of GPs and general public remain rooted in using oral antibiotics for UTIs that occur handful of times in a year, as oral drugs are quicker, easier, safer and cheaper to administer [81]. However, as the threat of AMR persists, alternative treatment methods might need to be considered as the new conventional treatments.

## 1.3. Nanotechnology: a solution for improved drug delivery

An increase in high-mortality diseases has identified that current traditional treatment options do not provide desired therapeutic results even when using highly potent active agents [87]. Therefore, nanoscale technology has provided novel methods in disease diagnosis, treatment and prevention to enter the scientific field [9,22,88,89]. Combining nanotechnology with pharmaceutical and biomedical sciences enhanced the development of novel drugs delivery systems, that improve the efficacy and safety of the treatment [9,22,89,90]. Encapsulation of drugs into nanocarriers could improve the metabolic stability of the drug, increase molecule penetration through permeability barriers, allow tissue targeting, reduce toxic side effects and provide sustained drug release [9,22,91].

Different carriers of nanosized agents, such as liposomes, micelles, polymeric or metal nanoparticles, dendrimers and nanocrystals (**Figure 1.5**), can be administrated through oral, intravenous, intravesical, transdermal, rectal or buccal mucosa delivery routes [92–94]. From these, liposomes, lipid and polymeric nanoparticles were considered to be most popular types of nanocarriers, due to their cost effectiveness, easy synthesis, and biodegradable properties [22,95]. Some of the drug loaded liposome and polymer nanoparticle products have been approved by FDA for nanomedicine use as early as 1990s, with steady increase of clinical trial approvals observed since the late 2000s [90]. In the last decade, more of micellar, metallic and protein-based particles have entered the development process [90].

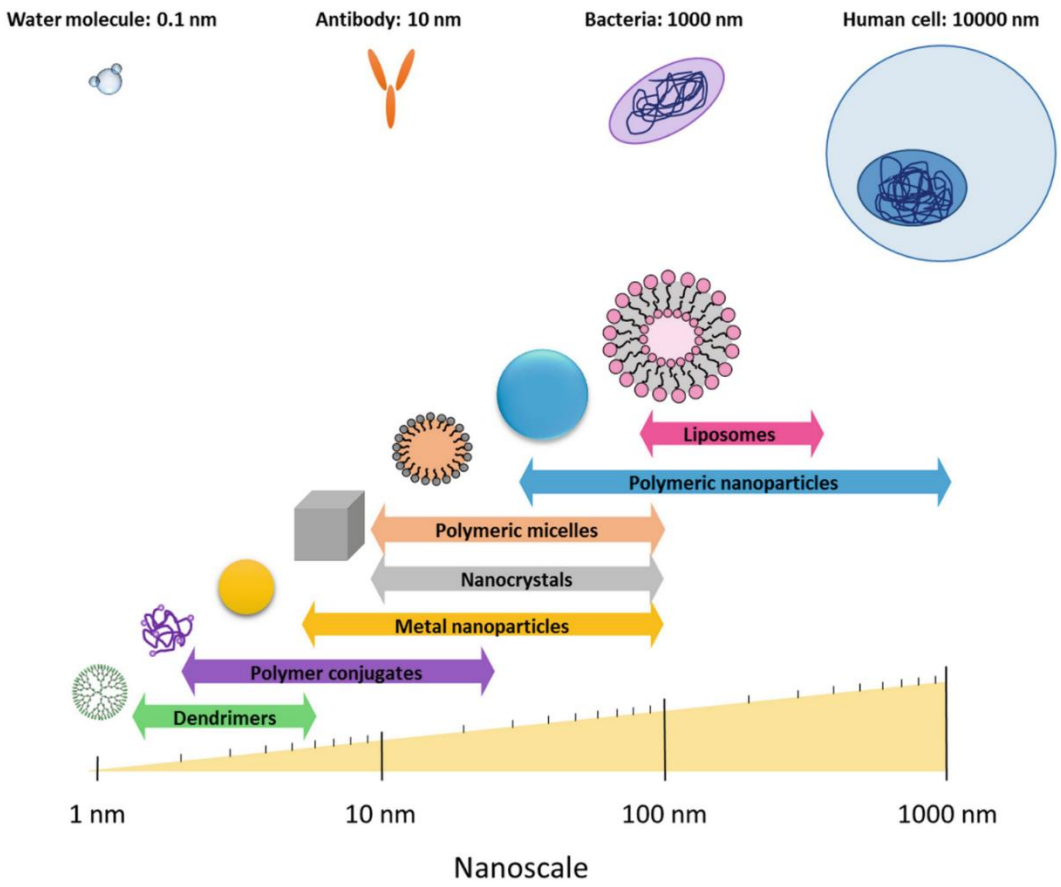


**Figure 1.5:** Illustrative representation of different nanocarrier types and their associated approximate size, compared with the size of biological structures. Figure reprinted with permission from Fornaguera et al., 2020 [94].

Due to the small particle size and large surface area, encapsulation of the drugs into nanosized carriers can improve the solubility and permeability properties of the drug, allowing the particles to cross even the most impermeable barriers [88,96]. In addition, drugs that were claimed to be no longer suitable for the market, due to high AMR or acute toxicity, can now have another chance with an improved drug formulation by using nanotechnology [97].

To ensure that the pharmaceutical agent has the capacity to reach its maximum efficacy, design of the drug formulation can be challenging [87]. By encapsulating active molecules, the biodistribution of the therapeutic agent relies on physicochemical properties of the carrier [98]. Therefore, alterations in particle size, shape and surface chemistry are the key factors that determine performance criteria [90].

## 1.4. Polymeric nanoparticles as drug delivery vehicle

One of the most used materials for nanocarriers are polymers, due to their wide applicability across the field and relatively easy synthesis [90]. Depending on the polymers selected and the composition of the nanoparticle formulations, physicochemical, toxicity and drug release profiles can be adjusted in order to achieve desired nanomedical product [2,94].

### 1.4.1. Composition of polymeric nanoparticles

Polymeric nanoparticles can be made from natural polymers, starches, cellulose, albumin, chitosan, as well as synthetic polymers synthesised from natural monomers, such as polylactic acid and poly(lactic-co-glycolic acid) (PLGA) [93,99]. Synthetic polymers were observed to be biocompatible, biodegradable and non-toxic, making them FDA-approved for drug delivery use in humans [90,100,101]. PLGA copolymer has been often used as delivery system for active drugs, genes and macromolecules [102]. Additionally, it has been employed in various fields of medicine, to enhance diagnosis, tissue engineering, facilitate vaccine, gene or protein delivery [103].

PLGA is a copolymer of lactic acid (LA) and glycolic acid (GA) [104]. It can be synthesised by ring opening polymerisation of two different monomers, which the cyclic dimers of GA and LA [105]. During the polymerisation, the two monomers are linked together in PLGA by ester linkages (**Figure 1.6**). Degradation of PLGA occur through cleavage of polymer chains by hydrolysis, therefore leaving LA and GA products in the body to be later naturally eliminated through Krebs cycle [105,106]. The time required for hydrolysis to degrade PLGA structure depends on LA to GA ratio, end group of the polymer and overall molecular weight (MW) [105,107].

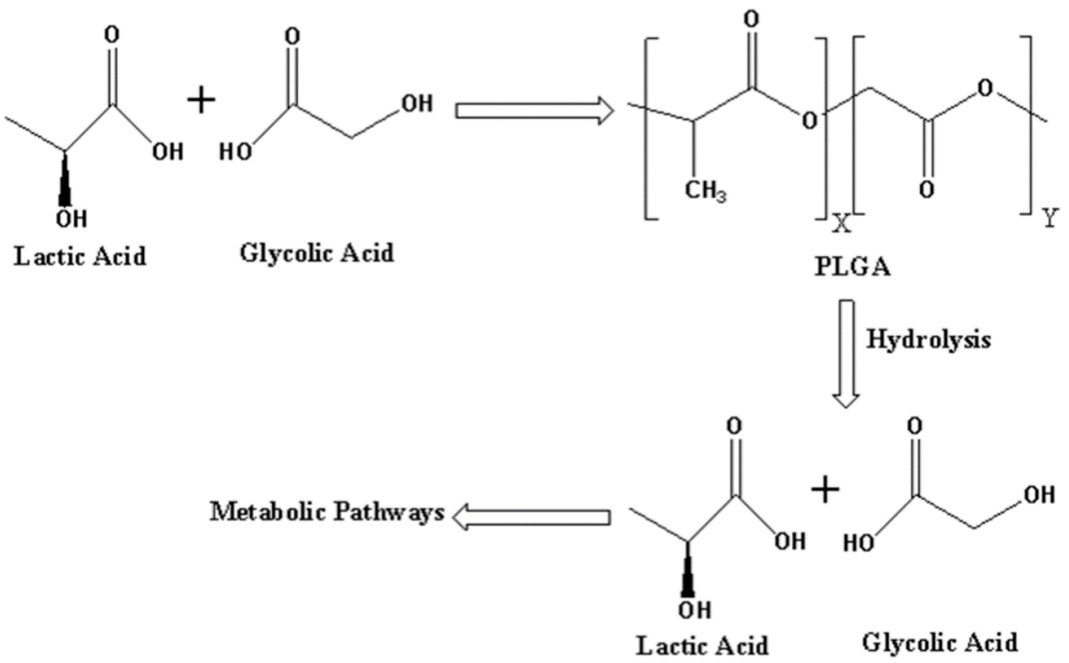


**Figure 1.6:** Chemical structure of LA, GA, and PLGA. Graph represents copolymerisation reaction of lactic acid and glycolic acid monomers, leading to formation of PLGA, followed by hydrolysis and monomer elimination through metabolic pathways. Figure reprinted with permission from Alvi et al., 2022 [108].

PLGA is known for its shorter degradation time compared with other synthetic polymers [106]. Degradation rate can be controlled by choosing the right composition of PLGA, where higher concentration of GA enhances the hydrophilicity of the polymer, leading to faster hydrolysis [107,109]. Study by Budhian et al., 2005 showed that increasing LA to GA ratio in PLGA from 50:50 to 95:5 significantly sustained the release of haloperidol from 2 days needed for complete drug release from 50:50 PLGA, to 13 days when drug was entrapped in 95:5 PLGA [110]. However, some studies suggest that shorter degradation time helps to reduce adverse reactions during treatment, which is often observed when polymers with longer degradation time are used [107,108]. In addition to LA to GA ratio, pH of the surrounding medium also plays important role in PLGA degradation. With increase in pH a decrease in polymer degradation rate and improved stability of the overall system can be observed [105,107]. Furthermore, studies have reported, that lower MW facilitates faster degradation of the polymer, therefore resulting in faster drug release rate [105]. Different grades of PLGA are available commercially, which provide different LA to GA ratio, as well as capped or uncapped ester or acid end group [107]. Ester end group polymers are reportedly more resistant to hydrolytic degradation, therefore prolonging the shelf life of the polymer [107].

Apart from PLGA, polymeric nanoparticle composition also often includes use of surfactants. They are mainly used to stabilise the nanoparticles and reduce the surface tension [111]. Surfactants are known to prevent particle aggregation due to their amphiphilic nature, where hydrophobic regions of the surfactants bind to the nanoparticles, while hydrophilic regions interact with water providing colloidal stability [111,112]. In addition to this, use of surfactants also often affects particle size, polydispersity index (PDI), zeta potential, sometimes also improving solubility of the drug, which can lead to improved drug loading into the particles [112]. Different surfactant materials are often used for polymeric nanoparticle preparation: poly(vinyl alcohol) (PVA), polysorbates (Tween 20, Tween 80), emulsifiers (Span 20, Span 80) and poloxamers (Pluronic F127, Pluronic F68) [113,114]. Out of these, PVA and poloxamers are most commonly used for manufacturing polymeric nanoparticles in the biomedical field [112].

### 1.4.2. Preparation methods of polymeric nanoparticles

Over the last decade, use of polymeric nanoparticles has increased exponentially due to their advantages when compared to conventional therapies or other nano-systems [94]. Most importantly, these particles can be obtained through easily scalable and affordable methods. Some of these methods have been extensively documented in polymeric nanoparticle synthesis: emulsion – solvent evaporation, nanoprecipitation (NPPT), emulsion – solvent diffusion, and salting out techniques [94,101,115]. According to the literature, out of these, emulsion – solvent evaporation and NPPT methods are most commonly used for PLGA nanoparticles synthesis. Therefore, they are discussed in detail in **section 1.4.2.1.** and **1.4.2.2.**

Polymeric nanoparticles usually carry an active pharmaceutical ingredient (API), gene or molecule of interest, which can be either encapsulated within the particle, adsorbed on the particle surface or chemically linked to the particles surface [101]. Mostly, polymeric nanoparticles exist as either nanocapsules or nanospheres (**Figure 1.7**) [94,101]. Nanocapsules are vesicular systems, where the substance of interest is entrapped in a cavity consisting of liquid core, while surrounded by a solid material shape [116]. In contrast, nanospheres are homogenous matrices, where the core and the outer surface made up of polymeric material, where substance of interest is either retained or absorbed into the structure [94,101]. In most studies both types are rarely differentiated, typically referring to both as nanoparticles [94].

However, for certain applications specific types of nanoparticles are aimed to be synthesised, which can be achieved based on the materials and synthesis methods used [115].

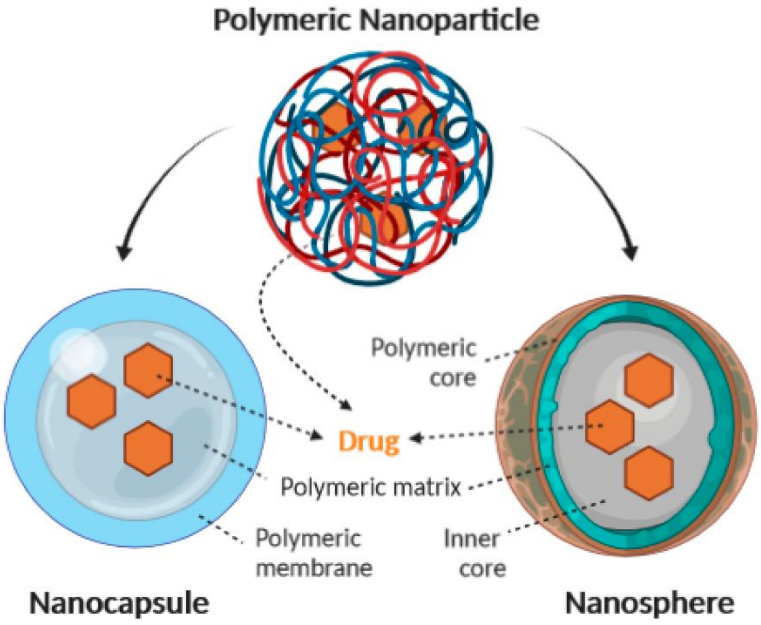


**Figure 1.7:** Schematic illustration of nanocapsules and nanospheres as structures of polymeric nanoparticles. Figure reprinted with permission from Zielińska et al., 2020 [115].

### 1.4.2.1. Emulsion – solvent evaporation

Emulsion – solvent evaporation was the first method to be developed for nanoparticle preparation, as well as most commonly used to this day for drug encapsulation [117–119]. Emulsion – solvent evaporation method relies on the use of volatile water immiscible solvent, which upon mixing with aqueous solution at high shear force forms nanoparticle droplets that after solvent evaporation harden into nanoparticles [119]. The main advantage of this technique is the ability to encapsulate not only hydrophobic drugs, but also hydrophilic drugs by including additional emulsification steps to protect the drug from surrounding aqueous phase [108,119]. In addition, this method synthesises high yield of small sized particle in a short reaction time, and despite the use of organic solvents, produces non-toxic particles [108,119]. However, some disadvantages are also observed. Various parameters in preparation methods need to be optimised depending on the properties of selected API and overall application of the formulation to achieve the best results [120]. Use of homogeniser or sonication is necessary to achieve small nanoparticles, however due to high energy and subsequently increased temperatures of the solution, this step could affect the stability of certain drugs [112].

During emulsion – solvent evaporation preparation method, organic phase, containing polymer and active agents (e.g. drug) dissolved in organic solvent, is mixed with aqueous phase containing a surfactant [115]. Then, the mixture is processed by using a high-speed ultrasonication, which creates a dispersion of nanodroplets. The nanoparticles are formed through the evaporation of organic solvent, after which the particles are centrifugated to obtain solidified nanoparticles [120].

In order to minimise the escape of the hydrophilic drug to the aqueous phase, the double emulsion – solvent evaporation method is used [117]. This method ensures that the active agents entrapped in the internal aqueous phase can facilitate slow and sustained release, while also protected from enzymatic degradation or oxidation [102]. However, this process is complex and thermodynamically unstable, and therefore it is often challenging to achieve a stable, good quality product [102]. The drawbacks of this methods are most often associated with polydisperse, large and non-uniform particles, due to at least two emulsification steps involved. Additionally, slow inner membrane formation might result in drug leaching out of the hydrophilic core into external aqueous phase [102,118].

Double emulsion process involves mixing aqueous phase, that contains the hydrophilic drug, with the organic phase, that contains dissolved polymer in the organic solvent [121]. The first emulsion is achieved after ultrasonication process, followed by addition of the second aqueous phase, that contains a surfactant. After another round of sonication, the final product is left stirring until organic solvent evaporates. Some common pharmaceutical drugs, such as anticancer drugs, anti-inflammatory and antibiotics, have been reported to be encapsulated into nanoparticles by double emulsification method [102].

### 1.4.2.2. Nanoprecipitation

NPPT technique is one of the most adopted techniques for nanoparticle synthesis, due to its single step process, good reproducibility, easy scalability, low energy input, and production of small nanoparticles with narrow size distribution [108,115,119,122]. Contrary to the technique of nanoparticle preparation by emulsion – solvent evaporation, NPPT method does not require use of surfactants [115]. However, use of NPPT is limited for mostly hydrophobic active ingredient encapsulation [102]. NPPT technique requires the use of two miscible solvents [115]. Polymer and drug are dissolved in water-miscible organic solvent, such as acetone or

acetonitrile, and then thoroughly mixing it with an aqueous antisolvent, which can be water or aqueous buffer [115,122]. Spontaneous diffusion of organic phase into aqueous phase and PLGA precipitation results in instant formation of nanoparticles [116,122].

During formation of drug loaded nanoparticles, some drug precipitation might occur, however that depends on the concentration of the drug and its solubility in the solvent/antisolvent mixture. Study by Hamdallah et al., 2024, refers to this as degree of supersaturation (DOS), which is defined as ratio of between component concentration in the solvent/antisolvent mixture after mixing and its equilibrium solubility in that mixture [122]. With high DOS, component precipitation time could be shortened, which would lead to precipitation occurring before homogenous component mixing is achieved [122]. This would result in reduced drug entrapment, as two phases are formed: PLGA nanoparticles and drug particles in nano or microparticle form [122]. Based on the DOS, other outcomes can also be observed, where drug is entrapped into a drug-enriched core of polymeric nanoparticles, drug is entangled within polymer chains, or drug is adsorbed onto the polymeric nanoparticles surface [122].

### 1.4.3. Physicochemical properties of polymeric nanoparticles

Physicochemical properties of polymeric nanoparticles, such as particle size, PDI, zeta potential and drug entrapment efficiency are crucial parameters that determine the quality of the nanoparticles. Multiple studies have investigated how changes in parameters of nanoparticle synthesis methods affect the particle characteristics. These are presented in detail in **Table 1.1**.

**Table 1.1:** Table presents a summary of different parameters that can be manipulated when preparing polymeric nanoparticles, how changes in those parameters affect the final characteristics of the particles, and underlying reason why changes in characteristics are observed. Supporting literature is split between publications investigating changes in particles prepared by emulsion – solvent evaporation (E-SE) and nanoprecipitation (NPPT) methods.

| **Parameters** | **Effect on particle characteristics** | **Underlying reason of the effect** | **Supporting studies** |
|---|---|---|---|
| Polymer concentration | Increase in polymer concentration | Increasing the concentration of the polymer in the organic phase increases the overall viscosity of the | E-SE: [119,123–127] NPPT: |

| | | | |
|---|---|---|---|
| | increases particle size | phase. This leads to higher resistance against shear forces, which in turn increases the size of the particles. Additionally, higher viscosity of the polymer phase contributes to slower diffusion rate of the organic phase into aqueous phase, which contributes to larger particle size. Size of the particles could also be affected by PLGA co-polymer structure, depending on the ratio of lactic acid and glycolic acid, as well as different MW of PLGA. | [119,128–130] |
| Polymer structure | Increased ratio of lactic acid in PLGA co-polymer prolongs the release of encapsulated active molecules | PLGA is a co-polymer made up of lactic and glycolic acids, where lactic acid is hydrophobic and has a slow degradation rate, while glycolic acid is hydrophilic, and therefore degrades much faster. Hence, PLGA with higher ratio of lactic acid takes longer release the entrapped molecules. | Applicable to both E-SE and NPPT: [107–110,131,132] |
| Surfactant concentration | Increase in surfactant concentration decreases particle size *(only applicable to E-SE method)* | Increased viscosity of aqueous phase improves the stability of the emulsion, leading to a decrease in particle coalescence and aggregation. | E-SE: [119,125,133] |
| | Increase in surfactant concentration increases particle size *(only applicable to NPPT method)* | Due to surfactant adsorption on the nanoparticle surface, higher concentrations of surfactant lead to increase in particle size. | NPPT: [119,134,135] |
| | Increased surfactant concentration leads | Several studies have demonstrated that surfactants coat the surface of | E-SE: [112,136–138] |

| | | | |
|---|---|---|---|
| | to decrease in their anionic charge, which could also reduce colloidal stability of the nanoparticle system | polymeric nanoparticles. PVA, which is often used in particle preparation by emulsion – solvent diffusion method, form hydrophobic bonds with acetyl groups of PLGA, therefore permanently attaching itself to the surface of the nanoparticles. | NPPT: [112,134,135] |
| Organic solvent evaporation rate | Faster evaporation of organic solvent leads to smaller particle size and lower polydispersity | Higher rate of solvent evaporation leads to increased solvent front kinetic energy, which results in higher degree of droplet dispersion in the aqueous phase. In contrast, slower solvent diffusion prolongs particle hardening process, which in turn can lead to droplet coalescence and aggregation during the early particle formation process. | Applicable to both E-SE and NPPT: [119,125,139] |
| Aqueous to organic phase volume ratio | Increase in organic phase decreases particle size and ensures overall stability of the particles | Larger volume of organic solvent reduces overall viscosity of the polymer phase, which then prevents the droplet aggregation due to faster organic phase diffusion into the aqueous phase. | E-SE: [123,125,140,141] NPPT: [123,129,130,142] |
| Sonication amplitude and time *(only applicable to E-SE method)* | Increased duration and power of the sonication reduces the particle size | By using high shear stress, the emulsion droplets are reduced in size upon formation, therefore providing reduced mean diameter as a result. Sonication also changes particle population distribution from bimodal to monomodal. | E-SE: [119,125,143,144] |

Particle size is the most important criterion of the nanoparticles, as it determines the *in vivo* distribution and biological fate, toxicity, targeting ability, drug loading, drug release kinetics,

and stability of the drug formulation [89]. Smaller nanoparticle size results in larger surface area to volume ratio, which could mean faster drug release as it is closer to the surface than in larger sized particles [96]. In contrast, larger nanoparticles can have larger drug enriched core, therefore being able to store more drug and release it in a prolonged manner [89,138]. However, nanoparticles sized above 200 nm were shown to trigger clearance by lymphatic system and therefore resulting in quicker removal from the circulation [89,96]. Alternatively, it has been shown that nanoparticles sized 100 nm had 2.5-fold greater uptake by Caco-2 cells than 1 μm sized particles [89,96]. Furthermore, depending on the size, some nanoparticles can cross even the most complex permeability barriers in human body, such as blood brain barrier or urothelium [88,96]. These findings indicate that due to their small size and mobility nanoparticles can be a desirable option for drug delivery to cellular and intracellular targets [89]. In addition, size distribution of the nanoparticles determines the quality of the system, as wide size distribution is often associated with particle aggregation, while uniform size distribution (PDI < 0.3) demonstrates good quality samples with no particle coalescence [134].

Manipulation of surface characteristics of the nanoparticles can prevent particle aggregation, ensure stability of the system, and facilitate receptor binding [89]. Surface charge shows the electrical potential of the particles, which is influenced by the composition of particles in the medium that they are dispersed in [89]. Generally, positively charged particles have been shown to be better internalised in various cell lines compared to neutrally or negatively charged nanoparticles [145]. Positively charged nanoparticles can interact with the negatively charged mucin, which facilitates the drug transportation across mucus and enhances internalisation of epithelial cells [97]. In addition, nanoparticles also can interact with each other, which affects particle system stability, as well as determines if any aggregates are formed. These outcomes depend on repulsive electrostatic forces and van der Waals attractive forces, as well as overall surface charge of the particles which can be measured by zeta potential [146]. In order to achieve stable formulations and prevent particle aggregation, it is recommended that particles demonstrate the highly positive or highly negative zeta potential [89,146]. To prevent nanoparticle coalescence, particles are often coated with surfactants, which decrease surface tension. In addition, they also improve pharmacokinetics, encapsulation efficiency and drug release profile [147]. Other surface modifications by membrane permeation enhancers or ligands, that bind the receptors expressed on the cellular membrane, can improve transcellular particle accumulation and specific tissue targeting [97].

The shape of the nanoparticles demonstrates significance in biodistribution, loading capacity and interactions with *in vitro* and *in vivo* systems [148]. Studies have shown that the radius of the curvature where the initial contact between the cells and particles occur could determine the rate of particle phagocytosis [149]. Study by Decuzzi et al., 2010 found that non-spherical particles had more effective internalisation into different types of *in vitro* tissues [150]. Rod-shaped nanoparticles were reported to have better cell uptake due to larger surface area for nanoparticle-cell interactions, while nanowires were demonstrated to evade phagocytosis due to their length [149,150]. However, many studies have shown that spherical particles have unmatched high surface area to volume ratio, high drug-loading capacity and dynamic characteristics, making them superior to non-spherical particles [151].

It is essential to understand the interactions between nanocarriers and target tissue or organs to ensure efficient nanodrug delivery and improved drug pharmacokinetics [152]. Generally, most critical nanoparticle-host interactions happens when particles enter the blood system, where the biodistribution, efficacy and toxicity of the drug is determined [153]. As nanoparticles are highly organised clusters of chemical groups and biomolecules, in some cases they can be considered as foreign agents by human body due to differences in sugars, polysaccharides, proteins or nucleic acids present on the surface of the nanoparticles [153]. This can lead to insufficient absorption and diffusion of the drug into tissues compromising the drug activity [152]. It can also have a contrasting effect, where excessive accumulation can result in enhanced tissue-specific toxicity [152]. However, nanoparticles can be delivered directly to an organ, such as the eye, lungs, gastrointestinal tract or bladder, which limits drug systemic exposure, significantly reduces the chances of the drug being cleared through the lymphatic system, as well as minimises the risk of toxicity [97,154–156].

Another important interaction between nanoparticles and target tissue is nanoparticle cellular internalisation, that depends on the intracellular processing pathways that are activated upon cell entry [94,153]. While traditional drugs with small molecules rely on passive diffusion or active transport for intracellular entry, nanoparticles enter the cells via endocytosis [46]. This process is defined as material transfer to the inside of the cell by the use of cell membrane as collector of solutes, molecules and different particles [94]. Endocytosis is considered to improve specific cell targeting and help nanoparticles to accumulate in the right location. Nanoparticles internalisation endocytosis pathways can be classified into phagocytosis and pinocytosis, which can be split into caveolar- or clathrin-mediated endocytosis, and

macrocytosis (**Figure 1.8**) [46,94,97]. Phagocytosis is internalisation and elimination of mainly larger than 0.5 μm particles by mammalian cells, such as macrophages, neutrophils and monocytes [46,94]. Pinocytosis focuses on intracellular fluid uptake, that can be surrounding fluid or all substances in fluid form [94]. Scientists have showed that the pathway of endocytosis depends on physiochemical characteristics of the particles, such as size, shape and charge [46,94]. However, the intracellular entrance of the nanoparticles can be often manipulated by using membrane permeation enhancers or ligands that bind with the receptors expressed on the cellular membrane [97]. Particle ability to bind and interact with biological material can alter nanoparticles surface characteristics, therefore highlighting the importance of therapeutic formulation optimisation and examination [94,101].

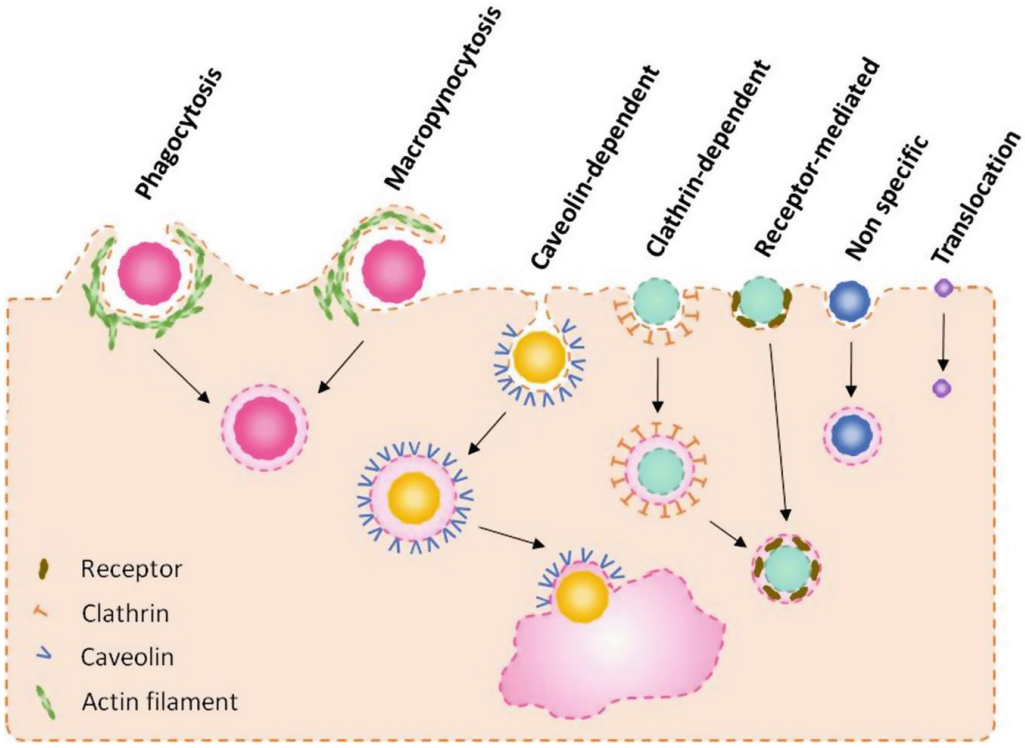


**Figure 1.8:** Schematic representation of the mechanisms of endocytosis internalisation pathways. Figure reprinted with permission from Fornaguera et al., 2020 [94].

Ensuring that nanoparticles interact with the target tissue or internalise intracellularly is important for enhanced particle accumulation at the target site, however efficient drug loading and drug release is crucial when developing nanoparticle drug delivery system. To achieve that, drugs can be loaded into nanoparticles by either incorporating the drug during particle preparation process or by adsorbing it to the nanoparticles after their formation is finished [89,157]. Different particle preparation methods can result in different types of drug

entrapment, where drug is entrapped in polymer matrix, encapsulated in liquid core, adsorbed on the particle surface, or trapped in the nanoparticle core by shell-like polymer membrane [105]. Thus, depending on the drug entrapment in the polymer, different drug release mechanisms can be observed: desorption of the drug from the surface of the particle, diffusion from particle matrix, diffusion through the polymeric shell of the nanoparticles, or diffusion out of particle matrix due to polymer erosion [105,157]. The rate of drug release depends on chosen polymer matrix, specifically its biodegradation, drug solubility, as well as pH and temperature of surrounding medium [96].

### 1.4.4. Toxicity profile of polymeric nanoparticles

With increasing attention of using polymeric nanoparticles as a drug delivery vehicle, potential toxicity related to increased human exposure and unknow dosage of nanomedicine has to be investigated to ensure safe and effective treatment. Due to different factors and different APIs involved in polymeric nanoparticles, it is challenging to establish cytotoxicity profiles of PLGA nanoparticles on different cell lines [158]. However, based on the results of multiple studies, it appears that cytotoxicity is increased with the length of the exposure of nanoparticle treatment, due to the high intracellular accumulation of the drug over treatment time [158–160]. Additionally, some studies have demonstrated that size-dependent cytotoxicity by nanoparticles is caused by their ability to internalise within cells and modify their crucial cellular functions, which leads to rupture of membrane of the subcellular structures and overproduction of reactive oxygen species (ROS) [161,162]. Overexpression of ROS results in oxidative stress, that affects the normal physiological functions of the cells and can cause DNA damage, dysregulation of cell signalling, and ultimately cell death [161].

Surface modification of nanoparticles, which is often implemented for specific tissue targeting or to improve particle attachment and permeation through biological barriers, can also contribute to the overall toxicity of the nanomedical treatment [158,161,162]. Nanoparticles with reactive surface moieties can interact with different intracellular and extracellular biomolecules, which could lead to disturbance of the tissue or cellular homeostasis [161]. Most reports demonstrate that cationic surface charge contributes to the enhanced cytotoxicity, however such reports are mostly based on studies examining inorganic nanoparticles [161,163,164]. In contrast, some studies have found that surface modifications can improve toxicity profiles of the nanoparticles. For instance, polyethylene glycol (PEG) is often used to

coat polymeric nanoparticles in order to enhance their systemic circulation time, enhance penetration of biological barriers, and prevent or enhance particle binding to mucous membranes, depending on the MW of the material used [104,115,165,166]. Findings demonstrate that API encapsulation into PEGylated PLGA nanoparticles had significantly reduced cytotoxicity compared to the free API treatment [161,167].

The components, that are usually used for polymeric nanoparticle synthesis, have been shown to be safe to use in human body. The most commonly used polymer for nanoparticles, PLGA, is a biodegradable polymer that has been approved for drug delivery purposes in humans by FDA [90]. Surfactants, such as poloxamers and PVA, have demonstrated some cytotoxicity systemically with higher concentrations of surfactants used, however it was proven by multiple studies that low concentrations used for nanoparticle synthesis do not seem to cause any cytotoxicity *in vitro* [136,168–170]. In addition, conventional nanoparticle synthesis methods use organic solvents, which are later evaporated from nanoparticle formulations [108,115,171]. However, even after several washes, some residual organic solvent remains in the nanoparticle system, which could lead to some undesirable toxic effects [171].

## 1.5. Nanomedicine: current and future products on the market

Nanomedicine is a field that combines nanotechnology with pharmaceutical and biomedical sciences for the development of therapies with higher efficacy and improved toxicology profiles [90]. Similarly to the traditional drugs, nanomedicines also require pre-market approval and their pre-clinical and clinical validation from FDA and European Medicines Agency (EMA) [90]. Although a clear interest in development of nanotechnology has been observed in most countries, researchers still face challenges related to insufficiency of specific regulatory guidelines for production of nanomedicines [172,173]. Due to diversity of nanoparticle composition, characteristics, and potential surface coatings, their interactions with the biological systems and interparticle interactions *in vivo* and are hard to predict, increasing the risk of unexpected therapeutic effects or toxicity [172,174]. Lack of standard protocols in the early development of the nanomedicine products leads to often unforeseen toxicity of the treatment in the later stages of clinical trials, resulting in overall failure of the product [172]. Most often, clinical trials are long, complicated, and expensive, which means that standardised and improved regulatory process for nanomedicines is necessary to enable novel nanotherapeutics to enter the market [174].

### 1.5.1. Approved polymeric nanoparticle products

The very first generation of nanoparticle-based therapies focused on liposomes and micelles, which have been approved by FDA for drug delivery use since the late 1990s [172]. Current nanomedicine products that are approved for clinical practise all revolve around the drugs that have low solubility and high toxicity, as encapsulation of these drugs into nanoparticles enabled better bioavailability and reduces toxicity [172]. However, since 2016 the majority of FDA approved nanoparticles for drug delivery were polymeric, with liposomal and lipid-based nanoparticles following closely [175]. Since the 1990s, there had been several PLGA-based injectable depot formulations that were approved for use by FDA [173]. These are long-acting formulations in form of microparticles, in-situ gels, or solid implants, where drug depot needs to be reintroduced after predetermined amount of time, ranging from 1-2 weeks, to several months [173]. Out of prolonged drug delivery depot types, polymeric nanoparticles appear to be most often ones used, with many products, such as Nutropin Depot®, Arestin®, Vivitrol®, Sublocade® and Rebinyn® products already in the market [173,175]. These products mainly focus on prolonged treatment of disorders such as cancers, haemophilia, control and reduce infections, help manage alcohol or opioid dependencies, or supplement crucial hormones [90,172,173,175,176]. Currently, there are no drug loaded PLGA nanoparticles that have been approved by FDA or EMA.

### 1.5.2. Nanomedicine for treating bladder infections

Extensive studies have attempted to treat bladder diseases and infections by using nanomedicine. Implementation of nanotechnology has overcome the limitations often exhibited by traditional drugs administrated orally, intravenously, or intravesically. by increasing drug retention time in the bladder, improving drug bioavailability and uptake through biological barriers, as well as reducing drug-related toxicity [2,177]. Most of the studies that explore nanoparticle facilitated drug delivery to the bladder focus on treating bladder cancer [88,95]. Despite that, multiple studies have investigated whether UTI treatment with drug loaded nanoparticles was possible. They demonstrated successful antibiotic encapsulation in PLGA nanoparticles, which resulted in sustained drug release, effective antimicrobial activity against pathogenic bacteria, and improved drug accumulation intracellularly, thus enhancing therapeutic efficacy and reducing drug toxicity [121,154,178–181].

In the past, GEN was used as one of the main antibiotics in treating bacterial infections, however due to high risk of side effects and AMR, it had to be substituted with other antibiotics [52]. However, several studies shown that encapsulating GEN into polymeric nanoparticles or microparticles can reduce the side effects of this drug and improve its efficacy. Study by Abdelghany et al., 2012 have observed elevated antimicrobial efficacy of gentamicin loaded PLGA nanoparticles *in vivo* when it was used to treat *Pseudomonas aeruginosa* infection in mice model [121]. In addition, after 96 hours of the treatment, free GEN seized to prevent the rise of the bacterial count, while significantly lower bacterial concentrations were detected in mice treated with GEN loaded PLGA nanoparticles due to continued sustained release of the drug [121]. Similarly, the study by Imbuluzqueta et al., 2013 provided evidence that localised delivery of hydrophobic GEN loaded PLGA nanoparticles improved the efficacy of GEN compared to the free drug [178]. Additionally, the study demonstrated reduced toxicity of the GEN nanoparticle treatment, whereas free GEN treated mice exhibited pathogenicity in kidney tissue [178]. Study by Dorati et al., 2018 showed that GEN loaded PEG-PLGA nanoparticles had the same antimicrobial activity *in vitro* compared to free GEN [182]. Results demonstrated successful 100% drug release achieved within 10 hours, which did not show significant impact on the antimicrobial properties of the drug [182].

Alternatively, some studies have attempted to encapsulate antibiotics such as nitrofurantoin and trimethoprim, which are currently used as first-choice treatment from uncomplicated UTIs. Due to effective and non-toxic systemic treatment of nitrofurantoin, only a few studies have attempted to encapsulate this drug into nanoparticles [183,184]. Study by Lau et al., 2020 provides evidence how encapsulated nitrofurantoin is more effective in destroying UPEC reservoirs than a free drug [185]. PLGA nitrofurantoin loaded microparticles demonstrated reduced bacterial count for the duration of 3 days, indicating that encapsulation of nitrofurantoin does not interfere with the efficacy of the drug. In addition, results showed enhanced intracellular drug delivery from nitrofurantoin microparticles *in vitro* and *in vivo*, compared to free nitrofurantoin treatment, which lead to poor drug accumulation of therapeutic levels in bladder cells. This research also found that microparticle entrapped nitrofurantoin does not show any adverse effects, additionally, encapsulation of the drug reduces its toxicity compared to the same dose of the free drug [185]. Alternatively, trimethoprim has been successfully encapsulated into nanoparticles and microparticles by Brauner et al., 2020 [186–188]. Studies found that higher drug loading was observed in PLGA nanoparticles, with

sustained release observed for 24 hours, while microparticles showed much poorer drug loading, however it prolonged drug release up to 9 days [187]. Study by Skoll et al., 2023 demonstrated successful trimethoprim encapsulation into human serum albumin nanoparticles, which could be used to treat UTIs [189].

Apart from antibiotic drug encapsulation, other methods of UTI treatment with nanoparticles have been investigated. Study by Macedo et al., 2017 found that incorporating amino-cellulose nanoparticles into silicone of standard urinary catheters had antibiofilm effect, preventing biofilm growth and formation by *E. Coli* [190,191]. Interestingly, some antibiofilm materials, such as amino-cellulose or glycerol monolaurate, did not exhibit any antimicrobial properties as free molecules, however their encapsulation into nanoparticles improved their solubility and bioavailability, as well as provided different particle surface characteristics [190,191]. This has allowed cellular penetration and accumulation in the target tissues, as well as cationic nanoparticles improved particle adhesion to the negatively charged cell membrane of the bacteria [191,192]. Alternatively, some studies demonstrated encapsulation of natural compounds, such as cranberry and polyphenol 60, that demonstrated enhanced antimicrobial activity against *E. Coli* due to enhanced bioavailability, improved pharmacokinetics, stability and cellular uptake [191,192].

Some nanoparticles have been synthesised to specifically target bacterial cells, that not only establish contact between drug loaded nanoparticles and bacteria, but also enhance bacterial recruitment to the treatment site [192]. These can be antibody-based, aptamer-based, or electrostatic interaction-based strategies [192]. Nanoparticle surface modification by antibodies or aptamers improves direct binding of the nanoparticles and bacteria, due to antibody or aptamer recognition of bacterial cell elements [192]. These have been especially utilised to be used as vaccines for UTI prevention and treatment, discussed in more detail in **section 1.2.2.2.** Alternatively, surface medication of nanoparticles to obtain a cationic surface charge has allowed electrostatic interactions with negatively charged bacterial membrane [88,192]. Nanoparticles made or coated with chitosan are probably the most established cationic nanoparticles in the nanotechnology field, as they are biodegradable, non-toxic and demonstrate mucoadhesive properties due to their positive surface charge [193]. This is further explored in **section 1.6.1**.

Great number of potential inorganic nanocomposites have been investigated for UTI treatment, such as silver, gold, copper and iron based nanocarriers [191,192]. Since they are metal nanoparticles, they do not aim to induce alterations in metabolic pathways of pathogens, meaning that cannot trigger bacterial resistance mechanisms [194]. Silver nanoparticles have attracted the most attention, as they have been shown to promote downregulation of the expression of the genes associated with citric acid cycle and amino acid metabolism, which are involved in the cellular growth of *E. Coli* [192,194]. This means, that silver nanoparticles can enter bacterial cells and inhibit DNA synthesis, as well as release silver ions, which cause oxidative stress to the bacteria and exhibits its antimicrobial activity [195]. While multiple studies showed that bacterial infection treatment with silver nanoparticles demonstrated comparative antimicrobial activity to common antibiotic treatments, study by Lopez-Carrizales et al., 2018 showed that combining the antimicrobials with silver nanoparticles significantly enhanced the efficacy of the treatment in multi-resistant uropathogens [191,196,197]. Zinc oxide nanoparticles have also gained a lot of attention, as it exhibits cell internalisation and bactericidal effects against several uropathogenic bacterial strains [191,194,197]. Several studies have reported zinc oxide nanoparticles exhibited significant antimicrobial properties against resistant bacteria, making it an excellent candidate for UTI treatment [194,197]. However, metallic nanoparticles demonstrate some limitations too. Synthesis of metallic nanoparticles uses toxic elements, which questions the safety of the treatment, as well represent environmental problems due to hazardous waste [191]. Additionally, issues such as difficulty in scale-up production, instability and aggregation are often mentioned [191,197].

## 1.6. Intravesical drug delivery (IDD) to the bladder

Human urinary bladder is a hollow organ with a urethral access, therefore, localised treatment through injecting the drug via catheter are an attractive option for drug delivery. Intravesical drug delivery (IDD) ensures that the drug is not affected by first pass metabolism, which in turn significantly enhances therapeutic effect on desired tissue, along with significantly reducing drug degradation before reaching the target location [198]. Localised delivery of the drug also contributes to lower drug levels in the serum, therefore eliminating the risk of side effects caused by toxic drugs [199]. Intravesical drug delivery to bladder specifically ensures minimal systematic drug exposure, as urothelium is known to be the most impermeable biological barrier in human body [81,82,198]. In addition, minimised drug exposure to the whole body reduces the risk of AMR [200].

However, IDD system has its own limitations. IDD to the bladder requires catheterisation, and as discussed in **section 1.2.2.5.**, current standard catheters used for urine drainage are not approved for drug delivery purposes and their use is linked with increased risk of contracting bacterial infections [86]. It is also important to mention that catheterisation and IDD to treat uncomplicated UTI cases, that are normally successfully treated orally, is seen as unnecessary procedure by the GPs and general public [81]. However, one of the biggest limitations of the bladder is low permeability of the urothelium, which prevents drug or particle internalisation into the bladder cells [9,198]. In addition, as the main function of the bladder is to store and void urine, frequent dilution and washing out of the drug might require more frequent dosing [9]. However, over the last decade researchers have explored different options to overcome challenges associated with IDD to the bladder.

### 1.6.1. Urothelium permeability enhancement

Urothelium constantly maintains urine-to-blood electrochemical gradient by regulating passive diffusion [9]. If manipulated, this barrier can be made more permeable to allow better passage for solutes. Electromotive drug administration (EMDA) is a technique that allows aqueous drug transport into the urothelium using small electric current on bladder wall [9]. The mechanism of EMDA is based on iontophoresis, electro-osmosis and electroporation [201,202]. Iontophoresis is defined as ionised particle transportation across membrane due to the application of electrical current [201,202]. Non-ionised particles are then transported through the membrane due to electro-osmosis, that occurs based on the concentration gradient of ionised molecules [201]. Finally, electroporation increases the permeability of the membrane following the application of the electric current [201]. It has been confirmed to be an effective drug delivery system to treat low-risk bladder cancers with mitomycin C, with several trials and cohort studies demonstrating significant benefit in this type of treatment [202–204]. Side effects of the EMDA treatment were comparable with side effects observed with other bladder cancer treatments, such as passive mitomycin C or passive bacille calmette-guerin (BCG) [201,202,204]. However, EMDA is a complicated drug delivery method, as it requires a strict monitoring of voltages to ensure no damage is caused to the bladder wall [9]. At the moment, this method has not been widely embraced by urologists as larger RTCs are needed to confirm the efficacy and safety of this treatment [205]. While EMDA application in delivering

antibiotics to treat UTIs have not yet been studied, it could be a potential treatment method for patients suffering from recurring UTIs.

Chemical penetration enhancers have been reported to interact with tightly packed umbrella cell layer [9]. One of the enhancers, dimethyl sulfoxide (DMSO) is known as an organic solvent that has anti-bacterial and anti-inflammatory properties, as well as ability to penetrate tissues without inflicting damage. However, use of chemical penetration enhancers can irreversibly disrupt the barrier function of the urothelium and cause side effects, such as painful and frequent urination [177,198]. Interestingly, use of DMSO was shown to enhance chemotherapeutical drug delivery to bladder tumours [9]. In addition, 50% of DMSO has been marketed as intravesical treatment, called Rimso-50, for interstitial cystitis/painful bladder syndrome. DMSO is known to stimulate bladder afferent pathways and release of nitric oxide from afferent neurons, which desensitise the nociceptive pathways leading to symptomatic relief [206].

Other biomolecules have also demonstrated effective ways to improve permeability layer of urothelium. For example, cell-penetrating peptides (CPPs), which are short peptides that can transfer various cargoes across cell membranes [177]. These cargoes can either be attached directly to a CPP or can be encapsulated into CPP-modified nanocarriers. Study by Hsieh et al., 2011 found that a small amino acid CPP called R11 successfully passed through bladder wall and was found internalised into bladder urothelium in the mice model [207]. Authors hypothesised that attaching antibiotics to R11 could enhance the drug uptake into bladder cells and provide faster treatment of bladder infections. Several other studies demonstrated promising outcomes from CPP based treatment of bladder disorders, such as interstitial cystitis, bladder overactivity or even bladder cancer [208–211]. However, no CPP-conjugated drugs have been FDA approved, with several clinical trials also terminated [212]. Use of CPP for enhanced permeability for improved drug delivery reported limitations such as poor stability *in vivo*, increased risk of immune system response, cellular toxicity due to increased levels of internalisation of therapeutic molecules, low specificity and endosomal degradation after entering the cytosol of the cell [212].

Chitosan has been proposed as a polymer that could be used to enhance permeability of the urothelium [213]. Chitosan is a biocompatible, biodegradable and non-toxic polymer, that has bio-adhesive properties and is often used for drug absorption enhancement during IDD [214].

Chitosan is a polysaccharide composed of *N*-acetyl-D-glucosamine and D-glucosamine, linked by 1-4-β-glycosidic bonds, and is obtained through alkaline deacetylation of chitin [215,216]. Due to its positive charge, chitosan is known to interact with negatively charged epithelial surfaces, and therefore is widely used as a mucoadhesive agent, as discussed in detail in **section 1.6.2.** [213,215]. However, chitosan also enhances urothelium permeability by disrupting the tight junctions between umbrella cells [9,217,218]. It has been demonstrated by Hsu et al., 2013 that during electrostatic interactions between chitosan and integrin αVβ3, confirmational change of integrins occurs arranging integrins into clusters along the cell border (**Figure 1.9**) [219]. This, in turn, leads to F-actin rearrangement, protein CLDN4 down-regulation and increased paracellular permeability, which indicated disruption of tight junctions [219]. Electrostatic interaction between the chitosan and the cells is essential for disruption of tight junctions, as increasing pH and subsequent deprotonation of chitosan reduces paracellular permeability [219]. It is important to note, that Hsu et al., 2013 study was performed on Caco-2 cells line, that is originally derived from colon carcinoma and therefore could have cancerous properties.

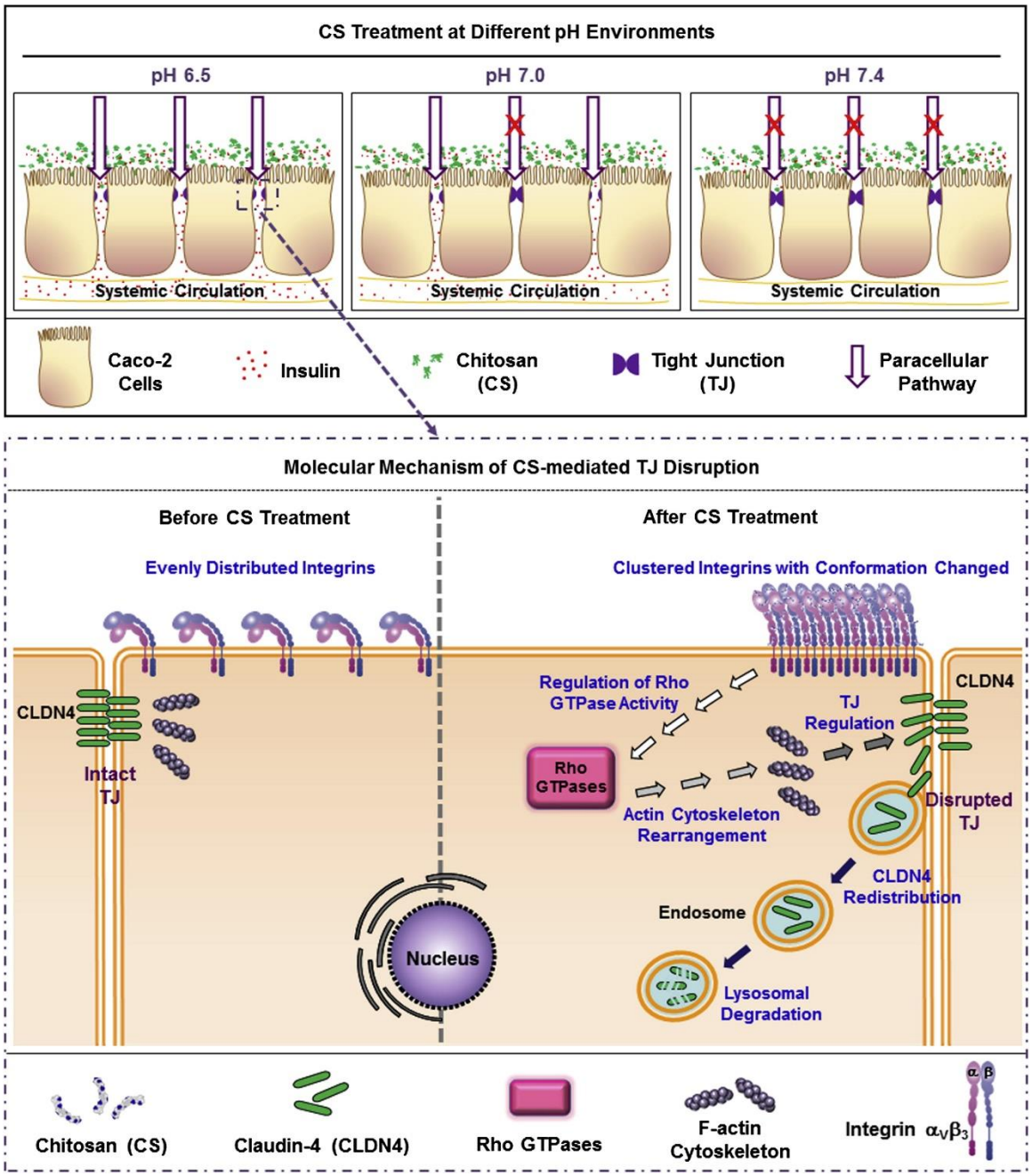


**Figure 1.9:** Schematic representation of molecular mechanisms that occur as a consequence of electrostatic interactions between positively charged chitosan and negatively charged epithelium cells and disrupt tight junction function in a pH-dependent manner. Figure reprinted with permission from Hsu et al., 2013 [219].

Studies have showed that once chitosan adheres to the apical membrane of umbrella cells, it then causes necrotic changes and desquamation of the umbrella cells [213,217]. Although the mechanism of desquamation induction is unknown, it has been observed that higher concentrations of chitosan and longer cell exposure to chitosan lead to significantly increased

permeability of the urothelium [220]. Despite this, no long-term toxic effects have been reported, with several studies demonstrating differentiation of umbrella cells almost immediately following chitosan induced cell desquamation [213,217,221]. Interestingly, chitosan has been suggested as potential treatment to combat recurring UTIs. As discussed in **section 1.1.2.**, UPEC QIRs can be found in the inner layers of urothelium and lay dormant for long periods of time before triggering resurgent growth of UPEC, causing an UTI episode. Study by Erman and Veranič, 2018 propose that by using several instillations of chitosan, combined with antibiotics, exfoliation of umbrella cells can be triggered, followed by regeneration process until UPEC QIRs are destroyed [213]. They have demonstrated success of this treatment on mice model, where four rounds of chitosan and ciprofloxacin lead to complete bacterial eradication, with no reported relapse episodes or recorded toxicity to the urothelium [221].

### 1.6.2. Mucoadhesive nanocarriers for direct to bladder delivery

Incorporating mucoadhesive materials onto drug loaded nanoparticles for IDD have gained a lot of interest, especially in drug delivery to treat bladder disorders. Mucoadhesive nanocarriers could prolong drug residence in the bladder by adhering to the bladder wall and prevent it from being flushed out by the urine [222]. It has been shown that mucoadhesive materials can interact with GAG layer components via free hydroxyl or carboxyl groups, therefore allowing prolonged attachment to the urothelium [9]. The adhesion of mucoadhesive molecules to mucin layer involves physical interaction, followed by mucoadhesive particle interpenetration into the GAG layer, then electrostatic and/or covalent bond formation between the surface and the mucoadhesive polymers [177].

Multiple studies have demonstrated mucoadhesive properties of chitosan, as due to its cationic charge it forms electrostatic interactions with negatively charged GAG layer on the bladder surface [9,223]. As stated previously, chitosan is a biocompatible, biodegradable and non-toxic polymer, that has been FDA approved for wound dressing applications, as well as determined to be safe for human dietary use [215]. Advantages of chitosan have been widely reported in mucosal area targeting studies. Reports in literature state that chitosan coated nanoparticles have enhanced drug bioavailability due to prolonged drug residency time in the target tissue [223]. Several studies have shown that higher MW of the chitosan used for polymeric nanoparticle coating demonstrated enhanced mucoadhesive properties, suggesting that longer

polymer chains achiever stronger interaction with GAG layer [88,224,225]. Additionally, concentration of chitosan used for nanoparticle coating was also shown to influence overall mucoadhesive properties, with higher concentrations of chitosan leading to stronger mucoadhesive properties [224]. Some studies have proved, that adding chitosan coating to PLGA nanoparticles have reduced initial burst effect observed during the *in vitro* drug release assay [193,226,227]. It is suggested that chitosan coating reduced the amount of drug that could be absorbed onto the nanoparticle surface, therefore reducing the concentration of loaded drug released at the beginning of the drug release assay [193]. Another important criterion for mucoadhesive properties of chitosan is pH of the surrounding media. Chemical structure of chitosan shows that this polymer possesses reactive hydroxyl and amino groups, of which the latter have a pKa value of 6.3 [228]. At pH above 6, chitosan becomes deprotonated, which leads to loss of its cationic charge and solubility [228,229]. Therefore, the chitosan coated nanoparticles demonstrate strongest mucoadhesive properties in acidic pH medias [224]. Several studies have confirmed the mucoadhesive properties of chitosan coated polymeric nanoparticles on *ex vivo* porcine or lamb bladder tissues [222,230,231].

Chitosan derivatives have gained interest as multiple studies provided evidence that derivatisation improved mucoadhesive properties of chitosan [216]. Additionally, some derivatisations showed increased permeation of hydrophilic drugs, protection of the acid sensitive drugs, enhanced drug release in basic environment, and overcome limited solubility in neutral pH [215]. Chitosan derivatives can be produced by alteration of hydroxyl or amine functional groups [215].

One of the well-known chitosan derivatives is a thiolated chitosan. Thiolated polymers are known to form disulphide bonds with cysteine domains in mucous [88,232]. Therefore, thiolated chitosan demonstrates enhanced mucoadhesive properties, achieved through disulphide bonds between thiolated polymers and mucous, as well as disulphide bonds between chitosan and cysteine-rich mucous glycoprotein domains [88]. Study by Barthelmes et al., 2013 found that chitosan-thioglycolic acid (chitosan-TGA) nanoparticles have exhibited significantly higher adhesion to the urinary bladder mucosa, compared to unmodified chitosan nanoparticles. This was shown in *in vivo* rat model, where more than 50% of the chitosan-TGA nanoparticles were present on the bladder mucosa 6 hours after the treatment, compared to only 15% of unmodified chitosan nanoparticles remaining on the bladder surface.

Chitosan derivatisation with methacrylate groups has also demonstrated to enhance mucoadhesive properties more than unmodified chitosan [88]. Methacrylate groups form covalent bonds with thiol-groups present in the cysteine-rich domains on mucosal surface [233]. Study of Kolawole et al., 2018 tested mucoadhesive properties of the methacrylated chitosan [233]. This chitosan derivative was achieved through amino groups of chitosan reacting with methacrylic anhydride. Results of the study found that highly methacrylated chitosan had superior mucoadhesive behaviour compared to unmodified chitosan. In addition, the study reported no significant different in toxicity on *in vitro* bladder tissue when treated with unmodified or methacrylated chitosan, therefore indicating that this chitosan derivative can be used safely to enhance mucoadhesive properties [88,233]. Other chitosan derivatives, such as trimethyl chitosan, carboxymethyl chitosan, glycol chitosan, have been reported to improve mucoadhesive properties [216].

Alternatively, a new approach for mucoadhesive drug delivery to the bladder has been gaining interest. A mucoadhesive in-situ forming gel has been investigated as drug delivery system for IDD to the bladder [234–238]. One of the main advantages the in-situ forming gel is the relatively easy administration, as it could be facilitated by a standard catheter and sol-gel transition should be triggered only within the bladder due to exposure to the body temperature [235]. Study by Sherif et al., 2018 demonstrated that the hydrogel would not interfere with the physiological functions of the bladder, as mucoadhesive hydrogel adhered to the bladder wall and did not block the urethral passage needed for urine voiding [239]. Alternatively, study by Lin et al., 2014 presented an in-situ gel, which after gel-sol transition in the bladder exhibited production of $CO_2$, which when attached to the surface of the hydrogel, allowed it to float on the urine [240]. Mucoadhesive properties of the nanoparticles entrapped in chitosan hydrogel were compared with free chitosan coated solid-lipid nanoparticles in study by Shawky et al., 2022 [234]. Results revealed that after 5 rounds of urine washes, nanoparticles entrapped in hydrogel demonstrated 12% to 24% better retention on the bladder wall, compared to free mucoadhesive nanoparticles [234]. In addition, nanoparticle entrapment into hydrogels demonstrated sustained release of the encapsulated drugs [234,238].

## 1.7. Thesis objectives

UTIs are one of the most common bacterial infections in the world, requiring urgent solutions and improved treatment to combat increasing infection rates, economic burden on healthcare

institutions, and rising AMR cases. Current treatment of orally administrated antibiotics continues to contribute towards AMR disaster, increasing the possibility that in the next several decades bacterial strains will show ineffectiveness to most antimicrobial agents [48]. Therefore, new therapeutical agents and drug administration routes need to be investigated to improve effectiveness of UTI treatment, reduce the risk of side effects associated with systemic antibiotic exposure, and minimise the risk of AMR.

This project aims to combine nanotechnology with IDD, creating a mucoadhesive nanoparticle system for drug delivery directly to the bladder to treat UTIs. Combined therapy of antibiotic and COX-2 inhibitor drug was proposed, with therapeutical agents encapsulated in separate nanoparticle systems tailored to enhance the loading of each drug. In addition, nanoparticle coating with mucoadhesive materials is explored to prolong particle retention time in the bladder. **Chapter 3** focuses on improving GEN therapy for treatment of UTIs, as entrapment of this antibiotic into nanoparticles and direct to bladder delivery could place this drug back on the market for UTI treatment, based on minimised associated risk of AMR and side effects. The work in this chapter studies hydrophobic ion pairing (HIP) with hydrophilic GEN to reduce hydrophilicity of the antimicrobial agent and improve its entrapment into the PLGA nanoparticles. **Chapter 4** examines the physicochemical properties and toxicity of the polymeric nanoparticles coated with different types, MWs and concentrations of mucoadhesive polymer chitosan, with mucoadhesive properties of the nanoparticles assessed on *ex vivo* porcine bladder tissue. In addition, mucoadhesive properties of water-soluble chitosan derivative, called carboxymethyl chitosan, were investigated on bladder urothelium, which has not yet been reported in the literature. Finally, the work in **Chapter 5** aimed to develop a novel therapeutical treatment of UTIs using a COX-2 inhibitor drug. Two nanoparticle preparation methods were compared to obtain desired physicochemical characteristics of the CLX loaded nanoparticle formulations. Mucoadhesive coating, which was optimised in **Chapter 4**, was then successfully applied to the CLX loaded nanoparticle formulations, presenting stable colloidal particle systems.

Thus, the aims of this study include the following:

**Discussed in Chapter 3:**

- To investigate which counterion achieves most efficient binding to GEN, as well as full dissociation from the drug once in physiologically accurate medium.

- To prepare polymeric nanoparticles loaded with high concentration of ion paired GEN complexes.
- To evaluate if GEN complexation into HIP enables *in vitro* sustained drug release from ion paired GEN (GEN:HIP) loaded polymeric nanoparticles.
- To compare antimicrobial sensitivity of ion paired GEN loaded nanoparticles with free, un-paired GEN (UNP-GEN) loaded nanoparticles and observe whether HIP enhances GEN antimicrobial properties.

**Discussed in Chapter 4:**

- To study the impact of formulation parameters, such as type, concentration and MW of chitosan, as well as concentration of surfactant, on the physicochemical characteristics, such as size, polydispersity index, and particle charge, of mucoadhesive polymeric nanoparticles.
- To investigate pH dependency of mucoadhesive properties of chitosan coated PLGA nanoparticles.
- To measure mucoadhesive properties of mucoadhesive polymeric nanoparticles *in vitro* and *ex vivo*, as well as compare the results of both assays.
- To evaluate toxicity and mucopenetrative properties of mucoadhesive polymeric nanoparticles on *ex vivo* porcine bladder tissue.

**Discussed in Chapter 5:**

- To compare two nanoparticle preparation methods (nanoprecipitation and single emulsion – solvent diffusion) by analysing how the selected parameters (polymer amount, drug amount, volume of the organic phase) affect the characteristics of CLX loaded PLGA nanoparticles.
- To utilise DoE technique to achieve colloidally stable CLX loaded PLGA nanoparticle system, with small particle size and polydispersity index, but high drug entrapment and drug loading.
- To apply mucoadhesive coating on the optimised CLX loaded PLGA nanoparticles and examine how it affects nanoparticle physicochemical and biological parameters.

# Chapter 2

## Materials and methods

## 2.1. Introduction

This chapter provides insights into the materials, methodologies and characterisation techniques used throughout the project. During the project, polymeric nanoparticles were developed using poly(lactic-co-glycolic acid) (PLGA) polymer, with additional use of chitosan to coat the nanoparticle surface. In order to achieve this, conventional nanoparticle preparation techniques were used: emulsification – solvent evaporation and nanoprecipitation (NPPT). The preparation of polymeric nanoparticles also included the use of excipients poloxamer 407 (P407) and poly(vinyl alcohol) (PVA). Obtained PLGA nanoparticles were loaded with either hydrophilic antibiotic Gentamicin (GEN), or hydrophobic non-steroidal anti-inflammatory drug (NSAID) Celecoxib (CLX). Polymeric nanoparticles obtained for fluorescent analysis were loaded with hydrophobic fluorescent dye Coumarin-6 (C6). For particular experiments and studies blank polymeric nanoparticles were examined.

Several analytical chemistry techniques were used to examine the physicochemical properties of the crude materials and formulated nanoparticles. These techniques included dynamic light scattering (DLS), attenuated total reflectance – Fourier transform infrared spectroscopy (ATR-FTIR), transmission electron microscopy (TEM), and powder X-Ray diffraction (PXRD), and *in vitro* drug release. The drug quantification for encapsulation efficiency calculations was performed by high-performance liquid chromatography (HPLC), while fluorescence of the fluorescent dye C6 was measured using spectrofluorometer. Additionally, histology studies were conducted on *ex vivo* porcine bladder tissue.

This chapter describes general techniques and main materials used for this project. However, some specific protocols that were used in the certain sections of this study are detailed in the **"Materials and methods"** sections of the relevant results chapters.

## 2.2. Materials

### 2.2.1. Poly(lactic-co-glycolic acid)

Poly(lactic-co-glycolic acid) (PLGA) is a copolymer, formed by copolymerisation of lactic and glycolic acid monomers via ester linkages (**Figure 2.1**). The molecular weight (MW) and composition of the polymer depends on the ratio of lactic and glycolic acid, which also determines the degradation rate of the polymer [241]. PLGA is an amorphous polymer, which is often used as nanocarrier due to good biocompatibility and biodegradability. Additionally,

this polymer is soluble in wide variety of solvents, water miscible and immiscible, and therefore can be processed into any shape and size, making it a versatile tool for encapsulation of variety of biomolecules. Since it was developed, PLGA has been used to encapsulate wide variety of molecules, including drugs, proteins, chemotherapeutics, hormones and genes [242]. For this study, amorphous PLGA with 50:50 lactic to glycolic acid ratio was chosen. The MW of this polymer was 38,000 – 54,000 Da, with reported glass transition ($T_g$) temperature of 46 – 50 °C, and a terminal ester group.

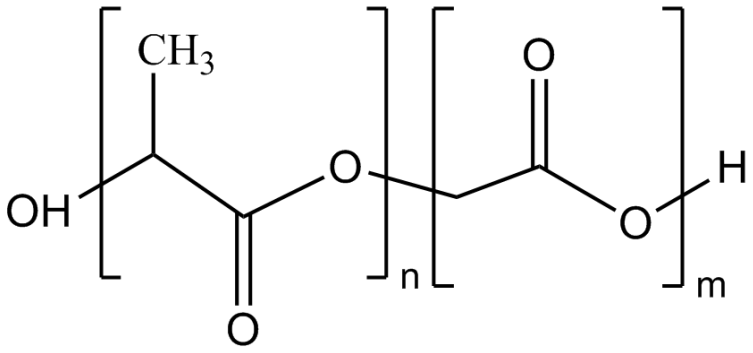


**Figure 2.1:** Chemical structure of Poly(lactic-co-glycolic acid) (PLGA).

### 2.2.2. Chitosan

Chitosan is a biodegradable polysaccharide, that was derived from chitin via deacetylation [243]. It is generally accepted that over 70% deacetylation of chitin results in chitosan, with MW of the polymer also depending on the deacetylation percentage [244]. Higher deacetylation increases MW of the chitosan, leading to improved stability, but it also reduces its solubility in most solvents. Chitosan is water-insoluble, however it is soluble in aqueous acidic media below its pKa (pH = 6.5) [244]. To improve solubility of chitosan in water and other solvents, several chitosan derivatives have been established by chemical modification of the reactive functional groups, such as hydroxy and amine groups [245].

In this study, different MWs of chitosan are selected: low MW (50-190 kDa, 75-85% deacetylated chitin), medium MW (190–310 kDa, 75-85% deacetylated chitin), high MW (310-375 kDa, >75% deacetylated chitin) (**Figure 2.2**). The form of the chitosan changes from off-white powder of low MW to increasing amount of coarse ground flakes within the powder of higher MW. Additionally, chitosan derivative carboxymethyl chitosan (≥80% deacetylated chitin) is also used in this study (**Figure 2.2**). It appears as off-white fine powder and demonstrates improved solubility in water, where no acid is needed for full solubilisation.

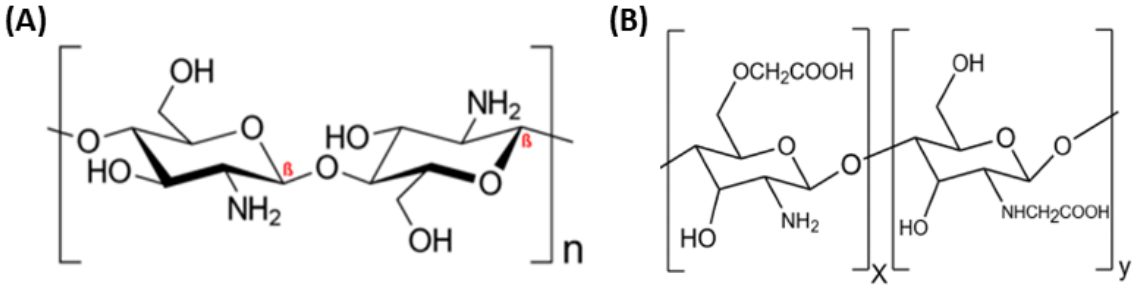


**Figure 2.2:** Chemical structure of (A) chitosan and (B) carboxymethyl chitosan.

### 2.2.3. Poloxamer 407

Poloxamers, also sometimes referred to as Pluronics, are block copolymers, that are comprised of hydrophilic ethylene oxide (EO) and hydrophobic propylene oxide (PO) blocks arranged in a triblock structure of $EO_x$-$PO_y$-$EO_x$ (**Figure 2.3**) [138,168]. Poloxamers are widely used in pharmaceutical formulations, often added to the nanoparticle formulations as surfactant or solubilising agent. They coat the particle surface through hydrophobic interactions between the polymer and hydrophobic PO moieties, with hydrophilic EO block extending into the aqueous media [138]. For this study Kolliphor® P 407 (P407) was selected, with reported 95 to 105 EO units and 54 to 60 PO units, totalling a MW of 10,000 to 14,600 g/mol. Poloxamer was of off-white colour, formed of coarse-grained powders with a waxy consistency. It demonstrated a great solubility in some solvents, including acetonitrile and dichloromethane, and water, with reported critical micelle concentration (CMC) at 34.2 mg/L (at 37 °C).

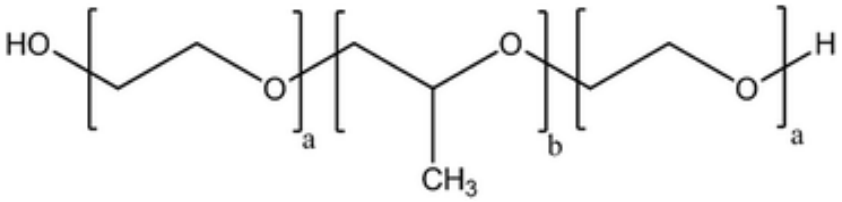


**Figure 2.3:** General structure of poloxamers. Figure reprinted with permission from Guan et al., 2016 [246].

### 2.2.5. Gentamicin

Gentamicin (GEN) is an antibiotic drug that belongs to the group of aminoglycosides, which are known to be an effective therapy for treating urinary tract infections (UTIs). It is mostly used to treat Gram-negative bacteria, with limited effectiveness reported on Gram-positive bacteria. Aminoglycosides are considered to be one of the critically important antibiotics due

to its retained effectiveness against bacteria with multidrug resistance [247]. GEN is known to cause nephrotoxicity in 10% to 20% of patients, as well as ototoxicity [247,248], therefore in the recent years the focus was aimed at developing a safe and non-toxic way of delivering the drug to the site of the infection. The structure of GEN is made up of 4 major congeners, which are C1, C1a, C2 and C2a, and 1 minor congener C2b (**Figure 2.4**) [247]. These five components mainly differ at the methylation sites and methylation of these components can influence antimicrobial activity of the antibiotic drug [249]. GEN belongs to the Biopharmaceutics Classification System (BCS) class III, due to high solubility but poor permeability. Its hydrophilicity and small MW make the encapsulation of the drug into polymeric nanoparticles very challenging. For this study, GEN with the composition of 33.4% of C1, 19.8% of C1a, and 46.8% of C2 + C2a + C2b was used. It demonstrated white hydroscopic powder and reported pH of the drug was 4.7. Melting point temperature ($T_m$) was reported to be 218 to 237 °C, LogP of -3.1 and pKa of 12.55. Gentamicin is freely soluble in water and aqueous buffers, and practically insoluble in ethanol and in ether.

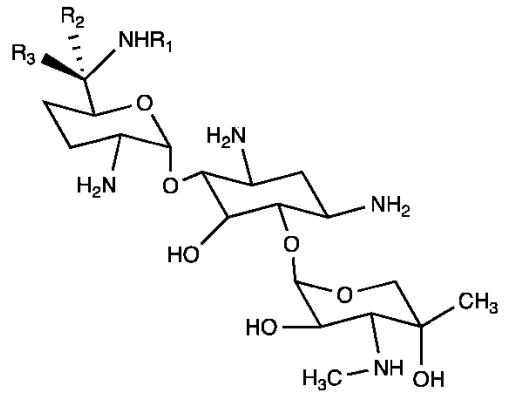


| | Gentamicin C1 | C1a | C2 | C2a | C2b |
|---|---|---|---|---|---|
| R1 | $CH_3$ | H | H | H | $CH_3$ |
| R2 | H | H | H | $CH_3$ | H |
| R3 | $CH_3$ | H | $CH_3$ | H | H |

**Figure 2.4:** Chemical structure of gentamicin, where five congeners (C1, C1a, C2, C2a, C2b) can be seen. Composition of gentamicin differs at each R site, as depicted in the image. Figure reprinted with permission from Wei et al., 2019 [249].

## 2.2.6. Celecoxib

Celecoxib (CLX) belongs to the group of non-steroidal anti-inflammatory drugs (NSAIDs), often used to treat pain and inflammation. In addition, CLX was evaluated as potential anti-

cancer treatment and has been labelled as chemopreventative agent by Food and Drug Administration (FDA) of the United States of America [250]. CLX is a selective cyclooxygenase-2 (COX-2) inhibitor drug, reportedly 10 to 20 times more selective for COX-2 than COX-1. It is BSC type II drug, as it is mostly insoluble in water but have strong permeability properties (**Figure 2.5**). CLX has demonstrated some cardiovascular toxicity when used in high dosages, however it reports significantly lower cases of gastrointestinal or renal adverse effects compared to other non-selective COX-1 and COX-2 inhibitor NSAIDs [250]. CLX used for this study was a powder to crystalline powder, that demonstrated white to off-white colour. Reported $T_m$ of CLX was at 164 °C, with LogP of 3.53, and pKa of 11.1. CLX is practically insoluble in water, but freely soluble in methanol, ethanol, dimethyl sulfoxide and other organic solvents.

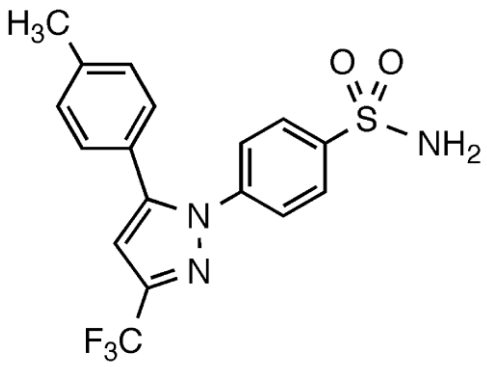


**Figure 2.5:** Chemical structure of Celecoxib. Figure reprinted with permission from Yamakawa et al., 2014 [251].

## 2.2.7. Coumarin-6

Coumarin-6 (C6) is a derivative of coumarin, where a benzothiazolyl group is added to the position 3. Due to its fluorescence in the green-blue spectrum, it is often used as fluorescent dye in visualisation of nanocarriers in biological applications. C6 demonstrates excitation peak at 450 nm and emission peak at 501 nm. Its structure is presented in **Figure 2.6**. Coumarin-6 comes as an orange to dark orange crystalline powder, with variable solubility in solvents and poor solubility in water.

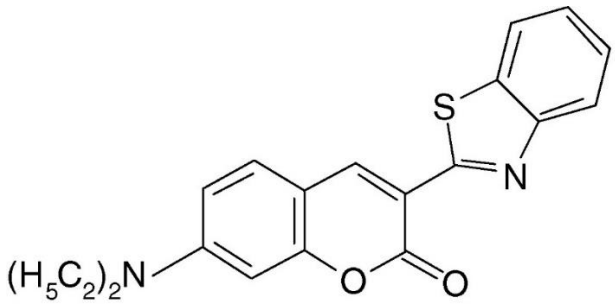


**Figure 2.6:** Chemical structure of Coumarin-6. Figure reprinted with permission from Raikar et al., 2006 [252].

## 2.3. Methods

### 2.3.1. Nanoparticle preparation methods

Several nanoparticle preparation methods have been developed for polymeric nanoparticle synthesis. This study focuses on the use of conventional methods, which are used most often in polymeric nanoparticle preparation [115]. In addition, nanoparticle preparation methods were selected for each formulation based on the properties of the drug that is to be loaded into the nanoparticles [115].

#### 2.3.1.1. Nanoprecipitation

Nanoprecipitation (NPPT) method, also sometimes referred to as solvent displacement, involves the use of two miscible solvents [115]. Once organic solvent phase is added to the aqueous phase during a constant stirring, the nanoparticles are formed instantly [253]. During NPPT method, polymer, hydrophobic drug and surfactant were all dissolved in acetonitrile (ACNT) and added dropwise into aqueous phase comprised of MilliQ water (MQW), as shown in **Figure 2.7** [254]. For mucoadhesive formulations, chitosan was dissolved in the aqueous phase. Detailed formulation compositions are reported in **Chapter 4** and **Chapter 5**. Evaporation of organic solvent was facilitated by Rotavapor R-210 system (Buchi UK Ltd, UK), equipped with B-491 heating bath set at 55 °C and V-700 vacuum pump. Samples were then stirred at 250 RPM for at least 1 hour to remove residual organic solvent.

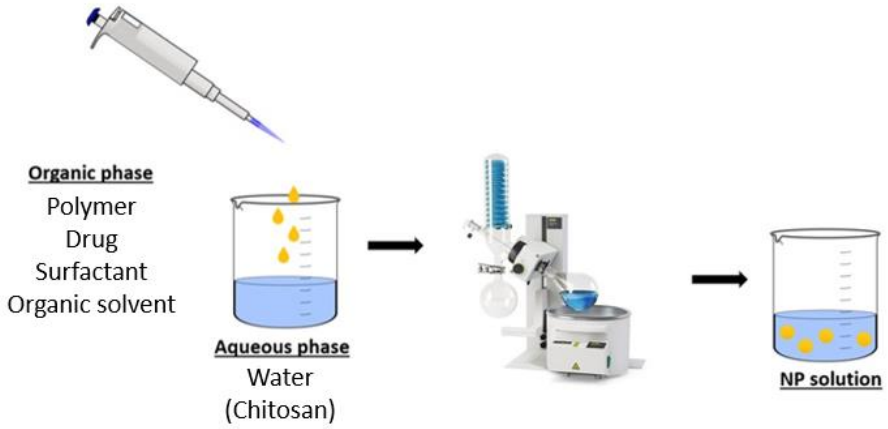


**Figure 2.7:** Schematic representation of the hydrophobic drug loaded polymeric nanoparticle preparation by nanoprecipitation method.

### 2.3.1.2. Emulsification – solvent evaporation

Oil-in-water (O/W) is often used for encapsulation of hydrophobic or poorly soluble agents. Encapsulation of hydrophilic molecules using the same method have demonstrated poor loading into the particles due to their diffusion into the aqueous phase, as well as lack of solubility in the organic phase [102]. Therefore, multiple emulsions, such as water-in-oil-in-water ($W_1/O/W_2$), are often used to encapsulate water-soluble agents, as they are trapped in the inner aqueous phase and are surrounded by hydrophobic polymer phase, preventing the diffusion of hydrophilic molecules [102].

In this study, polymeric nanoparticles, encapsulating hydrophobic drugs, were prepared using water-in-oil (W/O) single emulsification – solvent evaporation method (SE) [255]. Organic phase (O) was comprised of polymer and the drug dissolved in dichloromethane (DCM), while aqueous phase (W) was comprised of surfactant dissolved in MQW. For mucoadhesive formulations, chitosan was dissolved in the aqueous phase along with surfactant. Detailed formulation composition is reported in **Chapter 5**. The organic phase (O) was added dropwise to the aqueous phase (W), then emulsified using probe sonicator (Fisherbrand$^{TM}$ 505 sonicator, UK) at 20% amplitude for 3 min in a 20:5 second on-off cycle (**Figure 2.8**). The formulations were then left stirring at 250 RPM overnight at room temperature, to ensure complete evaporation of organic solvent.

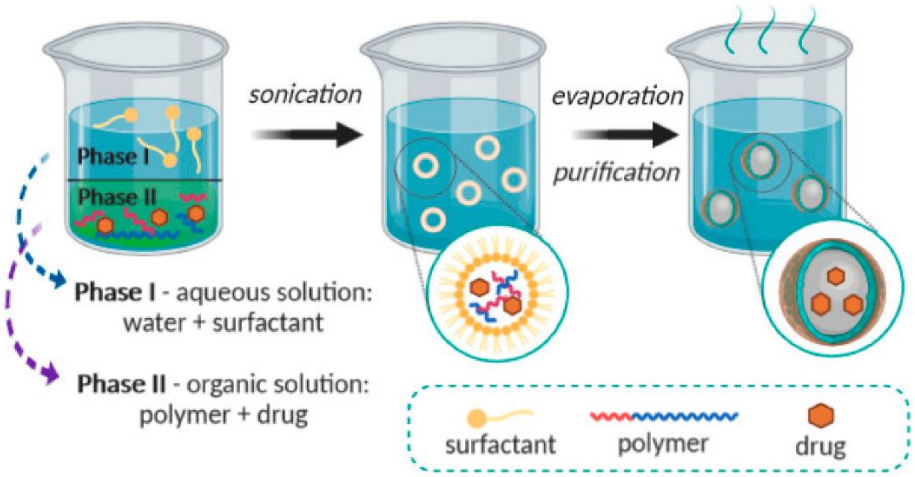


**Figure 2.8:** Schematic representation of the hydrophobic drug loaded polymeric nanoparticle preparation by single emulsion – solvent evaporation method. Figure reprinted with permission from Zielińska et al., 2020 [115].

For encapsulation of hydrophilic drugs, polymeric nanoparticles were prepared using water-in-oil-in-water ($W_1/O/W_2$) double emulsification – solvent evaporation method [121]. The first emulsion ($W_1/O$) was prepared by adding the drug dissolved in MQW ($W_1$) to the organic phase comprised of polymer dissolved in DCM (O), then using the probe sonicator (Fisherbrand™ 505 sonicator, UK) at 20% amplitude for 3 min in a 20:5 second on-off cycle to yield dispersion of nanodroplets (**Figure 2.9**). This emulsion was then added dropwise to the second aqueous phase ($W_2$), which was comprised of surfactant dissolved in MQW, followed by probe sonication and evaporation process as described above. Detailed formulation composition is reported in **Chapter 3**.

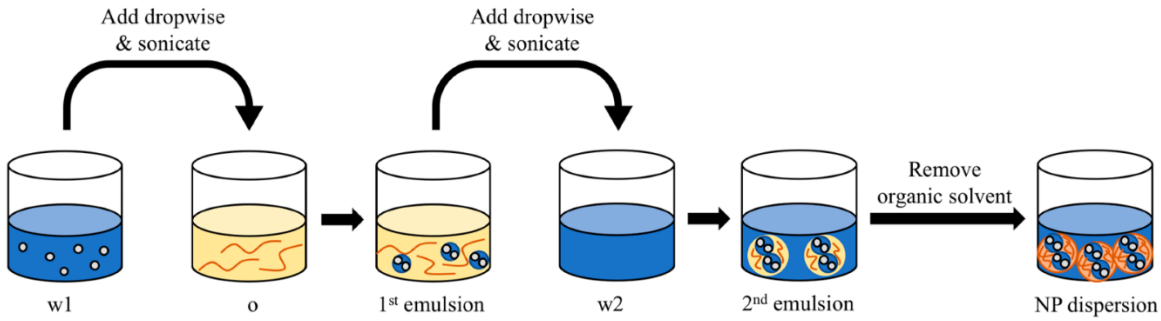


**Figure 2.9:** Schematic representation of the hydrophilic drug loaded polymeric nanoparticle preparation by double emulsion – solvent evaporation method. In the image, (w1) contains the hydrophilic drug, (o) contains polymer, (w2) contains surfactant. Figure reprinted with permission from Kim et al., 2019 [256].

## 2.3.2. General physicochemical characterisation methods

### 2.3.2.1. Dynamic light scattering (DLS)

Dynamic light scattering (DLS) is used to determine the nanoparticle size and aggregation state in a colloidal solution [257]. DLS measures the hydrodynamic size of the particles by mechanism of scattered light that passes through the colloidal solution, analysing the modulation of intensity of scattered light as function of time [258]. Hence, when light encounters the particles, it scatters in all directions and the intensity is recorded by a detector.

A hydrodynamic diameter of the particle can be measured based on the Brownian motion of the particles. Brownian motion is defined as a random movement of the particles suspended in fluids and achieved due to particle collision with fast-moving particles of the solvent [259]. The speed of Brownian motion is influenced by sample viscosity and temperature, therefore as long as those parameters are known and the temperature is kept constant, the hydrodynamic size of the particles can be measured based on the Brownian motion [257,259]. Additionally, particle size can also influence Brownian motion, where smaller sized particles lead to faster Brownian motion, while larger sized particles decrease the speed of Brownian motion [259]. The hydrodynamic diameter ($d_H$) is calculated by converting the velocity of Brownian motion, which is defined by the translational diffusion coefficient (D), into particle size using the Stokes – Einstein equation (**Eq. 2.1**):

$$d_H = \frac{kT}{3\pi\eta D} \qquad \textbf{Eq. (2.1)}$$

Where $d_H$ is the hydrodynamic diameter of the particles, k is Boltzmann's constant, T is the absolute temperature, η is the viscosity of the dispersion media, and D stands for diffusion coefficient [259]. It is important to note that hydrodynamic diameter of the particles will depend on the particle core, as well as any surface structure or the concentration of any ions in the media (**Figure 2.10**) [259].

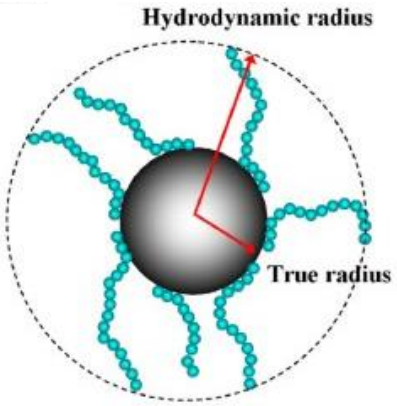


**Figure 2.10:** Schematic demonstration of hydrodynamic diameter versus the true nanoparticle diameter measurement obtained by DLS. Figure reprinted with permission from Lim et al., 2013 [260].

DLS uses single - frequency laser to scatter the light at the angles of 90° and 173°, with detector positioned at the back angle of 173° and right angle 90° to incident light [258]. Scattered light is detected over a period of time, during which its intensity will fluctuate due to the particle movement. Smaller sized particles move faster and therefore fluctuation is much faster than in larger particles [261]. However, larger sized particles demonstrate larger amplitude between the minimum and maximum intensities, as shown in the two top panels of **Figure 2.11**. These fluctuations are then used to generate a correlation function, which describes the time that particle spent at the same location within the sample [261]. As demonstrated in the bottom two panels of the **Figure 2.11**, at the beginning of the correlation function is linear and constant, therefore suggesting that the particle is at the same position within the sample. Later, an exponential decay observed in the correlation function indicates of the particle movement. Shorter decay indicates quicker movement of the particles, which is attributed to their small size, while longer decay indicates longer movement time, therefore suggesting larger particle size. Therefore, size-dependent movement is included in the decay of correlation function [261].

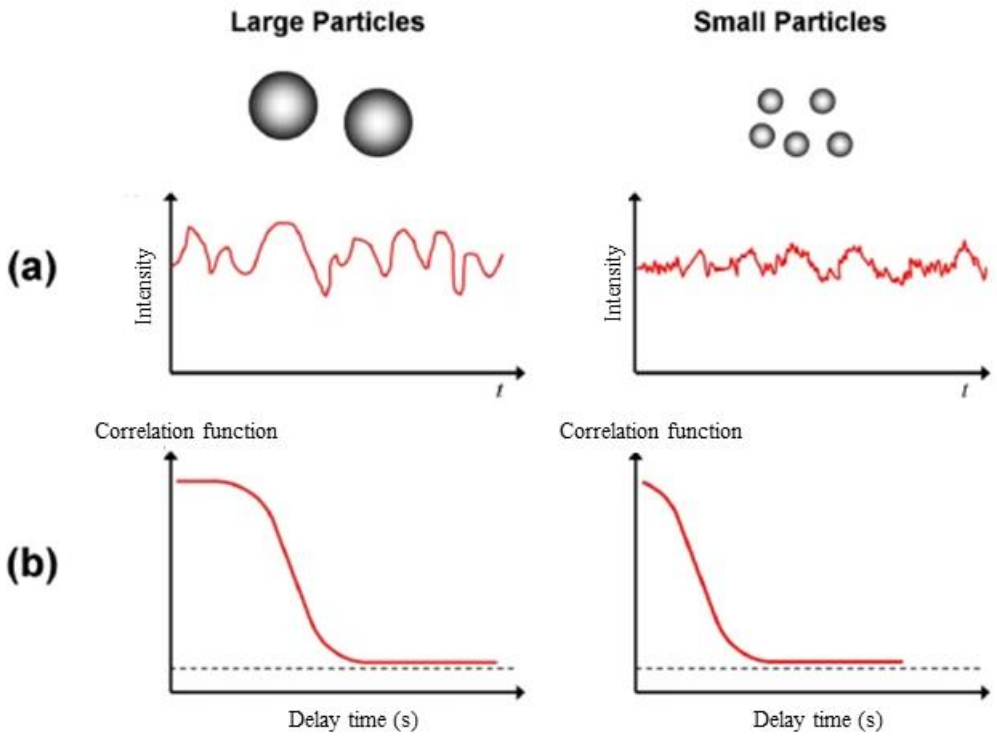


**Figure 2.11:** Schematic representation of (A) intensity measurement and (B) the corresponding correlation function in DLS based on the particle size. Figure reprinted with permission from Lim et al., 2013 [260].

Particle size measurements by DLS are usually expressed as Z-average, which are based on intensity, due to fluctuations of intensity that are detected over time [261]. However, it can also be expressed as volume or number based distributions. All three distributions represent the same physical reality of a distribution of differently sized particles. However, intensity distribution is very sensitive to the presence of aggregates compared to other two distributions, which in turn usually leads to reports of larger sized readings [261].

The polydispersity index (PDI) is another important parameter that can describe the width of the particle size distribution [258]. PDI measurements values vary from 0.1 to 1, where colloidal particles with PDI less than 0.1 show monodispersed particle size distribution, while PDI higher than 0.1 demonstrates some degree of polydispersity, which increases as PDI values gets closer to 1. PDI is calculated by equation (**Eq. 2.2**) presented below:

$$PDI = (\frac{\sigma}{d})^2 \qquad \textbf{Eq. (2.2)}$$

Here, PDI equals the square of standard deviation of particle size distribution (σ) divided by the mean of particle diameter (d) [258].

For this study, DLS (Zetasizer Nano, Malvern Instruments Ltd., Malvern, UK) was used to measure the mean particle size and PDI. The dispersant (medium) was set to water with viscosity (cP) of 0.8872 with an equilibrium temperature of 25 °C. All measurements were done in triplicate and expressed as mean ± standard deviation (SD).

### 2.3.2.2. Zeta potential

Zeta potential is electrostatic potential at the electrical double layer that surrounds the nanoparticles in aqueous solution [262]. The electrical double layer is comprised of layer of ions often referred to as Stern layer, where ions are bound to the nanoparticle surface and present opposite charge to the particle itself, and a second layer situated upon the Stern layer, composed of loosely associated counterions [262]. During the movement of the nanoparticles in the aqueous solution, the double layer moves with it, forming a hydrodynamic parameter of the particle [262]. The edge of this layer is called slipping plane, also called plane of shear, and the electrical potential measured at this point is called zeta potential [263]. This measurement is frequently used to determine relative surface charge of the particles, along with determining the stability of the nanoparticle suspension by measuring the electrostatic repulsion between similarly charged particles in the suspension. If the determined zeta potential is high (negative or positive), the particles of the same charge repel each other in the suspension, however if zeta potential is low (close to zero), the attractive forces might exceed repulsion forces, leading to aggregation and flocculation of the particles and poor colloidal stability [263].

Zeta potential is measured by electrophoresis light scattering, also referred to as Doppler microelectrophoresis [263]. This process can be defined as the movement of a charged particle relative to the fluid it is suspended in under the influence of an applied electric field [259]. The velocity at which the charged particles move is used to calculate the zeta potential of the nanoparticles [259,263]. Zeta potential is typically measured in millivolts (mV). For this study, measurement of zeta potential was determined using Zetasizer Nano (Malvern Instruments, Malvern, UK), samples for analysis were prepared by 1:1 dilution with 1 mM sodium chloride (NaCl). All measurements were done in triplicate and expressed as mean ± SD.

### 2.3.2.3. Attenuated total reflectance – Fourier transform infrared (ATR-FTIR) spectroscopy

FTIR spectroscopy is a label-free, non-destructive analytical technique used to characterise chemical and structural information of selected materials [264]. This technique is often used to identify denaturation or aggregation of biopharmaceutical agents, study composition changes in the material, predict and identify metabolites, as well as quantify their concentrations [264]. Infrared spectroscopy obeys to the Beer-Lambert's law and therefore can be used for quantitative purposes [265]. FTIR spectroscopy studies the interaction of the infrared light with the matter, during which molecular vibrations of the substance leads to absorption of electromagnetic radiation at different wavenumbers [266]. Most molecules present infrared bands in the mid-infrared region (4000 – 400 $cm^{-1}$), demonstrating vibrational bands that relate to the intensity and position of the underlying molecular motion of atoms participating in a chemical bond [265].

FTIR spectroscopy can be used in transmittance or attenuated total reflectance (ATR) mode. As transmittance FTIR spectroscopy requires sample preparation for the light to traverse the sample, ATR-FTIR spectroscopy is considered to be a superior technique with no sample preparation required. ATR-FTIR spectroscopy involves directing the infrared light at an interface between an infrared transparent material with a high reflective index called internal reflection element (IRE) and a sample on the surface of IRE [266,267]. The infrared beam is directed through the IRE, often referred to as ATR crystal, by a set of mirrors, where it is internally reflected at least once before reaching the FTIR detector by the use of mirrors, as demonstrated in **Figure 2.12**.

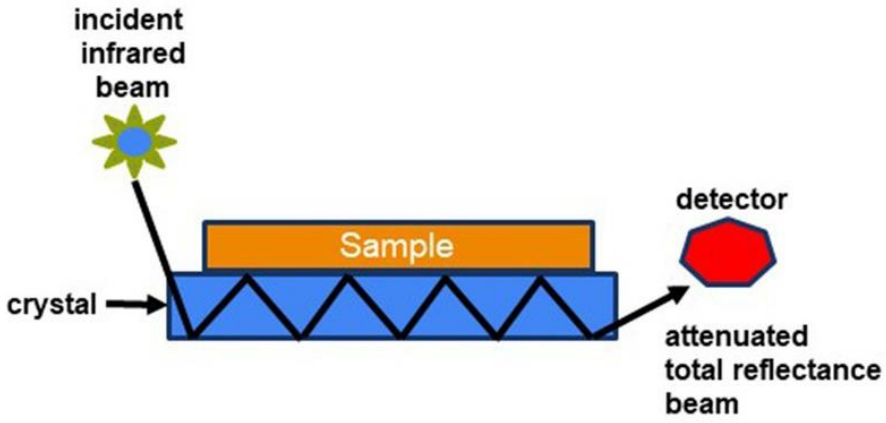


**Figure 2.12:** General working principle of ATR-FTIR spectroscopy. Figure reprinted with permission from Tiquia-Arashiro et al., 2023 [268].

FTIR analysis for this study was performed using FTIR spectrophotometer (Vertex 70, Bruker Optics Limited, United Kingdom) connected with an internal reflection diamond ATR accessory (Specac Ltd., Orpington, United Kingdom). Nanoparticle samples were freeze dried and placed directly onto the diamond disk. The spectra were acquired from 128 scans in the range of 500 – 4000 $cm^{-1}$ at a resolution of 4 $cm^{-1}$. All measurements were carried out in triplicate, and data was analysed using OPUS software.

### 2.3.2.3. Powder X-Ray diffraction (PXRD)

Powder X-Ray diffraction (PXRD) is a non-destructive analytical technique to study the crystallinity of the selected materials. This technique is useful when studying how crystalline structure of active pharmaceutical ingredients (APIs) can affect its physicochemical properties, as well as investigating polymorphs [269]. PXRD is based on constructive interference of monochromatic X-rays, which are generated by the cathode ray tube and filtered to produce monochromatic radiation, paralleled to concentrate and then directed at the sample (**Figure 2.13**) [270]. As a beam of X-ray is passed through the specimen and is scattered or diffracted, the atoms that are in the path of the X-ray are investigated [258]. The crystalline characteristics and structure of the material is determined by observing the interference of scattering X-rays, which with the sample produces constructive interference (and a diffractive ray) when conditions satisfy Bragg's Law (**Eq. 2.3**) [258,270]. In order to attain all possible diffraction directions of the lattice, the sample is scanned through a range of 2θ angles due to random orientations of the powdered material [270].

$$n\lambda = 2d \sin\theta \qquad \textbf{Eq. (2.3)}$$

Where $n$ is a positive integer, λ is the wavelength of the X-rays, $d$ is the distance between the lattice planes in crystal, and θ is the diffraction angle [270]. The Bragg's Law relates to the angular position of the X-rays to the lattice spacing and forms the basis of all X-ray diffraction measurements (**Figure 2.13B**) [270,271].

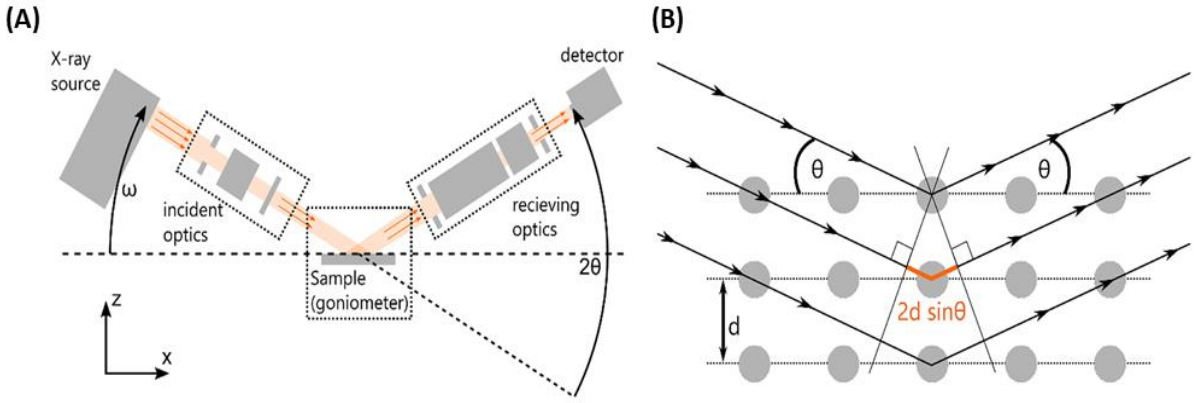


**Figure 2.13:** Schematic representation of (A) a diffractometer and a working principle of PXRD, (B) the Bragg's Law. Figures reprinted with permission from Harrington et al., 2021 [271].

For this project, Rigaku Miniflex 600 Powder X-ray diffraction system (SmartLab SE/PC, Japan) with Cu-sealed tube – $K^{\alpha}$ X-rays at 0.15419 nm, with voltage of 40 kV and current of 15 mA was used to investigate the crystallinity of crude materials and nanoparticle solutions. The range of scanned 2θ was from 3 ° to 60 ° at scanning speed of 4 ° per minute and step of 0.02 °.

### 2.3.2.4. Transmission electron microscopy (TEM)

Transmission electron microscopy (TEM) is the most commonly used microscopy technique to characterise physicochemical properties of the nanoparticles. Additionally, due to very high resolution, this technique can be used to investigate relationships between nanoparticulates and cell or tissue components [272]. The images of the nanoparticles are obtained by a beam of electrons transmitted through a thin specimen, when the beam of electrons is transformed into elastically and inelastically scattered electrons upon electron beam interaction with the

specimen [257]. TEM can achieve a sub-nanometre resolution, which corresponds to 0.2 nm in conventional TEM, due to the very short wavelength of the electron beam [272]. TEM is considered to be more advantageous compared to scanning electron microscopy (SEM), due to precise particle characteristics provided in both brightfield and darkfield images, as well as detailed information on particle morphologic, compositional, and crystallographic properties [257].

In this study, the TEM mode of a Gemini 300 series scanning transmission electron microscope (Zeiss, Germany) was used to analyse the morphology and characteristics of obtained polymeric nanoparticles. Samples were prepared by pipetting 10 µl of nanoparticle solution onto the 400-mesh grid (Agar scientific, UK), letting the solution soak into the grid for 5 minutes and then wiping off the excess with filter paper. The grid was then stained with phosphotungstic acid (2%, pH = 6.8) to contrast the sample.

### 2.3.3. *In vitro* drug release studies

Drug release studies are used to identify the accurate quantification of drug release kinetics *in vitro*. This data provides important information on how encapsulation of the APIs might alter the rate of drug release, which can be of crucial importance when assessing the safety, efficacy and quality of the obtained formulations [273]. *In vitro* drug release profiles can be obtained by three methods: sample and separate, continuous flow, and dialysis membrane techniques, of which the latter is used most often [273,274]. Dialysis membrane technique uses a semi-permeable membrane, that separates the nanoparticle solution and released drug. The set-up involves use of the dialysis bag, which is then placed into reservoir of known volume, meaning that over time the drug will diffuse from the dialysis bag and will travel into the reservoir (**Figure 2.14**) [274]. This technique does have some limitations, that can influence the drug release profiles of nanoparticle formulations. Due to two diffusion barriers, the diffusion of the drug might be affected and the drug concentration in the receiver compartment might not timely reflect the actual concentration of the free drug released from the nanoparticle formulation [273,274].

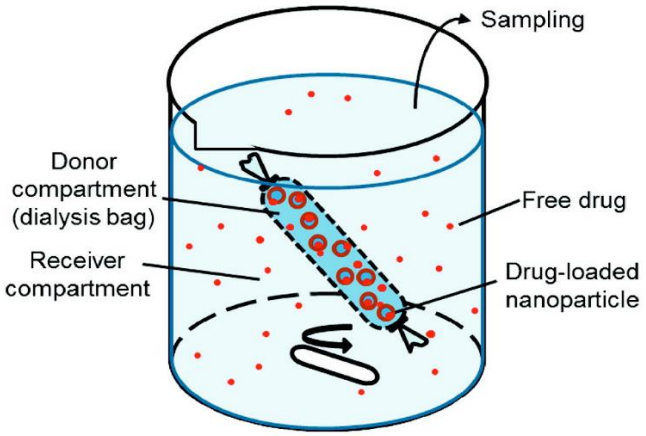


**Figure 2.14:** Schematic representation of *in vitro* drug release assay with dialysis membrane. Figure reprinted with permission from Zhou et al., 2016 [275].

*In vitro* drug release studies for this project used a dialysis bag (Thermo Scientific™ SnakeSkin™ Dialysis Tubing, 10K MW cut-off, regenerated cellulose, Fisher Scientific, UK), which was then submerged into the release media, which consisted of phosphate buffered saline (PBS), with additional surfactant or salt as required for specific experiments (detailed in **Chapter 3** and **Chapter 5**). Samples were incubated in shaking incubator (KS3000 i control IKA®, UK) at 37 °C degrees, with rotary speed of 100 RPM, with sink conditions maintained throughout the assay. At predetermined time intervals, a 1 ml sample from the total volume of 20 ml of the release media was collected and replaced with equal volume of the fresh release medium. Study was performed in triplicate to generate an average drug release profile of drug concentration versus time.

## 2.3.5. Histology

Histology is a branch of biology that studies the microscopic anatomy of the biological tissues. Histology is often used in observing structural changes in the diseased tissues to obtain insight on potential treatment options, as well as in diagnostics, forensic investigations, autopsy and education [276]. Preparation of the tissue involves fixation, embedding, sectioning and staining. Fixation is used to preserve the natural tissue and cell structure, as well as harden the tissue for the sectioning and delay tissue degradation [276]. Afterwards follow the dehydration of the tissue, which facilitates tissue hardening, and embedding the tissues into paraffin wax. Finally, tissue staining is performed for general assessment of the cell and tissue morphology [277]. Haematoxylin and eosin staining (H&E) is one of the principal tissue stains in histology. Firstly, the samples are stained with haematoxylin, which stains nuclear components of the cell

giving them a blue/purple hue, following a staining with eosin, which stains cytoplasmic components of the cells by giving them pink/red hue [276].

In this study, freshly excised porcine bladders were used for histology studies. Preparation of porcine bladder tissue and tissue treatment followed protocol adapted from Khutoryanskiy group [230,237,278]. Bladders were obtained from a local abattoir, transported to the laboratory on ice and used within the same day. After removing urethra, bladders were cut into quarters, each piece rinsed with PBS (pH 7.4) buffer and then left to dry off residual buffer for 10 min in 37 °C. Afterwards, 400 µl of nanoparticle formulation was carefully pipetted onto the centre of the tissue, ensuring that the whole solution stays on the tissue throughout the incubation period. Tissues were left to incubate in petri dishes for 1 hour at 37 °C in dark conditions. Afterwards, samples were dissected into smaller pieces to fit embedding cassettes and fixed in 10% neutral buffered formalin overnight at 4 °C degrees. The following day samples went through dehydration process, starting with samples immersed in PBS, to which gradually increasing concentrations of EtOH were introduced until a pure water-free EtOH is reached, as shown in **Table 2.1**. Afterwards, samples were immersed in Histo-clear for 1 hour and 30 minutes, then leaving samples in paraffin wax overnight. Next day samples were embedded in disposable moulds (15mm x 15mm x 5mm) and stored at 4 °C degrees until sectioning.

**Table 2.1:** Protocol of tissue dehydration process in buffers with gradually increasing concentrations of EtOH.

| **Time** | **Buffer** |
|---|---|
| 1 h 30 min | PBS 7.4 |
| 45 min | 50% EtOH |
| 45 min | 70% EtOH |
| 45 min | 95% EtOH |
| 1 h 30 min | 100% EtOH |
| 1 h 30 min | Histo-Clear |
| Overnight | Paraffin wax |

Eight-micrometre-thick cross-sections were cut using Rotary Microtome HM 355S (Fisher Scientific, UK). Sections were deparaffinized and hydrated through decreasing graded

concentrations of EtOH. Sections were then stained with H&E and dehydrated again, following the same procedure as described above. Sections were then mounted onto the Superfrost Plus microscope slides (Fisher Scientific, UK) using DPX mounting media (Fisher Scientific, UK). Slides were observed under brightfield light using Zeiss Imager Z2 upright microscope (ZEISS, UK). Study was performed in triplicate.

### 2.3.6. Statistical analysis

Data was analysed using GraphPad Prism 10 software. All measurements were done in triplicate, with results represented as average mean ± SD. Unpaired t-test was used to evaluate the significance of the difference between the means of the two variables. The statistically significant differences were represented as * ($P < 0.05$), ** ($P < 0.01$), *** ($P < 0.001$), **** ($P < 0.0001$), and non-significant differences as ns ($P \geq 0.05$)

# Chapter 3

## Application of hydrophobic ion pairing (HIP) to enhance intravesical drug delivery of hydrophilic drug loaded polymeric nanoparticles

## 3.1. Introduction

Urinary tract infections (UTI) refer to the presence of bacterial infection in the urine or urinary tract and are one of the most common infections across the world [22,29]. According to The National Institute for Health and Care Excellence (NICE), current UTI treatment is orally administrated antibiotics, which exposes the whole body to the drug, not only enhancing chances of side effects, but also increasing risk of bacteria acquiring antimicrobial resistance (AMR) [279]. In recent years, intravesical treatment for bladder diseases, such as bladder cancer or cystitis, has emerged as an appealing treatment option, as poorly permeable urothelium barrier reduces side effects of the drugs by preventing their systemic circulation [82,88]. However, intravesical drug delivery (IDD) still has its own limitations, as drug doses can be reduced to subtherapeutic levels due to urine filling and prematurely washed out by urine voiding [88]. Therefore, encapsulation of therapeutical agents into micro or nano-sized agents, especially if they have mucoadhesive coatings, can prolong drug release within the bladder by elongating nanoparticle retention time at the site of action.

Gentamicin (GEN) belongs to aminoglycosides, a class of antibiotics commonly used to treat serious bacterial infections caused by mainly gram-negative bacteria [247]. It is no longer prescribed as first choice treatment for UTI due to high AMR risk, as well as common side effects of ototoxicity and nephrotoxicity [121,248]. However, several studies have demonstrated the advantages of performing bladder instillations of high GEN dose to eradicate the infection and prevent systemic exposure to the drugs due to highly impermeable barrier of urothelium [78–85]. Based on this, combining intravesical GEN treatment with nanotechnology could achieve an appealing new treatment of UTIs, where initial high dose of GEN would kill bacterial infection, while GEN loaded nanoparticles would ensure prophylactic monitoring of the bladder to prevent recurring infections.

Encapsulation of highly hydrophilic drugs into polymeric nanoparticles have been widely researched, with results demonstrating low drug mass loaded into the particles and burst drug releases *in vitro* [182,280,281]. As a solution, hydrophobic ion pairing (HIP) has been proposed. Charged hydrophilic molecules can form ionic interactions with anionic counterion, resulting in a hydrophobic complex without irreversibly affecting the chemical structure of the therapeutic drug [282,283]. As ion paired hydrophilic drug is complexed into a hydrophobic complex, drug solubility in polar solvents, such as water, is reduced, and drug encapsulation

into nano-sized delivery vehicles is enhanced [13]. The hydrophobicity of the drug and HIP complex can be achieved by HIP agent masking the natural charge of the drug, and therefore reducing solubility of the complex in aqueous medium [282]. To form HIP complexes, counterions should have at least one ionisable group and one hydrophobic domain, therefore surfactants, fatty acids, and sulphates are often used [282]. In addition, therapeutic agents must also present at least one charged group for successful HIP, with many antibiotics presenting at least one amine group that can be positively charged in physiological pH [282,283]. For formation of stable pairs, it is recommended that ΔpKa between the counterion and the drug should be $\geq 2.5$, where counterions would demonstrate low pKa and the therapeutic drug would present a high pKa value [284]. Hydrophobicity of the counterions, measured as logP, can also play an important role in HIP formation [282]. Longer and more saturated alkyl tails of the counterion, or more alkyl tails present, demonstrate higher logP values, and therefore higher hydrophobicity of the HIP complex [282]. However, while this is an important criterion to consider, most hydrophobic counterions might not be the optimal HIP agents, as they often have high molecular weight (MW), which reduces the drug fraction in the final HIP complex, as well as are difficult and costly to obtain [282]. The evaluation of suitable counterions for selected therapeutic drug depends on further investigation on pKa values of both molecules, as well as surrounding pH, as it can influence pair stability, dissociation and overall hydrophobicity [282,284].

The objectives of this chapter are:

- To investigate which counterion achieves most efficient binding to GEN, as well as full dissociation from the drug once in physiologically accurate medium.
- To prepare polymeric nanoparticles loaded with high concentration of ion paired GEN complexes.
- To evaluate if GEN complexation into HIP enables *in vitro* sustained drug release from ion paired GEN (GEN:HIP) complex loaded polymeric nanoparticles.
- To compare antimicrobial sensitivity of ion paired GEN loaded nanoparticles with free, un-paired GEN (UNP-GEN) loaded nanoparticles and observe whether HIP enhances GEN antimicrobial properties.

## 3.2. Materials and methods

### 3.2.1. Materials

Poly(lactic-co-glycolic acid) (PLGA, 50:50 ester terminated, MW 38,000–54,000 Da), poly(vinyl alcohol) (PVA, MW 9,000–10,000 Da, 80% hydrolyzed), Docusate sodium salt (AOT), sodium oleate (OA), dextran sulphate sodium salt (DSS), O-phthalaldehyde (OPA), Ampicillin (AMP), boric acid, thioglycolic acid, sodium 1-heptanesulfonate monohydrate, calcium chloride, sodium acetate, phosphate buffered saline, artificial urine diluent, Mayer's haematoxylin solution, Eosin Y solution (aqueous), dichloromethane (DCM), methanol (MeOH, HPLC grade), isopropanol (HPLC grade), ethanol (EtOH) were purchased from Sigma-Aldrich (Merck Life Science, UK). Sodium chloride (NaCl), sodium dodecyl sulphate (SDS), potassium chloride, potassium hydroxide, 10% neutral buffered formalin, and glacial acetic acid was purchased from Fisher Scientific, UK. Gentamicin sulphate (GEN) was supplied by Fujian Fukang Pharmaceutical (Fujian Fukang Pharmaceutical Co., Ltd, China). Histo-clear II was purchased from Scientific Laboratory Supplies (Scientific Laboratory Supplies Ltd, UK). Freshly excised porcine urinary bladders were kindly supplied by Arthur Howell Butchers (Wells-next-the-Sea, Norfolk, UK).

### 3.2.2. Synthesis and characterisation of ion paired GEN complexes

#### 3.2.2.1. Preparation of ion paired GEN complexes

The ionic complex of gentamicin (GEN) and anionic surfactant was prepared by hydrophobic ion pairing (HIP) technique following previously reported methodology [280,285]. Four different counterions were chosen for this study: sodium oleate (OA), docusate sodium salt (AOT), sodium dodecyl sulphate (SDS), and dextran sulphate sodium salt (DSS). Stocks of counterions were prepared by dissolving anionic surfactant in MilliQ water (MQW), while GEN stock was prepared in buffered aqueous solution (10 mM sodium acetate, 10 mM potassium chloride, 10 mM calcium chloride, at pH = 5) to achieve better ionisation of amino acids present in GEN [280,285]. In brief, 0.5 ml of 5 mg/ml GEN solution was mixed with equal volume of counterion solution, then sonicated for 5 min and vortexed. Both phases were mixed in different mole (mol) ratios, where GEN was kept at constant 1 mol and mixed with 1 mol, 3 mol or 5 mol of anionic surfactant.

### 3.2.2.2. Binding efficiency of GEN and counterion

The amount of GEN that has been ion paired to a counterion in GEN:HIP complexes were determined by indirect method. After preparation of GEN:HIP complex described in **section 3.2.2.1.**, centrifugation was used to separate formed GEN:HIP complexes from the unpaired drug. Formed GEN:HIP complexes were hydrophobic and thus they were precipitating out by forming aggregates, while unpaired drug remained dispersed in the aqueous phase due to its hydrophilicity. Samples were centrifuged (Megafuge$^{TM}$ 16 centrifuge, Thermo Fisher Scientific, UK) at 12,000 RCF for 30 minutes. Supernatant with unpaired GEN was collected and samples were prepared for high-performance liquid chromatography (HPLC) analysis described in **section 3.2.3**. Binding efficiency of HIP (HIP%) of GEN was calculated using equation:

$$HIP\% = \frac{Amount\ of\ GEN\ initially\ added - unpaired\ GEN}{Amount\ of\ GEN\ initially\ added} \times 100\% \qquad \textbf{Eq. (3.1)}$$

### 3.2.2.3. Dissociation efficiency of ion paired GEN complexes

Dissociation efficiency (DS%) of GEN:HIP complex was measured after incubating GEN:HIP complexes in salt buffers. For this study, salt buffers refer to 0.5 M, 1 M, or 1.71 M of NaCl dissolved in PBS, with final pH of the solutions changed to pH=4.5 or pH=7. Increasing concentrations of salt buffers were chosen to facilitate HIP dissociation, with 1.71M of NaCl concentration selected as the highest safe hypertonic solution to be used in bladder without causing adverse effects on bladder tissue, as reported by Tahtali et al., 2022 [286]. Additionally, acidic pH was tested alongside neutral pH to observe whether pH below pKa of ion pairing agents improve its dissociation from the drug.

Briefly, GEN:HIP complex was incubated in the selected salt buffer, vortexed for 5 min and sonicated for 30min, then centrifuged at 12,000 RCF for 45 min. Supernatant with free dissociated GEN was collected and filtered using 0.2 µm PES filter to remove any leftover GEN:HIP complex. Samples were then prepared for HPLC analysis as described in **section 3.2.3**. DS% of GEN:HIP complex was measured by quantifying the amount of GEN that has disassociated from the counterion, which was calculated using equation:

$$DS\% = \frac{Free\ \ dissociated\ GEN}{Amount\ of\ GEN\ initially\ added} \times 100\% \qquad \textbf{Eq. (3.2)}$$

### 3.2.3. Quantification of GEN using HPLC analysis

The quantification of GEN was carried out using HPLC as previously reported [287]. The HPLC system was composed of Quaternary Pump VL (Agilent, UK) and 1260 Infinity II Variable Wavelength Detector (Agilent, UK). A reverse phase column HC-C18, 4.6×100 mm, 5µm, 400 bar (Agilent, UK) was connected to a guard column HC-C18, 4.6×12.5 mm, 5µm, 400 bar (Agilent, UK) and kept at 30 °C degrees throughout runs. Isocratic mobile phase, containing 5 g of sodium 1-heptanesulfonate monohydrate dissolved in 50 ml glacial acetic acid, 250 ml of MQW and 700 ml of MeOH, was injected into machine at 1.2 ml/min flow rate. GEN peaks were detected at 330 nm wavelength.

Samples were prepared for HPLC by derivatizing GEN with OPA, as GEN has a naturally weak UV chromophore, which UV detectors are not sensitive enough to detect in low levels [287,288]. Briefly, OPA reagent was prepared by dissolving 1 g of OPA in 5 mL of MeOH, then mixing it with 95 ml of 0.4 M boric acid, followed by adjustment of final solution to pH = 10.4 using potassium hydroxide and thioglycolic acid. Afterwards, 0.4 ml of the sample containing GEN was mixed with 0.44 ml of isopropanol and 0.16 ml of OPA reagent, followed by 15 min of heating in the water bath set at 60 °C degrees. Samples were then cooled to room temperature and 40 µl of each sample was injected into HPLC machine.

### 3.2.4. Synthesis of blank, UNP-GEN, and GEN:HIP complex loaded PLGA nanoparticles

Polymeric nanoparticles were prepared using water-in-oil-in-water ($W_1/O/W_2$) double emulsification – solvent evaporation method [121]. Briefly, 5 mg GEN dissolved in 0.5 ml of MWQ was used as first aqueous phase ($W_1$) to prepare free, un-paired GEN (UNP-GEN) loaded PLGA nanoparticles. DCM containing 10 mg of dissolved PLGA was used as organic phase (O), and MQW containing 2% of PVA was used as a second aqueous phase ($W_2$). Briefly, first aqueous phase ($W_1$) was added dropwise to 2 ml of organic phase (O), then emulsified using probe sonicator (Fisherbrand$^{TM}$ 505 sonicator, UK) at 20% amplitude for 3 min in a 20:5 second on-off cycle. First emulsion ($W_1/O$) was then added dropwise to 10 ml of second aqueous phase ($W_2$), followed by probe sonication as described before. The formulations were then left stirring at 250 RPM overnight at room temperature, to ensure complete evaporation of organic solvent. Next day, formulations were filtered using 1 µm glass fibre filter (VWR,

UK) and topped up with MQW to make up 10 ml total volume of obtained nanodispersions. No washing steps were performed post nanoparticle formation, meaning that residual PVA was likely present in the samples.

To prepare blank PLGA nanoparticles, 0.5 ml of MQW water without any drug was used as $W_1$ phase. To prepare GEN:HIP loaded nanoparticles, 1 ml of GEN:HIP complex was used as $W_1$ phase. It was prepared by mixing GEN and selected HIP agent in 1:1, 1:3, or 1:5 mol ratios, where 5 mg of GEN dissolved in 0.5 ml of buffered aqueous solution (10 mM sodium acetate, 10 mM potassium chloride, 10 mM calcium chloride, at pH = 5) was pipetted into equal volume of counterion dissolved in MQW. Obtained $W_1$ phase was then swiftly pipetted into the organic phase, followed by the rest of the protocol as described above.

### 3.2.5. Drug loading and encapsulation efficiency

Indirect method was used to measure loading capacity (LC%) and encapsulation efficiency (EE%) of GEN:HIP and UNP-GEN loaded PLGA nanoparticles. Nanoparticle formulations were centrifuged at 12,000 RCF for 1 hour, supernatant was collected and prepared for HPLC analysis as described in **section 3.2.3**. LC% and EE% of GEN was calculated using equations:

$$LC\% = \frac{(Mass\ of\ GEN\ added - mass\ of\ GEN\ in\ supernatant)}{Mass\ of\ PLGA} \times 100\% \qquad \textbf{Eq. (3.3)}$$

$$EE\% = \frac{(Mass\ of\ initial\ GEN\ added - mass\ of\ GEN\ in\ supernatant)}{Mass\ of\ initial\ GEN\ added} \times 100\% \qquad \textbf{Eq. (3.4)}$$

### 3.2.6. *In vitro* drug release

Drug release profiles of GEN were investigated using dialysis bag method [289]. For this study, 1 ml of GEN:HIP complex solution (made of 5 mg GEN mixed with selected counterion in 1:3 or 1:5 mol ratios), UNP-GEN or nanoparticle formulation was placed inside dialysis bag (Thermo Scientific™ SnakeSkin™ Dialysis Tubing, 10K MW cut-off, regenerated cellulose, Fisher Scientific, UK). Samples were incubated in release media, which was made up of 20 ml of PBS, with addition of 0.5 M, 1 M, or 1.71 M of NaCl to the PBS when GEN:HIP samples were used, at pH = 4.5 or pH = 7.4. Samples were incubated in shaking incubator (KS3000 i control IKA®, UK) at 37 °C degrees, with rotary speed of 100 RPM, with sink conditions

maintained throughout the assay. At predetermined time intervals, 1 ml of the sample was collected and replaced with 1 ml of fresh release medium. Collected samples were analysed for drug content by HPLC. Study was performed in triplicate and the average percent of GEN released per each timepoint was expressed in mean ± standard deviation (SD).

### 3.2.7. Antimicrobial sensitivity assay

Antimicrobial sensitivity of UNP-GEN or GEN:HIP loaded nanoparticles was assayed using micro broth dilution method as described in Clinical and Laboratory Standards Institute (CLSI) with minor modifications [182,290]. Cultures of *Escherichia Coli* ER2738 were grown on LB agar plates 24 hours before the assay. On the day of the assay, *E. Coli* cultures were incubated in LB broth and the optical densities of cell growth at 600 nm ($OD_{600}$) were measured by micro-plate reader SpectraMax® M2 (Molecular Devices Limited, UK) using UV-Vis detection. Bacterial culture was then diluted to achieve bacterial concentration of $1x10^8$ colony-forming unit (CFU)/ml. In a 96-well plate, 50 µl of each nanoparticle formulation in twofold dilutions was inoculated with 50 µl of prepared bacterial culture, leaving the plate to incubate at 37 °C overnight. Next day, plates were investigated visually, along with $OD_{600}$ measurements of each well recorded using microplate reader SpectraMax® M2. The minimum inhibitory concentrations (MICs) of nanoparticle formulations were recorded at lowest encapsulated GEN concentration where no bacterial growth was observed by eye and confirmed by $OD_{600}$ measurement. Study was performed in triplicate.

## 3.3. Results and discussion

### 3.3.1. GEN quantification by HPLC

GEN quantification was performed using HPLC method, that was adapted from previously reported study [287]. Derivatization step was performed before sample analysis by HPLC, as UV detectors are not sensitive enough to pick up naturally weak UV chromophore of GEN [287,288]. Due to the composition of GEN comprising of 4 major congeners C1, C2, C2a and C1 [247], 4 peaks were detected at retention time ($R_t$) of 1.9, 6.4, 8.5 and 10.1 min, respectively (**Figure 3.1**). GEN congener separation has been well documented when liquid chromatography is used to analyse this drug [247,291,292]. While obtained peaks can be used to quantify each congener concentration to identify exact GEN composition [247,291,292], the purpose of this project was to quantify total GEN concentration in the sample. Therefore, bulk calculation of the congeners was used, where absorbance of all four peaks of each concentration

were summed and calibration curves for GEN in MQW, GEN in PBS, and GEN in artificial urine (AU) were prepared. Increasing concentrations of GEN showed linear correlations with increasing areas of the HPLC peaks, demonstrating high $R^2$ value of 0.999 and generating regression equation of Y = 15938x + 25.896.

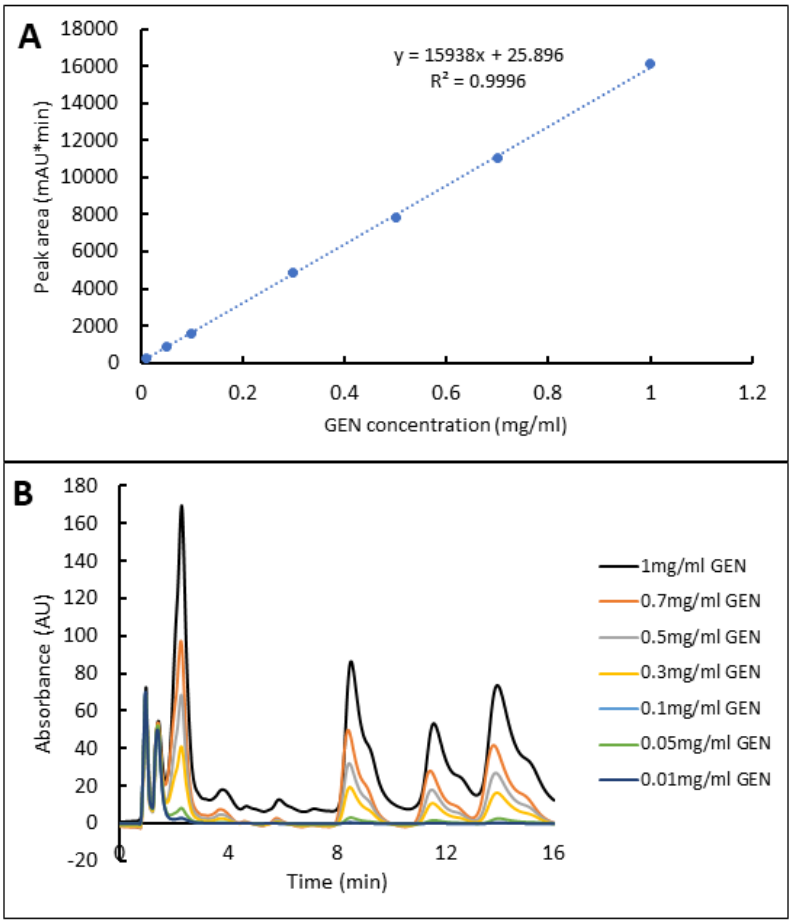


**Figure 3.1:** Calibration curve (A) and HPLC chromatogram (B) of GEN in MQW, measured at concentration range from 1 to 0.01 mg/ml, UV detected at 330 nm.

Limit of detection (LOD) and limit of quantification (LOQ) was calculated using equations:

$$LOD = \frac{3.3\,\sigma}{S} \qquad \textbf{Eq. (3.5)}$$

$$LOD = \frac{10\,\sigma}{S} \qquad \textbf{Eq. (3.6)}$$

Where σ is the standard deviation of the intercept, and S is the slope of calibration curve. From the obtained calibration curve, LOD was calculated to be 0.04 mg/ml, with LOQ calculated to be 0.12 mg/ml. Although these values are quite high, there we no issues associated with quantification of GEN, as larger concentrations than 0.12 mg/ml of the drug were used and quantified throughout this project.

Although GEN quantification by HPLC was selected, certain limitations of this assay were observed. Due to pre-column derivatisation needed for GEN detection by UV, this assay is often associated with low sensitivity, time-consuming process, poor reproducibility of the results, and possible introduction of non-controlled impurities and degradation products [288,293,294]. Alternatively, GEN quantification assay by ultraviolet-visible (UV-Vis) spectroscopy was investigated, however this method also required GEN derivatisation step. Multiple studies reported using indirect assay to measure GEN content in the nanoparticles, by derivatising unencapsulated drug dispersed in the supernatant with ninhydrin or OPA, followed by sample analysis using UV-Vis spectroscopy [182,295–297]. However, in present study obtained results from UV-Vis were less accurate (lower $R^2$ value) than results obtained from GEN quantification by HPLC, therefore HPLC method was used for all quantification experiments. HPLC methods without pre-column derivatisation have been reported in the literature, where GEN was quantified using Mass Spectrometry (MS) [293], Charged Aerosol Detection [288,298], or Evaporative Light Scattering Detection [294]. Out of these, GEN quantification by MS was considered, however surfactant use is not compatible with liquid chromatography-MS (LC-MS), as they contaminate the machines. Alternatively, some studies have used bioassays to determine GEN concentrations in the samples, however this technique has been deemed inaccurate, it demonstrates low sensitivity and lack of specificity, as other antibacterial substances in the sample can interfere with bacterial inhibition associated with the drug [293].

Despite discussed limitations of the HPLC analysis used for quantification of GEN, this method showed most reliable results out of available quantification assays, with minor fluctuation in results expected due to derivatisation step involved. In order to limit sample variability, derivatisation was performed on the same day as sample analysis by HPLC, therefore removing the possibility of derivatised GEN degradation over time.

### 3.3.2. Preparation and characterisation of GEN:HIP complexes

HIP technique was used to increase GEN (pKa ≈ 12.5) hydrophobicity by binding oppositely charged counterions through electrostatic interactions to create water-insoluble complexes [299]. Four different ion pairing agents were selected for formation of ion paired GEN complexes: OA (pKa ≈ 5), AOT (pKa ≈ -0.75), SDS (pKa ≈ 3.3) and DSS (pKa≈ 2). These were chosen to observe which ion pairing agent would demonstrate best results for drug delivery application, which includes strong binding efficiency, as well as complete drug detachment from the complex once target site is reached.

Choosing an ion pairing agent that is fatty acid based was previously described to show pH triggered dissociation between the active ingredient and counterion [282]. For this study, OA was chosen (**Figure 3.2**) instead of oleic acid, as it is a fatty acid-based salt and has much higher solubility in water. It was expected that with pH conditions below the pKa of OA (pKa ≈ 5), molecules of OA would become protonated and form oleic acid [300]. This in turn, would lead to protonation of carboxyl group present in the oleic acid, which would form a free acid and detach from the cationic counterpart that is GEN [282].

Alternatively, SDS, DSS and AOT (**Figure 3.2**) were chosen as additional counterions, as due to their low pKa values they exhibit stable anionic charge in wide range of pH conditions [282,283,301]. Studies where DSS was used as ion pairing agent have demonstrated almost 100% dissociation of the HIP complex in normal physiological conditions or water, therefore exhibiting appealing properties for drug delivery applications [285,301]. Anionic surfactant SDS has been widely used to ion pair hormones, enzymes, proteins, and antibiotics [282,283,285], with one study reporting hydrophobic GEN-SDS complex being encapsulated into nano carriers by flash nanoprecipitation method [281]. Our attempt at replicating these results has been unsuccessful, however we hypothesised that pre-formed GEN:SDS complex could be encapsulated into PLGA nanoparticles by double emulsification – solvent evaporation method. Finally, AOT was chosen as a counterion of interest due to many studies reporting successful GEN:AOT complexation, which in turn lead to high encapsulation rates of the complex into nano or micro-sized carriers, unaffected or enhanced bactericidal properties and, in some cases, sustained drug release [178,280,302]. Here, our aim was to replicate previous studies and observe how HIP between GEN and AOT compared to binding efficiency,

dissociation, encapsulation into nanoparticles, drug release and antimicrobial sensitivity of HIP between GEN and other selected counterions.

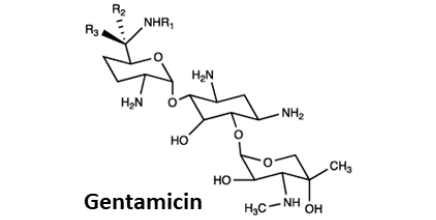


| | Gentamicin C1 | C1a | C2 | C2a | C2b |
|---|---|---|---|---|---|
| R1 | $CH_3$ | H | H | H | $CH_3$ |
| R2 | H | H | H | $CH_3$ | H |
| R3 | $CH_3$ | H | $CH_3$ | H | H |

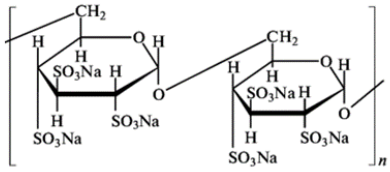


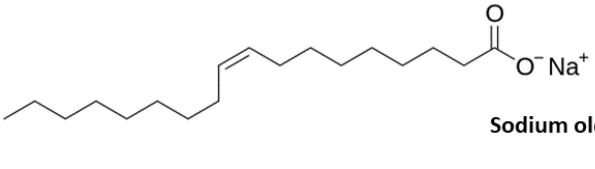


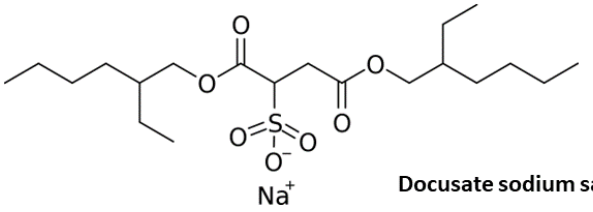


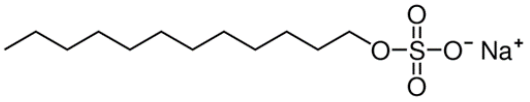


**Figure 3.2:** Chemical structures of gentamicin (GEN), sodium oleate (OA), docusate sodium salt (AOT), sodium dodecyl sulphate (SDS), and dextran sulphate sodium salt (DSS).

### 3.3.2.1. Binding efficiency of GEN:HIP complexes

HIP is a process of forming ionic interactions between a charged hydrophilic molecule and oppositely charged surfactants [282]. Once the complex is formed, hydrophilic groups of cationic molecule become shielded by hydrophobic moieties of the counterion, with hydrophobic parts of the counterion extending into the outer parts of the complex and thus decreasing the solubility of the whole complex in aqueous environments [282,302]. Obtained hydrophobic complex has been shown to demonstrate lack of hydrogen bonding in polar solutions, therefore confirming increased hydrophobicity [303]. As HIP is formed by non-covalent interactions, the complex can easily dissociate in the presence of ions that outcompete the counterion [282].

Ionized GEN (at pH=5) and anionic counterions OA, AOT, SDS and DSS (dissolved in water) were mixed in different mol ratios to form GEN:HIP complexes. These complexes were made in ratios of 1 mol of GEN to 1, 3 or 5 mol of counterion. As GEN chemical structure suggests (**Figure 3.2**), this drug demonstrates 5 amine groups, which if ionised could form ionic interactions with 5 molecules of counterion, that presents a single charged group [178]. In this case, the stoichiometry would be equimolar [304]. However, based on GEN composition, five

amine groups differ in their methylation pattern at one or more sites in the molecule [305], meaning that it is challenging to predict the exact GEN to counterion ratio needed for stoichiometric binding. Therefore, increasing mol ratios of GEN:HIP-agent were examined to fully saturate free amino groups of GEN with counterion, which would result in fully ion paired GEN [280,306]. This was achieved by measuring the binding efficiency between GEN and counterion, as fully ion paired GEN would demonstrate 100% HIP-agent binding efficiency [285,306].

Results have demonstrated that increase in mol ratio between GEN and counterions improve their ionic binding efficiency (**Figure 3.3**). With ratios of GEN:HIP complex set to 1:1 mol, less than 50% of GEN was ion paired, as evidently not enough counterion was used to bind all available amino groups of GEN. Increased mol ratio to 1:3 GEN:HIP-agent revealed counterions AOT and SDS to perform better compared to OA or DSS, as the former two reached 98.6 ± 2% and 96.4 ± 2% HIP%, respectively. Similar results were reported by Griesser et al., 2017, where they compared OA, AOT and SDS as ion pairing agents to several cationic peptides [307]. Their findings show AOT superiority in terms of binding efficiency compared to the other counterions, which highlights that chemical structure of anionic surfactants could be a key factor in achieving most efficient ion pairing results [307]. Additionally, Claus et al., 2023 have shown that counterions with sulphonate groups, such as AOT, demonstrate more efficient HIP performance than counterions with sulphate groups, such as SDS, also revealing that presence of highly electron-dragging head formation of the counterion ensures efficient HIP formation [299]. This also suggests that the reason why DSS, which has two sulphate groups on each α-glucose unit, does not achieve as high HIP efficiency as AOT or SDS, as the sulphate groups of DSS are not structured in the anionic head position [308].

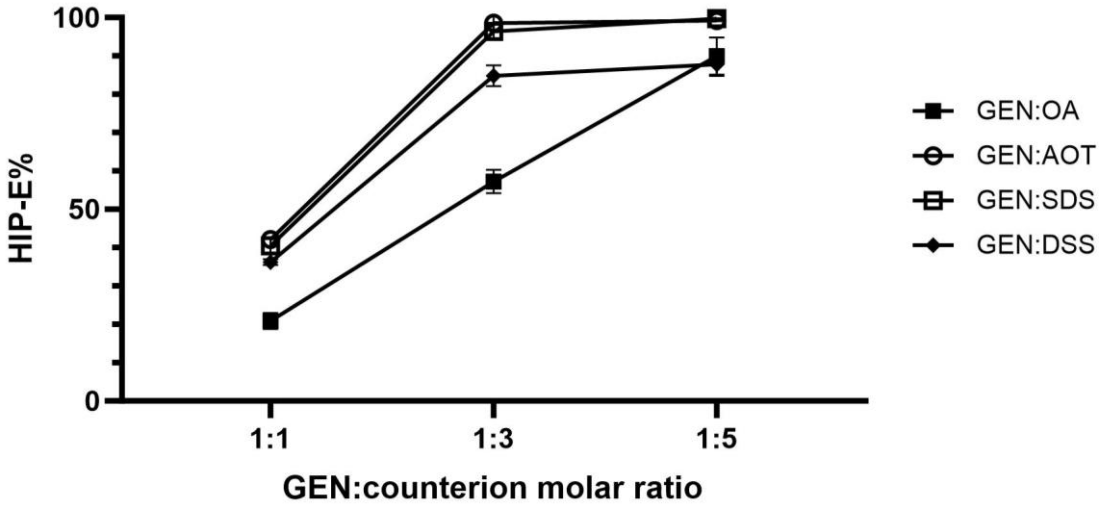


**Figure 3.3:** Graph demonstrating the ionic binding efficiency (HIP%) of GEN with HIP agents OA, AOT, SDS and DSS, when increasing mol ratios of counterions are used. Error bars represent the SD (n = 3).

It is important to note that both AOT and SDS counterions have achieved almost 100% pairing efficiency with GEN when mol ratio of 1:3 GEN:counterion was used [34,37]. Several studies reported that after the most efficient HIP formation was achieved, increase in counterion ratio often resulted in micellar formation, as concentration of counterion surpassed its critical micelle concentration (CMC) [282,307,309]. Based on the reported CMC values in other publications, where CMC of OA is 0.09%, CMC of AOT is 0.02%, and CMC of SDS is 0.2% (w/v) [310–312], all concentrations of counterion used for preparation of GEN:HIP were above the CMC level. Therefore, it is highly likely that GEN:AOT and GEN:SDS complexes with higher ratios than 1:3 exhibited micellar formation, as increase in GEN:counterion ratios demonstrated continuing 100% ion pairing efficiency. All following experiments for GEN:AOT and GEN:SDS complexes were performed in 1:3 drug to counterion ratios.

Similarly, DSS exhibited no significant difference ($P > 0.05$) between HIP% results of 1:3 and 1:5 mol ratios of drug to counterion complexes. Resulting 84.2 ± 3% to 87.8 ± 3% GEN pairing efficiency was significantly lower than observed in GEN:AOT and GEN:SDS complexes at the same ratios. However, around 90% binding efficiency was also observed in GEN:OA complex, demonstrating 89.9 ± 5% of GEN paired when 1:5 mol ratios were used. A possible reason why both OA and DSS counterions could not 100% effectively pair with GEN could be due to other intra-molecular interactions occurring between drug and surfactants [306].

All four counterions examined have demonstrated increase in HIP% when mol ratios of counterions were increased in GEN:HIP agent complexes. Results showed generally high ion paired GEN percentage of > 88%. Similar results have been widely reported in the literature when OA, AOT, SDS and DSS were used as counterions [285,299,301,307,309].

### 3.3.2.2. Ion pairing of GEN and counterions confirmation by ATR-FTIR

ATR-FTIR analysis was performed to investigate interactions between GEN and selected counterions, and results are presented in **Figure 3.4**. GEN spectrum showed nitrogen-hydrogen (N-H) bending vibrations of primary amines at peaks 1618 and 1525 $cm^{-1}$, with two characteristic peaks for GEN present at 1024 and 605 $cm^{-1}$ [313,314]. For counterions AOT and SDS peaks of vibration of sulphate groups (SOO-) could be observed at 1209 and 1217 $cm^{-1}$, respectively, for asymmetric stretching, and 1047 and 1082 $cm^{-1}$, respectively, for symmetric stretching [301,315]. These peaks were observed at the same wavenumber in physical mix of GEN and AOT, and GEN and SDS. Once GEN:AOT complex was formed, symmetric stretching of SOO- peak formed a hump on shifted GEN peak (from 1024 $cm^{-1}$ to 1111 $cm^{-1}$), with asymmetrical stretching SOO- peak disappearing completely. This indicates sulphate group binding to GEN during their complex formation. As for SDS, both asymmetric and symmetric stretching peaks of SOO- were no longer visible once 1:1 and 1:3 mol ratio complexes of GEN:SDS were formed. Instead, a characteristic GEN peak shifted from 1024 to 1109 $cm^{-1}$, therefore suggesting GEN and SDS interaction during complex formation.

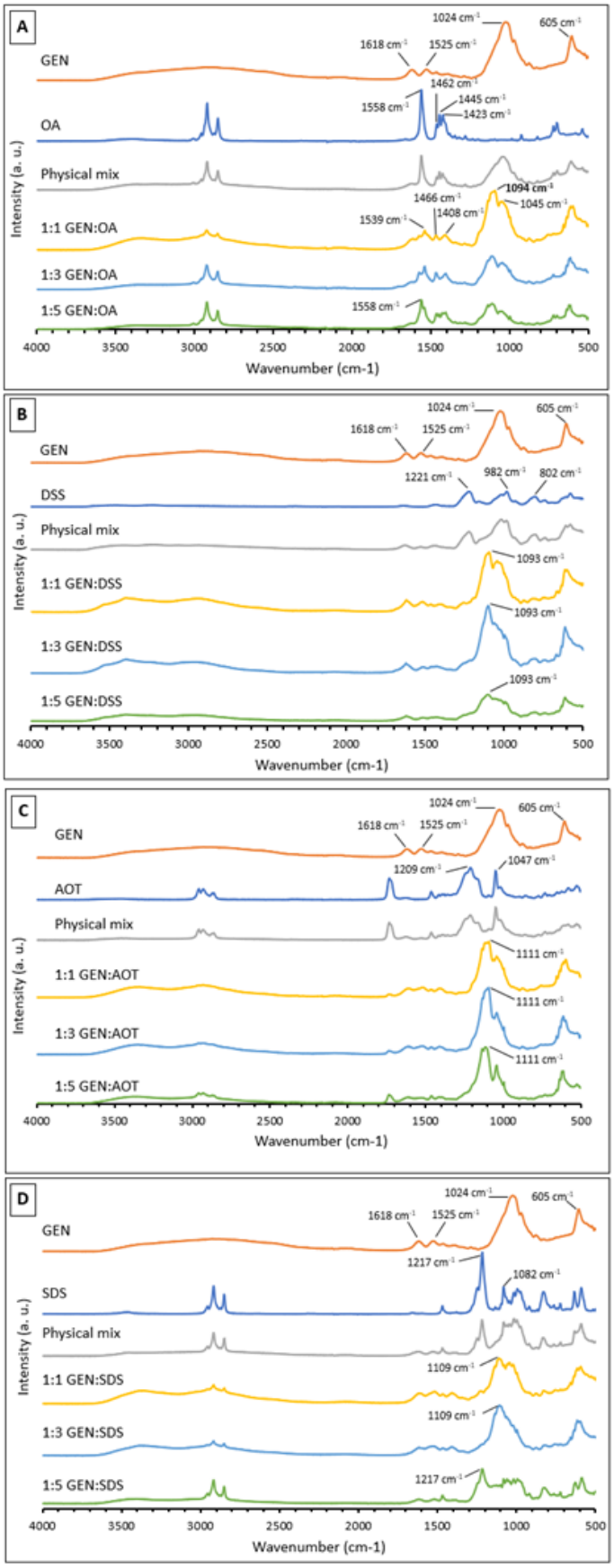


**Figure 3.4:** ATR-FTIR absorbance spectrum of (A) GEN:OA, (B) GEN:DSS, (C) GEN:AOT and (D) GEN:SDS complexes, with their raw materials and physical mixtures.

Similarly to AOT and SDS, spectrum of DSS showed peaks of asymmetric and symmetric stretching vibrations of SOO- at 1221 and 982 $cm^{-1}$, respectively [285,301,315]. Additionally, S-O-S vibration has been observed at peak 802 $cm^{-1}$ [285,301]. After GEN:DSS complex formation, these peaks were diminished, while GEN peak shifted to 1093 $cm^{-1}$, indicating ionic interactions between the drug and counterion.

OA demonstrated asymmetric stretching vibration of carboxyl group (-COO-) at peak 1558 $cm^{-1}$, whereas peaks 1462, 1445 and 1423 $cm^{-1}$ exhibited symmetric stretching vibrations of -COO- [309,316]. After electrostatic interactions between anionic carboxyl group of OA and cationic amino group of GEN, the asymmetric -COO- peak demonstrated a shift to 1539 $cm^{-1}$. Instead of 3 peaks of symmetric stretching vibrations of OA and 2 peaks of primary amines of GEN, two peaks at 1466 and 1408 $cm^{-1}$ appeared in GEN:OA complex samples, which therefore suggests interactions between the drug and counterion. Additionally, GEN:OA complex spectrum also reveals a characteristic GEN peak at 1024 $cm^{-1}$ shifting and splitting into two peaks at 1094 and 1045 $cm^{-1}$.

It is interesting to mention that in some GEN:HIP agent complexes, which were formed in 1:5 mol ratios, distinctive peaks of counterions can be observed. For instance, spectrum of GEN:OA complex shows strong peak of asymmetric stretching vibration of carboxyl group at 1558 $cm^{-1}$ reappearing again. Similarly, peak at 1217 $cm^{-1}$ corresponding to asymmetric stretching vibration of sulphate group can be clearly identified in 1:5 mol GEN:SDS complex sample. These observations strongly suggest that excess quantities of free counterion are present in the sample and not interacting with the drug, as there are no available GEN amino groups to form a GEN:HIP complex with.

### 3.3.2.3. Dissociation of GEN:HIP complexes

For this study, complete ion paired complex dissociation is necessary to achieve therapeutical concentrations of the drug within target site, which would inhibit bacterial growth and kill the bacterial infection. Due to the nature of ionic interactions being easily influenced by presence of high ionic strength, dissociation of GEN:HIP complexes can be enhanced by addition of NaCl, which outcompetes counterions and releases the drug from HIP complex. Dissociation experiments were performed by dispersing the GEN:HIP complexes in PBS (originally

contains 0.137 M NaCl) with increasing concentrations of NaCl added. Up to 1.71 M (10%) of NaCl used was per sample, as it is reportedly the highest salt concentration that was safely used in bladder with minimal adverse effects observed [286]. Additionally, dissociation of GEN:HIP complexes was examined in AU buffer with same NaCl concentrations as mentioned earlier. Finally, two pH conditions were tested: neutral at pH = 7.4 and acidic at pH = 4.5. Here, inclusion of acidic pH was important for a couple of reasons. Firstly, pH conditions lower than pKa of certain counterions can facilitate protonation, which in turn would lead to detachment of the drug from GEN:HIP complex. Secondly, acidic pH significantly improves mucoadhesive properties of the PLGA nanoparticles, that are coated with mucoadhesive polymers, such as chitosan [317,318]. As chitosan is protonated in acidic pH, it becomes positively charged and thus achieves strong mucoadhesive interactions with negatively charged mucin [317,318]. Strong mucoadhesive interactions between nanoparticles and mucous layer are important in order to prolong the retention time of the nanoparticles in the bladder, facilitating sustained drug release. Although nanoparticles used in this chapter do not have mucoadhesive coating, addition of chitosan to these formulations would be part of further optimisation work, which demonstrates the need to test how dissociation of GEN:HIP complex is affected by acidic pH. Mucoadhesive interactions between chitosan coated nanoparticles and mucous layer are further explored in **Chapter 4** and **Chapter 5**.

Results of dissociation tested in PBS pH = 7.4, PBS pH = 4.5 and AU pH = 4.5 buffers are demonstrated in **Figure 3.5**. Dissociation of GEN:DSS complex in PBS + NaCl buffers at both acidic and neutral conditions demonstrate detachment of over 100% when high concentration of salts are used. Based on this, we speculate that during preparation of GEN:DSS samples for HPLC analysis, DSS gets derivatized along with GEN, which later on interferes with GEN peak readings. To the best of our knowledge, there are no prior reports of chemical reactions between DSS and OPA. During the sample preparation of GEN:HIP complexes for HPLC assay, samples are filtered using 0.2 μm PES filter to remove any leftover complex, however water-soluble UNP-GEN and free counterion (below CMC) remained dispersed in the aqueous solution. Once the supernatant of GEN:DSS is derivatized, samples turn into a dark red colour, which is not seen after derivatization of UNP-GEN or supernatants of GEN:OA, GEN:AOT or GEN:SDS. Hence, results of GEN:DSS samples were deemed unreliable and this complex was not investigated in further experiments.

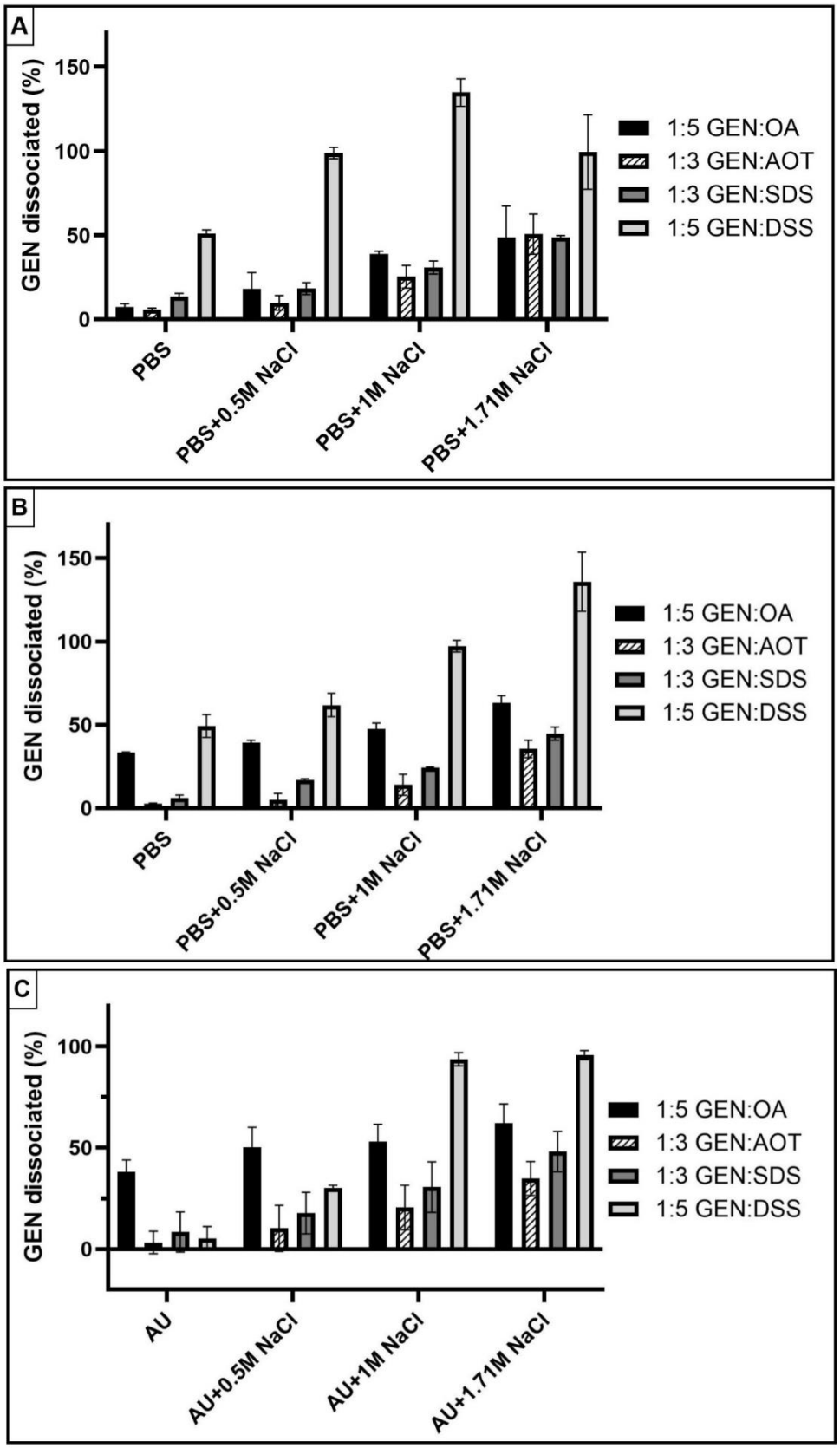


**Figure 3.5:** Dissociation of GEN:HIP complexes in (A) PBS pH = 7.4, (B) PBS pH = 4.5, (C) AU pH = 4.5 buffers with increasing concentrations of NaCl added. Error bars represent the SD and n = 3.

Looking at the dissociation rates of complexes GEN:OA, GEN:AOT and GEN:SDS, none of the counterions showed full 100% dissociation from the drug. Highest dissociation rates were observed in GEN:OA complex, resulting in 63.2 ± 4% of GEN freed from the counterion, when the highest concentration of NaCl was used in acidic PBS buffer. Failure to fully dissociate HIP complexes was also reported in other studies, as evidently non-ionic interactions, such as covalent bonding and hydrophobic interactions, have been observed between therapeutics and counterions [285,301,319]. For counterions AOT and SDS, highest percentage of dissociated GEN of 50.7 ± 12% and 48.7 ± 1%, respectively, was achieved in 1.71 M NaCl PBS buffer at pH = 7.4. Based on this data, the most effective dissociation was achieved in buffers with highest salt concentrations. Other studies have also demonstrated similar results of improved dissociation of HIP complex with increasing concentration of salts used [301,320].

As mentioned before, we hypothesised that acidic pH conditions could act as dissociation trigger to GEN:OA complex, as protonation is expected in pH conditions below pKa of OA (pKa ≈ 5) [282,300]. Therefore, when buffer pH was 4.5, OA showed significantly higher ($P < 0.05$) percentage of dissociated GEN in all NaCl concentrations tested, except for 1.71 M, when compared against GEN:OA dissociation in neutral conditions. A likely reason why no further dissociation is observed at highest NaCl concentration even at pH = 4.5 is likely due to other non-ionic interactions between GEN and OA [285,301,319]. GEN:AOT samples showed no significant difference in dissociation when tested in pH = 4.5 or pH = 7.4, except for when tested in PBS buffer alone, however in both conditions the dissociation was incredibly poor, with an average of 2.6 ± 1% and 6 ± 1%, respectively, of GEN dissociated. Complex of GEN:SDS showed significantly higher dissociation percentage at pH = 7.4 in PBS alone and PBS + 1M NaCl buffers, however at highest concentration of salt used dissociation percentage was similar to the one obtained in pH = 4.5. These results of AOT and SDS dissociation were expected, as pH change did not drop below the pKa values of these counterions (AOT pKa ≈ -0.75), SDS pKa ≈ 3.3).

Results of GEN and counterion dissociation were similar in both PBS and AU buffers at pH = 4.5. Similar trend of increase in dissociation with increasing concentrations of salt added was observed in AU buffer, with GEN:OA complex showing highest percentage of released drug from the complex. It is important to note, that results of dissociation in AU buffer showed quite

large error bars indicating around 10% fluctuation of the outcome, which could suggest challenging reproducibility.

### 3.3.3. Characterisation of GEN:HIP loaded PLGA nanoparticles

PLGA nanoparticles loaded with GEN:HIP complexes were prepared by a double emulsion – solvent evaporation method [121]. Nanoparticles ranged in size from 128 to 299.5 nm, with polydispersity index (PDI) average of 0.31 (**Table 3.1**). Nanoparticles loaded with GEN:HIP complexes showed no significant difference to blank PLGA nanoparticles when particle size was compared, except for 1:1 GEN:OA complex nanoparticles, which were significantly larger ($P < 0.05$). Nanoparticles loaded with UNP-GEN showed lowest particle size of 128 ± 15 nm, and although some GEN:HIP complex loaded formulations showed significantly higher particle size, there was no clear trend observed that suggested increased particle size when GEN:HIP complex was loaded. Similar size range of PLGA nanoparticles loaded with GEN:AOT complex was reported previously [280,321]. Most nanoparticles showed narrow size distribution, as their PDI values ranged from 0.2 to 0.3, with only exception of 1:1 GEN:OA formulation showing much larger value of 0.6. All nanoparticles showed minimal negative particle charge. As PLGA is negatively charged polymer, expected zeta potential should be at around -20 mV, however our formulations contained 2% of stabilizer PVA, which decreased zeta potential values to almost neutral [169,280]. Encapsulation of UNP-GEN or GEN:HIP complex did not demonstrate a significant difference on nanoparticle charge, therefore indicating no drug adsorption on the particle surface.

**Table 3.1:** Characteristics of blank PLGA nanoparticles, UNP-GEN loaded and GEN:HIP complex loaded PLGA nanoparticles prepared by double emulsification – solvent evaporation. Error bars represent SD and n = 3.

| GEN concentration (mg) | Counterion | Drug to counterion mol ratio | Particle size (nm) | PDI | Zeta potential (mV) |
|---|---|---|---|---|---|
| N/A | N/A | N/A | 165.4±40 | 0.33±0.02 | -0.8±1 |
| 5 | | | 128.0±15 | 0.23±0.06 | -0.7±0 |
| | OA | 1:1 | 299.5±73 | 0.55±0.12 | -0.4±0 |
| | AOT | | 154.9±38 | 0.26±0.02 | -0.8±0 |
| | SDS | | 167.0±33 | 0.35±0.14 | -1.5±1 |

| | | | | | |
|---|---|---|---|---|---|
| | OA | 1:3 | 202.2±68 | 0.31±0.06 | -1±1 |
| | AOT | | 175.8±14 | 0.30±0.05 | -2.8±2 |
| | SDS | | 171.1±20 | 0.28±0.02 | -1.2±0 |
| | OA | 1:5 | 187.2±16 | 0.25±0.04 | -1.7±0 |
| | AOT | | 187.8±79 | 0.25±0.08 | -9.6±12 |
| | SDS | | 175.1±32 | 0.35±0.09 | -1.9±1 |

The shape and surface morphology of blank PLGA nanoparticles, UNP-GEN loaded PLGA nanoparticles, and GEN:OA, GEN:AOT, GEN:SDS complex loaded PLGA nanoparticles were inspected by TEM (**Figure 3.6**). Images demonstrate spherical shaped nanoparticles in size range from 150 to 250 nm, which is agreement with data obtained from DLS analysis (**Table 3.1**). Some smaller sized particles can be observed in all formulations, indicating some degree of particle polydispersity, which is expected with an average PDI of 0.3, as measured by DLS. Most of the formulations demonstrated smooth particle surface morphology, except for 1:3 mol ratio of GEN:SDS complex loaded PLGA nanoparticles, which surface was covered by irregular structures. It is likely to be excess SDS or PVA forming a coating on the surface of nanoparticles [322].

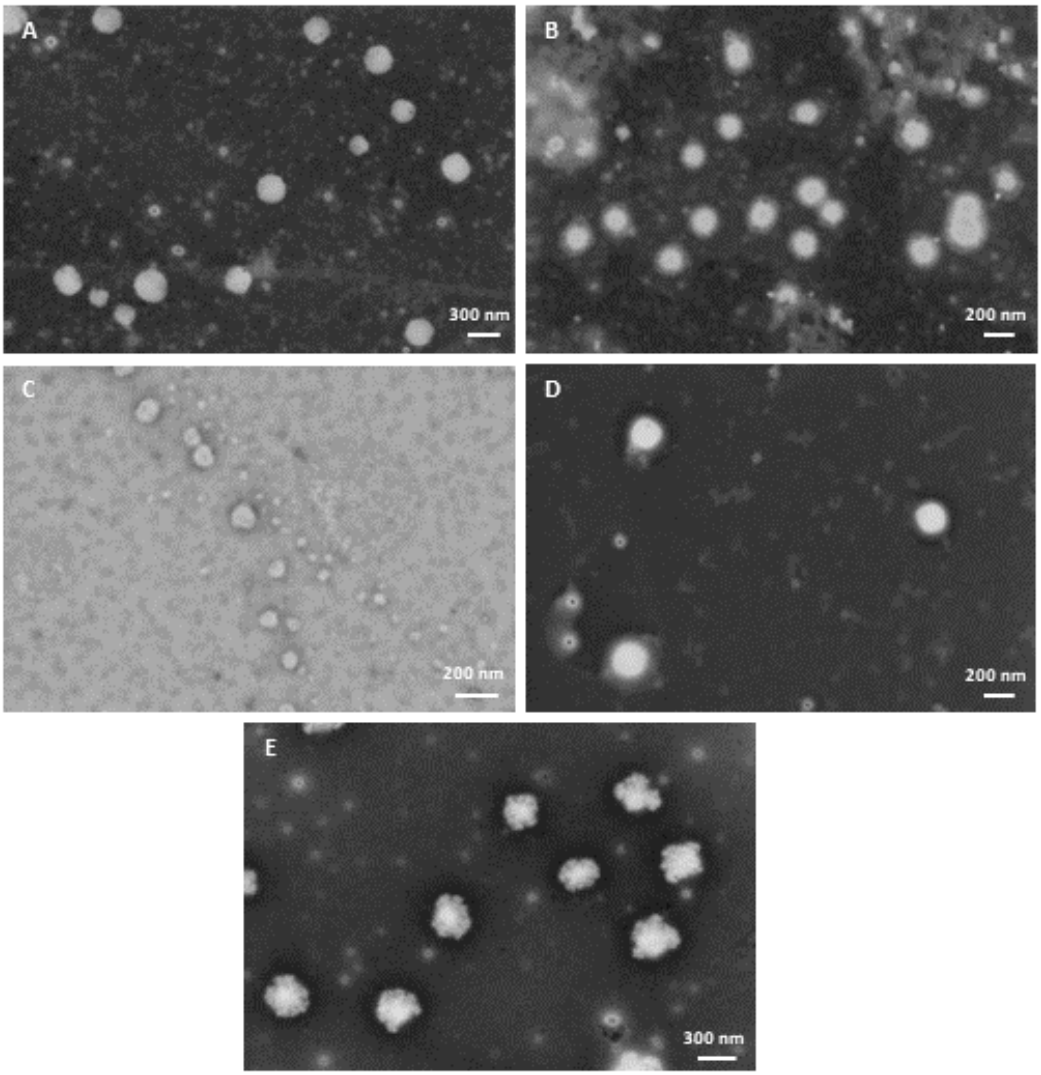


**Figure 3.6:** TEM images of (A) blank PLGA nanoparticles, (B) UNP-GEN, (C) 1:5 GEN:OA, (D) 1:3 GEN:AOT, (E) 1:3 GEN:SDS loaded PLGA nanoparticles.

Different mol ratios of GEN:HIP complexes were encapsulated in PLGA nanoparticles to observe how binding efficiency (HIP%) correlates with encapsulation efficiency (EE%) of GEN. Due to high water solubility of GEN, encapsulation of it in hydrophobic polymers such as PLGA can be challenging [296,297,323]. Use of double emulsion – solvent evaporation method enables to trap hydrophilic drugs in an internal oil phase, which is then distributed in external aqueous phase containing surfactant to stabilize the external interface [324]. However, sometimes it does not fully prevent the drug from diffusing out of the oil core during the preparation and particle formation process. Therefore, use of HIP is an appealing technique that changes hydrophobicity of the drug without altering its chemical structure, and then enables this hydrophobic complex to partition into polymers matrix during the encapsulation process [322].

As seen from results demonstrated in **Figure 3.7**, increase in mol ratios of GEN:HIP increases encapsulation efficiency of GEN. By comparing these results to HIP% results discussed in **section 3.3.2.1.**, it is clear that with more hydrophobic GEN:HIP complex present in the sample, more GEN is encapsulated into the nanoparticles. For instance, 1:5 mol ratio GEN:OA complex showed HIP% of 89.3 ± 5% and the same complex showed encapsulation of 90.9 ± 5% into PLGA nanoparticles. In contrast, when GEN:HIP complexes made of mol ratios 1:1 drug to counterion were used, much smaller amount of GEN was complexed with its counterion, therefore EE% values were considerably lower, ranging from 36.8% to 53.7% as most of the unpaired GEN has diffused from the core of the nanoparticles. It is important to note that some of the unpaired GEN is expected to be loaded into the PLGA nanoparticles too. UNP-GEN loaded nanoparticles demonstrated EE% of 33.1 ± 2%, with LC% of 16.5 ± 1%, which represents an average mean of EE% and LC% values of GEN loaded polymeric nanoparticles reported in the literature [182,296,297,321,323]. Interestingly, when comparing EE% of 1:1 mol ratios of GEN:HIP complexes and UNP-GEN formulations, only GEN:AOT loaded nanoparticles showed significantly higher ($P < 0.01$) EE% compared to UNP-GEN loaded nanoparticles.

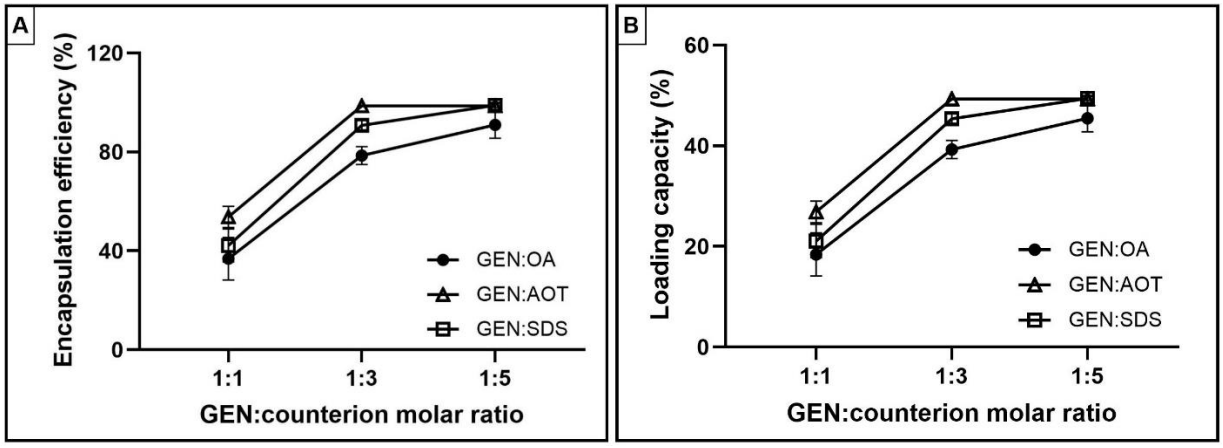


**Figure 3.7:** (A) Encapsulation efficiency (EE%) and (B) loading capacity (LC%) of different mol ratios of GEN:OA, GEN:AOT and GEN:SDS complexes loaded PLGA nanoparticles. Error bars represent the SD and n = 3.

Complexes GEN:OA and GEN:SDS achieved highest EE% and LC% values once encapsulated into PLGA nanoparticles at 1:5 mol drug to counterion ratios. This is expected, as their HIP% values were highest at the same ratios. As for GEN:AOT, no significant difference ($P > 0.05$)

was observed between ratios 1:3 and 1:5 when comparing their values of EE% and LC%, as no significant difference was found between the same ratios in HIP% values too.

Highest EE% values achieved were 90.9 ± 5%, 98.6 ± 1% and 98.9 ± 1% for GEN:OA, GEN:AOT and GEN:SDS complex loaded nanoparticles, respectively. This data aligns with previously reported results of ion paired GEN encapsulation into PLGA nanoparticles reaching around 100% entrapment efficiency [178,280,321]. Additionally, similar LC% values were also reported [321].

### 3.3.4. *In vitro* drug release profiles of GEN:HIP loaded PLGA nanoparticles

*In vitro* drug release profiles of GEN:HIP loaded formulations were investigated to observe whether complexation of GEN into a HIP complex, as well as encapsulation into polymeric nanoparticles, provides a sustained drug release of this highly hydrophilic drug. Firstly, UNP-GEN diffusion rate out of dialysis bag was established in 3 different release media: PBS pH = 7.4, PBS pH = 4.5 and AU pH = 4.5. As mentioned previously in **section 3.3.2.3.**, lower pH of 4.5 was included in the *in vitro* drug release assay to examine whether pH below pKa of a counterion can trigger complete dissociation of GEN:OA complex. Additionally, as the envisioned site of action for these formulations is urinary bladder, acidic pH conditions are needed to improve mucoadhesive properties of chitosan coated nanoparticles, which are further explored in **Chapter 4** to enhance nanoparticle retention time in the bladder. Therefore, based on the application intended for these formulations, our goal was to ensure that drug release properties are not crucially affected by change in pH. In addition, AU was used as a release medium option to mimic release conditions in the bladder.

Results of drug release profiles of UNP-GEN, that was solubilised in MQW, in different release medias are reported in **Figure 3.8**. GEN demonstrates 100% release from dialysis bag in both PBS pH = 7.4 and pH = 4.5 buffers within 4 hours, showing almost identical drug release profiles. As GEN is freely soluble in water, it is expected to fully diffuse out of the dialysis bag in a burst effect. However, it appears that GEN diffusion rate through the membrane is controlled by the permeation rate of the drug through the dialysis membrane, which reportedly has been shown to slow down the release kinetics of the drug release studies [274,325]. Despite these limitations, drug release studies using dialysis membrane have been widely used to

observe drug release kinetics *in vitro* and can be still used effectively when comparing the drug release profiles between formulations, as well as obtaining relevant controls [274].

UNP-GEN failed to reach 100% release in AU pH = 4.5, at 4 hours demonstrating peak of 88.4 ± 7% of UNP-GEN released. The reason why GEN fails to achieve complete diffusion out of dialysis bag is unknown, as GEN was observed to be freely soluble in AU buffer. However, it could be attributed to GEN degradation in AU over time, additional bi-product formation that interfere with GEN diffusion through dialysis bag, or with GEN quantification by HPLC assay.

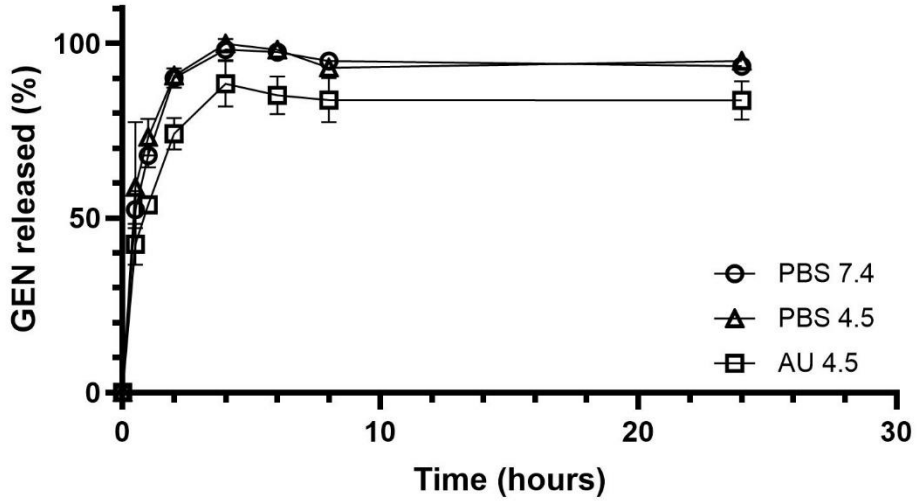


**Figure 3.8:** *In vitro* UNP-GEN release from UNP-GEN solution (drug dissolved in MQW) in different buffers, incubated 24 hours using dialysis bag, at 37 °C degrees and shaking at 100 RPM. Error bars represent the SD and n = 3.

Afterwards, release of GEN from GEN:HIP complexes were investigated in the same 3 buffers, with 1.71M of NaCl included to enhance the dissociation of drug and counterions. Based on results reported in **section 3.3.2.3.**, dissociation studies have showed only 48.7% to 63.2% dissociation of GEN from its HIP complexes. This could be an issue observed in *in vitro* drug release studies if almost half of the drug is being trapped inside of a complex unable to be released. Despite this, all 3 GEN:HIP complexes demonstrated around 90% to 100% release of GEN after dissociation from its HIP complex in PBS at acidic and neutral conditions as shown in **Figure 3.9**. The only instant where GEN release was different between PBS pH = 7.4 and PBS = 4.5 buffers was observed in GEN:SDS samples, where less GEN was released in acidic conditions. In contrast, GEN:OA complex demonstrated a burst release in the first 2 hours in

PBS pH = 4.5 buffer, which was not observed when the same complex was incubated in PBS pH=7.4 buffer. However, overall GEN release did not show many differences between different pH conditions of PBS. When comparing these GEN:HIP release profiles to UNP-GEN release shown in **Figure 3.8**, a sustained release of GEN can be observed when the drug is coupled with a counterion. While UNP-GEN control was fully released in PBS pH = 7.4 and PBS pH = 4.5 within 4 hours, the drug released from GEN:HIP complex reached almost 100% after 8 to 24 hours. Therefore, coupling GEN into a HIP complex can be beneficial in order to sustain drug release by at least several hours, compared to fast free drug diffusion rate.

GEN release from GEN:HIP complexes in AU pH = 4.5 was recorded at around 60% even after 14 days (not shown), since demonstrating a plateau after 48 hours. Incomplete GEN release was previously observed when measuring how fast UNP-GEN diffuse out of the dialysis bag into AU release media (**Figure 3.8**). Although the reason why full release of the drug cannot be achieved in this release media is unknow, several theories were considered.

Firstly, we questioned whether NaCl in the release media failed to facilitate full dissociation of GEN:HIP complex due to complex chemical composition of AU. Dissociation of GEN from ion paired complex was previously discussed in **section 3.3.2.3.**, where that amount of GEN that dissociated from its counterion was similar in all three buffers used: PBS pH = 7.4, PBS pH = 4.5 and AU pH = 4.5. As shown in **Figure 3.9**, full GEN dissociation from GEN:HIP complex was achieved in PBS pH = 7.4 and PBS pH = 4.5, which included 1.71M of NaCl, therefore complete dissociation of GEN was also expected in AU pH = 4.5 with additional NaCl. However, as mentioned above, only 60% of GEN was released after 14 days in AU pH = 4.5. Since NaCl concentration in all buffers were the same, and previous experiments showed similar dissociation results of GEN:HIP complexes in all buffers, it seems unlikely that difference in chemical composition of release buffers had such an impact on dissociation of the GEN:HIP complex and release of GEN. Alternatively, wide chemical composition of AU buffer could have resulted in potential GEN degradation over time. This, however, was not investigated further. Finally, failure to fully release drug could be attributed to additional complexes being formed between GEN and chemicals that comprise AU, which could affect how the drug is derivatized and then analysed in HPLC. In this instance, the drug could be dissociated from the GEN:HIP complex and fully released in the media, but not correctly measured due to interference with quantification process. Although we hoped to demonstrate more therapeutically relevant GEN release profiles by mimicking a more accurate release

medium, based on the limitations observed in the results, AU buffer was deemed unusable for the present study. Further research could provide insight on why GEN failed to release fully in AU buffer, as well as potentially eliminate previously discussed limitations of using this release media.

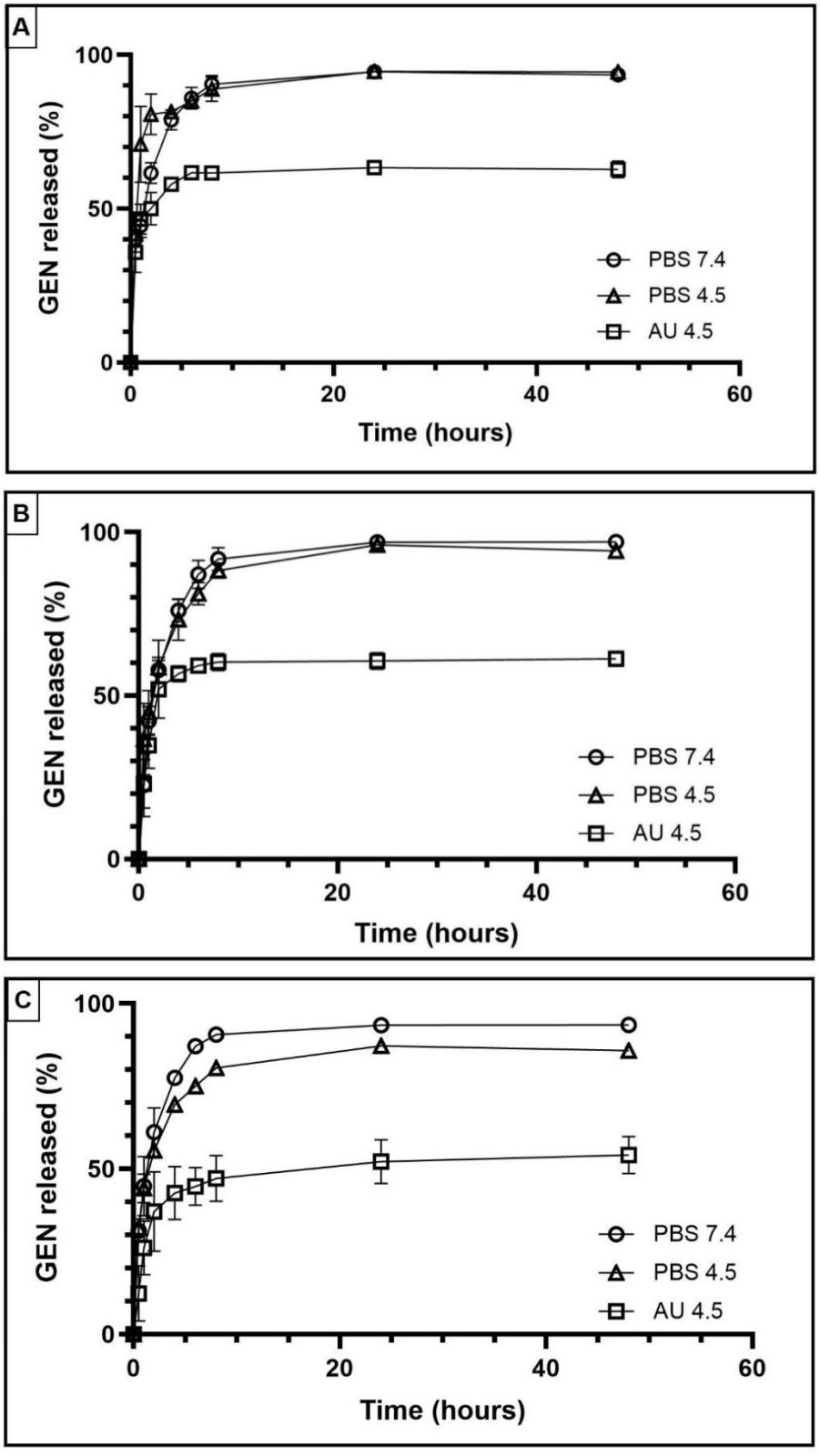


**Figure 3.9:** Cumulative *in vitro* GEN release from (A) GEN:OA (B) GEN:AOT (C) GEN:SDS complexes in PBS pH = 7.4, PBS pH = 4.5 or AU pH = 4.5 release media, over 48 hours using dialysis bag method, incubated at 37 °C degrees and shaking at 100 RPM. Error bars represent the SD and n = 3.

PBS buffer at pH = 4.5 was selected as a final release medium, due to acidic pH needed to trigger GEN:OA complex dissociation, as well as enhanced mucoadhesive properties that would be tailored to these formulations in the future. These requirements suggest that in order to achieve the right conditions *in vivo*, a bladder pre-treatment with acidic solution might be necessary to remove residual urine and establish the right pH conditions for efficient treatment.

The next step was to investigate concentration of NaCl used in release media in order to facilitate dissociation of the GEN:HIP complexes. Based on preliminary dissociation study performed in **section 3.3.2.3.**, highest concentration of salt showed best dissociation results. However, with highest concentration of NaCl used in release media, GEN:HIP complexes achieved their full release within 24 hours, mainly releasing most of GEN by 6 hour mark. When comparing this data to UNP-GEN release, this demonstrates a small sustained effect on GEN release just by ion pairing GEN into a GEN:HIP complex. However, we hypothesize that release could be sustained more by reducing concentration of salt in the release medium to reduce or slow down dissociation.

Results presented in **Figure 3.10** and **Figure 3.11** demonstrate that reduction of NaCl concentrations to 1 M instead of 1.71 M helps to reduce initial burst effects, however lower concentrations of salt also reduce overall amount of GEN released. Reduction in salt concentration in release medium has reduced burst effect from 88.3 ± 2% to 44 ± 3% of GEN released from GEN:AOT, and from 80.5 ± 1% to 48.5 ± 1% of GEN released from GEN:SDS in the first 8 hours of the assay. However, overall GEN released after 7 days of incubation has also dropped once 1 M of NaCl was used, with GEN:AOT samples demonstrating total 65 ± 2% of GEN released, while GEN:SDS showed 65.2 ± 1% of GEN released. With 1.71M of NaCl used in release media, complexes GEN:AOT and GEN:SDS reached total of 93.3 ± 3% and 91.9 ± 1%, respectively, of GEN released after 7 days, overall releasing roughly 30% more drug than with 1 M NaCl in PBS buffer. Based on this data, 1.71 M of NaCl was chosen for further drug release assays for complexes GEN:AOT and GEN:SDS.

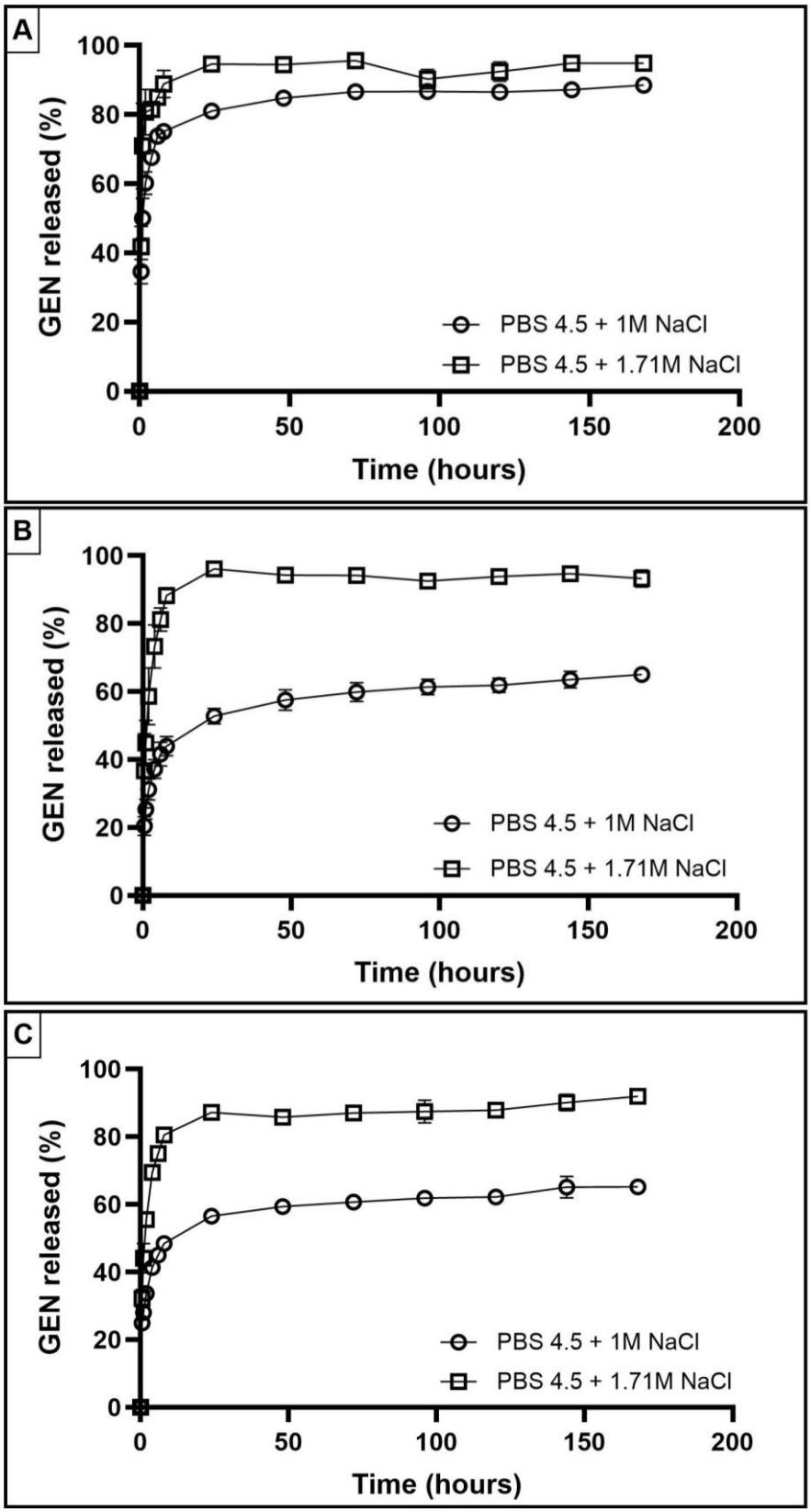


**Figure 3.10:** Cumulative *in vitro* GEN release from (A) GEN:OA (B) GEN:AOT (C) GEN:SDS complexes in PBS pH = 4.5 with different concentrations of NaCl, over 7 days using dialysis bag method, incubated at 37 °C degrees and shaking at 100 RPM. Error bars represent the SD and n = 3.

Focusing on the results of GEN:OA release, decrease in salt concentration did show a small reduction in overall GEN released in 7 days of the assay, however the reduction was much smaller than in the other two GEN:HIP complexes. Initial burst effect of GEN:OA samples was reduced from 88.9 ± 4% to 75.2 ± 1% of GEN released within the first 8 hours when salt concentration was reduced from 1.71 M to 1 M. Importantly, overall GEN released from GEN:OA complex after 7 days of the assay was very similar for both salt concentrations – 94.9 ± 2% when 1.71 M NaCl was used, and 88.5% when 1 M NaCl was used. The reason why reduction of salt did not impact GEN:OA release profiles as much as it did for GEN:AOT and GEN:SDS could be due to acidic pH below the pKa of OA used, which helped to protonate counterion and dissociate it from the drug complex. Due to small drug release profile differences observed between NaCl concentrations in release media, 1 M concentration of NaCl was selected for further experiments of GEN:OA release in order to reduce initial burst effect.

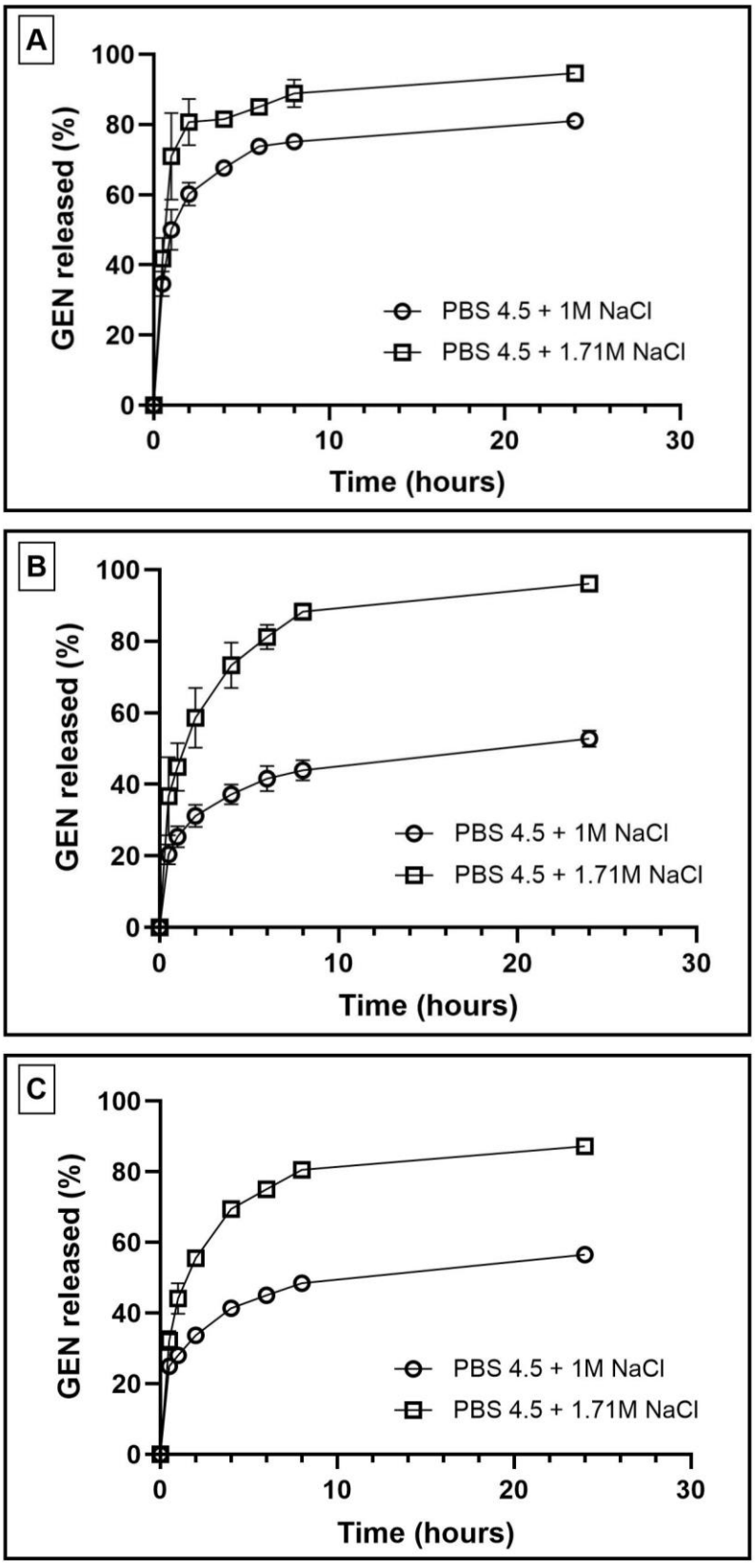


**Figure 3.11:** Cumulative *in vitro* GEN release from (A) GEN:OA (B) GEN:AOT (C) GEN:SDS complexes in PBS pH = 4.5 with different concentrations of NaCl, over the first 24 hours using dialysis bag method, incubated at 37 °C degrees and shaking at 100 RPM. Error bars represent the SD and n = 3.

Finally, GEN:OA, GEN:AOT and GEN:SDS complexes were encapsulated into polymeric nanoparticles and their drug release profiles were investigated in PBS pH = 4.5 buffer with additional NaCl. Results presented in **Figure 3.12** demonstrate that less than 10% of GEN is being released from GEN:HIP complex loaded PLGA nanoparticles over 7 days. The same formulations were checked at 1 month, 10 week and 6 month time points and no increase in GEN concentration in PBS was recorded. While the reason for poor GEN release from GEN:HIP loaded PLGA nanoparticles is unknown and requires further investigation, we hypothesised that GEN:HIP complexes might not be fully loaded into the polymeric nanoparticles, despite the high EE% and LC% values presented in **section 3.3.3**. This could occur due to potential limitations in nanoparticle preparation method. As described in **section 3.2.4.**, GEN:HIP complex was pre-formed prior to entrapment into polymeric nanoparticles. Due to hydrophobicity of the complex, it is likely that precipitation of the complex has started before this phase was added to the organic phase, which could have impacted the complex loading into the PLGA nanoparticles. However, it is important to stress that this hypothesis have not been confirmed and thus requires a further investigation.

In the event that GEN:HIP complex loading in the PLGA nanoparticles was affected by limitations in selected nanoparticle preparation method, the reason behind potential discrepancy between poorly loaded nanoparticles and high EE% and LC% values needs to be addressed. Indirect assay to quantify the GEN encapsulated in nanoparticles rely on measurement of free, unencapsulated GEN, from which a theoretical calculation of the amount of GEN inside of nanoparticles can be made. Nanoparticles and free unencapsulated drug are separated by centrifugation, where nanoparticles sediment into a pellet, while free drug remains dispersed in the supernatant. Therefore, based on the principle of the indirect assay, the true drug content within the pellet remains unknown. Measurement of precise GEN amount in supernatant becomes especially challenging when formulation includes surfactants and stabilisers, as they could form micelles and entrap GEN inside of very small nano-sized vehicles which do not sediment into a pellet when centrifuged. Additionally, based on the HIP binding efficiency discussed in **section 3.3.2.1.**, at least 90% of GEN should be ion paired, meaning that if the complex is not encapsulated into PLGA nanoparticles, it would still precipitate into the pellet due to its hydrophobicity. This means that less than 10% of UNP-GEN remains in the supernatant, which in turn leads to high EE% and LC% values. Therefore, the accuracy of indirect quantification assay seems to suffer when more complicated

nanoparticle systems are involved, as drug content is distributed in different forms within the nanoparticle solution. For more precise results, new EE% values were calculated based on the *in vitro* drug release data of GEN:HIP loaded nanoparticles. As shown in **Table 3.2**, the EE% values obtained from indirect assay (**section 3.3.3.**) and EE% based on *in vitro* drug release (**Figure 3.12**) demonstrate significantly different results. Although most studies use direct assay for drug quantification, as pellet of centrifuged PLGA nanoparticles can be dissolved and drug can be solubilised in a solvent to then be used for quantification analysis [326], GEN is not soluble in any solvents that could dissolve PLGA.

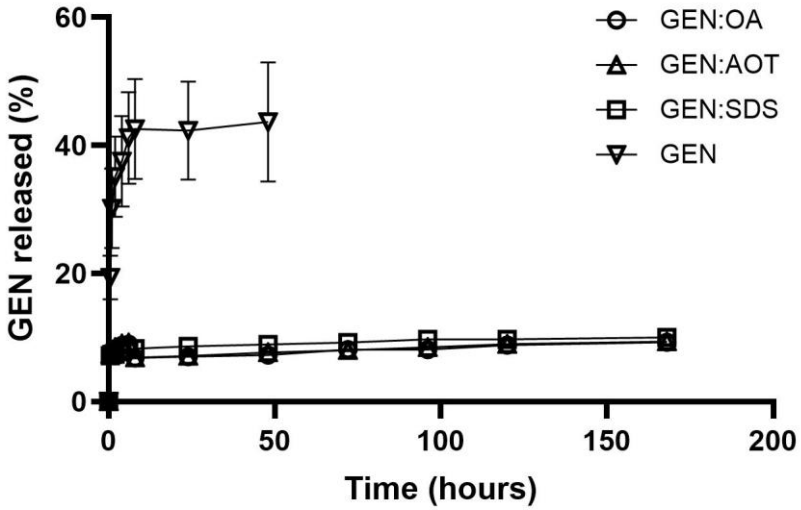


**Figure 3.12:** Cumulative *in vitro* GEN release from UNP-GEN loaded PLGA nanoparticles in PBS pH = 4.5 over 48 hours. In addition, cumulative GEN release from GEN:OA, GEN:AOT, and GEN:SDS complex loaded PLGA nanoparticles in PBS pH = 4.5 (with release media containing 1 M NaCl for GEN:OA, and 1.71 M NaCl for GEN:AOT and GEN:SDS) over 7 days using dialysis bag method, incubated at 37 °C degrees and shaking at 100 RPM. Error bars represent the SD and n = 3.

Alternatively, another hypothesis as to why GEN:HIP demonstrated poor drug release data was considered. We hypothesised that perhaps no GEN is being released from its complex and/or polymeric nanoparticles, however data presented in this section, as well as dissociation results shown in **section 3.3.2.3.**, demonstrate that GEN can successfully dissociate from its HIP complex in selected medium. Additionally, control formulation of UNP-GEN loaded PLGA nanoparticles demonstrated an increasing amount of GEN released over 48 hours, demonstrating successful drug release out of obtained PLGA nanoparticles (**Figure 3.12**).

Despite that, in order to reject the hypothesis that GEN is trapped inside the polymeric nanoparticles or in its GEN:HIP complex that is encapsulated into PLGA nanoparticles, samples were left to incubate for 6 months, after which PLGA is expected to fully degrade [327,328]. Usually, 1 to 6 months are reportedly needed for PLGA degradation to complete, depending on ratio of lactic to glycolic acid used [327,328]. GEN concentrations in the release media were measured after 1 month, 10 weeks and 6 months to observe whether degradation of PLGA has any impact on drug release. Even after 6 months of incubation, total of GEN released from GEN:HIP loaded PLGA nanoparticles was still below 10%. Based on all collected data and literature research, it was concluded that < 10% of GEN was entrapped into the polymeric nanoparticles.

In contrast, several studies reported *in vitro* drug release profiles of GEN:AOT loaded polymeric nanoparticles. Imbuluzqueta et al., 2011 demonstrated 100% of GEN released over 70 days from GEN:AOT complex loaded PLGA nanoparticles [280], while Rotman et al., 2020 demonstrated over 60% of GEN released from GEN:AOT complex encapsulated into polymeric microspheres over 2 week period [329]. Similarly, study by Kwiecien et al., 2022 reported over 60% of GEN released from encapsulated GEN:AOT complex into PLGA nanoparticles over 5 to 6 days, after which the release seem to stabilise and plateau [321].

**Table 3.2:** Amount of GEN present in UNP-GEN loaded and GEN:HIP loaded PLGA nanoparticles based on results from drug release assay. In addition, new EE% values, that are based on drug release data, are presented and compared to the values first reported in **section 3.3.3.**

| **Nanoparticle formulation** | | | **Amount of GEN released after 7 days (mg)** | **EE% based on drug release (after 7 days)** | **EE% based on indirect assay and HPLC quantification** |
|---|---|---|---|---|---|
| **GEN concentration (mg)** | **Counterion** | **Drug to counterion mol ratio** | | | |
| 5 | OA | 1:5 | 0.44±0.01 | 8.8±0.2% | 90.9±5% |
| | AOT | 1:3 | 0.46±0.01 | 9.3±0.2% | 98.6±1% |
| | SDS | 1:3 | 0.48±0.02 | 9.5±0.4% | 90.8±2% |

Looking at the data presented in **Figure 3.12**, it is important to mention, that UNP-GEN loaded PLGA nanoparticles showed 43.7 ± 9% of GEN released over 48 hours, demonstrating a plateau after hour 8 time point. Although the assay was not continued afterwards, a plateau of GEN release for at least 24 hours indicates that no more of the hydrophilic drug was expected to release. Due to high hydrophilicity of GEN, a small reduction in the burst effect and somewhat sustained release of the drug was expected due to encapsulation of the drug into polymeric nanoparticles, as previously reported [182,330]. A plateau after initial burst of around 50% was observed by Kwiecien et al., 2022, with no increase in released GEN observed for the remaining weeks of the study [321]. In contrast, multiple studies demonstrate a sustained release of encapsulated GEN into PLGA nanoparticles that does not include a burst effect and takes at least 7 days or more to reach 100% release from the polymeric nanoparticles [121,296,297,323]. However, these results do not align with results reported in present study, as based on hydrophilic nature of GEN, a fast drug release profiles are expected in sink conditions.

Some might argue that sustained release of antibiotics in the bladder could only contribute to the problem of AMR due to subtherapeutic concentrations of antibiotic exposure to the bacteria [279]. In order to achieve therapeutical concentrations of GEN inside the bladder, much higher drug loading would need to be achieved first, as well as bulking up the nanoparticle concentration in the solution. However, with emerging trials of using free GEN solution instillation in high doses to instantly kill the bacterial infection [78–85], our mucoadhesive formulations containing encapsulated antibiotic could ensure prophylactic monitoring and prevention of recurrent infection in the bladder for the following days after initial GEN solution instillation.

### 3.3.5. Antimicrobial sensitivity assays

For antimicrobial sensitivity assay *E. Coli* ER2738 strain was selected. This project focuses on treatment of UTIs, which are most commonly caused by UroPathogenic *E. Coli* (UPEC) [29]. Although ER2738 strain is not considered to be UPEC, a *E. Coli* strain was selected for the study. Antimicrobial susceptibility of GEN:HIP complexes or PLGA nanoparticles, loaded with either UNP-GEN or GEN:HIP complexes, was measured by broth micro-dilution method carried out against *E. Coli* to identify minimum inhibitory concentrations (MIC) of formulations tested. For this experiment, 10ml of each nanoparticle formulation was

concentrated to 400 µl, to ensure that 50 µl of nanoparticle solution contained enough drug to calculate MIC value. Concentrating of the sample was done by collecting nanoparticles in a pellet, removing the supernatant and then resuspending nanoparticles in 400 µl of MQW. Achieved drug concentrations of the samples presented in **Table 3.3**.

For this assay, concentrations of GEN in each formulation were determined based on the data acquired during *in vitro* drug release assays, as presented in **Figure 3.12** from **section 3.3.4**. Each formulation concentration was based on the amount of GEN released in PBS buffer (including high concentrations of salt for GEN:HIP loaded PLGA nanoparticles) after 24 hours at 37 °C degrees, 100 RPM (**Table 3.3**). Due to the nature of the assay, where MIC is calculated from freshly prepared nanoparticles containing full amount of the encapsulated drug, theoretical entrapped drug concentration data was used.

**Table 3.3:** Starting concentrations of GEN in UNP-GEN or GEN:HIP complex loaded PLGA nanoparticle formulations, which were used for antimicrobial sensitivity assay. Nanoparticle solutions were concentrated from 10 ml to 400 µl. Original GEN concentrations in nanoparticle formulations were obtained from *in vitro* drug release assay (results shown in **Figure 3.12** of **section 3.3.4**).

| **Nanoparticle formulation** | | | **Starting concentration of GEN inside PLGA nanoparticles calculated from drug release data (mg/ml)** |
|---|---|---|---|
| **GEN amount (mg)** | **Counterion** | **Drug to counterion mol ratio** | |
| 5 | N/A | N/A | 1.7±0.2 |
| | OA | 1:5 | 0.8±0.1 |
| | AOT | 1:3 | 0.9±0.0 |
| | SDS | 1:3 | 1.0±0.1 |

After 24 hours of formulations being incubated with bacteria, the resulting MICs were reported in **Table 3.4**. GEN dissolved in water was used as a control, so its effectiveness against *E. Coli* could be used as comparison for encapsulated UNP-GEN or GEN in HIP complexes. Additionally, ampicillin (AMP) dissolved in water was used as a control of another antibiotic that also inhibits *E. Coli* growth. Blank PLGA nanoparticles were also used as control to

demonstrate that blank nanoparticles do not show any antimicrobial properties and no inhibition of bacterial growth is observed. Most of the PLGA nanoparticle formulations showed higher MIC values than MIC of unencapsulated UNP-GEN or unencapsulated GEN:HIP complexes. This seems to indicate that entrapment of GEN into polymeric nanoparticles reduces its antimicrobial efficacy. Similar effects have been observed in studies Sun et al., 2021 and Abdelghany et al., 2012, where encapsulation of GEN into PLGA nanoparticles has led to decreased effectiveness in preventing bacterial growth [121,330]. On the contrary, studies by Dorati et al., 2018 and Dhal et al., 2019 demonstrated that encapsulation of GEN either had no effect on its effectiveness against different bacterial strains or showed lower MIC values then unencapsulated GEN [182,296]. Results obtained from present study shows no data to support this statement.

Interestingly, nanoparticles encapsulating GEN in a HIP complex showed lower MIC than UNP-GEN encapsulated into PLGA nanoparticles, which could indicate that GEN in HIP complex improves the antimicrobial properties of the drug. This was confirmed by measuring MIC values of GEN:OA and GEN:SDS complexes against *E. Coli*, where resulting MICs were significantly lower than MIC of UNP-GEN. Similar observations were reported by Ter Boo *et al.*, 2015 and Rotman *et al.*, 2020, where they observed that GEN:AOT complex was more efficient in killing *Staphylococcus aureus* and *Staphylococcus epidermidis* than the UNP-GEN, which they hypothesised could be due to anionic AOT destabilising the bacterial membrane [329,331].

**Table 3.4:** MIC of nanoparticles loaded with UNP-GEN, GEN:OA complex, GEN:AOT complex, GEN:SDS complex, as well as GEN:HIP complexes without being loaded into nanoparticles, UNP-GEN solution and AMP solution against *E. Coli*. NPs = nanoparticles.

| **Sample name** | **Organism** | **MIC (µg/ml)** |
|---|---|---|
| Blank NPs | *Escherichia Coli* ER2738 | N/A |
| UNP-GEN loaded NPs | | 108.8 |
| 1:5 GEN:OA loaded NPs | | 13.1 |
| 1:3 GEN:AOT loaded NPs | | 54.9 |
| 1:3 GEN:SDS loaded NPs | | 63.9 |
| 1:5 GEN:OA complex | | 2.4 |

| | | |
|---|---|---|
| 1:3 GEN:AOT complex | | 19.5 |
| 1:3 GEN:SDS complex | | 4.9 |
| 1 mg/ml UNP-GEN solution | | 7.8 |
| 1 mg/ml AMP solution | | 7.8 |

Most of previous literature examining how HIP affects antimicrobial properties of an antibiotic drug that is encapsulated into polymeric nanoparticles are focused on GEN and AOT complex [178,280,321,329,331,332]. Studies by Imbuluzqueta *et al.*, 2011 and 2013 report that GEN coupled with AOT has enhanced effectiveness of the drug against *Brucella melitensis*, but also encapsulation of GEN:AOT complex into PLGA nanoparticles improved its efficacy against bacterial strain even more than just GEN:AOT complex [178,280]. Results from study by Kwiecień *et al.*, 2022 agreed with Imbuluzquenta *et al.*, as enhanced inhibition zone against *S. aureus* was reported with GEN:AOT loaded PLGA nanoparticles, compared to UNP-GEN loaded nanoparticles [321]. Therefore, results from the present study agree with prior literature as nanoparticles encapsulating GEN:OA, GEN:AOT or GEN:SDS complexes showed much lower MIC than UNP-GEN loaded PLGA nanoparticles [178,280,321].

### 3.3.6. Histology and toxicity studies

Adverse effects of UNP-GEN and GEN:HIP loaded PLGA nanoparticles were examined on freshly excised porcine bladder tissue. Porcine bladders were collected from a local abattoir, dissected in the lab and treated with 400 µl of each nanoparticle formulation. Tissues were fixed, embedded in paraffin and sectioned. Following dehydration process and H&E staining, then rehydration and tissue preparation for microscope analysis, samples were observed under the microscope for any pathological changes in urothelium tissue. Resulting histology images can be observed in **Figure 3.13**.

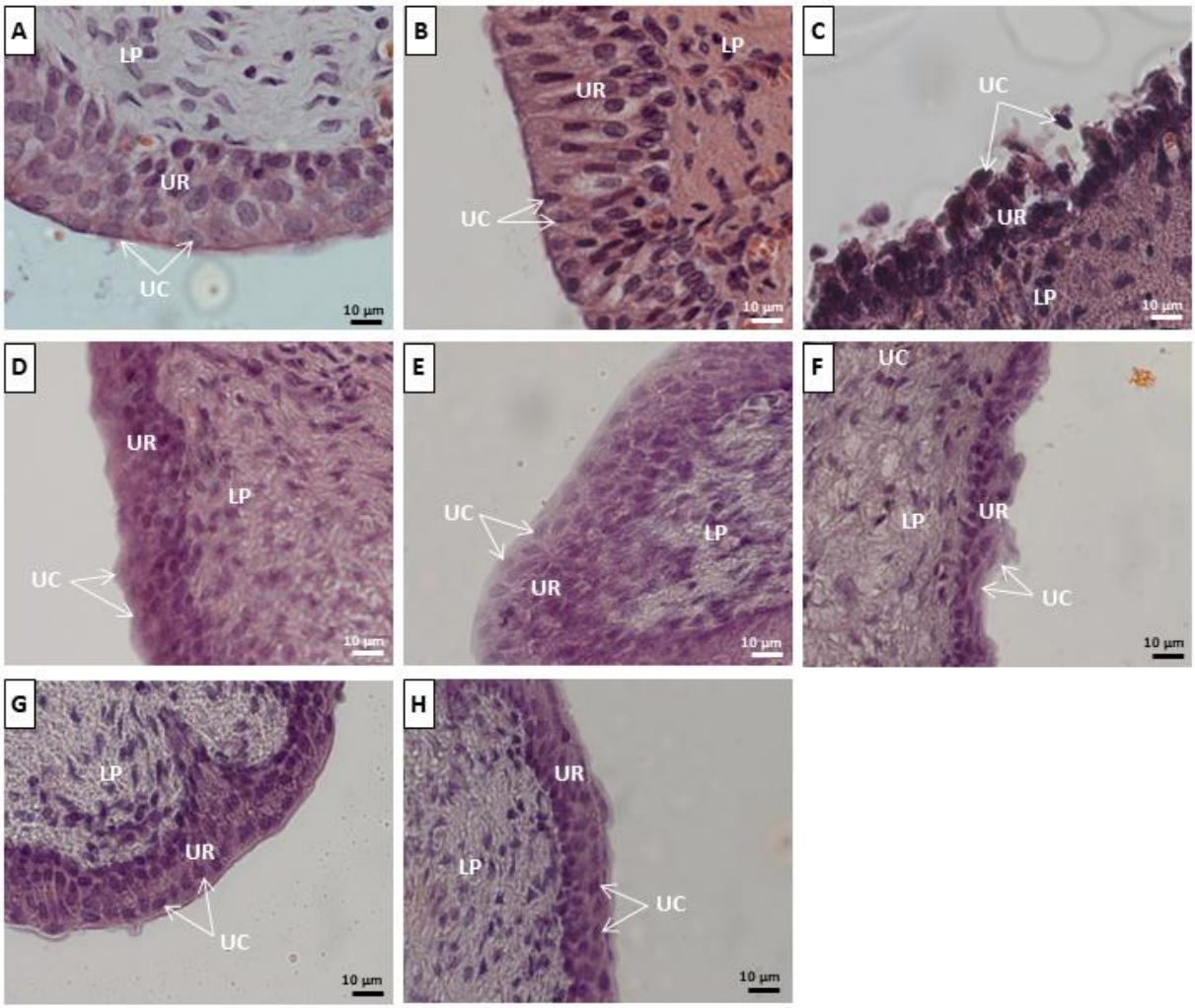


**Figure 3.13:** Microscopic images of H&E stained porcine bladder tissue sections of 8 µm thickness. Images demonstrate freshly excised porcine bladder tissues that (A) were stored at 4 °C during transportation, (B) followed the washing and incubation at 37 °C procedure, but did not undergo any treatment, (C) were treated with 10 mg/ml protamine sulphate (PS) in PBS pH = 7.4 resulting in urothelium desquamation. Images also show tissues treated for 1 hour at 37 °C with (D) blank PLGA nanoparticles, and PLGA nanoparticles encapsulated with (E) UNP-GEN, (F) 1:5 GEN:OA complex, (G) 1:3 GEN:AOT complex, (H) 1:3 GEN:SDS complex. Scale bar denotes 10µm, UC = umbrella cells, UR = urothelium, LP = lamina propria.

In a healthy bladder, a tightly packed layer of urothelium can be observed, with umbrella cells and uroplakins forming an apical membrane plaque which acts as impermeable barrier [4]. Additionally, tight junctions and adherens junctions within cells of urothelium layer form a paracellular permeability barrier [4]. To confirm no adverse changes in urothelium layer that could have been caused during bladder excision or transportation, porcine bladder tissues were kept on ice while other tissues undergone treatment and were used as negative control (**Figure**

**3.13A**). Additionally, no pathological changes were observed in tissues that had undergone process of treatment, such as washing with PBS and incubation at 37 °C without treatment administration, confirming no harm caused by treatment procedure alone (**Figure 3.13B**). Intentional harm to urothelium layer was caused by 1 hour treatment of 10 mg/ml protamine sulphate (PS), after which destruction of tight junctions and adherens junctions was observed (**Figure 3.13C**), leading to desquamation of urothelium cells and damaged structural integrity of the permeability barrier [333]. Finally, formulations of UNP-GEN, 1:5 GEN:OA, 1:3 GEN:AOT, or 1:3 GEN:SDS loaded PLGA nanoparticles were tested on the porcine urothelium, with no toxicity observed after 1 hour treatment (**Figure 3.13D-H**). Although urothelium lining shown in **Figure 3.13F** appears non-uniform, it is likely that this can be attributed to artefacts, as umbrella cells of the layer seem to be intact.

GEN is known to cause ototoxicity, which causes damage to the inner ear, and nephrotoxicity, which affects the kidneys [248]. However, as the treatment proposed in present study would be applied directly to bladder, side effects of the drug are significantly reduced due to limited systemic adsorption of the drug [79]. Multiple studies have shown off-label treatment of UTIs by GEN instillation through intermittent catheters, which have successfully treated bacterial infections without any toxic effects reported [79,81,334]. As for counterions, no reports of toxicity were reported for OA, AOT and SDS for use in bladder, however some toxicity were reported when counterions were used systemically. For instance, OA was mentioned to be safe and non-toxic [309,335,336], however some publications mention that it can permeate skin or disrupt cell membranes [309,337]. AOT showed toxicity during *in vitro* haemolysis assay [338], but demonstrated no toxicity on Caco-2 cells [306]. SDS was reported to cause skin and respiratory irritation [339]. However, most of these side effects are linked to cases where surfactants would have systemic exposure, which is unlikely to happen if they are administered through intravesical route.

PLGA nanoparticles have been deemed safe to use for drug delivery in human body by Food and Drug Administration (FDA) [90]. During preparation of nanoparticles, PVA was used to stabilise the emulsions and prevent particle aggregation [136]. Cytotoxic effects on lung cells have been reported with high concentrations (>1 mg/ml) of PVA used or after prolonged treatment time [136,169]. However, the challenge of removing PVA from nanoparticle formulations has been widely documented, as PVA permanently attaches to the nanoparticle surface due to hydrophobic bonding of partially hydrolysed PVA and PLGA acetyl groups

[169,170]. Despite this, multiple studies have reported that PLGA nanoparticles synthesised with PVA were safe for use [170,340,341], as well as toxicity studies in present study demonstrated no indication of harm to urothelium tissue when 2% PVA concentration was used in PLGA nanoparticle formulations. As obtained nanoparticle formulations would be administered directly to bladder, no systemic toxicity is expected from residual PVA in the samples.

## 3.4. Conclusion

GEN was ion paired with counterions OA, AOT and SDS to form HIP complexes, with counterions AOT and SDS showing highest binding efficiency to the drug. DSS was also examined as a potential counterion to form GEN:HIP complex with, however it was quickly discovered that DSS seems to interfere with HPLC assay of GEN quantification, therefore the use of DSS was not pursued further. GEN:OA complex showed best dissociation values in high salt buffer in acidic pH, however only 63% of the drug was found to be dissociated, showing concern for its performance in therapeutical release medium.

Prepared GEN:OA, GEN:AOT and GEN:SDS complexes were then encapsulated in PLGA nanoparticles. Results of EE% showed almost 90% to 100% of the complexes being encapsulated into polymeric nanoparticles, which was significantly higher compared to 33% of UNP-GEN encapsulated into PLGA nanoparticles. However, once the drug release profiles of these nanoparticles were observed, results suggested that less than 10% of the GEN:HIP complexes were loaded into polymeric nanoparticles. Based on the data collected, it seems that indirect method of GEN quantification, as well as nanoparticle preparation method demonstrate some limiting factors resulting in potentially questionable EE% values. Due to the poor drug loading, no conclusions could be made on sustained drug release when GEN:HIP was encapsulated into PLGA nanoparticles. On the other hand, UNP-GEN loaded nanoparticles demonstrated 43% of the drug released within 48 hours, which could suggest a burst effect within the first 8 hours, and much slower incline in drug release after that. Indication of sustained release was observed in unencapsulated GEN:HIP complexes, which dissociated most of GEN within 6 hours of the assay in PBS with highest salt concentration. Tailoring salt concentration could reduce initial burst effect and slow down the release of GEN, which was observed in GEN:OA complex where reduction of salt concentration in release media lead to most of GEN being released in 24 hours.

Antimicrobial sensitivity assay showed that encapsulation of UNP-GEN or GEN:HIP complexes into PLGA nanoparticles diminishes antimicrobial properties of the drug. Interestingly, GEN in an ion paired complex performed better in inhibiting bacterial growth than UNP-GEN, which suggests that ion pairing of GEN enhances antimicrobial properties of the drug.

Based on the results of this study, GEN:HIP application shows a lot of promise in terms of sustained drug release and enhanced drug antimicrobial properties. Although encapsulation of ion paired GEN into PLGA nanoparticles was challenging, perhaps other drug carrier types, such as nanoparticles made of other materials than polymers, or *in situ* forming gels, should be investigated to enhance true potential of using ion paired GEN to treat UTIs through intravesical route.

# Chapter 4

## *In vitro* and *ex vivo* evaluation of chitosan-coated PLGA nanoparticles for intravesical drug delivery

## 4.1. Introduction

Bladder infections and other bladder disorders are mostly treated via systemic administration of drugs, which leads to more prominent side effects and diminished concentrations of drug reaching the target site [2]. Hence, intravesical drug delivery (IDD) has been extensively researched and used in practise for bladder disorders, as it directly instils the pre-determined dosage to the bladder, significantly reducing side effects of therapeutic agents, and lowers the risk of antimicrobial resistance during antibiotic treatment [2,9]. To improve drug retention time in the bladder and prevent its expulsion through bladder voiding, mucoadhesive nanoparticles have been widely researched [222,230,342,343].

Poly(lactic-co-glycolic acid) (PLGA) nanoparticles have been extensively studied for IDD, due to their high drug loading, enhanced bioavailability, relatively short biodegradation time and approval of PLGA for drug delivery use by U.S. Food and Drug Administration (FDA) [136,344]. Additionally, PLGA nanoparticles can be easily synthesised by several conventional preparation methods [101,115]. Changes in formulation composition can be used to manipulate physicochemical characteristics of the nanoparticles, including enhanced drug loading and controlled drug release rate [9,344]. Use of chitosan has been shown to change particle charge from anionic to cationic, therefore allowing nanoparticles to establish electrostatic interactions with negatively charged mucosal surfaces, resulting in prolonged retention time at the target site [9,244,345]. However, it was proposed that these interactions can depend on the type, concentration and molecular weight (MW) of chitosan that was used for nanoparticle coating, as well as other factors, such as pH and other surface coatings [112,224]. Hence, the work described in this chapter aims to obtain colloidally stable, nanosized polymeric nanoparticle formulation exhibiting highly positive zeta potential values that indicate strong mucoadhesive properties.

The objectives of this chapter are:

- To study the impact of formulation parameters, such as type, concentration and MW of chitosan, as well as concentration of surfactant, on the physicochemical characteristics, such as size, polydispersity index, and particle charge, of mucoadhesive polymeric nanoparticles.
- To investigate pH dependency of mucoadhesive properties of chitosan coated PLGA nanoparticles.

- To measure mucoadhesive properties of mucoadhesive polymeric nanoparticles *in vitro* and *ex vivo*, as well as compare the results of both assays.
- To evaluate toxicity and mucopenetrative properties of mucoadhesive polymeric nanoparticles on *ex vivo* porcine bladder tissue.

## 4.2. Materials and methods

### 4.2.1. Materials

Poly(lactic-co-glycolic acid) (PLGA, 50:50 ester terminated, MW 38,000–54,000 Da), low MW chitosan (50-190 kDa, deacetylated chitin) (CS-L), medium MW chitosan (190–310 kDa, deacetylated chitin) (CS-M), high MW chitosan (310-375 kDa, deacetylated chitin) (CS-H), coumarin-6 (C6), protamine sulphate (PS), mucin from porcine stomach (type II), artificial urine diluent, phosphate buffer saline (PBS), 10% neutral buffered formalin, Mayer's haematoxylin solution, Eosin Y solution (aqueous), glacial acetic acid, acetonitrile (HPLC grade) (ACNT), and ethanol (EtOH) were all purchased from Sigma-Aldrich (Merck Life Science, UK). Kolliphor® P 407 Geismar was obtained from BASF (BASF, UK). Carboxymethyl chitosan (80% deacetylation, water soluble chitosan) (C-CS) was kindly gifted by Yuda Century (Qingdao, China). Histo-clear was purchased from Scientific Laboratory Supplies (Scientific Laboratory Supplies Ltd, UK). VECTASHIELD® Antifade Mounting Medium was purchased from Vector Laboratories (Vector Laboratories, Inc., USA). Freshly excised porcine urinary bladders were kindly supplied by Arthur Howell Butchers (Wells-next-the-Sea, Norfolk, UK).

### 4.2.2. Synthesis of chitosan coated PLGA nanoparticles by nanoprecipitation method

Nanoparticles were synthesised using nanoprecipitation method. Briefly, 5mg PLGA and 0.025% (w/v) of P407 were dissolved in 2ml of acetonitrile (ACNT) to make solvent phase, which was then added to 4ml of anti-solvent phase containing from 0.1 mg/ml to 2 mg/ml chitosan. Evaporation of organic solvent was facilitated by using rotary evaporator and 55 °C degree water bath. Samples were then stirred at 250 rpm for at least 1 hour to remove residual organic solvent. Samples were filtered using 1 µm glass fibre filter (VWR, UK) and topped up with MilliQ water (MQW) to make up 4 ml total volume. For synthesis of non-mucoadhesive formulations, no chitosan was added. For synthesis of fluorescent PLGA nanoparticles, from 0.5 µg to 3 µg of C6 was added to the organic phase containing PLGA and P407.

For this study, four types of commercially available chitosan were selected: low MW of 50-190 kDa (CS-L), medium MW of 190–310 kDa (CS-M), high MW of 310-375 kDa (CS-H), and carboxymethyl chitosan (C-CS). To solubilise CS-L, CS-M and CS-H in aqueous solution, 0.2 M acetic acid was added to the aqueous phase. Residual chitosan present in the solutions of nanoparticle formulations was not quantified.

### 4.2.3. Fluorescence quantification by spectrofluorometer

To quantify the amount of encapsulated fluorescent dye inside PLGA nanoparticles, a FS5 Spectrofluorometer (Edinburgh Instruments, UK) was used. A standard calibration curve was prepared for C6, with conditions on the instrument set as follows:

- Emission scan from 390 nm to 700 nm
- Step can of 1 nm
- Dwell time of 0.1 min
- Bandwidth of 2

Samples for C6 fluorescence measurement were prepared by mixing 0.5 ml of the nanoparticle solution and 0.5 ml of ACNT to dissolve PLGA and solubilise C6. Result for each measurement was adjusted by subtracting amount of soluble C6 in 0.025% (w/v) of P407. Encapsulation efficiency of C6 loaded PLGA nanoparticles was calculated using equation:

$$EE\% = \frac{Mass\ of\ encapsulated\ C6}{Mass\ of\ total\ C6\ used\ for\ encapsulation} \times 100\% \qquad \textbf{Eq. (4.1)}$$

### 4.2.4. *In vitro* muco-adhesion test

*In vitro* muco-adhesion properties of the formulations were investigated using previously established mucin particle method with minor modifications [346]. For this study, 0.5 mg/ml of mucin from porcine stomach (type II) was dispersed in PBS 7.4, the buffer was then mixed with an equal volume of chitosan coated PLGA nanoparticle formulations. Samples were vortexed, then left to incubate for 1 h at 37 °C, shaking at 100 RPM. After incubation, samples were prepared for zeta potential analysis by diluting the samples in 1:1 ratio with 1mM NaCl. Samples were analysed using Zetasizer Nano (Malvern Instruments, Malvern, UK).

### 4.2.5. *Ex vivo* muco-adhesion test

Freshly excised porcine urinary bladders were used for *ex vivo* mucoadhesion assay. Bladders were obtained from a local abattoir, transported to the laboratory on ice and used on the same day. After removing urethra, bladders were cut into quarters, each piece rinsed with PBS 7.4 and residual buffer left to dry for 10 min at 37 °C incubator. Afterwards, 400 µl of each chitosan coated PLGA nanoparticle formulation was carefully pipetted onto the centre of the tissue, ensuring that the whole solution stays on the tissue throughout the incubation period. Tissues were left to incubate in petri dishes for 1 hour at 37 °C in dark conditions. Once removed, any remaining rundown of the sample was collected from the petri dish and tissues were prepared for artificial urine washouts as described in the protocol developed by Khutoryanskiy group [343]. Each tissue was washed with 10 ml of artificial urine (stored at 37 °C) using a syringe pump set to 4 ml/min, repeating the process 7 times to a total of 70 ml urine wash-out. Each wash was collected separately and stored at room temperature in the dark. The study was performed in triplicate.

Fluorescence of each wash-out sample was measured using a FS5 Spectrofluorometer (Edinburgh Instruments, UK), following the protocol described in **section 4.2.3**. Wash-out samples were prepared for spectrofluorometric analysis by centrifugation at 12,000 RCF for 45 min, then removing the supernatant, and dissolving the pellet in 1ml ACNT. Percentage of polymeric nanoparticles washed off during each wash was calculated using equation:

$$\%\, NPs\ washed\ off = \frac{(\mu g\ of\ NPs\ washed\ off \times\ 100\%)}{\mu g\ of\ NPs\ on\ tissue\ before\ wash} \qquad \textbf{Eq. (4.2)}$$

### 4.2.6. Mucopenetration assay

Preparation of freshly excised porcine bladders for mucopenetration assay followed the same procedure as described in **section 2.3.5** of **Chapter 2**. Tissues were treated with C6 loaded chitosan coated PLGA nanoparticles for 1 hour at 37 °C in dark conditions. Afterwards, samples were rinsed with PBS 7.4. Eight-micrometre-thick cross-sections were deparaffinized and hydrated through decreasing graded concentrations of EtOH. Sections were mounted onto the Superfrost Plus microscope slides (Fisher Scientific, UK) using VECTASHIELD® antifade mounting media (Vector Laboratories, Inc., USA). Slides were then observed using Zeiss Imager Z2 upright microscope (ZEISS, UK). Samples were excited at 475 nm with 30% laser

power for green fluorescence, with emission peak measured at 500 nm, while blue fluorescence samples were excited at 385 nm using 20% laser power, with emission peak measured at 465 nm. Image J software was used to calculate mucopenetration of the tissue by measuring the width of penetrated tissue that exhibit green fluorescence and comparing it with the width of whole urothelium, visible under DAPI channel. Study was performed in triplicates.

## 4.3. Results and discussion

### 4.3.1. Characterisation of mucoadhesive PLGA nanoparticle formulations

Blank PLGA nanoparticle formulations were optimised and adapted for mucoadhesive purposes. Here, four types of chitosan were examined: CS-L, CS-M, CS-H and C-CS, along with their MWs, ranging from low to high, and concentrations, ranging from 0.5 mg/ml to 2 mg/ml. Residual chitosan present free in the nanoparticle solution was not quantified, meaning that true concentration of chitosan present on the particle surface is unknown. Other parameters such as use of surfactants and change of pH were studied to help achieve optimal mucoadhesive properties of chitosan coated PLGA nanoparticles.

#### 4.3.1.1. Effect of addition of surfactant on nanoparticle characteristics

Addition of chitosan to achieve mucoadhesive PLGA nanoparticle formulation significantly increased ($P < 0.05$) nanoparticle size. As shown in **Table 4.1**, Blank-NP formulation demonstrated particle size of 96.9 ± 12 nm, which was significantly lower ($P < 0.05$) than the size of nanoparticles with CS-L or C-CS coating, which ranged from 455 nm to 656 nm, and 581 nm to 4091 nm, respectively. An increase of the nanoparticle size was observed with larger amount of chitosan added to the formulations. Similar particle size results of chitosan coated nanoparticles have been extensively reported in the literature [347–350]. Hence, surfactants are often used to control nanoparticle size when adding high concentrations of chitosan [112]. For this study, poloxamers were chosen due to low toxicity to biological membranes, improved nanoparticle drug loading, easy dissolution and, in some cases, ability to enhance nanoparticle permeability into biological tissues [348,351]. Poloxamers have been commonly used to reduce the size of PLGA nanoparticles, as during nanoparticle formation their hydrophilic moieties (ethylene oxide blocks) extend into aqueous phase, which reduces interfacial tension during particle formation, hence reducing particle size and preventing from particle aggregation [352,353].

**Table 4.1:** Composition and characterisation of CS-L and C-CS coated PLGA nanoparticles with and without addition of P407. Error bars represent standard deviation (SD) and n = 3. PDI = polydispersity index.

| Formulation code | Chitosan type | Chitosan conc. (mg/ml) | P407 conc. (% w/v) | Particle size (nm) | PDI | Zeta potential (mV) |
|---|---|---|---|---|---|---|
| Blank-NP | N/A | N/A | N/A | 96.9±12 | 0.20±0.04 | -13.2±3 |
| 0.1CS-L | CS-L | 0.1 | N/A | 455.4±100 | 0.18±0.05 | 35.3±5 |
| 0.5CS-L | | 0.5 | | 623.8±53 | 0.19±0.02 | 51.1±1 |
| 1CS-L | | 1 | | 656.7±105 | 0.23±0.03 | 50.4±1 |
| 0.1CS-L-P407 | CS-L | 0.1 | 0.025 | 277.1±44 | 0.25±0.01 | 27.5±4 |
| 0.5CS-L-P407 | | 0.5 | | 259.0±60 | 0.25±0.05 | 38.8±1 |
| 1CS-L-P407 | | 1 | | 349.2±20 | 0.32±0.05 | 47.0±2 |
| 0.1C-CS | C-CS | 0.1 | N/A | 4091.7±3590 | 0.36±0.15 | 5.7±14 |
| 0.5C-CS | | 0.5 | | 581.5±83 | 0.23±0.01 | 33.5±3 |
| 1C-CS | | 1 | | 974.8±264 | 0.15±0.04 | 45.0±4 |
| 0.1C-CS-P407 | C-CS | 0.1 | 0.025 | 272.1±24 | 0.29±0.09 | 17.8±1 |
| 0.5C-CS-P407 | | 0.5 | | 391.5±80 | 0.29±0.05 | 30.9±5 |
| 1C-CS-P407 | | 1 | | 467.6±52 | 0.30±0.02 | 45.5±1 |

P407 was used in this study to reduce the size of chitosan coated nanoparticles, with very low concentrations such as 0.025% (w/v) successfully achieving desired results.

An upward trend can be observed in **Figure 4.1**, where particle size increases with increased concentration of CS-L and C-CS used in the formulations. However, when adding P407 to the same formulations, the similar upward trend is maintained but with significantly lower nanoparticles size (**Figure 4.1**). Significant difference was observed between 0.1CS-L and 0.1CS-L-P407 ($P < 0.05$), 0.5CS-L and 0.5CS-L-P407 ($P<0.01$), and 1CS-L and 1CS-L-P407 ($P < 0.01$) formulations, demonstrating the significant impact of P407 on particle size.

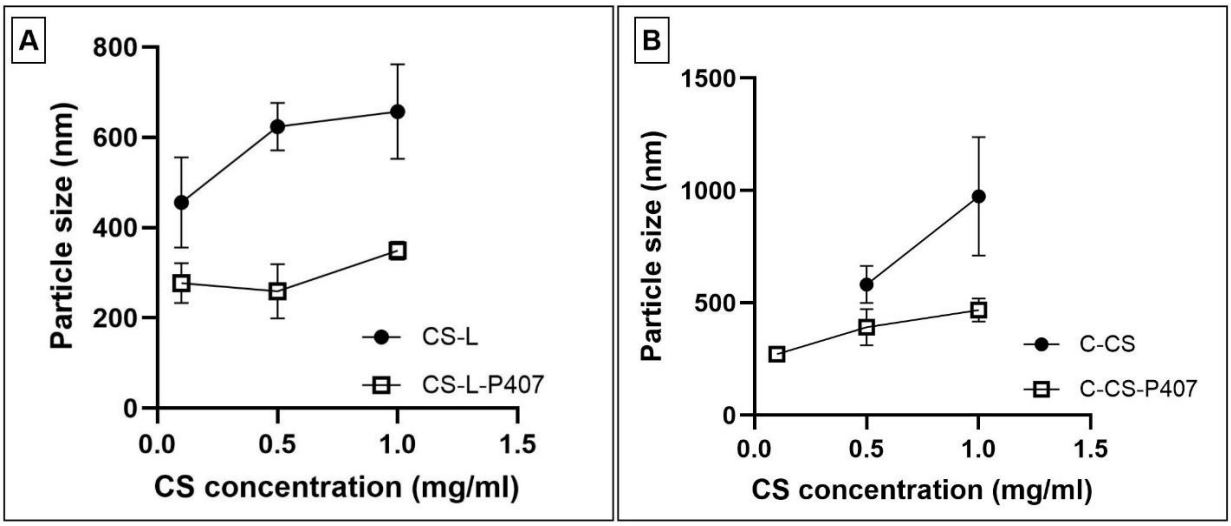


**Figure 4.1:** Particle size of PLGA nanoparticles coated with different concentrations and types of chitosan. Trends of particle size were observed in formulations containing P407 (data points marked with □) and containing no P407 (data points marked with ●). Two types of chitosan were used for this study: (A) CS-L and (B) C-CS (data point of 0.1C-CS formulation was excluded from the graph, due to poor quality sample as seen in the particle size data presented **Table 4.2**). Error bars represent the SD and n = 3.

C-CS coated PLGA nanoparticles that had no P407 demonstrated much higher particle size when compared with CS-L coated nanoparticles. Formulation 0.1C-CS demonstrated micro-sized particles, with high polydispersity index (PDI) and relatively low zeta potential, as well as large variability suggesting poor reproducibility and poor colloidal stability of this formulation. However, addition of surfactant in 0.1C-CS-P407 significantly improved physicochemical properties of the formulation, demonstrating a stable colloidal nanoparticle system with characteristics within expected range (**Table 4.2**). Addition of P407 to formulations 0.5C-CS-P407 and 1C-CS-P407 have significantly reduced their particle size ($P < 0.05$) compared with 0.5C-CS and 1C-CS, respectively.

All chitosan coated PLGA nanoparticles demonstrated positive particle charge, compared to the Blank-NP formulation that had no chitosan coating (**Table 4.2**). No significant change ($P > 0.05$) was observed in zeta potential values of CS-L and C-CS coated nanoparticles when P407 was added to the formulations, except for formulation 0.5CS-L-P407 which showed significantly reduced ($P < 0.05$) zeta potential with addition of surfactant (**Figure 4.2**). It has been reported in the literature, that a reduction of zeta potential can be seen when PLGA nanoparticles are coated in poloxamers [138,354]. Although it is unclear why surfactant coating

significantly reduced the charge of formulation 0.5CS-L-P407 specifically, it is likely that chitosan coating in most of the other formulations increases particle charge and diminishes P407 effects on zeta potentials due to higher concentrations of chitosan used in the formulations, compared to concentrations of surfactant.

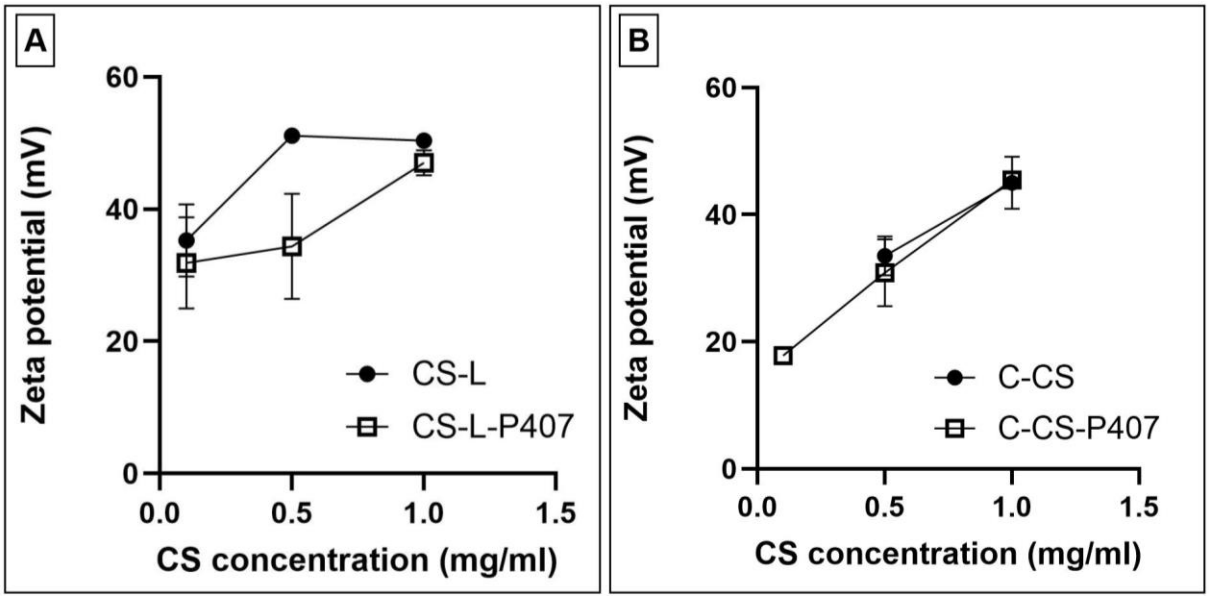


**Figure 4.2:** Graph representation of how increase in chitosan concentration in PLGA nanoparticle formulation correlates to increase in zeta potential. Zeta potential increase trends were observed in formulations with P407 (data points marked with □) and without P407 (data points marked with ●). Two types of chitosan were used for this study: (A) CS-L and (B) C-CS (data point of 0.1C-CS formulation was excluded from the graph due to poor quality). Error bars represent the SD and n = 3.

Additional testing was performed on Blank-NP formulation, using different concentrations of P407 to observe whether increases in P407 concentration had any significant effect on particle characteristics (**Table 4.2**). No significance was observed when comparing Blank-NP to formulations including P407, except for formulation with 0.025% (w/v) P407 which demonstrated significantly higher size and PDI compared to the blank formulation ($P < 0.05$). However, all nanoparticles were sized between 96 nm to 120 nm, with PDIs ranging from 0.2 to 0.28, which were considered a normal range for uncoated PLGA nanoparticles [136,169,355].

**Table 4.2:** Characteristics of Blank-NP formulation containing different concentrations of P407. Chitosan coating not added to the formulations. Error bars represent SD and n = 3.

| P407 concentration (% w/v) | Particle size (nm) | PDI | Zeta potential (mV) |
|---|---|---|---|
| N/A | 96.9±12 | 0.20±0.04 | -13.2±3 |
| 0.025 | 120.0±7 | 0.27±0.03 | -10.6±3 |
| 0.125 | 111.5±11 | 0.28±0.06 | -10.6±2 |
| 0.25 | 104.1±19 | 0.24±0.08 | -10.1±2 |

Overall, use of P407 was necessary to reduce the particle size of PLGA nanoparticles coated with chitosan for mucoadhesive properties. Even the smallest concentration of surfactant had a significant impact in reducing nanoparticle size. Based on these results, all further formulations included 0.025% (w/v) of P407, unless specified otherwise.

### 4.3.1.2. Effect of pH change on particle characteristics

Changes in pH are a very important factor in nanoparticle mucoadhesive behaviour. Different pH environments can significantly affect nanoparticle interactions with mucin, which is further explored in **section 4.3.3.** However, it was important to test how changes in pH affect nanoparticle characteristics. Formulations were adjusted to pH = 4.5 and pH = 7, because of pH conditions of 4.5 to 8 reported in a healthy bladder [356,357], which is an intended target site for nanoparticles delivery discussed in this study. Chitosan coated PLGA nanoparticles in acidic and neutral pH conditions were examined for any changes in particle characteristics or detect any issues with stability of colloidal system.

Firstly, nanoparticle formulations presented in **Table 4.2** (in **section 4.3.1.1.**) were analysed for their natural pH achieved after nanoparticle preparation process, with results demonstrated in **Table 4.3**. Due to CS-L insolubility in water, 0.2 M acetic acid was used to solubilise the polymer, which led to acidic pH of 3.5-4 observed in nanoparticle formulations coated with CS-L. Interestingly, low concentrations of C-CS demonstrated near neutral pH conditions, however with increased C-CS concentration, the pH of the samples dropped to 4.5. This is observed due to deprotonation of carboxyl groups of C-CS, which with increasing concentration of C-CS changes the pH of the sample from neutral to acidic [358]. Blank-NP

formulation with no chitosan coating exhibited pH of 7.26 ± 0.15, which explains why formulation 0.1C-CS-P407 demonstrates a similar pH when very low concentration of C-CS was used.

**Table 4.3:** pH conditions of chitosan coated PLGA nanoparticles before any pH modification. Error bars represent SD and n = 3.

| Formulation code | Chitosan type | Chitosan concentration (mg/ml) | pH (before modifications) |
|---|---|---|---|
| Blank-NP | N/A | N/A | 7.3±0.1 |
| 0.1CS-L-P407 | CS-L | 0.1 | 3.4±0.1 |
| 0.5CS-L-P407 | | 0.5 | 3.6±0.1 |
| 1CS-L-P407 | | 1 | 3.8±0.1 |
| 0.1C-CS-P407 | C-CS | 0.1 | 6.5±0.2 |
| 0.5C-CS-P407 | | 0.5 | 5.0±0.1 |
| 1C-CS-P407 | | 1 | 4.6±0.1 |

**Table 4.4** demonstrates previously established (**Table 4.2** in **section 4.3.1.1.**) mucoadhesive PLGA nanoparticle formulations in pH = 4.5 and pH = 7. A significant decrease ($P < 0.01$) in zeta potential was observed with increasing pH, which indicates reduced mucoadhesive properties of the formulation. Lower values of zeta potential can be observed due to pH of sample rising over pKa of chitosan, which is around 6.5, and in turn significantly reducing cationic charge of the polymer [229,358]. Interestingly, formulations C-CS-P407 in pH = 7 conditions demonstrated overall higher zeta potential (15.4 – 16.1 mV) than CS-L-P407 in pH = 7 (4.1 – 9.7 mV). Due to carboxyl groups present in C-CS, the pKa of C-CS (pKa ≈ 4.5) is much lower than pKa of chitosan (pKa ≈ 6.5) making C-CS a stronger acid, which is why neutral pH conditions do not decrease the positive particle charge as significantly as nanoparticles coated with CS-L [358]. However, significant difference ($P < 0.05$) in zeta potential can still be observed between C-CS nanoparticles in pH = 4.5 and pH = 7. Overall, most studies report significantly higher zeta potential of chitosan coated PLGA in acidic conditions, compared to more neutral pH [224,359,360].

**Table 4.4:** Characterisation of mucoadhesive nanoparticle formulations in acidic and neutral pH conditions. Error bars represent SD and n = 3.

| Formulation code | Chitosan type | Chitosan concentration (mg/ml) | pH | Particle size (nm) | PDI | Zeta potential (mV) |
|---|---|---|---|---|---|---|
| 0.1CS-L-P407 | CS-L | 0.1 | 4.5 | 231.1±11 | 0.17±0.04 | 21.3±4 |
| | | | 7 | 294.6±8 | 0.18±0.03 | 4.1±2 |
| 0.5CS-L-P407 | | 0.5 | 4.5 | 282.7±58 | 0.22±0.03 | 31.6±2 |
| | | | 7 | 312.6±19 | 0.25±0.01 | 7.9±0 |
| 1CS-L-P407 | | 1 | 4.5 | 341.4±30 | 0.28±0.01 | 38.8±2 |
| | | | 7 | 534.5±126 | 0.39±0.07 | 9.7±1 |
| 0.1C-CS-P407 | C-CS | 0.1 | 4.5 | 332.4±48 | 0.28±0.03 | 20.6±1 |
| | | | 7 | 1029.3±691 | 0.40±0.14 | 16.0±1 |
| 0.5C-CS-P407 | | 0.5 | 4.5 | 326.4±53 | 0.28±0.02 | 25.7±2 |
| | | | 7 | 894.1±537 | 0.41±0.16 | 15.4±0 |
| 1C-CS-P407 | | 1 | 4.5 | 383.2±49 | 0.30±0.01 | 35.0±2 |
| | | | 7 | 856.5±229 | 0.54±0.06 | 16.1±0 |

Nanoparticles in neutral pH conditions demonstrated higher mean particle size than nanoparticles in acidic conditions, with formulations 0.1CS-L-P407 and 1C-CS-P407 showing significant difference ($P < 0.05$) between particle sizes in different pH environments. In formulations with C-CS coating, nanoparticles showed abnormally large nanoparticle sizes, which was no longer consistent with results reported in **section 4.3.1.1**. This suggested that neutral pH negatively affected colloidal stability of C-CS coated nanoparticles, increasing nanoparticle aggregation and reducing result reproducibility in this pH.

The main purpose of these formulations is to exhibit mucoadhesive properties, which are likely to be enhanced in acidic pH conditions, as nanoparticles demonstrated significantly higher zeta potential values compared to neutral pH. In addition, particles in acidic environments showed smaller mean of particle size with narrow size distribution.

### 4.3.1.3. Optimisation of chitosan coated PLGA nanoparticles

Optimisation of chitosan coating for PLGA nanoparticles was undertaken with the aim of achieving a stable colloidal system, with relatively small particle size and low polydispersity, maintaining high zeta potential for enhanced mucoadhesive properties. Concentrations of four types of chitosan used in PLGA nanoparticle formulations were examined in this section: low MW (CS-L), medium MW (CS-M), high MW (CS-H), and water-soluble carboxymethyl chitosan (C-CS).

Many previous studies reported that chitosan with higher MW tends to demonstrate better mucoadhesive properties [224,225,361], therefore characteristics of nanoparticles coated with CS-L, CS-M and CS-H chitosan were investigated (**Table 4.5**). With set chitosan concentration at 1 mg/ml, CS-L samples showed significantly smaller ($P < 0.05$) nanoparticle size when compared to the CS-M and CS-H samples. No significant difference was observed in PDI and zeta potential of all 3 types of chitosan. All formulations showed similar zeta potential values, indicating similar mucoadhesive properties, with detailed investigation into mucoadhesion of the particles explored in **section 4.3.3.** and **4.3.4**. CS-L coated PLGA nanoparticles demonstrated the smallest particle size with lowest SD values, as well as lowest mean PDI, in comparison to high particle size and PDI values obtained from nanoparticles coated with CS-M and CS-H. This therefore indicates good suitability of CS-L coated nanoparticles for mucoadhesive coating, due to good quality and stability of the particles.

**Table 4.5:** Characteristics of nanoparticles coated with CS-L, CS-M and CS-H. Error bars represent SD and n = 3.

| Chitosan type | Chitosan concentration (mg/ml) | P407 concentration (% w/v) | Particle size (nm) | PDI | Zeta potential (mV) |
|---|---|---|---|---|---|
| CS-L | 1 | 0.025 | 349.2±20 | 0.32±0.05 | 47.0±2 |
| CS-M | | | 634.6±125 | 0.41±0.08 | 49.0±2 |
| CS-H | | | 690.9±159 | 0.48±0.11 | 49.7±2 |

Particle size of nanoparticles can be of crucial importance in some drug delivery applications, for example when crossing blood-brain barrier [347]. However, due to highly impermeable urothelium barrier comprised of tightly arranged umbrella cells, covered by hydrophilic

glycosaminoglycan (GAG) layer and uroplakin plaques [333], cellular uptake or paracellular permeability into the urothelium of the nanoparticles is likely to be challenging. Therefore, this study focuses on localised delivery of the drug, which is expected to be enhanced due to adherence of the nanoparticles to the mucin layer of the bladder. Despite that, some permeation into the urothelium of the bladder is to be expected, as some studies reported that smaller sized nanoparticle increased the likelihood of permeating deeper into the mucin network [2,342,362]. Nanoparticles could also successfully permeate through disruptions in the urothelium, caused by cell necrosis or desquamation of umbrella cells due to bacterial infection or toxicity of the treatment [214,217]. Mucoadhesive chitosan nanoparticles have been shown to enhance bladder permeability, as they accumulate in the GAG layer and form a micro-concentration gradient, which enables increased diffusion of the drug into the bladder wall [363]. It is important to mention, that particle size increase of nanoparticles coated with chitosan has been widely documented [347–350], as addition of chitosan into the formulation increases the concentration of overall polymer phase. Therefore, our aim is to enhance concentration of chitosan as much as possible while ensuring that the size of chitosan coated nanoparticles remains below 450 nm, based on the particle size range reported by other studies [348,364,365].

Further optimisations were undertaken to increase the chitosan concentration to enhance mucoadhesive properties, while ensuring that stable, colloidal nanoparticle system is maintained. As demonstrated in **Table 4.6**, higher concentrations of CS-L were used to coat PLGA nanoparticles, with additional changes to P407 and PLGA concentrations in order to stabilize and reduce particle characteristic fluctuation. As explained in **section 4.3.1.1.**, higher concentrations of P407 were tested to see if addition of surfactant could reduce particle size and PDI. No significant difference ($P > 0.05$) was found in nanoparticle characteristics of formulations containing either 0.025% or 0.125% (w/v) of P407 in nanoparticles coated with 1.5 mg/ml of chitosan. Formulation 2CS-L-5P-5P407 showed significantly decreased zeta potential values ($P < 0.05$) when compared to 2CS-L-5P-1P407 formulation, which had lower surfactant concentration. Apart from this, formulations with 2 mg/ml CS-L showed no significant difference ($P > 0.05$) in their characteristics despite changes in P407 and PLGA concentrations. Matching results were observed in formulations coated with 1.5 mg/ml CS-L.

Overall, increasing CS-L concentration from 1 mg/ml to 1.5 mg/ml or 2 mg/ml increased the mean particle size with enlarged SD values, while PDI stayed in expected range of 0.2 – 0.4.

Higher chitosan concentration did not show any significant difference ($P > 0.05$) on zeta potential values. Additionally, formulations with 1.5 mg/ml and 2 mg/ml chitosan showed poor quality during dynamic light scattering (DLS) analysis, as well as physical precipitation was observed after a couple of days of samples being left at room temperature. Due to this, 1CS-L-P407 formulation was selected for further experiments due to good colloidal stability over 7 days and relatively small particle size of 349.2 ± 20 nm.

**Table 4.6:** Characteristics of PLGA nanoparticles coated with 1mg/ml, 1.5mg/ml and 2mg/ml CS-L. Error bars represent SD and n = 3.

| Formulation code | Chitosan type | PLGA conc. (mg) | Chitosan conc. (mg/ml) | P407 conc. (% w/v) | Particle size (nm) | PDI | Zeta potential (mV) |
|---|---|---|---|---|---|---|---|
| 1CS-L-1P407 | CS-L | 5 | 1 | 0.025 | 349.2±20 | 0.32±0.05 | 47.0±2 |
| 1.5CS-L-5P-1P407 | | | 1.5 | | 675.2±320 | 0.28±0.07 | 48.5±2 |
| 1.5CS-L-5P-5P407 | | | | 0.125 | 561.9±134 | 0.41±0.11 | 46.5±3 |
| 1.5CS-L-10P-1P407 | | 10 | 1.5 | 0.025 | 577.0±179 | 0.31±0.00 | 46.4±2 |
| 1.5CS-L-10P-5P407 | | | | 0.125 | 426.0±50 | 0.32±0.01 | 44.6±4 |
| 2CS-L-5P-1P407 | | 5 | 2 | 0.025 | 673.0±194 | 0.30±0.03 | 45.8±1 |
| 2CS-L-5P-5P407 | | | | 0.125 | 776.1±15 | 0.23±0.08 | 42.1±2 |
| 2CS-L-10P-1P407 | | 10 | 2 | 0.025 | 952.8±371 | 0.30±0.06 | 47.2±2 |
| 2CS-L-10P-5P407 | | | | 0.125 | 583.8±178 | 0.36±0.03 | 46.1±4 |

Although PLGA nanoparticles demonstrated large sizes when coated with 1 mg/ml CS-M (**Table 4.5**), optimisation of the formulation was attempted to minimise particle size and PDI

by increasing concentration of chitosan and changing concentrations of P407 and PLGA. The same parameters listed in **Table 4.6** were investigated with CS-H coated nanoparticles. Increased CS-M concentration of 1.5 mg/ml and 2 mg/ml used in preparation of PLGA nanoparticles demonstrated the average particle size was 607.8 ± 128 nm and 915.7 ± 249 nm, respectively. Increase in P407 or PLGA did not show any significant results on particle size, PDI or zeta potential. Based on these results, optimisation to enhance CS-H concentrations in nanoparticle formulations was not performed, as both CS-M and CS-H coated formulations showed large particle size, high PDI and overall large standard error bars, demonstrating poor colloidal stability and poor formulation reproducibility.

However, large particle size and poor sample colloidal stability has led to consideration of using much lower concentration of CS-M to coat PLGA nanoparticles. Addition of 0.5 mg/ml CS-M to the formulation resulted in 287.5 ± 22 nm sized particles, with PDI of 0.272 ± 0.05 and zeta potential of 47 ± 1 mV. Although this formulation had relatively low concentration of chitosan, zeta potential values were comparable with 1CS-L-P407, suggesting potentially similar mucoadhesive properties due to higher MW [224,225,361]. Additionally, we hypothesised that nanoparticles with MW weight of chitosan coating could achieve strong interactions with mucin, despite having low concentration. These results were further explored in **sections 4.3.3.** and **4.3.4.**

Finally, same optimisation studies were undertaken for C-CS coated nanoparticles to increase concentration of chitosan used to coat nanoparticles and enhance mucoadhesive properties. Formulation composition and formulation codes are shown in **Table 4.7**. All nanoparticles demonstrated particle size between 297 nm and 569 nm, however due to inter-batch variability in particle size, only formulation 1.5C-CS-10P-5P407 demonstrated significantly smaller ($P < 0.05$) size compared to 1C-CS-P407 formulation. Here, nanoparticle size was shown to decrease from 467.6 ± 52 nm to 337.1 ± 58 nm, despite increased concentrations of chitosan, PLGA and P407. Additionally, an increase in P407 concentration was associated with a reduction in particle size from 529.1 ± 28 nm to 362.3 ±4 7 nm for 2C-CS-5P-1P407 and 2C-CS-5P-5P407, respectively. No significant difference was found in PDI values of all formulations tested, which were in 0.2 – 0.4 range.

**Table 4.7:** Composition of additional C-CS coated PLGA nanoparticle formulations, that were used to investigate changes in particle characteristics in increasing chitosan, P407 and PLGA concentrations. Error bars represent SD and n = 3.

| Formulation code | Chitosan type | PLGA conc. (mg) | Chitosan conc. (mg/ml) | P407 conc. (% w/v) |
|---|---|---|---|---|
| 1C-CS-1P407 | C-CS | 5 | 1 | 0.025 |
| 1.5C-CS-5P-1P407 | | | 1.5 | |
| 1.5C-CS-5P-5P407 | | | | 0.125 |
| 1.5C-CS-10P-1P407 | | 10 | | 0.025 |
| 1.5C-CS-10P-5P407 | | | | 0.125 |
| 2C-CS-5P-1P407 | | 5 | 2 | 0.025 |
| 2C-CS-5P-5P407 | | | | 0.125 |
| 2C-CS-10P-1P407 | | 10 | | 0.025 |
| 2C-CS-10P-5P407 | | | | 0.125 |

Interestingly, the zeta potential of some C-CS coated nanoparticles significantly decreased despite having higher concentrations of C-CS used for nanoparticle synthesis (**Figure 4.3**). Formulations 1.5C-CS-5P-5P407, 1.5C-CS-10P-1P407, 1.5C-CS-10P-5P407 and 2C-CS-5P-5P407 were all compared to 1C-CS-P407 formulations and displayed significantly lower ($P < 0.05$) zeta potential values, even if 1C-CS-P407 had lower concentration of chitosan. It is important to note, that these 1.5 mg/ml and 2 mg/ml C-CS coated nanoparticles did have higher P407 and PLGA concentrations, depending on the composition of specific formulations (**Table 4.7**). Additionally, a significant decrease ($P < 0.05$) in zeta potential can be observed with increase of P407 concentrations in nanoparticle formulations, except for 1.5C-CS-10P-1P407 and 1.5C-CS-10P-5P407 formulations (**Figure 4.3**). Although not all samples demonstrated significant decrease, but overall means of zeta potentials did show lowered zeta potential values with increased concentration of surfactant. It appears that higher concentration of non-ionic surfactant P407 used interferes with cationic properties of chitosan [134]. However, it is important to note that using the same formulation composition but different C-CS concentrations, the difference between zeta potentials is very small as seen in formulations 1C-CS-P407 and 1.5C-CS-5P-1P407, as well as 1C-CS-P407 and 2C-CS-5P-1P407.

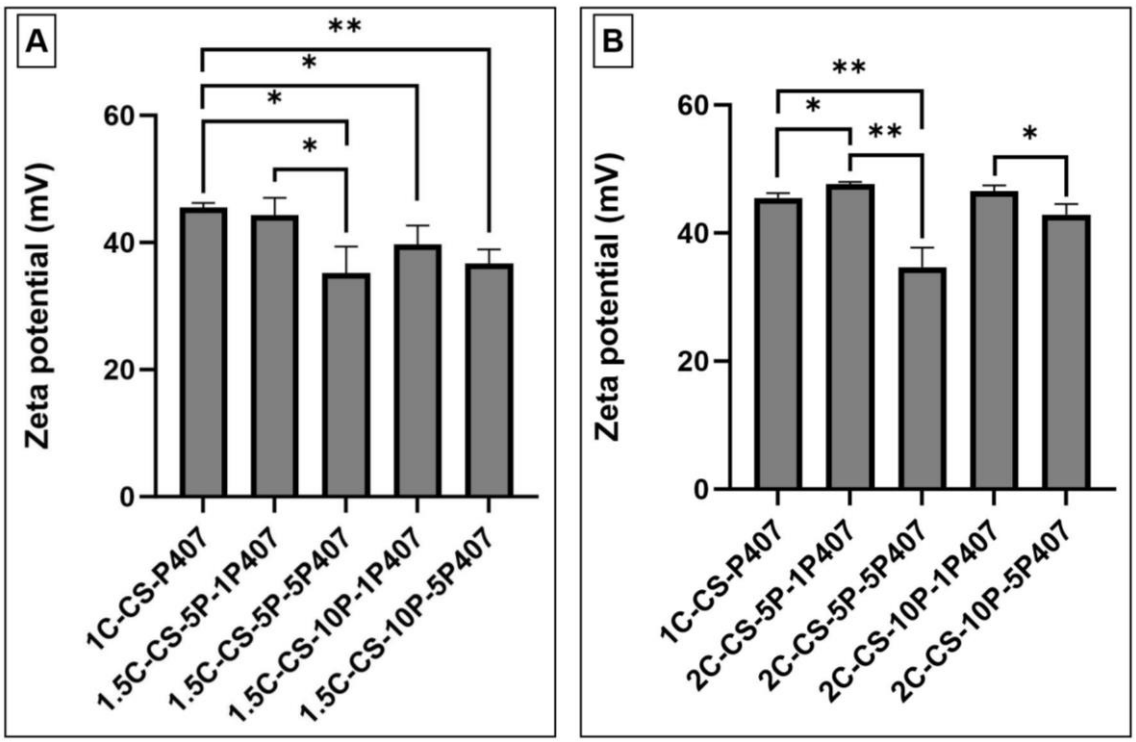


**Figure 4.3:** Zeta potential values of (A) 1.5 mg/ml C-CS and (B) 2 mg/ml C-CS coated PLGA nanoparticles, with increasing concentration of P407 and PLGA. * ($P < 0.05$), ** ($P < 0.01$). Error bars represent the SD and n = 3.

All formulations with CS-L, CS-M or C-CS coated nanoparticles, demonstrated that increase in P407 and PLGA concentrations either does not show significant effect on particle characteristics or enlarges particle size and decreases zeta potential. However, opposite to CS-L and CS-M samples, higher concentrations of C-CS used in the PLGA nanoparticles did not negatively affect particle size and therefore was considered for further experiments.

Based on the results reported in this section, five formulations were selected for further experiments (**Table 4.8**). Concentration of 1 mg/ml CS-L and 0.5 mg/ml CS-M were chosen for mucoadhesive coating of PLGA nanoparticles as they demonstrated good colloidal stability and highly positive zeta potential values, while also demonstrating relatively small particle sizes. Further experiments with these formulations are expected to demonstrate whether small particle size has any positive impact on particle mucoadhesive or mucopenetrative properties. As for C-CS, 3 final concentrations were selected. Formulations 1C-CS-P407 and 2C-CS-P407 both demonstrated very similar characteristics, despite having different concentrations of chitosan coating. Formulation 2C-CS-P407 has the highest concentration of chitosan coating, therefore will be observed for superior mucoadhesive properties in the following experiments.

Additionally, to have a comparison between low chitosan concentration formulations, 0.5C-CS-P407 was also included for comparison with 0.5CS-M-P407 formulation.

**Table 4.8:** Characteristics of mucoadhesive PLGA nanoparticles that were optimised for *in vitro* and *ex vivo* mucoadhesion assays. Error bars represent SD and n = 3.

| Formulation code | Chitosan type | Chitosan concentration (mg/ml) | P407 conc. (% w/v) | Particle size (nm) | PDI | Zeta potential (mV) |
|---|---|---|---|---|---|---|
| 0.5CS-M-P407 | CS-M | 0.5 | 0.025 | 287.5±22 | 0.27±0.05 | 47.0±1 |
| 1CS-L-P407 | CS-L | 1 | | 349.2±20 | 0.32±0.05 | 47.0±2 |
| 0.5C-CS-P407 | C-CS | 0.5 | | 391.5±80 | 0.29±0.05 | 30.9±5 |
| 1C-CS-P407 | | 1 | | 467.6±52 | 0.30±0.02 | 45.5±1 |
| 2C-CS-P407 | | 2 | | 529.1±28 | 0.39±0.06 | 47.6±0 |
| NoCS-P407 | N/A | N/A | | 120.0±7 | 0.27±0.03 | -10.6±3 |

## 4.3.2. Characterisation of C-6 loaded PLGA nanoparticles

Fluorescent dye loaded PLGA nanoparticles were prepared for assays requiring quantification of mucoadhesion or mucopenetration. C6 was selected as fluorescent dye due to low limit of detection and its hydrophobic properties, which were necessary for enhanced encapsulation into PLGA nanoparticles prepared by nanoprecipitation method. Different amounts of C6 were encapsulated into uncoated PLGA nanoparticles in order to observe how change in C6 mass affects particle characteristics (**Table 4.9**). Results demonstrated no significant difference ($P \geq 0.05$) on particle size, PDI or zeta potential with increasing concentration of C6. Although there was no significant difference observed in EE% values when increasing C6 concentration, a small increase in mean EE% was observed with increasing C6 concentrations, with highest EE% values achieved with 3 µg of C6 loaded into PLGA nanoparticles. Therefore, highest amount of 3 µg of C6 was selected for further nanoparticle formulations.

**Table 4.9:** Particle size, PDI, zeta potential and EE% of increasing concentration of C6 encapsulated into PLGA nanoparticles, prepared by nanoprecipitation method. Error bars represent SD and n = 3.

| C6 loaded (µg) | P407 conc. (% w/v) | Particle size (nm) | PDI | Zeta potential (mV) | EE% |
|---|---|---|---|---|---|
| 0.5 | 0.025 | 119.1±12 | 0.25±0.03 | -8.3±2 | 45.7±2 |
| 1 | | 120.9±35 | 0.21±0.04 | -10.2±3 | 47.5±7 |
| 2 | | 158.9±72 | 0.29±0.12 | -11.8±1 | 47.5±7 |
| 3 | | 123.0±13 | 0.25±0.06 | -11.7±0 | 53.7±5 |

Chitosan coated nanoparticle formulations determined in **section 4.3.1.3.**, were encapsulated with 3 µg of C6, with characteristics of the nanoparticles shown in **Table 4.10**. Similarly to the results reported previously, a significant increase ($P < 0.05$) in particle size can be observed in formulations with chitosan coating, compared to the uncoated nanoparticles. The size range of C6 loaded, chitosan coated nanoparticles was between 274 nm and 430 nm, which are considered to be a larger size of polymeric nanoparticles. C6 loaded nanoparticles without chitosan coating demonstrated small nanoparticle size of 123 ± 13 nm. Encapsulation of C6 in PLGA nanoparticles did not show any effect on zeta potential values, while addition of chitosan coating of the nanoparticles increased particle charge from negative to positive.

**Table 4.10:** Particle size, PDI, zeta potential and EE% of different concentrations and types of chitosan coated PLGA nanoparticles, encapsulated with 3 µg C6, prepared by nanoprecipitation method. Error bars represent SD and n = 3.

| Formulation code | Chitosan type | Chitosan conc. (mg/ml) | P407 conc. (% w/v) | Particle size (nm) | PDI | Zeta potential (mV) | EE% |
|---|---|---|---|---|---|---|---|
| 0.5CS-M-C6 | CS-M | 0.5 | 0.025 | 400.2±82 | 0.32±0.02 | 46.5±3 | 60.2±3 |
| 1CS-L-C6 | CS-L | 1 | | 430.7±120 | 0.26±0.03 | 47.9±2 | 60.9±6 |
| 0.5C-CS-C6 | C-CS | 0.5 | | 274.1±34 | 0.26±0.01 | 34.6±1 | 88.4±7 |
| 1C-CS-C6 | | 1 | | 303.6±8 | 0.32±0.06 | 42.8±3 | 89.9±1 |
| 2C-CS-C6 | | 2 | | 383.9±22 | 0.32±0.01 | 46.3±2 | 92.3±2 |

| | | | | | | | |
|---|---|---|---|---|---|---|---|
| NoCS-C6 | N/A | N/A | | 123.0±13 | 0.25±0.06 | -11.7±0 | 60.4±3 |

The efficiency of C6 entrapment into PLGA nanoparticles was measured using spectrofluorometer (**Figure 4.4**). Results demonstrated higher EE% when nanoparticles were coated with C-CS, while no significant difference in EE% was observed between NoCS-C6, 0.5CS-M-C6 and 1CS-L-C6 formulations. Overall encapsulation values were between 60% to 92% which confirmed good entrapment of fluorescent agent, as well as demonstrated a robust fluorescent formulation obtained for quantification experiments. The morphologies of these formulations were examined using transmission electron microscopy (TEM) demonstrating relatively monodisperse nanoparticles (**Figure 4.5**), demonstrating smaller particle size results compared to results obtained by DLS, as reported in **Table 4.10**. This occurs as TEM measures the true radius of the nanoparticles, compared to the hydrodynamic radius measurement obtained by DLS. This is explained in detail in **section 2.3.2.1** of **Chapter 2.**

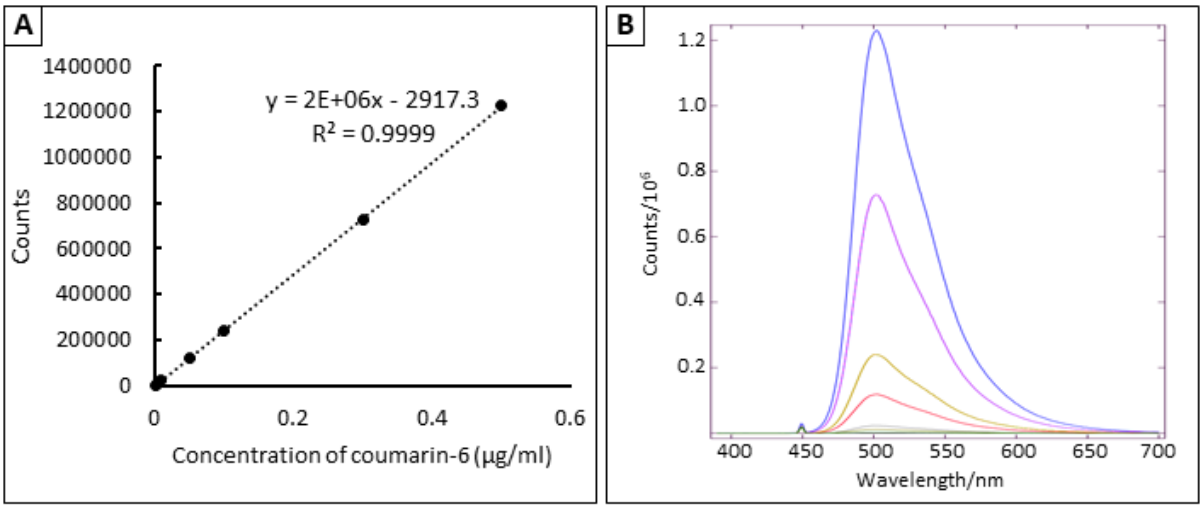


**Figure 4.4:** (A) Calibration curve of C6 measured using spectrofluorometer at excitation/emission wavelengths of 450/502 nm. (B) Fluorescence spectrum of C6 from 500 ng/ml to 1 ng/ml.

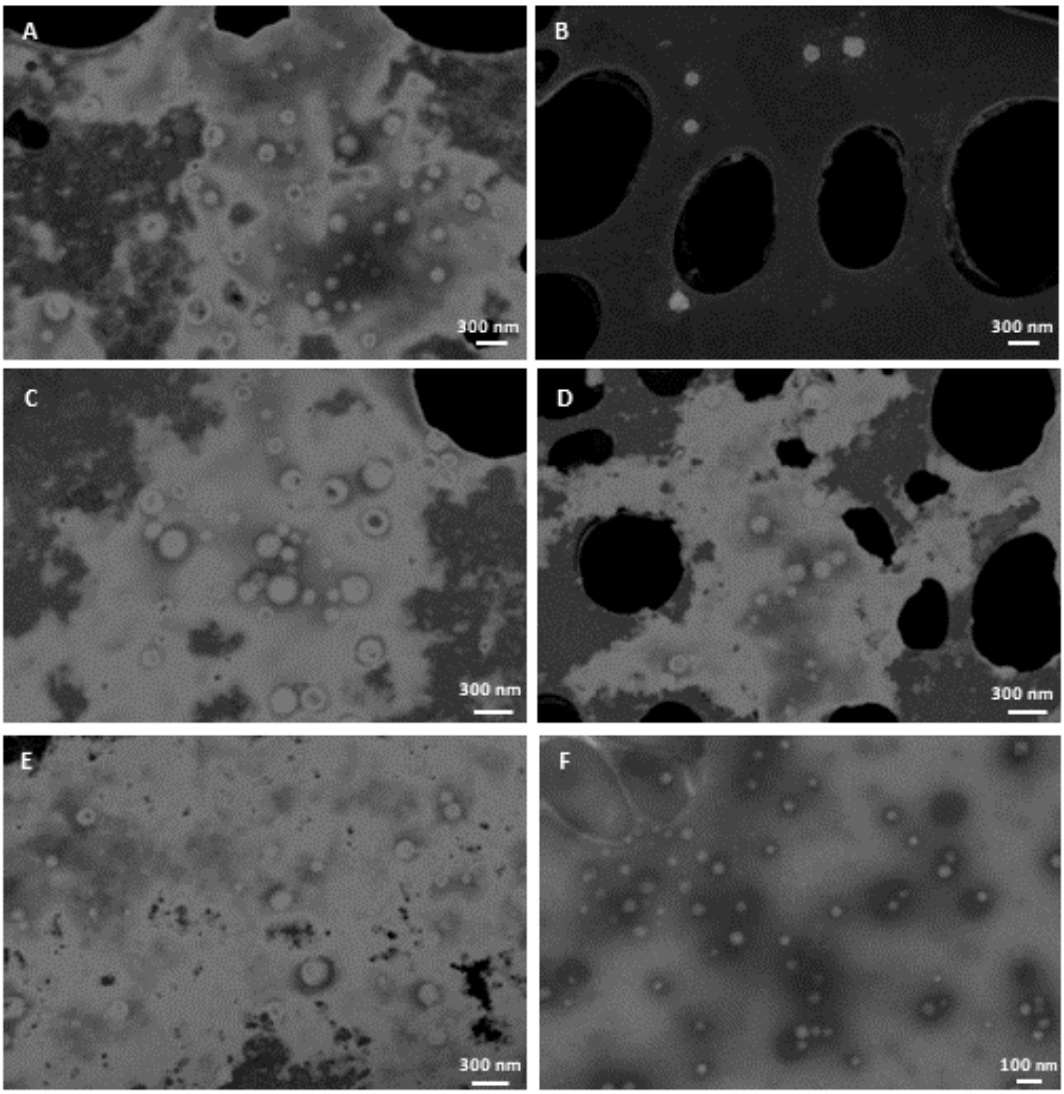


**Figure 4.5:** TEM characterisation of PLGA nanoparticles loaded with 3 µg C6, coated with (A) 0.5 mg/ml CS-M, (B) 0.5 mg/ml C-CS, (C) 1 mg/ml CS-L, (D) 1 mg/ml C-CS, (E) 2 mg/ml C-CS, and (F) no coating.

### 4.3.3. *In vitro* mucoadhesion study

For this study, *in vitro* mucoadhesion tests were performed by incubating mucin and chitosan-coated PLGA nanoparticles together. Mucin is often used to mimic mucosal tissues of nasal lining, gastrointestinal and urinary tracts, as well as surface of the eye, for the *in vitro* mucoadhesion assays [344,346,361,366–369]. By analysing how well anionic mucin interacts with cationic chitosan coated nanoparticles, mucin binding assays can provide useful preliminary data about mucoadhesive properties of the nanoparticle formulations. Separate zeta potential values of free mucin and nanoparticle formulations before the assay were compared to zeta potential values of mixed nanoparticle and mucin suspension. Changes in zeta potential

readings after nanoparticle samples were incubated with mucin would indicate ionic interaction between the particles [224,346]. Results of this assay were used to investigate how different types, concentrations and MWs of chitosan coating affected the mucoadhesive behaviour of the nanoparticles.

### 4.3.3.1. Effect of pH changes on mucoadhesive behaviour

Firstly, the mucoadhesive behaviour of nanoparticles (described in **section 4.3.1.2.**) was analysed under different pH conditions. As reported in the literature, healthy bladder pH varies from pH 4.5 to 8, however it is usually expected to be at around pH = 6-7, with more acidic and alkaline ends of the range experienced more rarely [356,357]. It has been widely reported that in acidic pH, amino groups present on D-glucosamine monomeric units of chitosan are protonated thus achieving positive charge [317,318]. Consequently, strongest mucoadhesive interactions between chitosan and porcine mucin particles can be achieved in acidic media, as D-glucosamine residue of chitosan and sialic acid residue of mucin can achieve highest ionization [370]. However, physiological limitations must be evaluated to achieve safe intravesical treatment. For this study, the most acidic pH was chosen to be pH = 4.5, due to it being the lowest pH that is still considered a healthy bladder environment [286,357]. A neutral pH = 7 has been selected as well, to observed what mucoadhesive properties could be expected in most common bladder environment. Zeta potential values of nanoparticles in these conditions are shown in **Table 4.11** All nanoparticles demonstrated positive zeta potential values, with generally higher zeta potential values exhibited in acidic pH. While zeta potential values between CS-L and C-CS coated PLGA nanoparticles were similar in pH = 4.5, nanoparticles containing C-CS showed much higher particle charge in pH = 7 compared to nanoparticles coated with CS-L. The effects of pH change on the physicochemical characteristics of these particles were discussed in detail in **section 4.3.1.2.**

**Table 4.11:** Zeta potential of chitosan coated PLGA nanoparticles (prior to *in vitro* mucoadhesion assay) in pH = 4.5 and pH = 7. Error bars represent SD and n = 3.

| Formulation code | Chitosan type | Chitosan concentration (mg/ml) | P407 conc. (% w/v) | Zeta potential (mV) | |
|---|---|---|---|---|---|
| | | | | pH=4.5 | pH=7 |
| 0.1CS-L-P407 | CS-L | 0.1 | 0.025 | 21.3±4 | 4.1±2 |
| 0.5CS-L-P407 | | 0.5 | | 31.6±3 | 7.9±1 |

| | | | | | |
|---|---|---|---|---|---|
| 1CS-L-P407 | | 1 | | 38.8±2 | 9.7±1 |
| 0.1C-CS-P407 | C-CS | 0.1 | | 20.6±1 | 16.0±1 |
| 0.5C-CS-P407 | | 0.5 | | 25.7±2 | 15.4±0 |
| 1C-CS-P407 | | 1 | | 35.0±2 | 16.1±0 |

Initial concentration of chitosan used to coat blank PLGA nanoparticles ranged from 0.1 mg/ml to 1 mg/ml. There was a clear difference between the mucoadhesive properties in acidic versus neutral pH noted when chitosan coated nanoparticles were mixed with mucin. Formulations 0.1CS-L-P407, 0.5CS-L-P407 and 1CS-L-P407 in acidic pH demonstrated significantly higher adhesion ($P < 0.05$) to mucin particles, compared to the same formulations in neutral pH (**Figure 4.6A**). Additionally, the zeta potential of nanoparticle and mucin mixture has proportionally increased with increasing concentration of chitosan used. This data agrees with results reported in previous studies [224,371,372].

A clear correlation can be observed between zeta potential of the CS-L coated PLGA nanoparticles and zeta potential of the nanoparticle and mucin mixture. The higher the zeta potential of the nanoparticles, the stronger they bind to the negatively charged mucin. Thus, some degree of charge neutralisation can be observed as a result of electrostatic interactions between cationic nanoparticles and anionic mucin [228].

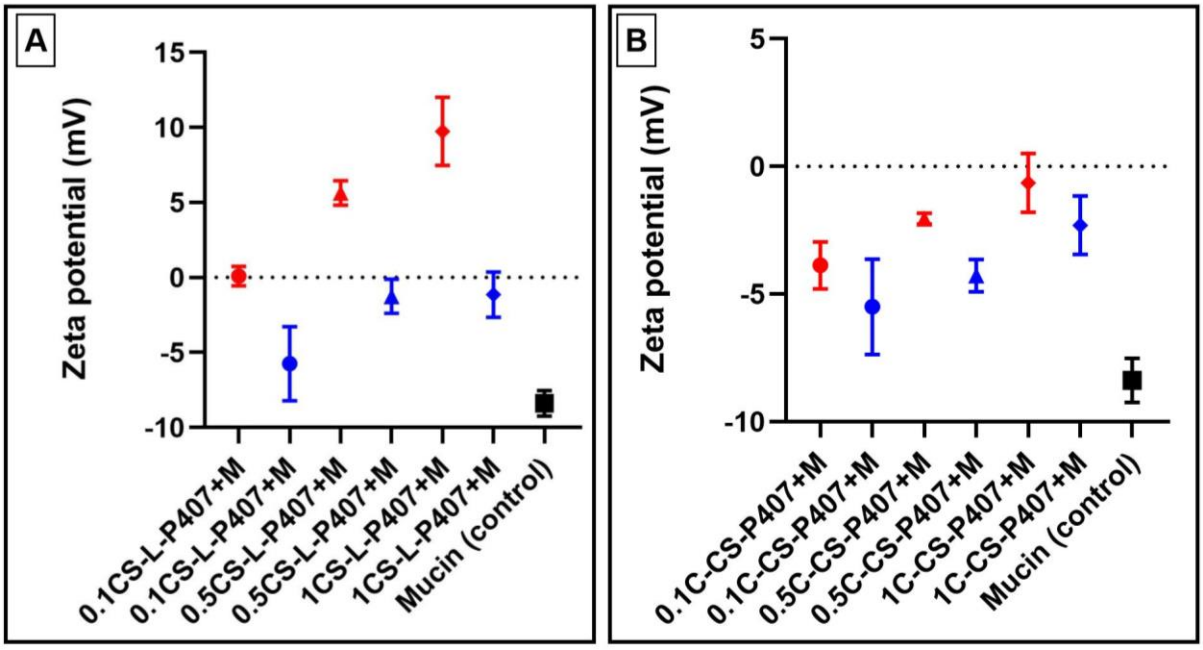


**Figure 4.6:** Zeta potential values of blank PLGA nanoparticle formulations coated with CS-L (A) and C-CS (B) in pH = 4.5 (in red) or pH = 7 (in blue) conditions, after incubation with mucin particles for 1 hour, at 100 RPM, 37 °C. Mucin (control) was measured at pH = 7.4. * (P-value < 0.05), ** (P-value < 0.01), ns (P-value ≥ 0.05). Error bars represent the SD and n = 3.

Interestingly, nanoparticle formulations 0.1C-CS-P407 and 1C-CS-P407 in mucin suspension demonstrated no significant differences on zeta potential values regardless of pH conditions (**Figure 4.6B**). While this can be expected for 0.1C-CS-P407 formulation, as its zeta potential values in pH = 4.5 and pH = 7 are similar (**Table 4.11**), formulation 1C-CS-P407 has significantly higher ($P < 0.05$) particle charge in acidic pH compared to neutral pH and therefore should demonstrate significantly higher zeta potential values when incubated with mucin. Similarly to CS-L coated PLGA nanoparticles, formulation 0.5C-CS-P407 showed significantly stronger interaction ($P < 0.05$) with mucin in pH = 4.5, compared to pH = 7 environment. However, the zeta potential of the nanoparticle and mucin mixture remained negative, indicating free mucin in the sample, as well as poor affinity between nanoparticles and mucin.

All samples, except for 0.1CS-L-P407 and 0.1C-CS-P407 at pH = 7, showed significant changes in zeta potential values when mixed with mucin compared to free mucin, indicating some degree of mucoadhesive interactions between the particles and mucin. It is likely that

formulations 0.1CS-L-P407 and 0.1C-CS-P407 cannot establish electrostatic interactions due to low concentration of chitosan coating, as well as neutral pH conditions impacting chitosan protonation.

Based on the results from this study, it was concluded that acidic pH is necessary to maintain strong mucoadhesive properties of PLGA nanoparticles. Therefore, these results imply that for effective mucoadhesive bladder therapies in the future, bladder must be pre-treated to ensure acidic pH for when the nanoparticle solution is instilled. Alternatively, instillation of nanoparticle formulation at low pH to an empty bladder could be sufficient as well. However, certain limitations can be expected as bladder filling over time will affect the pH of the bladder environment, which in turn could negate the mucoadhesive effect of the nanoparticles. In addition, it is unclear how effective the bladder pre-treatment or treatment with nanoparticles in acidic pH would be in reducing overall pH of the bladder environment during bacterial infection, as study by Lai et al., 2021 have demonstrated that more alkaline pH within the bladder have been documented in patients suffering from urinary tract infections (UTIs) [357]. Although direct to bladder treatments with prolonged retention time are an attractive option in treating many bladder conditions, including UTIs, this is still a relatively novel treatment proposal that needs more research to ensure its efficacy and safety.

Results from this section showed that neutral pH conditions failed to facilitate strong mucoadhesive interactions and therefore further mucoadhesive experiments were performed in pH = 4.5 conditions. However, the reason for CS-L and C-CS coated nanoparticle showing very different mucoadhesive properties remained unclear and therefore was investigated next (**section 4.3.3.2.**).

### 4.3.3.2. Mucoadhesive interactions between mucin and chitosan of different types and molecular weights

Mucoadhesive properties of nanoparticles coated with different types of chitosan and their MWs were investigated. Blank PLGA nanoparticles coated with 1 mg/ml of CS-L, CS-M, CS-H or C-CS (**Table 4.12**) in pH = 4.5, were mixed with mucin solution and incubated for 1 hour. Firstly, there was a sizable difference in zeta potential of the nanoparticles and mucin mixture compared to the zeta potential values of the individual components (**Table 4.12**). All samples of chitosan coated PLGA nanoparticles mixed with mucin demonstrated significant difference

(P < 0. 0001) when compared with free mucin particles, therefore confirming mucoadhesive interactions between them (**Figure 4.7**).

**Table 4.12:** Zeta potential values of mucin particles in PBS, nanoparticle formulation coated in different types of chitosan, and nanoparticles incubated with mucin. All nanoparticle samples were at pH = 4.5, incubated for 1 hour at 37 °C, shaking 100 RPM. Error bars represent SD and n = 3.

| **Chitosan type** | **Chitosan concentration (mg/ml)** | **P407 conc. (% w/v)** | **Zeta potential (mV)** | | |
|---|---|---|---|---|---|
| | | | **Mucin** | **Nanoparticles** | **Nanoparticles + mucin** |
| CS-L | 1 | 0.025 | -7.9±1 | 36.3±2 | 9.8±1 |
| CS-M | | | | 41.2±2 | 13.3±1 |
| CS-H | | | | 38.5±1 | 10.8±1 |
| C-CS | | | | 35.0±2 | -0.6±1 |

Formulations with CS-L, CS-M and CS-H mixed with mucin showed high zeta potential of 9.8 ± 1 mV, 13.3 ± 1 mV and 10.8 ± 1 mV, respectively, compared to C-CS + mucin zeta potential of -0.6 ± 1 mV. Although CS-L, CS-M and CS-H demonstrates significantly better mucoadhesive properties when interacting with mucin based on the measured zeta potential values, C-CS showed physical particle aggregation in the sample (**Figure 4.8**). This was initially considered to contradict zeta potential values that indicated its poor mucoadhesive properties. It was hypothesised that interactions between C-CS nanoparticles and mucin particles are particularly strong, which result in aggregation into physically visible clumps.

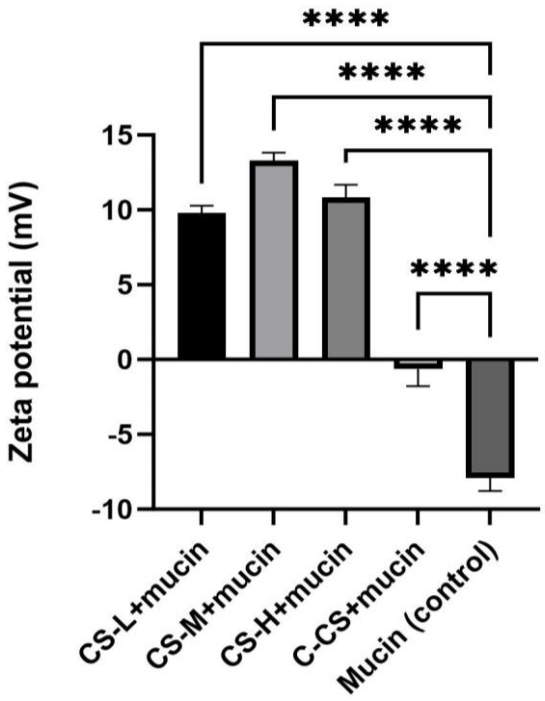


**Figure 4.7:** Interaction between different types and MWs of 1 mg/ml chitosan coated PLGA nanoparticles with porcine mucin measured in zeta potential. **** (P-value < 0.0001). Error bars represent the SD and n = 3.

However, the reason why C-CS interaction with mucin is seemingly different to CS-L, CS-M or CS-H is due to carboxyl group present in water soluble polymer [371]. The difference in mucoadhesive properties observed between chitosan and water-soluble chitosan in *in vitro* mucoadhesion assay can be explained by difference in their pKa values. When usually pKa of chitosan is ≈ 6.5, carboxyl groups on chitosan have pKa value of 4.5, meaning that protonation of C-CS is expected even in neutral pH ≥ 7 [358]. C-CS is considered to be an amphoteric polymer, as it has both cationic and anionic charges due to amino and carboxyl groups present [318,358]. These polymers have a unique isoelectric point, where pH above it makes polymer overall negatively charged, or pH below it makes polymer positively charged [373]. It was reported by Fu et al., 2024 that mucoadhesive interactions between amphoteric polymers and mucin were observed only when pH was below isoelectric point, where polymer exhibited positive charge forming electrostatic interaction with negatively charged mucin [373]. However, when C-CS formulations at pH = 4.5 are mixed with mucin in PBS pH = 7.4 during *in vitro* mucoadhesion assays, the pH of bulk solution changes and becomes closer to the isoelectric point, which for C-CS reportedly is 5.5 [358]. It has been reported that amphoteric polymers undergo aggregation when pH reaches near their isoelectric point [373,374], which can be seen in present study after C-CS coated nanoparticles are incubated with mucin (**Figure**

**4.8**). Under these conditions, amphoteric polymers become non-charged or negatively charged, in turn losing their electrostatic attraction with mucin and relying on weak hydrogen bonds or physical entanglement to ensure mucoadhesive interactions [373]. Due to this reason, poor zeta potential values can be observed of C-CS coated nanoparticles incubated with mucin in **Table 4.6** (in **section 4.3.1.3.**), as well as results in **section 4.3.3.1.** However, poor zeta potential values do not display accurate mucoadhesive properties of C-CS coated PLGA nanoparticles, as final pH of *in vitro* mucoadhesion assay is not equal to 4.5, due to addition of mucin that is dispersed in pH = 7.4. Therefore, theoretically, in pH = 4.5 conditions C-CS coated nanoparticles should demonstrate strong attractive interactions towards mucosal tissue, due to electrostatic interactions between negatively charged urothelium and highly positively charged C-CS [224,346].

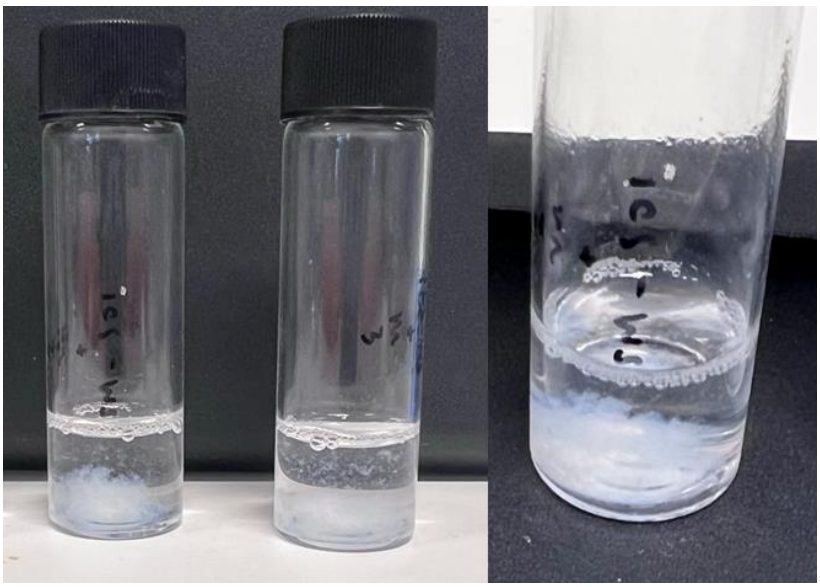

**Figure 4.8:** Physical aggregation observed in *in vitro* mucoadhesion assay, where 1 mg/ml C-CS coated PLGA nanoparticles in pH = 4.5 were mixed with 0.5 mg/ml mucin in PBS pH = 7.4 and incubated for 1 hour at 37 °C degrees, shaking at 100 RPM.

Mucin binding experiments to measure *in vitro* mucoadhesion properties have been widely used in the pharmaceutical research field [224,346,367,368]. Mainly, this assay is used as preliminary indication of any mucoadhesion behaviour of tested samples. Study by Takeuchi at el., 2005 have demonstrated enhanced chitosan affinity to mucin particles with increase in chitosan concentration and greater MW used [224]. While CS-M coated nanoparticles showed significantly stronger ($P < 0.001$) binding with mucin particles compared to CS-L coated nanoparticles, formulation containing CS-H failed to increase zeta potential further to indicate

even stronger mucoadhesive behaviour. The reason for this could be the overall poor quality and colloidal stability of the CS-H coated nanoparticles (**Table 4.5** in **section 4.3.1.3.**), which therefore impacted how well chitosan could interact with mucin particles.

Overall, CS-L, CS-M and C-CS coated nanoparticles demonstrated strong mucoadhesive interactions with mucin. However, different concentrations of chitosan still needed to be investigated in order to potentially enhance mucoadhesive interaction between nanoparticles and mucin.

### 4.3.3.3. Sample preparation for *ex vivo* mucoadhesion assay

Based on results of nanoparticle characteristics from **section 4.3.1.3.** and mucoadhesive properties of chitosan explored in **section 4.3.3.3.**, five final formulations of chitosan coated nanoparticles were selected for further testing. Formulations 0.5CS-M-P407, 1CS-L-P407, 0.5C-CS-P407, 1C-CS-P407, 2C-CS-P407 and NoCS-P407 were each incubated with mucin particles for 1 hour and then their zeta potential values were measured (**Figure 4.9**). Highly positive zeta potential readings of 0.5CS-M-P407 and 1CS-L-P407 samples indicated strong affinity between nanoparticles and mucin particles. It appears that zeta potential values of higher MW of CS-M samples have no significant difference ($P > 0.05$) when compared to values of lower MW CS-L samples. Therefore, it seems that despite having half the amount of chitosan used, CS-M samples can achieve the same mucoadhesive interaction as CS-L samples. These findings were consistent with already reported data in the literature, where higher concentrations of chitosan, along with higher MW of chitosan, will increase affinity of chitosan coated particles to the mucin particles [224,225]. Formulation No-CS-P407, which had no mucoadhesive coating, demonstrated negative zeta potential values, suggesting that polymeric nanoparticles did not show mucoadhesive behaviour towards mucin particles. Similar observations were reported in previous studies [225,361].

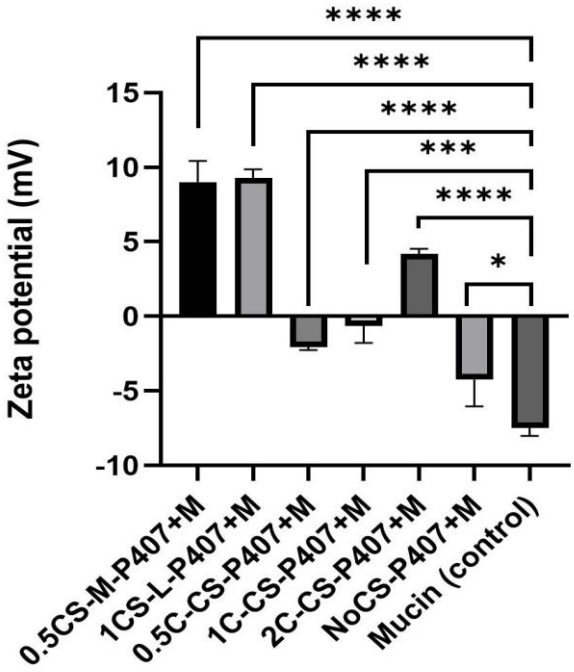


**Figure 4.9:** Graph demonstrates zeta potential values of chitosan coated PLGA nanoparticles incubated with mucin particles. Three different concentrations of chitosan and three different types of chitosan were used to coat nanoparticles. * (P-value < 0.05), *** (P-value < 0.001), **** (P-value < 0.0001). Error bars represent SD and n = 3.

The zeta potentials of 1 mg/ml and 2 mg/ml C-CS coated nanoparticles were similar to the zeta potentials of CS-M and CS-L coated nanoparticle formulations (**Table 4.8** in **section 4.3.1.3.**), however when tested in combination with mucin particles, the zeta potential values demonstrated very different results. Zeta potential values of C-CS nanoparticles with mucin ranged from -2 mV to 4.2 mV range, which was significantly lower than observed in CS-M-P407 and 1CS-L-P407 samples, 9 ± 1 mV and 9.3 ± 1 mV, respectively. Increase in concentration of C-CS samples from 0.5 mg/ml to 2 mg/ml showed significant increase ($P < 0.05$) in zeta potential values, which agrees with often reported enhancement of mucoadhesive properties with increased concentration of chitosan [224,225]. All C-CS samples demonstrated relatively low zeta potential values, therefore indicating poor affinity between nanoparticle formulations and mucin particles. The reason for this was explained in detail in **section 4.3.3.2.**

Despite limitations of our *in vitro* mucoadhesion assay, which demonstrated poor mucoadhesive properties of C-CS coated nanoparticles, several studies reported that water-soluble chitosan can achieve stronger mucoadhesive interactions than chitosan [361,366]. A

study by Pawar et al., 2013 used two different types of mucoadhesive polymers to coat their PLGA nanoparticles – a water-soluble glycol chitosan and chitosan (MW 110 – 150 kDa). It was observed that water-soluble chitosan showed better mucoadhesive properties than chitosan (MW 110-150 kDa) by having longer residence time in nasal cavity and better cell uptake [361]. Similar results were reported by Shinde et al., 2019, where they synthesised a water-soluble chitosan derivative N-trimethyl chitosan, which was then used to encapsulate flurbiprofen. These nanoparticles demonstrated higher affinity to mucin when compared to only chitosan nanoparticles [366].

Many published scientific papers use the results of *in vitro* mucin binding assay to confirm mucoadhesive interactions of their nanoparticle formulations [344,346,361,366–368]. This assay is quick to perform, inexpensive and does not require use of animal tissue or animal models. However, results from our study demonstrate how misleading conclusions can be drawn based on inaccurate zeta potential results, due to limitation of the assay and a complex protonation process of amphoteric polymers. Additionally, interactions between nanoparticle solution and mucin would be more complicated once exposed to the *ex vivo* or *in vivo* mucosal tissue, due to additional ionic, hydrophobic and Van der Walls interactions, as well as macromolecular entanglements [375].

The C6 loaded PLGA nanoparticles were prepared for *ex vivo* mucoadhesion assay to enable quantitative analysis of fluorescence (**Table 4.10** in **section 4.3.2.**), thus it was important to confirm that encapsulation of fluorescent dye or active agent, such as drugs for applications in drug delivery, does not have an impact on mucoadhesive properties of nanoparticle formulations. Therefore, *in vitro* mucoadhesion assay was performed with C6 loaded nanoparticles that were coated in 0.5 mg/ml CS-M, 1 mg/ml CS-L, 0.5 mg/ml C-CS, 1 mg/ml C-CS, and 2 mg/ml C-CS. Uncoated C6 loaded PLGA nanoparticle formulation was used as control. Results were comparable with unencapsulated formulations tested above.

### 4.3.4. *Ex vivo* mucoadhesive study on porcine bladder

Mucoadhesive properties of nanoparticle formulations established in **section 4.3.3.3.** were tested *ex vivo* on porcine bladder tissues. After 400 µl of each C6 loaded PLGA nanoparticle formulation was distributed on the tissue, samples were incubated for 1 hour in dark conditions at 37 °C degrees. Then, each tissue was subjected to 7 rounds of washing, washed off material

collected for every sample, and quantified using spectrofluorometer to measure the percentage of nanoparticles that were lost after each washing cycle. Results of washed-off nanoparticles per individual wash were plotted in **Figure 4.10**, with cumulative remaining percentage of nanoparticles on the tissue presented in **Figure 4.11.**

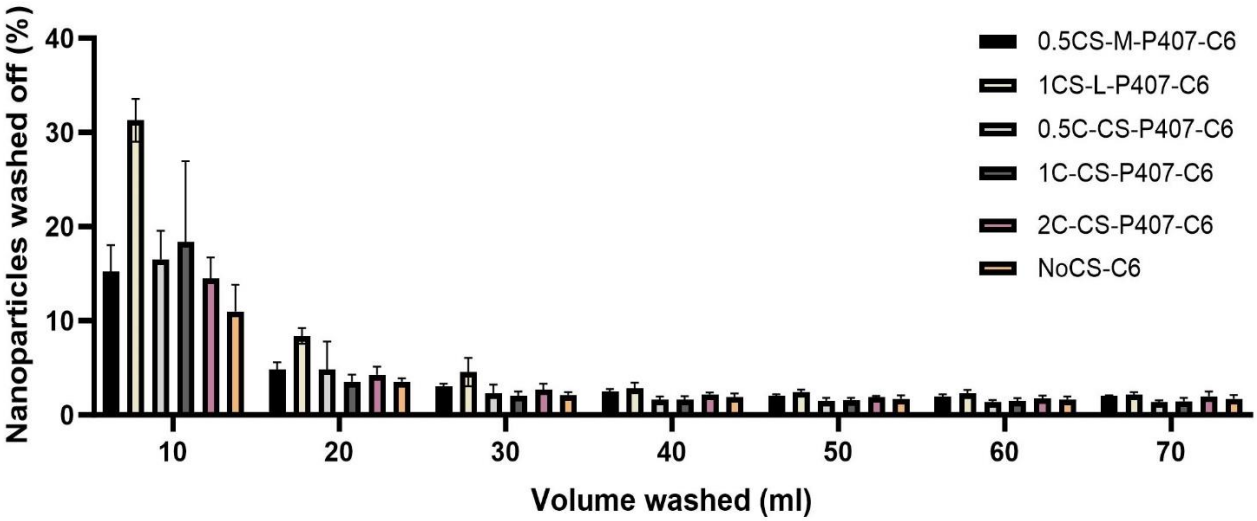


**Figure 4.10:** Graph presenting percentage of different types and concentrations of chitosan coated and C6 loaded PLGA nanoparticles washed off during each 10 ml wash of artificial urine, measured by fluorescence quantification. Error bars represent SD and n = 3.

Results of this study can conclude that most of nanoparticles were washed-off during the first 2 wash cycles. During the first wash a range from 11% to 31% of nanoparticles were lost, while second wash showed loss from 3.5% to 8%, depending on the nanoparticle formulation used. Formulation 1CS-L-C6 demonstrated highest ($P < 0.05$) percentage (31.3 ± 2%) of nanoparticles lost during the first wash. It was also the formulation that showed the highest overall loss of nanoparticles throughout all washing cycles reaching 54%. Interestingly, lowest percentage of loss was observed in NoCS-C6 formulation, which had no chitosan coating. Only 10 ± 3% were lost during the first wash, and overall mean loss throughout the cycles accumulated to 23.6%.

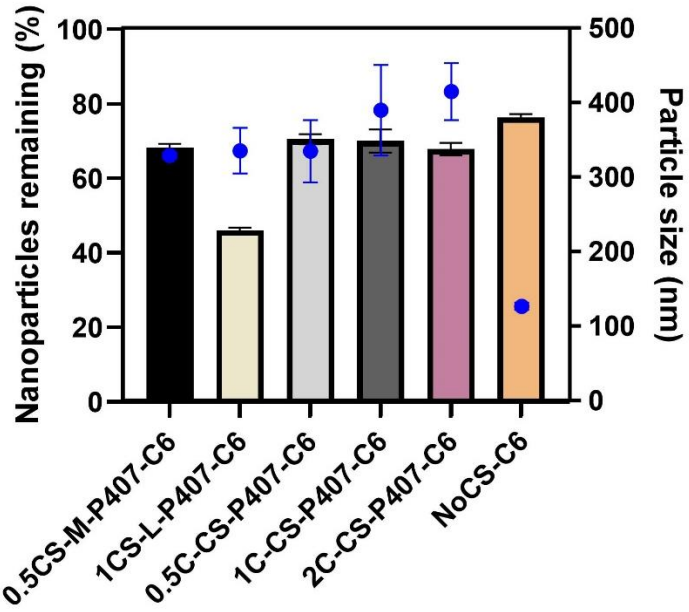


**Figure 4.11:** Graph showing the percentage of chitosan coated C6 loaded PLGA nanoparticles left on porcine bladder tissue after 7 cycles of washing with artificial urine, measured by fluorescence quantification. Blue data points demonstrate particle size values of C6-loaded PLGA nanoparticles coated with CS-L, CS-M or C-CS and used for *ex vivo* mucoadhesion testing. Error bars represent SD and n = 3.

It is important to highlight that even with the highest percentage of nanoparticles lost during 7 washing cycles, 46 ± 1% of them remained on the bladder surface (**Figure 4.11**). Majority of chitosan coated formulations demonstrated 67.9% to 70.5% retention of nanoparticles on bladder tissue. Highest percentage of nanoparticles remaining on mucosal tissue after the washes was achieved by NoCS-C6 formulation, which demonstrated 76.4 ± 1% retention. Porcine bladder tissues were observed under microscope after the first and final wash, with fluorescent images presented in **Figure 4.12**. After 7 rounds of washing, fluorescence could still be observed on certain parts of the tissue, confirming good particle retention.

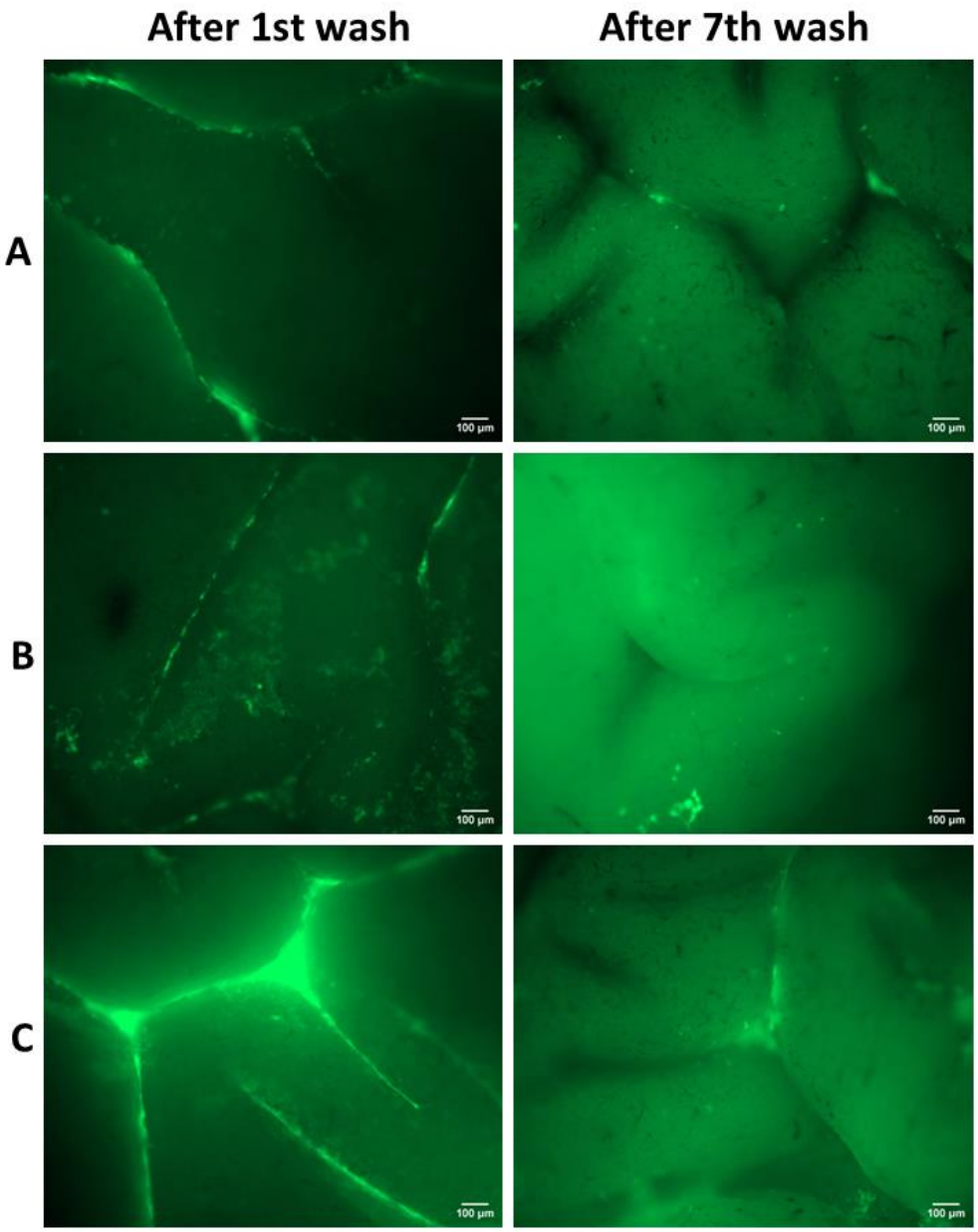


**Figure 4.12:** Images demonstrate fluorescent C6 loaded PLGA nanoparticles coated with (A) 0.5 mg/ml C-CS, (B) 1 mg/ml C-CS, and (C) 2 mg/ml C-CS remaining on *ex vivo* porcine bladder after first 10 ml wash with artificial urine (images on the left) and after 7th wash, or 70 ml total washed, of artificial urine (images on the right). Scale bar denotes 100 µm.

Formulations 0.5CS-M-C6, 0.5C-CS-C6, 1C-CS-C6 and 2C-CS-C6 demonstrated relatively similar mucoadhesive properties. During the first wash there was no significant difference ($P > 0.05$) between the samples as they all lost 14.5% to 18.3% of nanoparticles. During the second wash, formulations 0.5CS-M-C6, 0.5C-CS-C6 and 1C-CS-C6 performed better by losing 4.9 ± 1%, 4.8 ± 3 % and 3.5 ± 1% of nanoparticles, respectively, compared to 2C-CS-C6 formulation, which showed 7.2 ± 5% loss. However, no significant difference ($P > 0.05$)

was detected between these samples. Looking at overall mean of nanoparticles lost after all washing cycles, formulations demonstrated very similar values. 0.5C-CS-C6 and 1C-CS-C6 showed total loss of 29.5 ± 8% and 30 ± 6%, respectively, while formulations 0.5CS-M-C6 and 2C-CS-C6 accumulated loss of 31.7 ± 4% and 32.1 ± 3%, respectively.

Overall, the retention time of nanoparticles shown in **Figure 4.11** is considerably higher than results observed in previous studies. Study by Barthelmes et al., 2011 showed 14 times increase in mucoadhesive interaction between chitosan nanoparticle functionalised with thioglycolic acid (TGA) and porcine bladder tissue, compared to unmodified chitosan nanoparticles [231]. Their study reported that free thiol groups located on chitosan and TGA nanoparticles can form strong covalent bonds with cysteine-rich subdomains of glycoproteins on the mucous layer [231]. Although this group has used a continuous bladder rinsing method mimicking *in vivo* conditions, only 1% of nanoparticles remained on the bladder tissue after 3 hours of washing, while 14% of chitosan and TGA nanoparticles were discovered after the same amount of time. A similar approach to improve mucoadhesive properties of PLGA nanoparticle formulation was taken by Kaldybekov et al., 2019. They tested maleimide functionalised PLGA-poly (ethylene glycol) (PLGA-PEG) nanoparticles and their mucoadhesive properties on *ex vivo* lamb urinary bladder tissues [222]. Study reported poor retention of unfunctionalized PLGA-PEG nanoparticles of less than 20% of particles remaining after the first wash. Retention times of these nanoparticles were significantly improved by functionalising them with maleimide, which demonstrated 60% of nanoparticles remaining after the first wash, dropping to roughly 40% after the second wash [222].

Commonly, the most important parameters of nanoparticle formulation for mucoadhesive interactions are assumed to be the positively charged nanoparticle coating. However, the fact that formulation without chitosan demonstrated the lowest percentage of nanoparticles lost throughout washing cycles, seems to highlight importance of other particle characteristics. It is hypothesized that smaller particles can get stuck in the mucosal folds within the bladder wall and therefore be protected from artificial urine washouts. Oppositely, bigger sized particles can be easily washed away. This hypothesis is supported by significantly smaller ($P < 0.001$) nanoparticle size of NoCS-C6 formulation at 126.6 ± 5 nm, compared to chitosan coated formulations, which particle sizes range from 328.9 nm to 414.9 nm (**Figure 4.11**). While formulations 0.5CS-M-C6, 0.5C-CS-C6, 1C-CS-C6 and 2C-CS-C6 show significantly higher nanoparticle size, their mucoadhesive properties are similar to NoCS-C6 formulation (**Figure**

**4.10**). It appears that previously mentioned chitosan coated formulations have sufficient affinity to mucosal tissue, that despite their bigger particle size, they cannot be washed out with artificial urine. Similar results were reported by Barthelmes et al., in 2013 study, when they investigated mucoadhesive properties of nanoparticles and microparticles which were made from anionic and cationic thiolated polymers [342]. Their study confirmed the importance of particle size for mucoadhesive properties, as microparticles showed poorer adherence to the bladder wall when compared to nanoparticles.

Results also confirmed findings reported in **section 4.3.3.2.**, where it was stated that the strength of mucoadhesive interaction between nanoparticles and mucosal layer depends on the type of chitosan used and its MW chosen [224,225,361]. Results of *ex vivo* mucoadhesion assay demonstrated that nanoparticles coated with CS-L were much more easily washed off the bladder tissue, compared to formulations coated with CS-M and C-CS. Formulations containing different concentrations of C-CS and CS-M demonstrated roughly 16% loss of nanoparticles after the first wash cycle, while almost double the amount (31.2 ± 2%) of CS-L coated nanoparticles was washed off. In **section 4.3.3.2.**, comparison between different types of chitosan was challenging due to low zeta potential results of C-CS samples. The reason behind this was a limitation of the *in vitro* mucoadhesion assay, which impacted final sample pH to be higher than starting pH = 4.5. Due to carboxyl groups present in C-CS, this amphoteric polymer has reached its isoelectric point at a pH of ≈ 5.5 and became neutrally or negatively charged. Therefore, results achieved from *in vitro* mucoadhesion assays could not accurately predict mucoadhesive properties of C-CS coated formulations. However, in *ex vivo* mucoadhesion assays, all C-CS and CS-M samples demonstrated comparatively similar results.

Some of the large error bars observed in **Figure 4.10** indicate limitations of the chosen *ex vivo* mucoadhesion assay. Based on the results obtained in this study, it seems that bladder thickness and tissue viability can have an impact on retention of the nanoparticles on bladder surface. For instance, thicker bladder tissue with more mucosal folds resulted in higher retention time of nanoparticles. As smaller sized particles got entrapped within the folds, the more challenging it became to access particles during artificial urine wash-out process. Additionally, as *ex vivo* mucoadhesion assay was performed in triplicate, different porcine bladders were used to test the same formulation, which meant that some replicates with healthier and thicker bladders showed less nanoparticle loss than others. This can be clearly observed in 1C-CS-C6 formulation in **Figure 4.10**, where large standard error bar indicates variation in percentage of

particles washed-off during the first round of artificial urine. However, it is important to recognise that *ex vivo* results cannot be interpreted as accurate representation of formulation performance *in vivo*. Bladder is expected to expand and stretch its mucosal folds as it stores the urine [376], which in turn could allow urine to have better access to the nanoparticles. Without being entrapped into mucosal folds, mucoadhesive nanoparticles would be exposed to urine filling and voiding, which is hard to mimic in *ex vivo* conditions and then investigate mucoadhesive particle retention on the bladder tissue. Despite these limitations, *ex vivo* analysis allows to predict preliminary results, which could help to reduce number of samples, as well as lower number of animals needed for *in vivo* study.

Most of the studies on mucoadhesive properties choose *in vitro* assay instead of *ex vivo* due to less equipment and skill needed for these tests, as well as difficulty to obtain fresh tissue in relatively short time [225,348]. Studies by Khutoryanskiy group [222,230,278,343] and Benkorp-Schnürch group [231,342] focused on investigating *ex vivo* mucoadhesive properties of nanoparticles for intravesical delivery to urinary bladder. Most of their studies focus on functionalising nanoparticles with thiol groups that can form strong covalent linkage with glycoproteins in the mucosal lining [222,230,231,342]. This approach demonstrates stronger mucoadhesive properties compared to electrostatic interaction between negatively charged epithelium and positively charged chitosan [377]. Although our study uses a C-CS as one of the more commonly used chitosan derivatives, both chitosan and C-CS rely on electrostatic interactions to bind with mucin. Therefore, in the future it would be beneficial to attempt to improve and compare interactions with mucin between C-CS and thiolated chitosan.

A relatively novel approach of sustained drug delivery directly to bladder is using mucoadhesive *in situ* forming gels [234–238]. The main advantage of this approach is the injectable state of the hydrogel at low temperatures, which can undergo a sol-gel transition triggered by higher temperature once administrated into the body [235]. Viscosity of hydrogel changes into solid state gel, which if made with thiolated polymers, can ensure strong mucoadhesion properties and do not affect function of the bladder [236]. Earlier studies by Lin et al., 2014 and Sherif et al., 2018 raised the question of bladder obstruction by using *in situ* gels for drug delivery, however they have demonstrated that mucoadhesive or floating hydrogel has no impact on urine flow [239,240]. Study by Shawky et al., 2022 examined retention of chitosan coated solid-lipid nanoparticles on the bladder surface. Results revealed that chitosan coated nanoparticles showed 41% of nanoparticles remaining on the mucosal lining after 5

washes, which was enhanced to 53-65% when particles were entrapped in chitosan hydrogel [234]. Entrapment of nanoparticles into hydrogels could also additionally sustain nanoparticle drug release [234,238]. Use of mucoadhesive hydrogels to improve retention time of drugs or nanoparticles on bladder surface has demonstrated a lot of potential to safely and efficiently deliver drugs through intravesical route. Embedding nanoparticles obtained in our study into mucoadhesive hydrogels could significantly prolong retention time of drug loaded nanoparticles in the bladder, as well as negate the need for smaller sized particles, which appeared to be necessary to ensure particle entrapment into mucosal folds of *ex vivo* bladder tissue.

### 4.3.5. Histology and toxicity

Tissues of freshly excised porcine bladder were used to assay any toxic effects caused by mucoadhesive nanoparticle treatment discussed in **section 4.3.4**. Bladder tissues were dissected and treated with 400µl of each nanoparticle formulation and then fixed, embedded in paraffin and sectioned. After dehydration process and H&E staining, the tissue was rehydrated and mounted onto the microscope slides, which were later observed for any pathological indications in the urothelium layer.

For this study, *ex vivo* toxicity method was selected instead of more commonly used cytotoxicity assays. Due to the nature of this project, more commonly used cell lines of bladder cancer would only provide very limiting results due to not being biologically accurate. An established human cell line of urinary bladder epithelium cells called UROtsa was considered, however due to time restrains and already established access to fresh porcine bladder tissue, *ex vivo* toxicity assay was performed.

Untreated porcine bladder tissue was used as a negative control. H&E staining demonstrated a healthy tissue layer with tightly packed urothelial cells maintaining bladder wall structure. At the luminal surface of the urothelium, a layer of umbrella cells can be observed (**Figure 4.13**), which together with uroplakins make up a plaque that forms a strong permeability barrier [4]. No difference was observed between tissues kept on ice and tissues that underwent washing with PBS, 10 min drying and 1 hour incubation procedure, indicating no negative effects that could be associated with treatment procedure. In order to demonstrate what significantly toxic effects would look like on the porcine tissue, tissues were subjected to protamine sulphate (PS)

treatment for 1 hour at 37 °C. Here, desquamation of the urothelium layer can be seen as tight and adherens junctions are destroyed by PS downregulating ZO-1 protein, resulting in loss of structural stability and rigidity of the barrier [333,378–380]. Following the treatment of nanoparticle formulations 0.5CS-M-P407, 1CS-L-P407, 0.5C-CS-P407, 1C-CS-P407 and 2C-CS-P407 no adverse effects on urothelium were observed. Some haziness associated with the plaque on the urothelium layer can be observed in **Figure 4.13**, specifically in images E to I, however it is likely to be artefacts, as integral barrier structure made of tightly positioned umbrella cells does not appear to be affected. As a control to chitosan coated nanoparticle formulation, formulation with no chitosan coating was also used as a treatment and similarly to the other formulations, showed no toxicity. All formulations tested were at pH = 4.5.

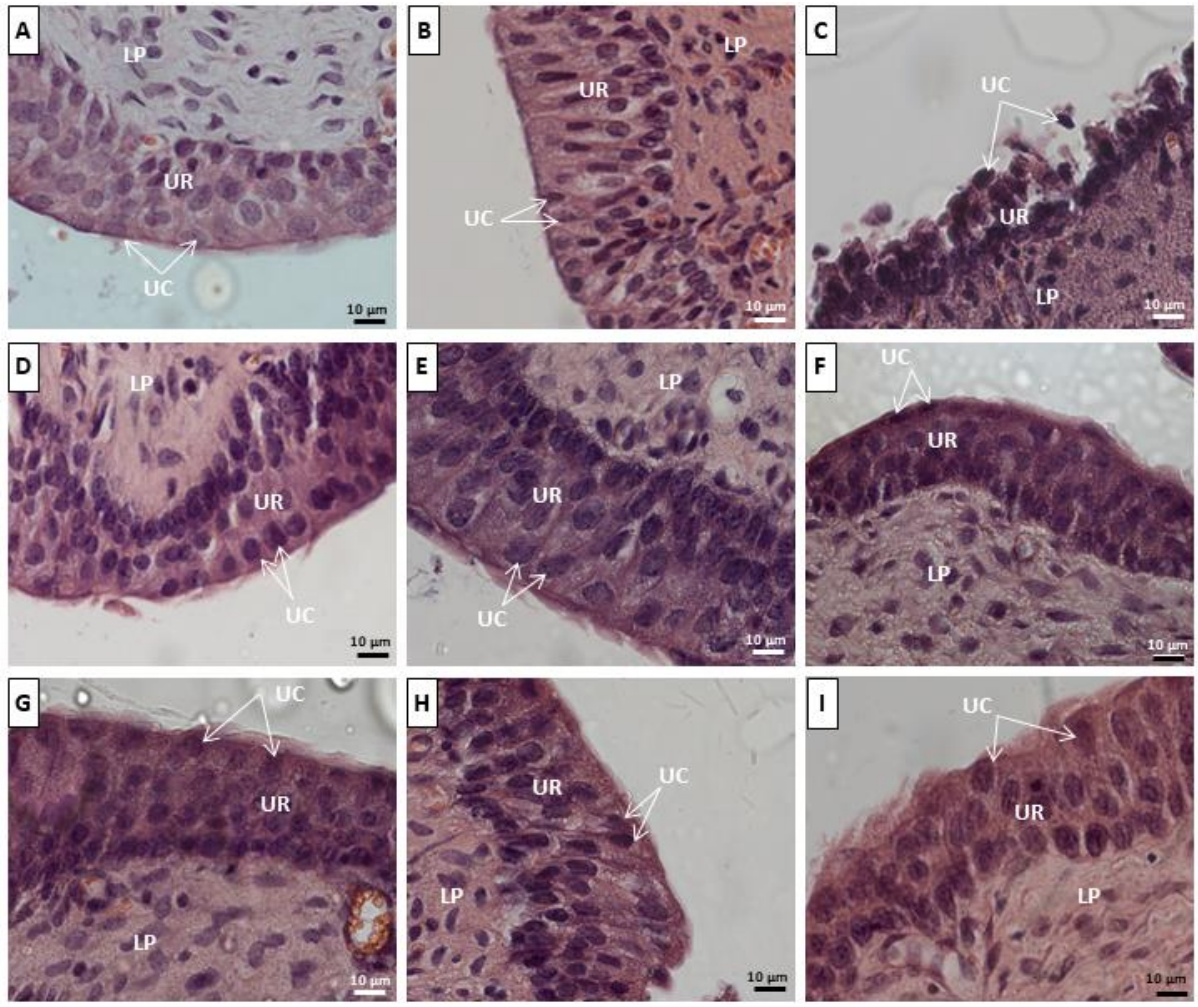


**Figure 4.13:** Microscopic images of H&E stained porcine bladder tissue sections of 8 µm thickness. Negative controls of (A) freshly excised porcine bladder, stored at 4 °C during transportation, (B) no treatment, tissues followed the washing and incubation in 37 °C procedure. Tissues treated for 1 hour at 37 °C with (C) 10 mg/ml PS in PBS 7.4, (D) 400 µl of

0.5CS-M-P407, (E) 400 µl of 1CS-L-P407, (F) 400 µl of 0.5C-CS-P407), (G) 400 µl of 1C-CS-P407, (H) 400 µl of 2C-CS-P407, and (I) 400 µl of No-CS. Study performed in triplicate. Scale bar denotes 10 µm, UC = umbrella cells, UR = urothelium, LP = lamina propria.

Obtained results from H&E stained tissues were expected, as all chemicals used in nanoparticle formulations were previously evaluated for their potential harmful effects. For example, it has been widely reported that PLGA is a safe, biodegradable polymer, that has FDA approval for drug delivery in human body [90]. On the other hand, some toxic effects of chitosan have been previously reported in the literature. Kos et al., 2006 highlighted that increasing concentration of chitosan (from 0.0001% to 0.5% (w/v)), along with increased incubation time, has caused necrosis of superficial cells and desquamation of umbrella cells [220,221]. In comparison, present study used 0.000005% to 0.00002% (w/v) of chitosan to coat PLGA nanoparticles, which is significantly lower than the range reported by Kos et al., 2006 [220]. A follow up study by Veranič et al., 2009 demonstrated that desquamation of umbrella cells occurs as fast as after 10 min of treatment, when cells start to detach due to becoming necrotic [217]. The group has confirmed that no apoptotic signs can be seen through microscope imaging, explaining why nuclei observed in **Figure 4.14** (in **section 4.3.6.**) appear healthy. Additionally, Veranič et al., 2009 shown that differentiation of umbrella cells is incredibly fast, with restoration of urothelium layer observed within an hour post treatment [217,221]. Therefore, although chitosan does evoke some negative effects on bladder tissue, they are restored quickly with no known long-term consequences. Study by Erman et al., 2017 has confirmed that there are no prolonged toxicity effects on urothelium even after administration of several doses of chitosan in a short period of time [221].

Chitosan use has been approved by FDA, however either for oral consumption as food supplement, or as application for wound or haemostatic dressings [244,381,382]. Although there are many published studies investigating chitosan use in drug delivery field, it is difficult to approve chitosan for drug delivery, due to different parameters of MWs or degrees of deacetylation used in many studies [382].

Since chitosan has demonstrated to cause some degree of desquamation, it was important to investigate how use of chitosan can influence particle permeation into urothelium. Known as the most impermeable barrier in the human body, urothelium penetration could be incredibly beneficial for UTI treatment and recurring UTI prevention.

### 4.3.6. Mucopenetration assay

Tissues of freshly excised porcine bladder were used to analyse whether nanoparticle treatment permeates into deeper levels of urinary bladder tissues. Tissues were treated with mucoadhesive C6 loaded nanoparticle formulations for 1 hour in dark conditions at 37 °C, afterwards they were fixed, embedded in paraffin and sectioned, later undergoing dehydration process. After rehydration, tissues were mounted using VECTASHIELD® antifade mounting media to prevent samples from photobleaching and fading during imaging and storing.

Distribution of C6 fluorescence within the urothelium demonstrated how permeable the tissue is for C6 loaded PLGA nanoparticles coated with chitosan. Overall thickness of urothelium layer was determined by observing the same area of the tissues under DAPI channel, under which nuclei of tightly assembled urothelium cells were visible. Results of urothelium thickness are presented in **Figure 4.14**. To quantify mucopenetration results, the width measurement of the green fluorescence was compared with width of urothelium layer as observed under DAPI channel (**Figure 4.15**).

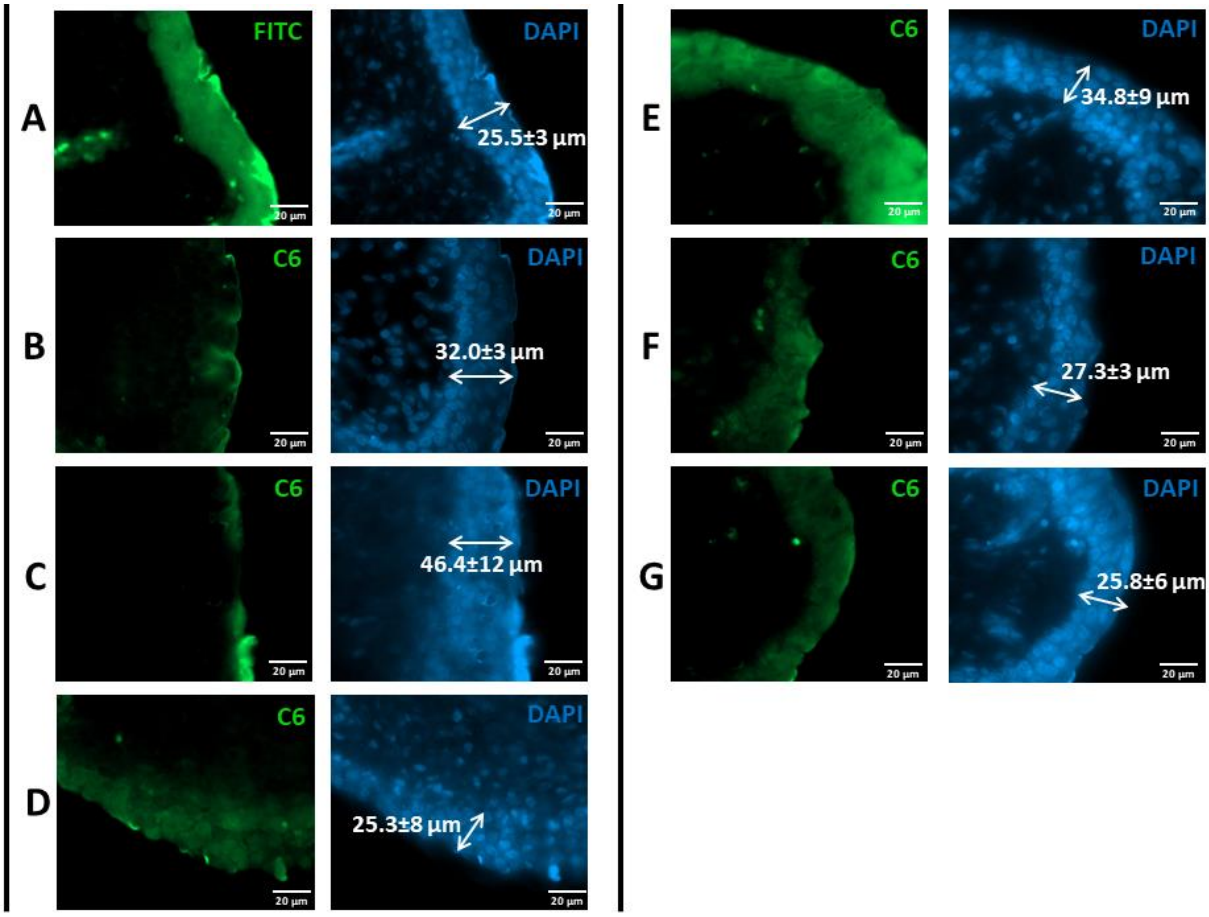


**Figure 4.14:** Visual representation of *ex vivo* mucopenetrative properties of mucoadhesive C6 loaded nanoparticle formulations on porcine bladder tissues. Tissues were incubated for 1 h in dark conditions at 37 °C after treatment with (A) 10 mg/ml PS and 10 µg/ml fluorescein isothiocyanate (FITC), (B) NoCS-C6, (C) 0.5CS-M-C6, (D) 1CS-L-C6, (E) 0.5C-CS-C6, (F) 1C-CS-C6, and (G) 2C-CS-C6. Tissues observed under green channel (FITC and C6 marked images), where green fluorescence represents nanoparticle permeated urothelium. Same tissues were captured under blue channel (DAPI marked images), where blue stained and densely packed nuclei indicate urothelium layer. Study performed in triplicate. Scale bars = 20µm.

To demonstrate a positive event of mucopenetration, a mixture of PS and fluorescent dye in PBS buffer were used. As C6 is a hydrophobic fluorescent dye, it had to be changed to a hydrophilic one, therefore 10 mg/ml of PS and 10 µg/ml of fluorescein isothiocyanate (FITC) were administered on the tissue (**Figure 4.14A**). Although this is not a true positive control, PS facilitated the disruption of cell-cell junctions in the urothelium, allowing FITC to fully penetrate through the layer [333]. Results demonstrated 22.8 ± 1 µm out of the 25.5 ± 3 µm of the overall urothelium thickness to be penetrated by the fluorescent dye, indicating successful

mucopenetration of urothelium layer. No mucopenetrative effects were observed past lamina propria for all samples tested.

Negative control of C6 permeability was challenging to obtain, as C6 is highly hydrophobic dye that would not permeate past hydrophilic mucin layer of the bladder due to hydrophobicity of this fluorescent dye [9]. Due to this, it was expected that C6 would form a uniform layer of fluorescence at the very top of the urothelium.

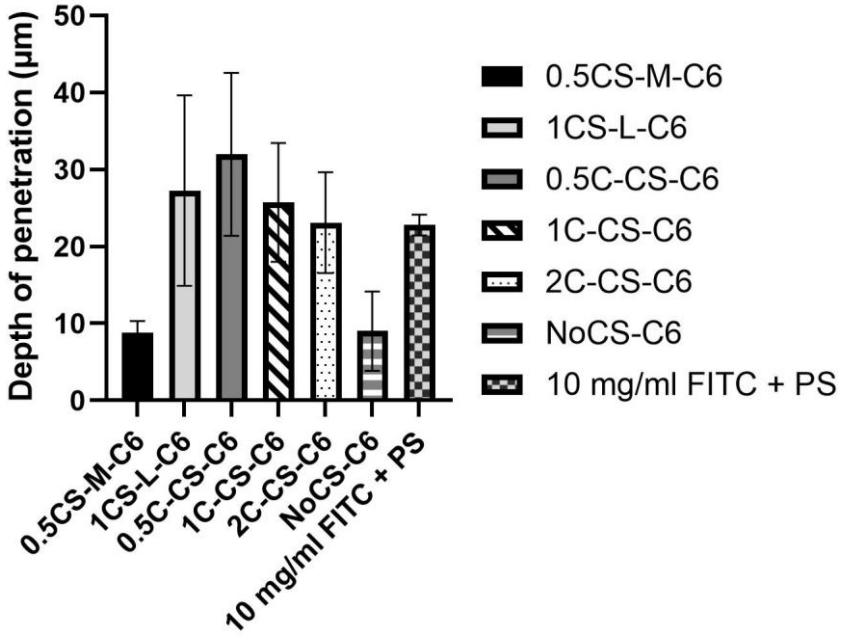


**Figure 4.15:** Graph demonstrating the depth of penetration into the urothelium tissue achieved by mucoadhesive C6 loaded PLGA nanoparticles after administrating them onto the bladder tissue, measured by fluorescence quantification. PS = protamine sulphate, FITC = fluorescein isothiocyanate. Error bars represent SD and n = 3.

Results demonstrated poor permeability of the tissue after the treatment with NoCS-C6 nanoparticle formulation, as formulation penetrated only 9 ± 5 µm of the tissue and most of the fluorescence was concentrated at the top of the urothelium layer. Interestingly, formulation 0.5CS-M-C6 showed similar mucopenetration results with the fluorescence detected up to 8.8 ± 2 µm of the tissue, which therefore indicated no significant difference ($P > 0.05$) between CS-M-coated and uncoated nanoparticles. However, other chitosan-coated nanoparticle formulations have showed significant enhanced mucopenetration properties when compared to NoCS-C6 formulation. Nanoparticles coated with C-CS demonstrated best mucopenetration

results, with tissues demonstrating 32 ± 11 μm of the urothelium permeated after treatment with 0.5C-CS-C6 formulation.

Additionally, the nuclei of the urothelium layer were observed under fluorescence for any indications of apoptotic cells that could signal of toxicity of the treatment. Fluorescent imaging under DAPI channel revealed non-toxic results, similarly to the results observed in H&E stained tissues in **section 4.3.5**. None of the tissues observed demonstrated presence of apoptotic cells, including tissue treated with PS which causes disruption of the cell-cell junctions of the urothelium but no evident toxicity to the cells or nuclei.

Mucopenetrative effects of chitosan have been previously reported in literature [220,383]. Kos et al., 2006 states that increase in urothelium permeability was achieved with higher concentration of chitosan used, as well as prolonged incubation time. Results of our study do not fully confirm this statement. Increase of C-CS in formulations 0.5C-CS-C6, 1C-CS-C6 and 2C-CS-C6 demonstrated no significant difference on permeability, however this could be due to overall deep permeation of 32 ± 11 μm, 25.7 ± 8 μm, and 23.1 ± 7 μm, respectively, of mucopenetration achieved. Nevertheless, the mean of these formulation was highest in 0.5C-CS-C6 formulation. Most formulations showed high SD values, suggesting permeability of certain parts of the tissue not being uniform as shown in **Figure 4.14**.

The reason why chitosan coated PLGA nanoparticles significantly increase the permeability of the urothelium is due to strong adhesion of the chitosan to the bladder wall and its low level of toxicity to the urothelium. As previously discussed in **section 4.3.5**, chitosan adheres to the urothelium via electrostatic interactions and causes short term toxicity to the umbrella cells. Along with causing necrosis of the umbrella cells, chitosan also affects the structure of the tight junctions within the urothelium layer [214,217,220,221], therefore pointing towards the mechanism in which chitosan can enhance the permeability of the bladder wall. Additionally, a study by Martin et al., 2013 have proved that PLGA nanoparticles coated with chitosan have demonstrated enhanced internalisation into urothelium of human *ex vivo* and mouse *in vivo* systems, relative to uncoated nanoparticles [383]. However, as mentioned before, Veranic et al., 2009 has shown that after chitosan exposure and first indications of umbrella cell desquamation, tight junction protein ZO-1 is present in the intermediate cell layer of the urothelium, that is exposed to the bladder lumen, indicating first signs of urothelium recovery [217]. Based on this, it is probable that mucopenetrative properties of the chitosan coated

nanoparticle formulations are achieved instantly or relatively quickly, before urothelium layer starts its differentiation. Due to desquamation and fast regeneration of the urothelium, it is challenging to predict mucoadhesive and mucopenetrative properties of chitosan coated PLGA nanoparticles *in vivo* and therefore further research within *in vivo* system is needed.

## 4.4. Conclusion

Chitosan coated PLGA nanoparticles demonstrated colloidally stable nanoparticle system. As reported in the literature, increasing chitosan concentration in the formulations lead to largely sized nanoparticles. Addition of low concentrations of surfactant P407 has significantly reduced particle size, without negatively affecting other characteristics, like PDI or zeta potential. It was also found that acidic pH conditions improve zeta potential of chitosan coated PLGA nanoparticles, achieving highly positively charge, compared to neutral pH conditions, which showed mainly neutral charge of the chitosan coated particles. In addition, PLGA nanoparticle coating with higher MW of chitosan resulted in larger and less colloidally stable nanoparticle systems. Therefore, further optimisation of formulation parameters was focused on achieving particle size under 450 nm, while ensuring the highest chitosan concentration is maintained to enhance positive zeta potential charge of the particles.

Five mucoadhesive formulations with varying concentrations of chitosan coating were tested *in vitro* and *ex vivo* to observe the strength of nanoparticle interactions with mucin. Results of *in vitro* assay, which is meant to predict nanoparticle *ex vivo* behaviour, indicated that formulations coated with CS-L and CS-M would demonstrate highest affinity with mucin, while C-CS coated and uncoated nanoparticles would not demonstrate strong mucoadhesive properties. This was contradicted by results of *ex vivo* assay, hence indicating limitations of *in vitro* mucoadhesion assay. *Ex vivo* mucoadhesion assay demonstrated that C-CS and CS-M coated nanoparticles and uncoated nanoparticles showed highest retention on the bladder tissue, maintaining around 70% of the nanoparticles after 7 cycles of washing with artificial urine.

Although chitosan is known to cause cell necrosis and desquamation, mucoadhesive polymeric nanoparticles demonstrated no toxicity on *ex vivo* porcine bladder tissue, after incubation with nanoparticle treatment for 1 hour. Uncoated nanoparticles, CS-L and CS-M coated nanoparticles showed poor mucopenetration into the urothelium. However, C-CS coated

nanoparticles showed mostly full permeation of the urothelium, comparable to the permeability of highly toxic PS, which disrupts tight junctions of the urothelium to enhance its permeability. Therefore, it was important to establish that while chitosan does show great permeation, it does not cause any toxicity if treatment time is kept short.

At the time of the study, C-CS has not been tested for mucoadhesive properties on the bladder urothelium. Our study shows that this chitosan derivative demonstrates enhanced mucoadhesive and mucopenetrative properties compared to chitosan, as well as form strong electrostatic interactions with mucosal tissue in the bladder. A recent study by Zhao et al., 2024 has also demonstrated increased retention time of the multilayer biomimetic scaffolds, made of polycaprolactone nanofibrous mats and C-CS hydrogel, in the *in vivo* environment of the urinary bladder.

# Chapter 5

## Development of celecoxib loaded PLGA nanoparticles for mucoadhesive intra-bladder drug delivery: A Design of Experiments (DoE) study

## 5.1. Introduction

Urinary tract infections (UTIs) and most of the other bladder disorders are commonly treated orally or through intravenous injections, which results in systemic exposure of the body to the therapeutical agents [9,21]. While some therapies rely on the drugs entering the blood system to achieve therapeutic results, in order to treat bladder infections drugs must accumulate in the bladder and achieve therapeutic concentrations to fight the infection [21]. Therefore, intravesical drug delivery (IDD) has been proposed as an effective way to diminish the risk of side effects due to reduced systemic exposure of the therapeutic agents, as well as reduce antimicrobial resistance (AMR) associated with antibiotic treatment of UTIs [9,21]. Despite this, IDD suffers from a few limitations, such as drug dilution in the bladder due to urine storing or early drug exposure due to urine voiding [2]. Therefore, IDD in combination with nanotechnology has showed promising drug delivery results to the bladder, especially with mucoadhesive nanoparticles offering prolonged drug retention time in the bladder and sustained drug release [21,222,342].

UTIs are mostly caused by UroPathogenic *Escherichia Coli* (UPEC), resulting in need of antibiotic treatment to manage bacterial infections [29]. Although antibiotic treatment in seen as crucial in reducing the duration and severity of the symptoms, it can also cause harm by sheltering bacterial reservoirs in the bladder cells and contributing towards AMR [29,384]. Therefore, many alternative ways of treating the UTIs have been investigated in the last decade, one of them being a symptomatic treatment of UTIs with non-steroidal anti-inflammatory drugs (NSAIDs) [74,76]. As pain experienced during voiding is classed as inflammatory reaction, UTI treatment with NSAIDs was shown to reduce the levels of cyclooxygenase-2 (COX-2) protein and prostaglandin E2, which are significantly elevated during the infection [71,385]. A small randomised controlled trial (RTC) was performed to evaluate ibuprofen, a non-specific COX-1 and COX-2 inhibitor drug, as alternative to antibiotics for treatment of uncomplicated UTIs [74,75]. The study demonstrated promising results, however larger trials were needed to confirm effectiveness of NSAIDs for UTI treatment [74,75]. Several publications have discussed an alternative NSAID drug for potential symptomatic treatment of UTI cases: a specific COX-2 inhibitor drug Celecoxib (CLX), which was also reported to increase the sensitivity of the bacteria to the antibiotic treatment [77,385].

Encapsulation of CLX into PLGA nanoparticles has been well documented in the literature [255,386–389]. While most of these CLX loaded PLGA formulations tend to be synthesised by single emulsion – solvent diffusion (SE) method [255,388,389], some other studies chose to use other well-known techniques, such as nanoprecipitation (NPPT) or salting-out [386,387]. The main difference between SE and NPPT techniques is the miscibility of the solvents that are used during these processes, along with the use of high shear force during SE method [119], with more detailed analysis of both methods described in **section 2.3.1.1.** and **section 2.3.1.2** of **Chapter 2**. Nanoparticle production can be challenging as minor changes in the selected nanoparticle preparation method or changes in the parameters can lead to significant changes in the physicochemical features [115,390]. Therefore, statistical design of experiments (DoE) tool is often used to understand and compare how input factors affect the final product [390].

The work described in this chapter aims to prepare mucoadhesive CLX loaded polymeric nanoparticle systems, which could be delivered directly to the bladder and used to treat UTIs in combination with antibiotics. In addition, this study aims to compare two commonly used nanoparticle preparation methods by implementing DoE technique. By analysing the same parameters in both preparation methods, the differences on how they affect the final product can be investigated.

The objectives of this chapter are:

- To compare two nanoparticle preparation methods (nanoprecipitation and single emulsion – solvent diffusion) by analysing how the selected parameters (polymer amount, drug amount, volume of the organic phase) affect the characteristics of CLX loaded PLGA nanoparticles.
- To utilise DoE technique to achieve colloidally stable CLX loaded PLGA nanoparticle system, with small particle size and polydispersity index, but high drug entrapment and drug loading.
- To apply mucoadhesive coating on the optimised CLX loaded PLGA nanoparticles and examine how it affects nanoparticle physicochemical and biological parameters.

## 5.2. Materials and methods

### 5.2.1. Materials

Poly(lactic-co-glycolic acid) (PLGA, 50:50 ester terminated, molecular weight (MW) 38,000–54,000 Da), poly(vinyl alcohol) (PVA, MW 9,000–10,000 Da, 80% hydrolyzed), low MW chitosan (50-190 kDa, deacetylated chitin) (CS-L), medium MW chitosan (190–310 kDa, deacetylated chitin) (CS-M), protamine sulphate (PS), artificial urine diluent, phosphate buffer saline (PBS), Tween 80, Mayer's haematoxylin solution, Eosin Y solution (aqueous), triethylamine acid, phosphoric acid, acetonitrile (ACNT, HPLC grade), dichloromethane (DCM) and ethanol (EtOH) were all purchased from Sigma-Aldrich (Merck Life Science, UK). 10% neutral buffered formalin and glacial acetic acid was purchased from Fisher Scientific, UK. Celecoxib (CLX) was purchased from Biosynth, UK. Kolliphor® P 407 Geismar was obtained from BASF (BASF, UK). Carboxymethyl chitosan (80% deacetylation, water soluble chitosan) (C-CS) was kindly gifted by Yuda Century (Qingdao, China). Histo-clear was purchased from Scientific Laboratory Supplies (Scientific Laboratory Supplies Ltd, UK). Freshly excised porcine urinary bladders were kindly supplied by Arthur Howell Butchers (Wells-next-the-Sea, Norfolk, UK).

### 5.2.2. Experimental design

For this study, a three-factor, two-level full-factorial design was chosen to optimise characteristics of CLX loaded PLGA nanoparticles synthesised by nanoprecipitation (NPPT) or single emulsion-solvent evaporation (SE) methods. Design-Expert® Software, V13 (Stat-Ease, Inc., Minneapolis, USA) was used to design matrixes with 8 runs total for each nanoparticle preparation method, with each experiment done in triplicate. Two-level screening design was chosen as initial study in order to identify significance of selected critical factors. Data obtained would then be used in future studies to generate more complex design, using only significant critical factors and higher number of levels, therefore generating more accurate statistical models.

Firstly, preliminary experiments were performed to narrow down the experiment numbers needed for DoE study. This included experiments to determine the levels for chosen critical factors, which were PLGA amount, drug amount, and the volume of organic solvent. Once critical factors were identified in both nanoparticle synthesis methods, their influence was investigated on selected nanoparticle characteristics (responses): particle size, polydispersity

index (PDI), encapsulation efficiency (EE%), and loading capacity (LC%). Experimental design can be observed in **Table 5.1**.

**Table 5.1:** Factors and corresponding levels used in optimisation of CLX loaded PLGA nanoparticles.

| Factor | Levels | |
|---|---|---|
| | **Low** | **High** |
| PLGA amount (mg) | 5 | 10 |
| CLX amount (mg) | 0.5 | 2 |
| Organic phase volume (ml) | 1 | 3 |

## 5.2.3. Synthesis of CLX loaded PLGA nanoparticles

### 5.2.3.1. Nanoprecipitation method

Nanoparticles were synthesised using NPPT method [254,348]. Some parameters of this study were predetermined beforehand from the preliminary experiments carried out to reduce the number of experiments for the DoE study. Briefly, 5 mg or 10 mg of PLGA, 0.5 mg or 2 mg of CLX and 0.075% of poloxamer 407 (P407) were dissolved in 1 ml or 3 ml of acetonitrile (ACNT), then added to 4 ml of aqueous phase. Evaporation of organic solvent was facilitated by Rotavapor R-210 system (Buchi UK Ltd, UK), equipped with B-491 heating bath set at 55 °C and V-700 vacuum pump. Samples were then stirred at 250 RPM for at least 1 hour to remove residual organic solvent. Samples were filtered using 1 µm glass fibre filter (VWR, UK) and topped up with MilliQ water (MQW) to make up 4 ml of total volume.

For mucoadhesive formulations, based on the results obtained in **Chapter 4** various concentrations (0.5, 1, or 2 mg/ml) of chitosan were dissolved in the 4 ml of aqueous phase during the preparation of nanoparticles. Three types of commercially available chitosan were used: low MW (CS-L), medium MW (CS-M) and carboxymethyl chitosan (C-CS). To solubilise CS-L and CS-M in aqueous solution, 0.2 M acetic acid was added to the aqueous phase.

### 5.2.3.2. Single emulsion – solvent evaporation method

Polymeric nanoparticles were prepared using oil-in-water (O/W) SE method [255]. Some parameters of this study were predetermined beforehand from the preliminary experiments

carried out to reduce the number of experiments for the DoE study. Briefly, organic phase (O) was comprised of 1 or 3 ml of DCM containing 5 or 10 mg of dissolved PLGA and 0.5 or 2 mg of CLX, and aqueous phase (W) was made of 2% of PVA dissolved in 4 ml of MQW. Briefly, organic phase (O) was added dropwise to the aqueous phase (W), then emulsified using probe sonicator (Fisherbrand$^{TM}$ 505 sonicator, UK) at 20% amplitude for 3 min in a 20:5 second on-off cycle. Formulations were then left stirring at 250 RPM overnight at room temperature, to ensure complete evaporation of organic solvent. Next day, formulations were filtered using 1 µm glass fibre filter (VWR, UK) and topped up with MQW to make up 4 ml total volume.

For mucoadhesive formulations, based on the results obtained in **Chapter 4**, various concentrations (0.5, 1, or 2 mg/ml) of chitosan were dissolved in 4 ml of aqueous phase during the preparation of nanoparticles. Three types of commercially available chitosan were used: CS-L, CS-M, and C-CS. To solubilise CS-L and CS-M in aqueous solution, 0.2 M acetic acid was added to the aqueous phase.

## 5.2.4. Characterisation of CLX loaded PLGA nanoparticles

### 5.2.4.1. Drug loading and encapsulation efficiency

The quantification of CLX by HPLC was done following the method previously reported by Song et al., 2013 [391]. The HPLC system was composed of Quaternary Pump VL (Agilent, UK) and 1260 Infinity II Variable Wavelength Detector (Agilent, UK). A reverse phase column HC-C18, 4.6×250 mm, 5µm, 400 bar (Agilent, UK) was connected to a guard column HC-C18, 4.6×12.5 mm, 5µm, 400 bar (Agilent, UK) and kept at 40 °C throughout runs. Mobile phase was comprised 70:30 of ACNT and 0.5% (w/v) of triethylamine acid, which was adjusted to pH = 7 with phosphoric acid. The flow rate of mobile phase was set to 1.5 ml/min. UV detection was performed at 256 nm, after 5 µl of the sample was injected into the machine.

To achieve more accurate measurements of how much CLX was entrapped into the PLGA nanoparticles, each CLX sample was tested in two steps: firstly, the 0.5 ml of the final nanoparticle solution was mixed with 0.5 ml of ACNT to solubilise and measure CLX present in the nanoparticles, along with free CLX that was soluble in the supernatant ($CLX_{total}$); remaining nanoparticle solution was centrifuged at 12,000 RCF, separating the pellet and supernatant, with the latter then measured to quantify how much CLX was freely soluble in the supernatant ($CLX_{supernatant}$). To obtain the true amount of CLX inside the nanoparticles, the

value of unencapsulated CLX ($CLX_{supernatant}$) was divided from the amount of total CLX in the sample ($CLX_{total}$). It is important to stress, that $CLX_{total}$ does not represent initial amount of CLX added, as we cannot exclude the possibility that some of the drug was lost during transfer and filtering stages of the particle preparation, as well as some of the drug could have precipitated out of the nanoparticles and sedimented at the bottom of the tube. Encapsulation efficiency (EE%) and loading capacity (LC%) of CLX was calculated using equations:

$$LC\% = \frac{(Initial\ CLX\ amount - (CLX_{total} - CLX_{supernatant}))}{Amount\ of\ PLGA} \times 100\% \qquad \textbf{Eq. (5.1)}$$

$$EE\% = \frac{(Initial\ CLX\ amount - (CLX_{total} - CLX_{supernatant}))}{Initial\ CLX\ amount} \times 100\% \qquad \textbf{Eq. (5.2)}$$

#### 5.2.4.2. *In vitro* drug release studies

Drug release profiles of CLX were investigated using dialysis bag method [289]. For this study, 1 ml of CLX solution or nanoparticle solutions, loaded with 0.5 mg to 2 mg of CLX, were placed inside dialysis bag (Thermo Scientific™ SnakeSkin™ Dialysis Tubing, 10K MW cut-off, regenerated cellulose, Fisher Scientific, UK). Samples were incubated in release media, which was made up of 20 ml of PBS, with addition of 1% Tween 80, at pH = 4.5. Samples were incubated in shaking incubator (KS3000 i control IKA®, UK) at 37 °C degrees, with rotary speed of 100 RPM and sink conditions maintained throughout the assay. At predetermined time intervals, 1 ml of the sample was collected and replaced with 1 ml of fresh release medium. Collected samples were analysed for drug content by HPLC. Study was performed in triplicate and the average percent of CLX released per each timepoint was expressed in mean ± standard deviation (SD).

## 5.3. Results and discussion

### 5.3.1. Full-factorial design

#### 5.3.1.1. Initial optimisation and critical factor identification

In order to compare which nanoparticle preparation method produce desired physicochemical characteristics, such as small particle size, narrow size distribution, and high drug loading, parameters that were shared between NPPT and SE methods were identified. For this study, a full-factorial design was selected, with 3 critical factors investigated: drug amount (mg),

polymer amount (mg), and volume of the organic phase (ml). Other factors such as surfactant concentration and sonication amplitude were considered, however they were specific to each method. It is important to clarify that although surfactant was used in both nanoparticle preparation methods, two different surfactants were used when preparing nanoparticles by NPPT and SE methods. Stabiliser PVA was used to prepare nanoparticles when using SE method, due to its effective stabilisation of suspensions and improvement of colloidal stability [112,392]. It is also the most used stabiliser when synthesis of nanoparticles involves emulsions, as PVA remains attached to the nanoparticles due to hydrophobic bonding between partially hydrolysed PVA and acetyl groups of PLGA, therefore forming an interconnected network between polymer and PVA at the interface [112,136]. However, some studies had reported using poloxamers instead of PVA for synthesis of PLGA nanoparticles by NPPT method, due to smaller sized nanoparticles achieved, partial nanoparticle surface coating, ensuring negative PLGA nanoparticle charge, as well as lesser toxicity [134,135,348,393]. Therefore, in order to maintain optimal nanoparticle characteristics, P407 was used as surfactant for nanoparticles prepared by NPPT method, while PVA was used as surfactant for nanoparticles prepared by SE method.

Prior to DoE study, parameters that were specific for each nanoparticle preparation method were optimised. PLGA nanoparticle formulation established in **Chapter 4** was used for optimisations of nanoparticles obtained by NPPT method. The lowest concentration of 0.025% (w/v) of P407 was used in preparation of CLX loaded PLGA nanoparticles. Results showed that low concentration of surfactant negatively affected stability of the nanoparticle system, leading to poor encapsulation of CLX as most of the drug precipitated out of the nanoparticles. Increase of P407 to 0.075% (w/v) improved drug solubilisation and encapsulation into nanoparticles, with no visible drug precipitation observed.

Formulation of PLGA nanoparticles prepared by double emulsion – solvent evaporation method in **Chapter 3** was used as a foundation for developing a nanoparticle formulation prepared by SE method. Therefore, optimisation of surfactant concentration and sonication process was performed. First, effects of amplitude of sonication on nanoparticle characteristics were investigated. Results revealed no significant difference ($P > 0.05$) on particle size and PDI when 20% amplitude or 40% amplitude was used, however the zeta potential values of formulations F1 and F2 were significantly lower ($P < 0.05$) when nanoparticles were sonicated at 40% amplitude (**Table 5.2**). It has been observed by other studies, that the increase in

sonication power and time lead to decrease in mean diameter of particle size, as well as formed monodispersed particle system [119,143,144]. Although no significant difference ($P > 0.05$) was found in these parameters in present study, increased amplitude did show reduced means of particle size in F2, as well as reduced mean polydispersity in both formulations. The lack of significant differences could be attributed to relatively short sonication time of 3 min, with 20 s on and 5 s pulse, as well as use of ice bath to reduce sample heating and product instability [119,143]. Although both sonication amplitude options could have been used in future experiments, sonication amplitude of 40% were selected due to smaller means of particle size results.

**Table 5.2:** Characteristics of CLX loaded PLGA nanoparticles after optimisation of sonication amplitude and PVA concentration parameters. Error bars represent SD and n = 3.

| Sample name | PLGA mass (mg) | Drug mass (mg) | Organic phase (ml) | Aqueous phase (ml) | Sonication amplitude (%) | PVA conc. (% w/v) | Particle size (nm) | PDI | Zeta potential (mV) |
|---|---|---|---|---|---|---|---|---|---|
| **F1** | 10 | 0.5 | 1 | 4 | 20 | 2 | 159.2±27 | 0.23±0.06 | -2±0.2 |
| | | | | | 40 | | 180.3±4 | 0.16±0.00 | -3.1±0.1 |
| | | | | | | 1 | 242.5±30 | 0.18±0.08 | -4.9±0.1 |
| **F2** | | | 3 | 4 | 20 | 2 | 439.1±197 | 0.58±0.39 | -3.6±0.4 |
| | | | | | 40 | | 295.1±22 | 0.52±0.03 | -4.5±0.2 |
| | | | | | | 1 | 285.9±53 | 0.52±0.11 | -5.2±1.1 |

Afterwards, effects of surfactant concentration on characteristics of nanoparticles, which were prepared by SE method, were investigated. Results shown in **Table 5.2** demonstrate that decrease in PVA concentration led to significantly decreased ($P < 0.05$) zeta potential of F1 nanoparticles, however it also significantly increased ($P < 0.05$) nanoparticle size. Formulation F2 showed no significant difference ($P > 0.05$) in any of the nanoparticle characteristics. Typically, the zeta potential of PLGA nanoparticles averages around -20 mV, due to the terminal carboxyl or ester groups of the PLGA [119]. However, it has been discussed in the literature that use of stabilisers can influence particle charge, as it coats the nanoparticle surface and in turn can reduce the originally negative nanoparticle charge [169]. Based on the optimisations done prior, as well as reports in the literature, further decrease in PVA concentration would result in further increase in particle size [119], therefore PVA

concentration remained at 2% for following experiments in order to limit the risk of increasing particle size of PLGA nanoparticles.

### 5.3.1.2. Optimisation of critical factors

A regular three-factor, two-level, full-factorial design was used to examine the influence of three critical factors, which were the amount of PLGA, the amount of CLX, and the volume of organic phase, on characteristics of CLX loaded PLGA nanoparticles. **Table 5.3** and **Table 5.4** show design matrix with levels of each critical factor, creating a total of 8 formulations each. **Table 5.3** represents data of nanoparticles prepared by NPPT method, while **Table 5.4** demonstrates data of nanoparticles prepared by SE method. Both tables also demonstrate results of four responses, which were determined to be particle size, PDI, encapsulation efficiency (EE%) and loading capacity (LC%).

**Table 5.3:** Design matrix for the preparation of CLX loaded PLGA nanoparticles prepared by NPPT method, with levels of critical factors for each formulation, along with results obtained from responses of particle size, PDI, encapsulation efficiency (EE%) and loading capacity (LC%). Values of particle size, PDI, EE% and LC% demonstrate mean of results from three individual repeats (n = 3). Error bars represent SD.

| Sample name | PLGA amount (mg) | CLX amount (mg) | Organic phase volume (ml) | Aqueous phase volume (ml) | Particle size (nm) | PDI | EE% | LC% |
|---|---|---|---|---|---|---|---|---|
| **N-F1** | 5 | 0.5 | 1 | 4 | 118.0±42 | 0.19±0.04 | 32.4±2 | 3.2±0 |
| **N-F2** | | | 3 | | 102.0±34 | 0.20±0.06 | 67.1±10 | 6.7±1 |
| **N-F3** | | 2 | 1 | | 114.4±25 | 0.20±0.03 | 6.4±0 | 2.6±0 |
| **N-F4** | | | 3 | | 93.0±19 | 0.23±0.03 | 7.0±0 | 2.8±0 |
| **N-F5** | 10 | 0.5 | 1 | | 140.4±25 | 0.17±0.06 | 75.4±4 | 3.8±0 |
| **N-F6** | | | 3 | | 106.9±12 | 0.22±0.01 | 83.3±6 | 4.2±0 |
| **N-F7** | | 2 | 1 | | 128.8±10 | 0.19±0.02 | 10.1±1 | 2.0±0 |
| **N-F8** | | | 3 | | 108.1±18 | 0.23±0.01 | 15.2±3 | 3.0±1 |

It is important to note that two-level screening design is often chosen to perform initial screening of the selected critical factors to then identify which of them are significant, while insignificant factors can be removed from the further design [394]. The selected significant

factors can be then investigated at higher numbers of levels, therefore generating more accurate statistical models and subsequently better predictions. However, due to time constraints and small number of critical factors selected, we only use the two-level screening design to investigate the significance and different effects of chosen factors on selected responses of CLX loaded PLGA nanoparticles prepared by two different nanoparticle preparation methods.

**Table 5.4:** Design matrix for the preparation of CLX loaded PLGA nanoparticles prepared by SE method, with levels of critical factors for each formulation, along with results obtained from responses of particle size, PDI, encapsulation efficiency (EE%), and loading capacity (LC%). Values of particle size, PDI, EE% and LC% demonstrate mean of results from three individual repeats (n = 3). Error bars represent SD.

| Sample name | PLGA amount (mg) | CLX amount (mg) | Organic phase volume (ml) | Aqueous phase volume (ml) | Particle size (nm) | PDI | EE% | LC% |
|---|---|---|---|---|---|---|---|---|
| **E-F1** | 5 | 0.5 | 1 | 4 | 200.8±53 | 0.19±0.01 | 30.0±1 | 3.0±0 |
| **E-F2** | | | 3 | | 285.9±43 | 0.54±0.04 | 14.0±6 | 1.4±1 |
| **E-F3** | | 2 | 1 | | 196.7±19 | 0.23±0.01 | 32.0±9 | 12.8±3 |
| **E-F4** | | | 3 | | 266.9±27 | 0.54±0.12 | 9.7±3 | 3.9±1 |
| **E-F5** | 10 | 0.5 | 1 | | 180.3±4 | 0.16±0 | 34.9±1 | 1.7±0 |
| **E-F6** | | | 3 | | 295.1±22 | 0.52±0.03 | 12.0±13 | 0.6±1 |
| **E-F7** | | 2 | 1 | | 197.8±7 | 0.20±0.02 | 64.9±1 | 13.0±0 |
| **E-F8** | | | 3 | | 308.9±120 | 0.54±0.28 | 50.5±10 | 10.1±2 |

### 5.3.1.3. Effect of critical factors on particle size

Experimental runs detailed in **Table 5.3** and **Table 5.4** demonstrate particle size of nanoparticles prepared by NPPT method to be between 92.97 nm to 140.43 nm, while nanoparticles prepared by SE method demonstrated size range of 196.7 nm – 295.1 nm. Based on these results, nanoparticles prepared by SE showed overall significantly ($P < 0.05$) higher particle size than nanoparticles prepared by NPPT. This could be attributed to higher concentration of surfactant used in nanoparticles prepared by SE, compared to NPPT method, as well as different surfactants selected for each method. In addition, the particle size of nanoparticles obtained through SE method can also be affected by homogenisation, unlike nanoparticles that are obtained without it by NPPT method. All of these factors have likely

contributed to the reason why significant difference in particle size is observed. As the aim of the study was to obtain smaller sized nanoparticles, with narrow size distribution, and high drug loading, particles synthesised by NPPT method appeared to be smaller in size, compared to the nanoparticles obtained by SE method.

Additionally, two different organic solvent evaporation techniques were used for different nanoparticle preparation methods. Solvent evaporation of nanoparticles prepared by NPPT was achieved by rotary evaporator, with complete solvent reduction attained within minutes. This method was not employed for formulations prepared by SE method, due to rotary evaporator destabilising the colloidal system by excessive frothing and air bubble formation in the sample, which have likely affected the hardening process of nanoparticle droplets. Therefore, the evaporation of the organic solvent in the formulations by SE method were facilitated by magnetic stirring. Study by Mainardes et al., 2005 demonstrated that particle size of PLGA nanoparticles had increased with longer solvent evaporation times by comparing solvent evaporation facilitated by rotary evaporation versus magnetic stirring [125]. This was also confirmed by Hernández-Giottonini et al., 2020, where the higher speed of agitation during solvent evaporation process resulted in decrease of particle size of PLGA nanoparticles [119].

The effect of three critical factors on particle size of CLX loaded PLGA nanoparticles was determined using ANOVA and presented in **Table 5.5**. Based on this data, both models established for prediction of particle size were significant as indicated by the F-value and P-value obtained. Predicted correlation coefficient ($R^2$=0.7907) and adjusted correlation coefficient ($R^2$=0.9084) of nanoparticles synthesised by NPPT were in reasonable agreement, as the difference between them was less than 0.2. Similarly, same outcomes were observed in model of nanoparticles prepared by SE, as predicted $R^2$=0.7829 and adjusted $R^2$=0.9050 were also in reasonable agreement. Overall $R^2$ values for both models were 0.9477 for NPPT and 0.9457 for SE, indicating that > 94% of the variation particle size, can be explained by the models [255]. The equations of both models for particle size are presented below:

$$SIZE\ (NPPT) = 120.38 + 2.84A - 3.84B - 11.47C \qquad \textbf{Eq. (5.3)}$$

$$SIZE\ (SE) = 132.6 + 1.59A + 1.36B + 47.65C \qquad \textbf{Eq. (5.4)}$$

Here, A stands for PLGA amount (mg), B for CLX amount (mg), and C for the volume of organic phase (ml). The sign of the coefficient corresponds to the relationship between the two variables, where a positive sign represents a synergistic effect, in which an increase in coefficient value will result in increase of the response value, while a negative sign correlates to antagonistic effect, where increase in coefficient value will result in decrease of the response [130,255,395,396].

**Table 5.5:** Statistical data obtained from ANOVA analysis of particle size of CLX loaded PLGA nanoparticles prepared by NPPT and SE nanoparticle preparation methods. * Statistically significant differences (P-value < 0.05), df = degree of freedom.

| Source | Nanoprecipitation | | | | Single emulsion | | | |
|---|---|---|---|---|---|---|---|---|
| | Sum of Squares | df | F-value | P-value | Sum of Squares | df | F-value | P-value |
| **Model** | 1522.61 | 3 | 24.15 | 0.005* | 18302.03 | 3 | 23.24 | 0.005* |
| | **Independent variables:** | | | | **Independent variables:** | | | |
| **PLGA amount** | 403.71 | 1 | 19.21 | 0.011* | 126.64 | 1 | 0.48 | 0.526 |
| **CLX amount** | 66.18 | 1 | 3.15 | 0.151 | 8.34 | 1 | 0.03 | 0.867 |
| **Organic phase** | 1052.72 | 1 | 50.09 | 0.002* | 18167.04 | 1 | 69.19 | 0.001* |

Organic phase was the only independent variable that showed to significantly influence particle size of nanoparticles prepared by both NPPT and SE methods. The statistical model of nanoparticles prepared by NPPT method indicated that PLGA amount also has statistically significant effect on particle size, while the model of SE nanoparticles showed no other significant variables. CLX amount did not influence particle size of nanoparticles synthesised either by NPPT method or SE method. The 3D response surface plots of the effect on particle size for both models are presented in **Figure 5.1**.

Statistical model of CLX loaded PLGA nanoparticles prepared by NPPT method demonstrates that PLGA amount has a positive significant (P > 0.05) effect on particle size, while organic phase has negative significant (P > 0.05) effect on the same response. This means, that increase

in PLGA amount will increase particle size, while increase in organic phase will lead to decrease in particle size (**Figure 5.1**). This is also confirmed by corresponding positive and negative signs of the coefficients in the equation (**Eq. 5.3**). Similar results on particle size of nanoparticles prepared by NPPT were reported by Joshi et al., 2010, where they used DoE to optimise anti-Alzheimer drug loaded PLGA nanoparticles, synthesised by NPPT method [142]. In their study they also observed that increase in PLGA concentration leads to increase in particle size, while increase in internal organic phase resulted in decrease of the same response [142]. The same observations were also reported by several other studies [129,130]. An increase in polymer concentration is linked with increase of particle size due to increased viscosity of the organic phase with higher amounts of polymer added [126–128]. With increased viscosity, the diffusion of the organic phase is into the aqueous phase is reduced by the higher mass transfer resistance, which leads to higher nanoparticle size [126]. Additionally, higher amount of PLGA per unit volume of the solvent carries higher amount of polymer chains, which during solvent evaporation process results in aggregation of higher number of polymer chains into larger sized nanoparticles [126].

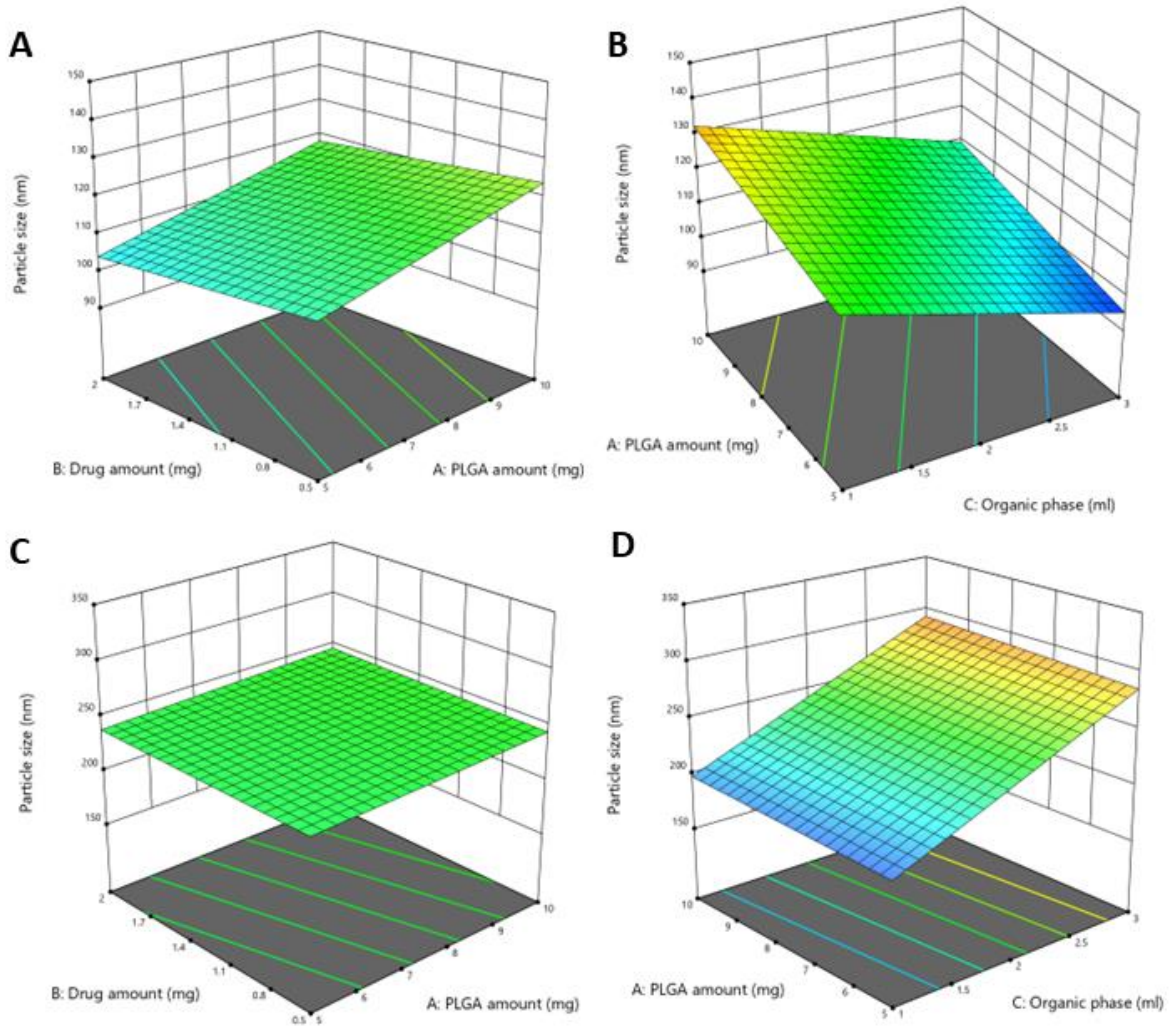


**Figure 5.1:** 3D response surface plots of the effect of PLGA amount (mg), CLX amount (mg), and volume of organic phase (ml) on particle size of CLX loaded PLGA nanoparticles. (A, B) plots for PLGA nanoparticles prepared by NPPT, (C, D) plots for nanoparticles prepared by SE.

Interestingly, PLGA amount did not show any significant influence on particle size when nanoparticles were synthesised using SE method. Based on results discussed above, increase in viscosity of the organic phase should have resulted in higher resistance against shear forces, as well as poorer PLGA solution dispersibility in aqueous phase, which in turn should have increased the particle size of the nanoparticles [125,127]. Other studies which examined how increase in PLGA amount affected the size of PLGA nanoparticles, have reported significantly positive effects [125,141,397]. We hypothesised that no significant effect was observed due to narrow range of PLGA amount used (5 mg to 10 mg) in present study, however this range was chosen in order to maintain small particle size of approx. 100 nm.

The effect of the volume of organic phase (ml) demonstrated significance in both DoE models, however contrasting effects were observed on the size of nanoparticles. When NPPT method was used to prepare the CLX loaded PLGA nanoparticles, an increase in organic phase volume resulted in a decrease of the particle size. In contrast, when SE method was used to synthesise polymeric nanoparticles, an increase in organic phase volume demonstrated an increase in particle size. Many other publications observed antagonistic effect between the independent variable of organic phase volume (ml) and the response of the particle size (nm) in formulations obtained by NPPT [129,130,142,398]. Study by Sharma et al., 2014, which aimed to optimise drug loaded PLGA nanoparticles prepared by NPPT method, explained that smaller volume of the organic phase could have resulted in poorer solubility of the drug, which in turn lead to higher particle size [398]. However, drug amount used in these formulations showed no significant effect on particle size in both NPPT and SE models, therefore seemingly rejecting this justification.

Interestingly, studies by Mainardes et al., 2005 and Ribeiro et al., 2015, which optimised PLGA nanoparticles prepared by SE method, reported an increase in particle size when organic phase volume was decreased, which is the opposite effect than observed in the present study [125,141]. Research by Mainardes et al., 2005 explained that larger volume of organic solvent prevented particle aggregation, as well as decreasing overall viscosity of the organic phase and thus decreasing particle size [125,130]. Therefore, it appears that the outcomes of changing the volume of organic solvent in present study conflict with the results reported by other studies [125,141]. Firstly, results obtained in present study agrees with Ostwald ripening theory, where increase in oil phase solubility leads to the larger droplet formation at the expense of smaller droplets, therefore increasing overall particle size of the obtained nanoparticle system [399]. Additionally, we hypothesise that increase in particle size was observed due to the use of larger volume of organic solvent, which was harder to evaporate using magnetic stirring at 250 RPM. More than 24 hours were often needed to fully evaporate 3 ml of the solvent, which was significantly longer than the time needed to evaporate 1 ml of organic solvent. These findings were supported by Mainardes et al., 2005 and Hernández-Giottonini et al., 2020, which demonstrated that short solvent evaporation time produced smaller sized particles [119,125]. Gradual decrease of the organic solvent prolongs the surface hardening of the nanoparticles, which can lead to coalescence and agglomeration of the droplets during the early stage of solvent removal [119,125,139].

Some studies also attempted to investigate how drug amount used affects the particle size, but reported no significant effects [125,398]. This was also observed in the present study (**Figure 5.1**). Results of this section, which focused on investigating the significant effect of critical factors on the particle size of CLX loaded PLGA nanoparticles, are presented in **Table 5.6**.

**Table 5.6:** Summary of the findings observed in section 5.3.1.3., showing significant effect of critical factors on the particle size of CLX loaded PLGA nanoparticles. Symbol "↑" demonstrates the increase, while symbol "↓" demonstrates decrease, "No effect" means no significant effect on the response.

| **Critical factors** | | | **Nanoparticles by NPPT** | **Nanoparticles by SE** |
|---|---|---|---|---|
| **Parameters tested** | **Levels of parameter** | | **Response in particle size** | |
| PLGA amount | ↑ | | ↑ | No effect |
| CLX amount | ↑↓ | | No effect | No effect |
| Volume of organic solvent | ↑ | | ↓ | ↑ |

## 5.3.1.4. Effect of critical factors on PDI

The PDI values of drug loaded PLGA nanoparticles prepared by NPPT and SE methods are presented in **Table 5.3** and **Table 5.4**. Despite different preparation methods, both types of formulations demonstrated no significant differences in PDI values, which ranged from 0.156 to 0.537. It is important to note that nanoparticles obtained through NPPT method showed lower means of PDI values, compared to the nanoparticles prepared by SE method. Highest PDI value of NPPT nanoparticles was 0.234, while 0.537 was reported as highest PDI value for SE nanoparticles, demonstrating wide size distribution in formulations E-F2, E-F4, E-F6 and E-F8. All of these formulations had higher volume of organic solvent, which also significantly increased particle size as discussed in **section 5.3.1.3**.

The effect of independent variables on PDI of CLX loaded PLGA nanoparticles was analysed using ANOVA and results are presented in **Table 5.7**. Individual models were prepared for nanoparticles synthesised using NPPT method and nanoparticles obtained by SE method. Both

models demonstrated significance based on reported F-values and P-values in **Table 5.7**. High $R^2$ values of both models suggest that 86.01% and 99.67% of variation can be explained by the independent variables of NPPT and SE models, respectively. While adjusted (R2 = 0.994) and predicted (R2 = 0.987) values of $R^2$ were in reasonable agreement in SE model, the difference between these values in NPPT model was higher than 0.2, which could be due to inclusion non-significant variables into the model. However, overall $R^2$ demonstrates a high value of 0.86, along significant F-value and P-value, meaning that the model is reliable and accurate. The effect of individual variables on the PDI can be explained by the following equations, generated for both models:

$$PDI\ (NPPT) = 0.165 - 0.002A + 0.012B + 0.018C \qquad \textbf{Eq. (5.5)}$$

$$PDI\ (SE) = 0.029 - 0.004A + 0.017B + 0.171C \qquad \textbf{Eq. (5.6)}$$

Here, A stands for PLGA amount (mg), B for CLX amount (mg), and C for the volume of organic phase (ml). Based on these equations, both B and C variables demonstrate synergistic effect with the response, where increase in CLX amount or organic phase volume would result in increase of PDI value. In contrast, independent variable A shows a negative sign of the coefficient, therefore meaning that decrease in PLGA amount will increase the PDI values. The 3D response surface plots demonstrating the effect of these variables on PDI are presented in **Figure 5.2**.

**Table 5.7:** Statistical data obtained from ANOVA analysis of PDI of CLX loaded PLGA nanoparticles prepared by NPPT and SE nanoparticle preparation methods. * Statistically significant differences (P-value < 0.05), df = degree of freedom.

| **Source** | | **Nanoprecipitation** | | | | | **Single emulsion** | | | |
|---|---|---|---|---|---|---|---|---|---|---|
| | | **Sum of Squares** | **df** | **F-value** | **P-value** | | **Sum of Squares** | **df** | **F-value** | **P-value** |
| **Model** | | 0.032 | 3 | 8.20 | 0.035* | | 0.235 | 3 | 400.00 | < 0.001* |
| | | **Independent variables:** | | | | | **Independent variables:** | | | |
| **PLGA amount** | | 0.0001 | 1 | 0.87 | 0.403 | | 0.001 | 1 | 4.19 | 0.110 |

| | | | | | | | | | | |
|---|---|---|---|---|---|---|---|---|---|---|
| **CLX amount** | | 0.0006 | 1 | 4.74 | 0.095 | | 0.001 | 1 | 6.77 | 0.059 |
| **Organic phase** | | 0.0024 | 1 | 18.97 | 0.012* | | 0.233 | 1 | 1189.04 | < 0.001* |

In both models obtained from formulations prepared by either NPPT or SE method, only a change in organic solvent volume demonstrated a significant difference on PDI of the nanoparticles (**Figure 5.2**). Our findings agreed with study by Bisht et al., 2018, where they reported that peptide loaded PLGA nanoparticles prepared by NPPT method demonstrated a significant increase in PDI when higher volume of organic phase was used [130]. Draheim et al., 2015 showed similar results, however they indicated that other variables, such as polymer concentration, stabiliser type, injection speed of the organic phase, as well as inner diameter of the needle used for injection, also have a significant effect on PDI of the PLGA nanoparticles [129]. Authors explained that an increase in PDI could be linked with PLGA concentration, due to PLGA distribution in each droplet. This means that high concentrations of PLGA ensure that polymer is more evenly distributed in solvent droplets, while lower concentrations of PLGA might have varying concentrations in each droplet, resulting in higher PDI values. While neither higher nor lower amounts of PLGA shown to affect the PDI of formulations in present study, a wide size distribution of nanoparticles could have been a result of generally low polymer amounts used in present study [126,129].

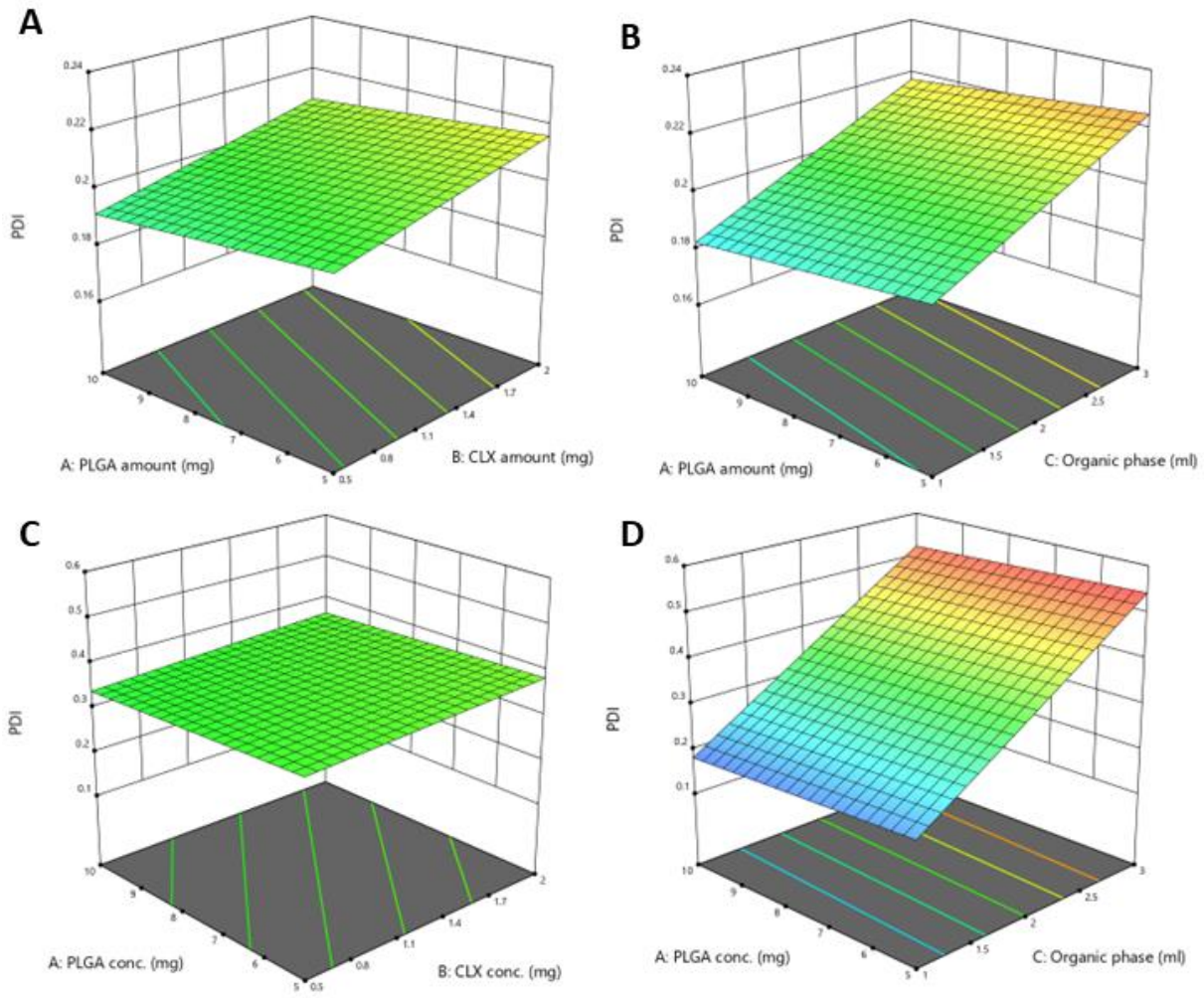


**Figure 5.2:** 3D response surface plots of the effect of PLGA amount (mg), CLX amount (mg), and the organic phase volume (ml) on PDI of CLX loaded PLGA nanoparticles. (A, B) plots for PLGA nanoparticles prepared by NPPT, (C, D) plots for nanoparticles prepared by SE.

While statistical model of formulations prepared by SE demonstrated that only change in organic solvent volume has shown to significantly affect the PDI values (**Figure 5.2**), several other publications have demonstrated contrary results [125,141,400,401]. For example, study by Ribeiro et al., 2015 on plant extract loaded PLGA nanoparticles, showed that both PLGA amount and the volume of organic phase did not have any significant effect on PDI of nanoparticles prepared by SE method [141]. On the contrary, study by Ahmad et al., 2022 demonstrated that increase of PLGA concentration significantly increased PDI of the chitosan coated, tannic acid loaded PLGA nanoparticles obtained by SE method [401]. However, it is likely that significant effect was observed due to much higher amounts of PLGA used in the study by Ahmad et al., 2022 compared to present study where a narrow range of 5 mg to 10 mg of PLGA was used. Both studies by Mainardes et al., 2005 and Das Neves et al., 2015 showed

that while organic phase volume did cause a significant effect on PDI values, a negative sign in front of the coefficient indicated an antagonistic effect of the variable, compared to the synergistic effect achieved in present study [125,400]. Das Neves et al., 2015 reasoned that increasing the volume of the organic phase lowers the overall viscosity of the phase, which in turn reduces interactions between nanoparticles during droplet formation and, subsequently, aggregation of the particles, therefore reducing the size distribution of the nanoparticles [400]. However, this explanation contradicts the results obtained in present study, where increase in the volume of the organic phase leads to increase in PDI, as presented in **Figure 5.2**. As mentioned earlier, high PDI values of > 0.5 were observed only in formulations that had higher volume of the organic solvent, which evaporation time was much longer than lower volumes of the same organic phase. As discussed in **section 5.3.1.3.**, during longer evaporation times droplets are more likely to agglomerate together, hence resulting in wider size distribution of the nanoparticles [119,125,139]. Therefore, the increase of the organic phase volume prolonged its evaporation rate, which in turn lead to more polydisperse colloidal system. This suggests that PDI is also influenced by the nanoparticle synthesis process and post-processing methods used, just as much as it is influenced by the changes in the formulation parameters or nanoparticle preparation methods selected.

No significant effect caused by increase in drug concentration loaded into PLGA nanoparticles was observed on the PDI values (**Figure 5.2**). Results of this section, which focuses on investigating the significant effect of critical factors on the PDI of CLX loaded PLGA nanoparticles, are presented in **Table 5.8**.

**Table 5.8:** Summary of the findings observed in section 5.3.1.4., showing significant effect of critical factors on the PDI of CLX loaded PLGA nanoparticles. Symbol "↑" demonstrates the increase, while symbol "↓" demonstrates decrease, "No effect" means no significant effect on the response.

| **Critical factors** | | | **Nanoparticles by NPPT** | **Nanoparticles by SE** |
|---|---|---|---|---|
| **Parameters tested** | **Levels of parameter** | | **Response in particle size** | |
| PLGA amount | ↑↓ | | No effect | No effect |
| CLX amount | ↑↓ | | No effect | No effect |

| | | | | |
|---|---|---|---|---|
| Volume of organic solvent | ↑ | | ↑ | ↑ |

### 5.3.1.5. Effect of critical factors on EE% and LC%

The quantification of CLX from CLX loaded PLGA nanoparticles was examined using HPLC method adapted from previously reported study [391]. Sharp peaks of CLX standard solution were detected at retention time ($R_t$) of around 6.1 min, as shown in **Figure 5.3**. A linear correlation between CLX concentration and area of the peak was observed, demonstrating $R^2$ = 0.9997 and generating a regression equation, where Y = 59.072x – 10.724.

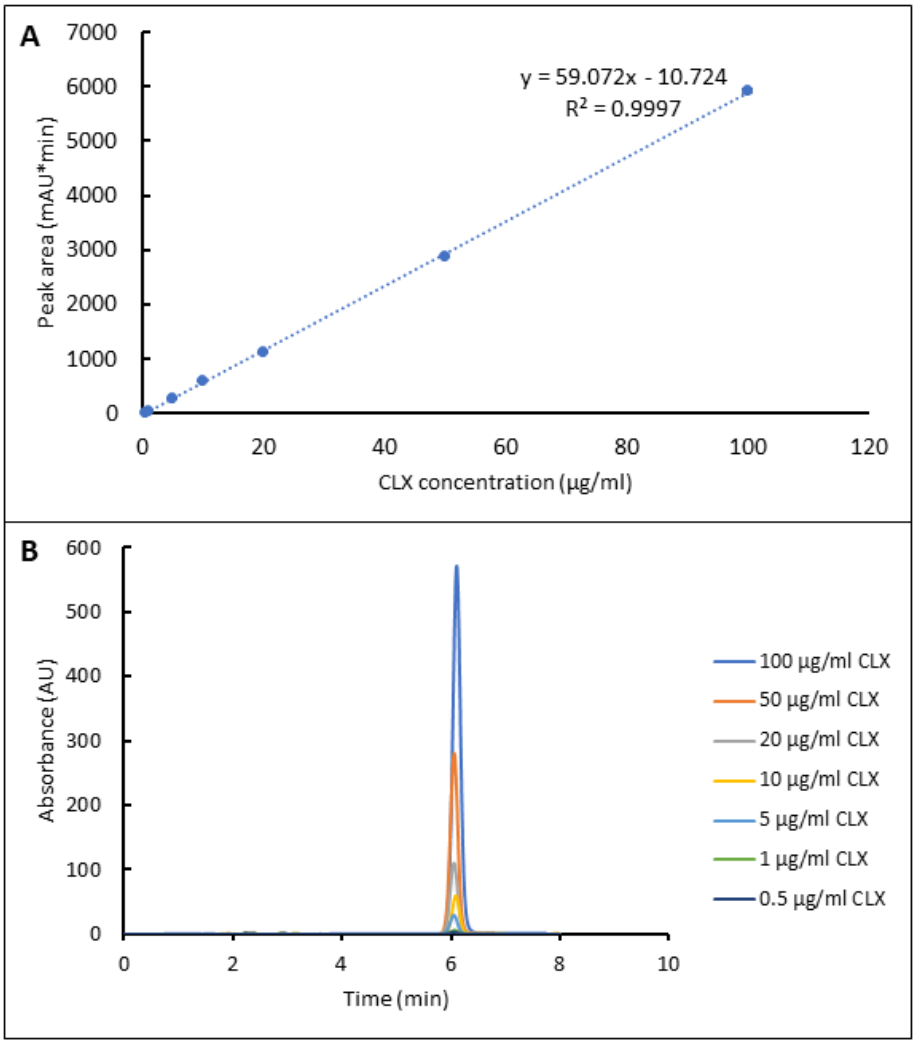


**Figure 5.3:** Calibration curve (A) and HPLC chromatogram (B) of CLX in ACNT, measured at concentration range from 100 to 0.5 µg/ml, UV detected at 256 nm.

Limit of detection (LOD) and limit of quantification (LOQ) were calculated using equations:

$$LOD = \frac{3.3\,\sigma}{S} \qquad \textbf{Eq. (5.7)}$$

$$LOD = \frac{10\,\sigma}{S} \qquad \textbf{Eq. (5.8)}$$

Where σ is the standard deviation of the intercept, and S is the slope of calibration curve. From the obtained calibration curve, LOD was calculated to be 0.015 mg/ml, with LOQ calculated to be 0.047 mg/ml.

As CLX amount (mg) was one of the independent variables in DoE models, it was more accurate to present both EE% and LC% values due to the different ways drug content in the nanoparticles is calculated (**Eq. (5.1)** and **Eq. (5.2)**). CLX loading into PLGA nanoparticles presented as LC% demonstrates an accurate guide to determine the drug mass per nanoparticle weight unit useful for clinical applications, however it can be misleading when comparing entrapment of drugs with different MWs [122]. Therefore, EE% measurement is often used in studies investigating and comparing different drug entrapment into nanoparticles, as EE% measurement is independent of MW of the drug, and it measures degree of interaction of the drug and polymer [122]. As present study focuses on CLX encapsulation only, both EE% and LC% results of the CLX loaded PLGA nanoparticle formulations are presented in **Table 5.3** for nanoparticles prepared by NPPT method, and **Table 5.4** for particles prepared by SE method. However, for the purpose of this study, LC% measurement is considered to be more accurate to express which formulations demonstrate highest drug loading. This is because based on EE% data only, E-F1 and E-F3 formulations demonstrate very similar EE% values of 30.0 ± 1% and 32.0 ± 9%, respectively (**Table 5.4**). However, looking at the overall drug content per unit weight of the nanoparticle, LC% values of the same formulations demonstrate that there is significantly more drug in the E-F3, with 12.8% of CLX loaded, compared to the E-F1, which shows only 3% of the nanoparticle mass can be attributed to CLX. This can be explained by looking at the initial amount of CLX added to the formulations: 2 mg of CLX was attempted to load into PLGA nanoparticles in E-F3, while only 0.5 mg of CLX was attempted to load into E-F1 formulation. Therefore, roughly 30% of 2 mg demonstrates four times higher amount of CLX loaded into E-F3, compared to 30% of 0.5 mg CLX loaded in E-

F1. Hence, LC% measurement was preferred for identifying which formulations encapsulated highest amount of CLX.

Focusing on the results of formulations prepared by NPPT method, EE% values varied widely based on the original amount of the drug added to formulations. With 0.5mg of CLX entrapped, EE% values ranged from 32.75% to 83.3%, while with 2 mg of CLX entrapped, EE% values dropped below 15.2%. Similar results were observed when CLX amount was calculated per unit weight of the formulation, where increasing amount of CLX caused LC% values to decrease. Opposite results were observed in nanoparticles prepared by SE method, where increase in CLX amount led to increase in LC% values. However, no trend was observed in EE% values with increasing or decreasing amount of the drug added to the formulations.

According to other publications, SE method is more commonly used in preparation of CLX loaded PLGA nanoparticles, due to higher EE% values achieved, compared to CLX loaded PLGA nanoparticles prepared by NPPT method [255,388,402]. Study by Alonso-González et al., 2022 showed that CLX had higher EE% values when prepared by SE method, compared to lower EE% when prepared by NPPT [255]. Authors reported over 60% of the CLX to be encapsulated into PLGA nanoparticles prepared by SE method, with some results demonstrating EE% over 90% [255]. Similarly, study by Emami et al., 2015 reported EE% of CLX loaded PLGA nanoparticles to be over 80% in all formulations tested, with LC% values rising to 24% [388]. Although in our study higher EE% values were observed in formulations by NPPT method, assessment of LC% data revealed the clear advantage of better drug loading in formulations prepared by SE method.

It was discussed earlier, that due to changes in the original amount of the CLX that was being loaded, LC% data more accurately represents the drug content per unit weight of the nanoparticle. While the EE% results of CLX loaded PLGA nanoparticles prepared by NPPT indicate good drug encapsulation, reported LC% results are not as high as LC% of nanoparticles prepared by SE method. Study by Kim et al., 2011 investigated characteristics of CLX loaded PLGA nanoparticles prepared by NPPT method, reporting EE% to be in range of 31.6 – 67.6%, while LC% ranged from 3.8% to 10.5% [387]. Similarly to these findings, our study reported the LC% values to be mostly around 3-4%, with some formulations increasing past 6% [387]. In present study, only N-F2 demonstrated LC% higher than 6%. While results of this study show lower EE% and LC% values than reports in the literature of the CLX loaded

PLGA nanoparticles prepared by either NPPT or SE methods, overall trend of SE nanoparticles demonstrating higher drug loading compared to NPPT nanoparticles agrees with prior research. The reason why nanoparticles prepared by SE method demonstrate higher EE% and LC% values compared to nanoparticles prepared by NPPT could be attributed to the organic solvent used during particle formation. For NPPT nanoparticle preparation method, ACNT or acetone are mostly used as organic solvents, which demonstrate higher and faster diffusion rates through aqueous phase compared to DCM, which is commonly used in particle preparation using SE method [255]. Therefore, increase in diffusion of CLX into external aqueous phase during NPPT could result in reduction of the amount of drug trapped inside the nanoparticles [255].

The effects of the critical factors on EE% and LC% of the CLX loaded PLGA nanoparticles were measured using ANOVA and results were presented in **Table 5.9**, for the response of EE%, and **Table 5.10**, for the response of LC%. Two models obtained for EE% prediction of CLX loaded PLGA nanoparticles demonstrated unequal outcomes: the model obtained of formulations prepared by NPPT showed to be significant ($P < 0.05$), with the factor of CLX amount significantly influencing the EE% values, while the model obtained from formulations prepared by SE model showed no significance ($P > 0.05$), as well as low F-value. The $R^2$ = 0.8535 for NPPT model predicting EE% values demonstrated that 85.35% of this response can be predicted by the model, while SE model for the same response demonstrated that only 56.66% of the EE% values can be predicted by this model due to $R^2 = 0.5666$. The predicted and adjusted $R^2$ values of NPPT models were 0.6651 and 0.8535, respectively, demonstrating a difference smaller than 0.2 and indicating a reasonable agreement between the values.

From the results of ANOVA test shown in **Table 5.10**, no critical factors showed significant influence on LC% of CLX loaded nanoparticles prepared by NPPT, with F-value and P-value demonstrating that overall model is not significant ($P > 0.05$). However, out of the three critical factors, CLX amount demonstrated significance in affecting LC% of CLX loaded nanoparticles prepared by SE. This statistical model was significant due to $P < 0.05$, along with high $R^2$ value demonstrating that 85.26% of the variation in response can be explained by the model. Interestingly, $R^2$ value of the NPPT model demonstrated relatively high number too, revealing that 74.42% of the variation in the response can be explained by the model. Both obtained models demonstrated a relatively larger difference between the predicted and adjusted $R^2$, which could be due to inclusion of non-significant values into the models. However, statistical

model obtained to predict LC% values of CLX loaded PLGA nanoparticles by SE method demonstrates significant P-values and F-values, along with high value of coefficient of determination, therefore confirming that the obtained model is accurate.

The equations of NPPT model for EE% and SE model for LC% are presented below:

$$EE\%\ (NPPT) = \ 44.082 + 3.553A - 36.592B + 6.054C \qquad \textbf{Eq. (5.9)}$$

$$LC\%\ (SE) = \ 0.951 + 0.218A + 5.498B - 1.823C \qquad \textbf{Eq. (5.10)}$$

Here, A stands for PLGA amount (mg), B for CLX amount (mg), and C for the volume of organic phase (ml). As described above, the sign before the coefficients corresponds to the relationship between two variables [130,255,395,396]. In **Eq. (5.9)**, increase in factors of PLGA amount and volume of organic phase leads to increase in the response, while increase in the CLX amount leads to decrease of EE%. In contrast, **Eq. (5.10)** demonstrates that increase in PLGA and CLX amount will result in increased LC%, while increase in the volume of organic solvent will decrease the result in response.

**Table 5.9:** Statistical data obtained from ANOVA analysis of EE% of CLX loaded PLGA nanoparticles prepared by NPPT and SE nanoparticle preparation methods. * Statistically significant differences (P-value < 0.05), df = degree of freedom.

| **Source** | **Nanoprecipitation** | | | | **Single emulsion** | | | |
|---|---|---|---|---|---|---|---|---|
| | **Sum of Squares** | **df** | **F-value** | **P-value** | **Sum of Squares** | **df** | **F-value** | **P-value** |
| **Model** | 6949.47 | 3 | 14.59 | 0.013* | 1995.20 | 3 | 4.05 | 0.105 |
| | **Independent variables:** | | | | **Independent variables:** | | | |
| **PLGA amount** | 631.01 | 1 | 3.97 | 0.117 | 732.11 | 1 | 4.46 | 0.102 |
| **CLX amount** | 6025.28 | 1 | 37.95 | 0.004* | 546.98 | 1 | 3.33 | 0.142 |
| **Organic phase** | 293.18 | 1 | 1.85 | 0.246 | 716.12 | 1 | 4.36 | 0.105 |

Based on the data obtained from both statistical models predicting responses of EE% and LC%, it appears that increasing the range of critical factors and increasing the number of runs could improve some of the results obtained from ANOVA analysis of the data, specifically to improve the clarity and accuracy of these models. With that, it can be expected that both EE% and LC% models would demonstrate significant influence on prediction of drug encapsulation and loading results. However, with current data, only formulations prepared by NPPT achieved significant model for EE% prediction, while formulations by SE achieved significant model for LC% prediction only.

In both EE% and LC% statistically significant models, only critical factor that influence the responses is CLX amount. It is important to note that it was previously observed in **Table 5.3** and **Table 5.4**, that the volume of the organic phase also seems to influence the EE% and LC% values: an increase in the volume of organic phase leads to an increase in EE% and LC% in all NPPT formulations, while an increase in the same factor leads to a decrease in the same responses of formulations prepared by SE (**Figure 5.4**). These observations are confirmed by coefficient signs presented in the **Eq. (5.9)** and **Eq. (5.10)**. However, despite this, the changes in the volume of organic phase do not significantly impact the EE% and LC% values based on the results reported from ANOVA analysis (**Table 5.9** and **Table 5.10**).

**Table 5.10:** Statistical data obtained from ANOVA analysis of LC% of CLX loaded PLGA nanoparticles prepared by NPPT and SE nanoparticle preparation methods. * Statistically significant differences (P-value < 0.05), df = degree of freedom.

| **Source** | **Nanoprecipitation** | | | | **Single emulsion** | | | |
|---|---|---|---|---|---|---|---|---|
| | **Sum of Squares** | **df** | **F-value** | **P-value** | **Sum of Squares** | **df** | **F-value** | **P-value** |
| **Model** | 10.96 | 3 | 3.65 | 0.112 | 165.02 | 3 | 7.71 | 0.039* |
| | **Independent variables:** | | | | **Independent variables:** | | | |
| **PLGA amount** | 0.66 | 1 | 0.70 | 0.451 | 2.37 | 1 | 0.33 | 0.595 |
| **CLX amount** | 7.01 | 1 | 7.45 | 0.053 | 136.07 | 1 | 19.08 | 0.012* |
| **Organic phase** | 3.29 | 1 | 3.49 | 0.135 | 26.58 | 1 | 3.73 | 0.126 |

Comparably to our approach, Alonso-González et al., 2022 also used DoE to observe how certain factors affect LC% of CLX loaded PLGA nanoparticles prepared by SE method. Similarly to results shown in the present study, the authors report that only statistical model predicting LC% response demonstrated significance, while model with EE% predictions did not [255]. Additionally, the authors showed that only change in drug to polymer ratio appeared to be a significant factor in changing the LC% results, while other factors such as surfactant concentration, sonication amplitude and time failed to significantly influence the response [255]. Finally, study by Alonso-González et al., 2022 along with our research agrees that increase in CLX amount in formulations prepared by SE method demonstrate an increase in LC% (**Figure 5.4**) [255], as also observed by the positive sign in front of the coefficient corresponding to the critical factor in the obtained equation (**Eq. 5.10**). However, studies by Ramalho et al., 2019 and Meng et al., 2018 demonstrated contrasting results, where increase in drug concentration led to decrease of EE% in drug loaded PLGA nanoparticles prepared by SE method [403,404]. Meng et al., 2018 suggests that increased concentration of the drug can lead to saturation of the organic phase, which can lead to partition of drug molecules into aqueous phase thus lowering the drug entrapment into polymer phase [403]. However, these reports do not appear to fit the data obtained in present study.

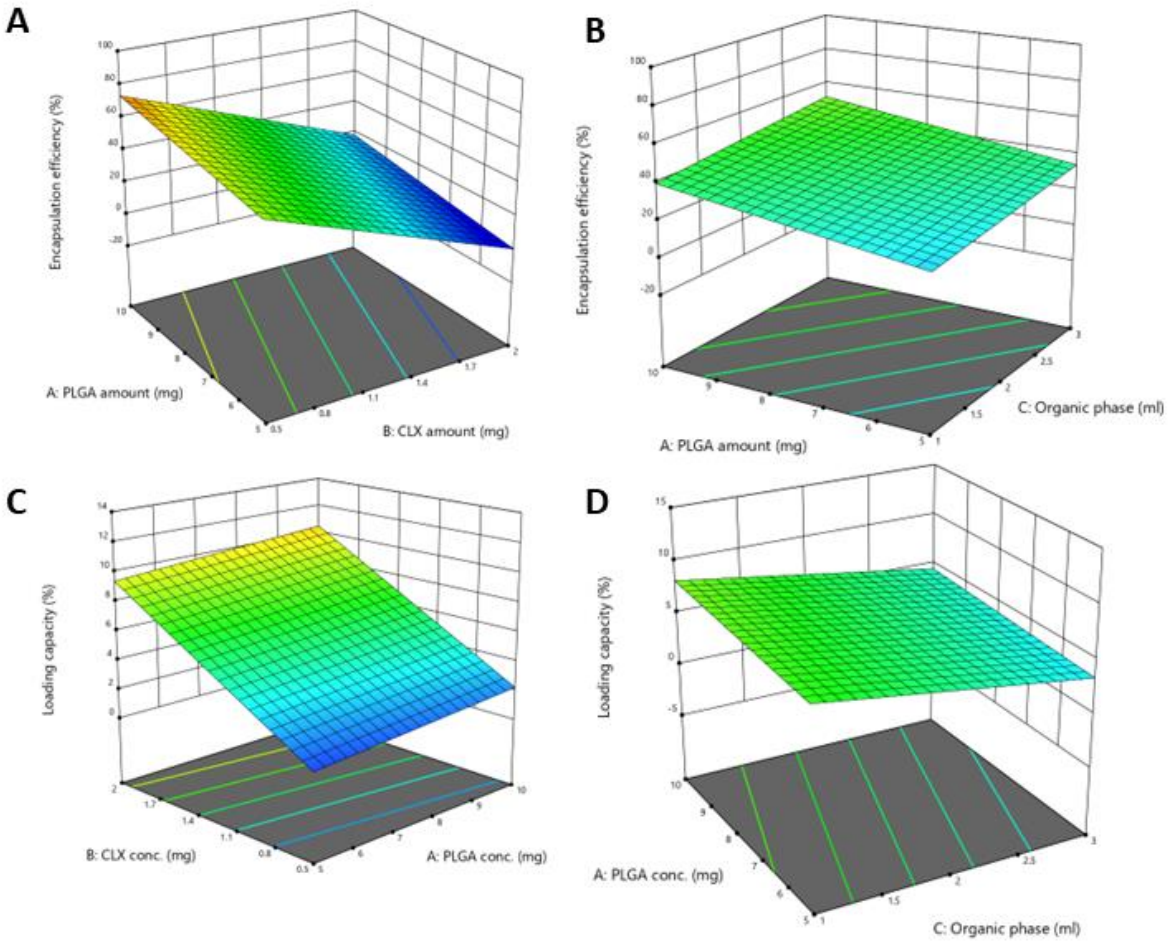


**Figure 5.4:** 3D response surface plots of the effect of PLGA amount (mg), CLX amount (mg), and the organic phase volume (ml) on EE% (A-B) and LC% (C-D) of CLX loaded PLGA nanoparticles. (A-B) plots for PLGA nanoparticles prepared by NPPT, (C-D) plots for nanoparticles prepared by SE.

Interestingly, some studies demonstrate that changes in PLGA amount also significantly affected the EE% and LC% responses in drug loaded PLGA nanoparticles prepared by SE method [401,405]. Both Ahmad et al., 2022 and Abbas et al., 2024 demonstrated that increase in PLGA concentration has significantly increased how much drug was entrapped in PLGA nanoparticles. Authors suggest that increased viscosity of the polymer phase reduces diffusion of the organic solvent into external aqueous phase, therefore enhancing the amount of the drug entrapped inside of the nanoparticles [401,405]. Similarly, increasing the PLGA amount was also reported to significantly enhance EE% of nanoparticles prepared by NPPT method [142,398]. However, changes in PLGA amount in present study did not show a clear trend in either reducing or increasing EE% or LC% values, which could be due to narrow range of PLGA amount used.

Results of this section, investigating the significant effect of critical factors on the EE% and LC% values of CLX loaded PLGA nanoparticles, are presented in **Table 5.11**. Interestingly, most of the studies investigating how critical factors influence chosen responses of PLGA nanoparticle formulations does not select the drug amount or drug concentration as one of the critical factors. Due to only several prior studies available, especially for nanoparticles prepared by NPPT method, as well as overall contrasting results reported, it is challenging to evaluate how the data from present study fits with available research. Improvement of obtained statistical model by increasing number of runs or widening the range of critical factors tested could be beneficial in improving the current statistical model.

**Table 5.11:** Summary of the findings observed in section 5.3.1.5., showing significant effect of critical factors on the EE% and LC% values of CLX loaded PLGA nanoparticles. Symbol "↑" demonstrates the increase, while symbol "↓" demonstrates decrease, "No effect" means no significant effect on the response.

| **Critical factors** | | | | **Nanoparticles by SE** | |
|---|---|---|---|---|---|
| | | **Nanoparticles by NPPT** | | | |
| **Parameters tested** | **Levels of parameter** | **Response in EE%** | **Response in LC%** | **Response in EE%** | **Response in LC%** |
| PLGA amount | ↑↓ | No effect | No effect | No effect | No effect |
| CLX amount | ↑ | ↓ | No effect | No effect | ↑ |
| Volume of organic solvent | ↑↓ | No effect | No effect | No effect | No effect |

## 5.3.1.6. Optimisation and validation of the DoE models

The optimum CLX loaded PLGA nanoparticle formulations prepared by NPPT and SE methods were selected by applying constrains on the critical factors. For the independent variables, PLGA amount was selected to be minimised and CLX amount to be maximised, to enhance the amount of drug per polymer used in the nanoparticle formulations. No contrains were set for the volume of organic solvent. For the reponses, particle size and PDI were set to be minimised, while EE% and LC% were set to be maximised.

Desirability factor of Design Expert Software was used to determine the parameters of critical factors which would help to achieve the desired reponses in the nanoparticle formulations. Based on the constrains selected, the software yielded solutions with desirability of 0.52 for NPPT model and 0.53 for SE model out of 1, which equals ideal desirability. Selected solutions and characterisation of those formulations are presented in **Table 5.12**.

**Table 5.12:** Formulations of CLX loaded PLGA nanoparticles, which were selected due to highest desirability by Desing Expert Software based on the constrains that were chosen. Responses are presented as predicted by the software in comparison to experimental data, obtained in in order to confirm predictions. Error bars of experimentally confirmed data represent SD and n = 3. EE% = encapsulation efficiency, LC% = loading capacity.

| Sample name | Nano-particle synthesis method | PLGA mass (mg) | CLX mass (mg) | Organic phase Volume (ml) | Aqueous phase volume (ml) | Particle size (nm) | PDI | EE% | LC% |
|---|---|---|---|---|---|---|---|---|---|
| **N-F9** | NPPT | 5 | 1.1 | 1.4 | 4 | **Predicted** | | | |
| | | | | | | 103.5 | 0.21 | 39.9 | 4.4 |
| | | | | | | **Confirmation** | | | |
| | | | | | | 93.7±5 | 0.09±0.02 | 11.5±3 | 2.5±1 |
| **E-F9** | SE | 5 | 2 | 1 | | **Predicted** | | | |
| | | | | | | 190.9±0 | 0.214 | 39.2 | 11.2 |
| | | | | | | **Confirmation** | | | |
| | | | | | | 182.9±17 | 0.19±0.06 | 27.8±0 | 11.1±0 |

Software presented additional formulations for verification of each NPPT and SE model, three confirmation runs (n = 3) were performed to validate the statistical models. The results were in good agreement with the predicted values, as well as within the 95%-confidence-interval, indicating validitity of the models. However, as demonstrated in **Table 5.12**, the characterisation of actual optimised final formulations N-F9 and E-F9 showed relative difference between predicted results and experimentally obtained data. Both predicted and actual responses of E-F9 were in reasonable agreement except for EE% values, however it was discussed in **section 5.3.1.5.** that obtained statistical model lacked significance in determining EE% response of PLGA nanoparticles obtained by SE method. In contrast, particle size of N-F9 was the only reponse with predicted and actual values in reasonable agreement. Other

responses, such as PDI, EE% and LC% demonstrated to be not accurate compared to the predicted values. This outcome could be linked to the use of two-level screening design as it included non-significant critical factors into the final model, which could have limited the accuracy of the predictions. Additionally, screening design is mainly used to identify which variables are significant, generating data that can be later used with other statistical design methods, such as Box – Behnken Design, for further optimisation of the experiments [390].

### 5.3.2. Optimisation and characterisation of selected formulations with mucoadhesive coating

Formulations N-F9 and E-F9, which were obtained through the use of DoE, were further optimised with mucoadhesive coating. The mucoadhesive coating of PLGA formulations containing encapsulated CLX was necessary to prolong nanoparticle retention time in the bladder, where formulations would be instilled intravesically in order to treat UTIs. Based on the optimisation of mucoadhesive nanoparticles investigated in **Chapter 4**, five concentrations and 3 types of chitosan were selected for present study: 0.5 mg/ml of CS-M, 1 mg/ml of CS-L, and 0.5 mg/ml, 1 mg/ml and 2 mg/ml of C-CS. Results for both formulations with chitosan coatings are presented in **Table 5.13**.

**Table 5.13:** Characteristics of CLX loaded PLGA nanoparticles with chitosan coating. Error bars represent SD and n = 3. EE% = encapsulation efficiency, LC% = loading capacity.

| Sample name | Chitosan type | Chitosan conc. (mg/ml) | Particle size (nm) | PDI | Zeta potential (mV) | EE% | LC% |
|---|---|---|---|---|---|---|---|
| **N-F9** | N/A | N/A | 93.7±5 | 0.09±0.02 | -8.3±2 | 11.5±3 | 2.5±1 |
| **N-F9-CSM** | CS-M | 0.5 | 295.5±83 | 0.29±0.01 | 33.4±2 | 14.8±6 | 3.3±1 |
| **N-F9-CSL** | CS-L | 1 | 273.9±4 | 0.31±0.02 | 28.8±2 | 19.3±7 | 4.2±2 |
| **N-F9-0.5CCS** | C-CS | 0.5 | 311.6±72 | 0.28±0.01 | 30.5±1 | 11.6±3 | 2.6±1 |
| **N-F9-1CCS** | | 1 | 282.2±15 | 0.27±0.01 | 35.3±3 | 10.4±2 | 2.3±1 |
| **N-F9-2CCS** | | 2 | 368.5±39 | 0.29±0.02 | 41.7±2 | 17.3±9 | 3.8±2 |
| **E-F9** | N/A | N/A | 182.9±17 | 0.19±0.06 | -3.1±0 | 27.8±0 | 11.1±0 |
| **E-F9-CSM** | CS-M | 0.5 | 212.6±22 | 0.32±0.05 | 5.4±3 | 22.3±2 | 8.9±1 |
| **E-F9-CSL** | CS-L | 1 | 194.6±16 | 0.29±0.05 | 7.5±1 | 18.0±2 | 7.2±1 |
| **E-F9-0.5CCS** | C-CS | 0.5 | 215.5±9 | 0.29±0.04 | 19.9±1 | 26.3±3 | 10.5±1 |
| **E-F9-1CCS** | | 1 | 207.3±28 | 0.29±0.08 | 22.6±2 | 28.9±5 | 11.6±2 |

| | | | | | | | |
|---|---|---|---|---|---|---|---|
| **E-F9-2CCS** | | 2 | 223.0±35 | 0.37±0.08 | 21.1±2 | 27.3±5 | 10.9±2 |

Based on the obtained data, addition of chitosan has significantly ($P < 0.05$) increased the zeta potential of the particles from negative to positive. Normally, PLGA nanoparticles exhibit negative charge due to terminal ester or carboxyl groups of PLGA [119], however addition of cationic chitosan coating changes the particle charge into positive, depending on the concentration, MW, and sometimes even derivative of chitosan used [345]. Positively charged nanoparticles are known to form electrostatic interactions with negatively charged mucosal surfaces, therefore making the formulations mucoadhesive [9]. The results observed in **Table 5.13** demonstrate that zeta potential was highest in chitosan coated PLGA nanoparticles by NPPT method, compared to nanoparticles prepared by SE method. Some reports suggest that it could be due to surfactant, which coats the particles and shields the surface charge [137,138]. It is important to note, that formulation N-F9 was prepared by NPPT method, which means only 0.075% of P407 was used, while E-F9 was prepared by SE method, which used 2% of PVA. It has been established that due to hydrophobic bonding of partially hydrolysed PVA and acetic groups of PLGA, PVA is permanently attached onto the nanoparticle surface [169,170]. Based on this, several studies have demonstrated that increasing the concentration of PVA reduces the surface charge of PLGA nanoparticles [119,137].

Slight increase in particle size and PDI of nanoparticles coated with different types of chitosan was observed, however this outcome is expected and has been extensively documented in other publications of chitosan coated nanoparticles [347–349]. No other major changes were observed comparing chitosan coated formulations to the non-coated formulations.

Based on obtained results, formulations N-F9-1CCS and E-F9-1CCS, which contained 1 mg/ml C-CS, were selected for further experiments. As explained in **Chapter 4**, zeta potential and particle size were the main characteristics influencing how well particles adhere to the mucosal surface [224,342]. Hence, formulations N-F9-1CCS and E-F9-1CCS demonstrated smallest particles of all chitosan coated formulations, resulting in particles sized 282.2 ± 15 nm and 207.3 ± 28 nm, respectively. More importantly, formulations with 1 mg/ml C-CS coating demonstrated highest zeta potential values out of all combinations of chitosan used. The only exception was N-F9-2CCS formulation, which showed highest zeta potential of 41.7 ± 2 mV, however it also showed highest particle size of 368.5 ± 39 nm and therefore was not used in further experiments.

As the aim of this study was to prepare mucoadhesive CLX loaded PLGA nanoparticles for intravesical delivery to the bladder, the pH of selected formulations was investigated. Initial pH of the N-F9 was 7.0 ± 0.1, while addition of chitosan coating demonstrated pH of 4.8 ± 0.3 of the N-F9-1CCS. Similarly, the pH of E-F9 formulation was close to neutral with pH of 6.4 ± 0.2, while addition of chitosan turned the pH more acidic showing pH of 5.1 ± 0.1 of the formulation E-F9-1CCS. In order to enhance mucoadhesive properties, the pH of all formulations was changed to 4.5. Acidic pH was found to be the optimal pH for strong mucoadhesive properties of the nanoparticles, as well as non-toxic acidity to the bladder environment, as discussed in depth in **Chapter 4** [224,357]. Nanoparticle characteristics after pH change were presented in **Table 5.14**.

The shape and surface morphology of these formulations were also investigated by TEM (**Figure 5.5**). TEM images showed a spherically shaped nanoparticles, with chitosan coated formulations N-F9-1CCS and E-F9-1CCS demonstrating size range of 118.8 ± 34 nm and 82.8 ± 18 nm, respectively. Uncoated formulations N-F9 and E-F9 demonstrated smaller particle size of 51.6 ± 12 and 63.0 ± 15 nm, respectively. While TEM results show significantly smaller particles than reported by DLS (**Table 5.14**), this outcome is expected as DLS measurement normally reports larger particle size due to measurement of hydrodynamic radius of the particles, instead of true radius of the particles as is measured by TEM. The detailed explanation of particle measurement principles of the DLS and TEM techniques were reported in **section 2.3.2.1.** and **section 2.3.2.4.** of **Chapter 2**.

**Table 5.14:** Characteristics of CLX loaded PLGA nanoparticles with and without chitosan coating after the pH of nanoparticle solution was changed to 4.5. Error bars represent SD and n = 3.

| Sample name | Chitosan type | Chitosan concentration (mg/ml) | Particle size (nm) | PDI | Zeta potential (mV) |
|---|---|---|---|---|---|
| **N-F9** | N/A | N/A | 133.5±25 | 0.20±0.01 | -3.7±1 |
| **N-F9-CCS** | C-CS | 1 | 295.9±33 | 0.28±0.02 | 32.9±2 |
| **E-F9** | N/A | N/A | 210.7±46 | 0.26±0.10 | -0.6±1 |
| **E-F9-1CCS** | C-CS | 1 | 194.8±15 | 0.25±0.03 | 14.3±2 |

Uncoated formulations N-F9 and E-F9, along with chitosan coated formulations N-F9-1CCS and E-F9-1CCS were further characterised by powder X-ray diffraction (PXRD) and attenuated total reflectance – Fourier transform infrared (ATR-FTIR) spectroscopy to analyse the drug distribution within the nanoparticle system. Results of PXRD results are plotted in **Figure 5.6**. Multiple sharp peaks visible in the raw CLX sample demonstrate that the drug is in crystalline state. Once the drug in encapsulated into the nanoparticles, only one broad diffraction peak at 2θ of 19.7 ° can be observed in all nanoparticle formulations prepared by SE. Blank formulations are presented in order to demonstrate that the same diffraction peak is also observed when no CLX is present in the samples. This draws the conclusion that the broad peak at 2θ of 19.7 ° belongs to the polymer diffraction pattern and it demonstrates that the polymer is an amorphous state [406,407]. Interestingly, some smaller peaks can be observed at 2θ of 19.2 °, 23.4 °, 31.2 ° and 45.2 ° in formulations N-F9 and N-F9 (no CLX) that correspond to the peaks at the same degrees as observed in P407. P407 was used as surfactant in these formulations. Some of these peaks are also visible in N-F9-1CCS and N-F9-1CCS (No CLX) samples. These results appear to confirm that P407 coats parts of the surface of the nanoparticles prepared by NPPT. Interestingly, it appears that addition of chitosan coating reduces the exposure of P407 on the surface of the particles to some capacity due to disappearance of a few peaks in chitosan coated formulations. Most importantly, no sharp peaks of CLX are observed in formulations N-F9, N-F9-1CCS, E-F9 and E-F9-1CCS, suggesting that the drug is encapsulated into the nanoparticles and is in an amorphous state [389].

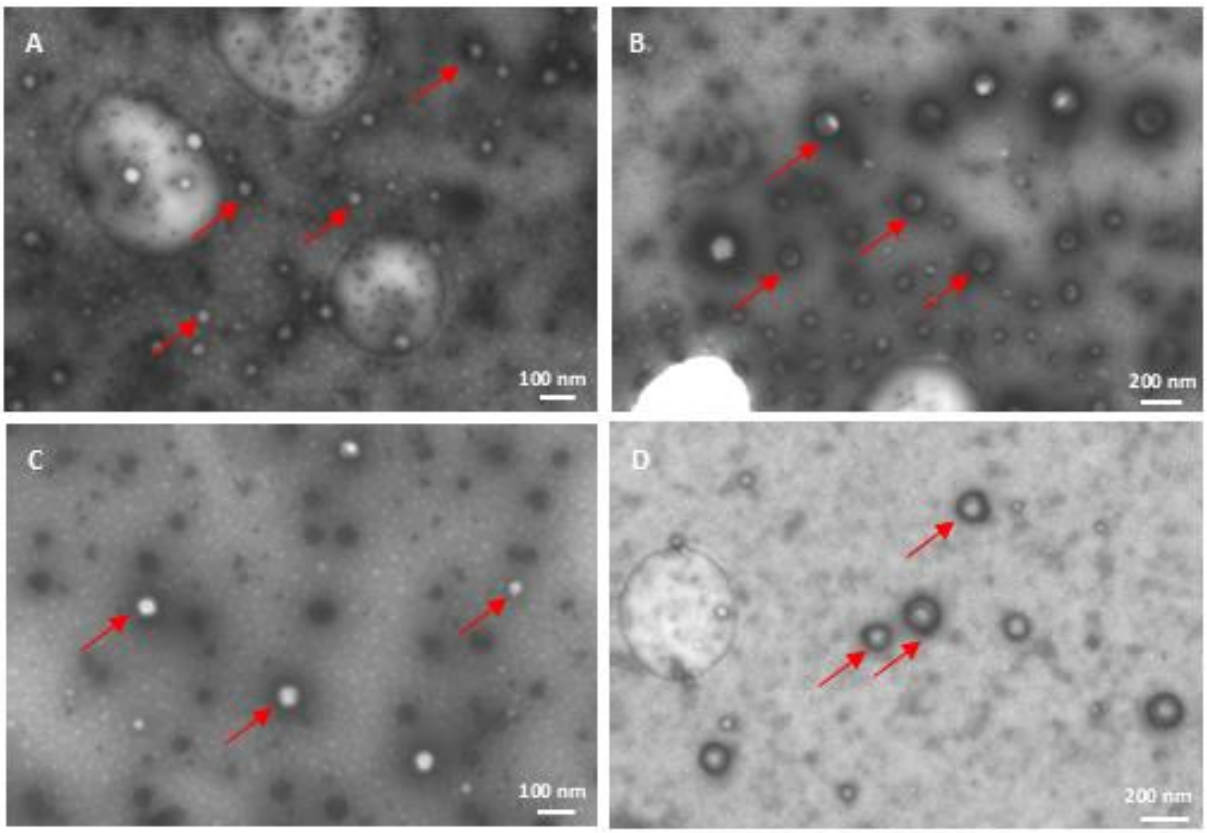


**Figure 5.5:** TEM images of CLX loaded PLGA nanoparticle formulations: (A) N-F9, (B) N-F9-1CCS, (C) E-F9, (D) E-F9-1CCS.

The ATR-FTIR spectra of CLX, presented in **Figure 5.7**, demonstrated characteristic peaks of CLX at 3333 and 3227 $cm^{-1}$, which are attributed to stretching vibration of primary amine N-H of $SO_2NH_2$ group, along with characteristics peaks of asymmetric and symmetric stretching of $S=O_2$ observed at peaks 1346 and 1130 $cm^{-1}$ [389,408]. The ATR-FTIR spectra of PLGA showed two characteristic peaks at 1749 and 1086 $cm^{-1}$, where first peak was attributed to C=O stretching, while the latter peak indicated C-O-C group stretching [193]. The spectrum of raw PVA, which was used in nanoparticle preparation by SE method, demonstrated a peak at 1734 $cm^{-1}$ indicating stretching of C=O, a peak at 1238 $cm^{-1}$, which demonstrated a wagging of $CH_2$, and peaks at 1022 and 845 $cm^{-1}$, which were attributed to stretching of C-O-C group and C-C group, respectively [409]. Alternatively, P407 was used as a surfactant for preparation of nanoparticles by NPPT, with its spectra demonstrating characteristic peaks at 2882 $cm^{-1}$ (C-H stretch aliphatic) and 1099 $cm^{-1}$ (C-O stretch), as well as two peaks at 962 and 841 $cm^{-1}$ that were also reported in prior literature [410].

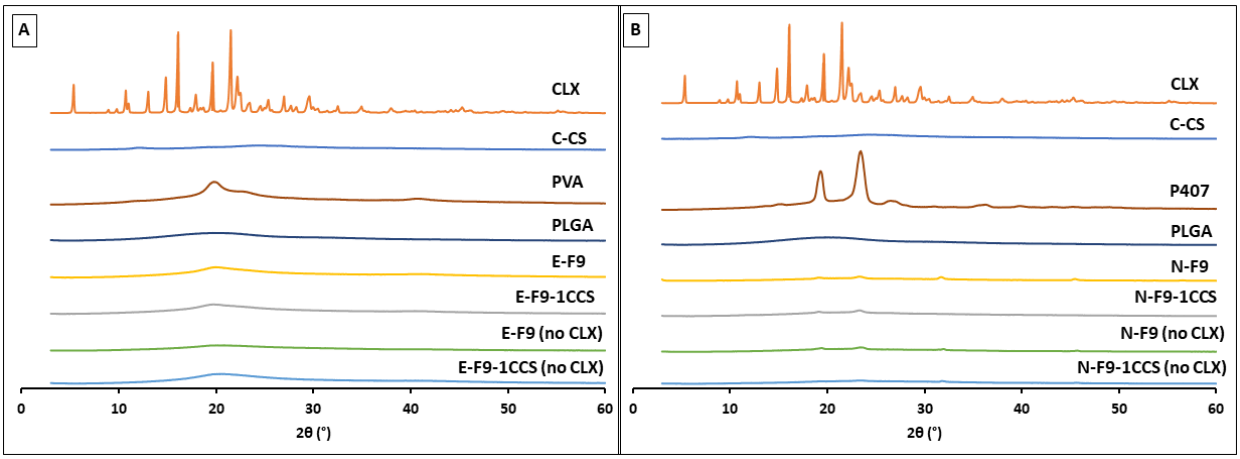


**Figure 5.6:** Powder X-ray diffraction patterns of (A) raw materials and nanoparticles prepared by SE method, (B) raw materials and nanoparticles prepared by NPPT method.

Formulations N-F9, N-F9-1CCS, E-F9, and E-F9-1CCS demonstrated clear characteristic peaks as observed in PLGA spectra at 1734 – 1755 and 1086 – 1090 $cm^{-1}$, with diminished peaks of CLX, suggesting that the drug was encapsulated inside the PLGA nanoparticles. In formulations N-F9-1CCS and N-F9-1CCS (without CLX) some reduction in peak intensities can be observed, due to addition of chitosan. Additionally, peaks at 2882 $cm^{-1}$, 962 $cm^{-1}$ and 841 $cm^{-1}$ can be observed in all nanoparticle formulations prepared by NPPT method, indicating that P407 coats parts of the nanoparticle surface (**Figure 5.7A**). In contrast, peaks at 1238 and 845 $cm^{-1}$, which are associated with PVA, can be clearly seen in all formulations prepared by SE method (**Figure 5.7B**). This outcome is to be expected due to hydrophobic binding of PVA and PLGA, which permanently attaches PVA onto the nanoparticle surface [169,170]. Additionally, the same reasoning can be used to explain why some PLGA peaks at 1734 and 1090 $cm^{-1}$ of nanoparticle formulations prepared by SE method appear to lack intensity. Minimal peak shifting was also observed from the characteristic peaks of PLGA at 1749 and 1086 $cm^{-1}$ to 1734 and 1090 $cm^{-1}$, respectively. Diminished peaks at 1734 $cm^{-1}$ of E-F9 and E-F9-1CCS, including the same formulations that had no CLX, were likely the consequence of PVA and chitosan coating the nanoparticle surface.

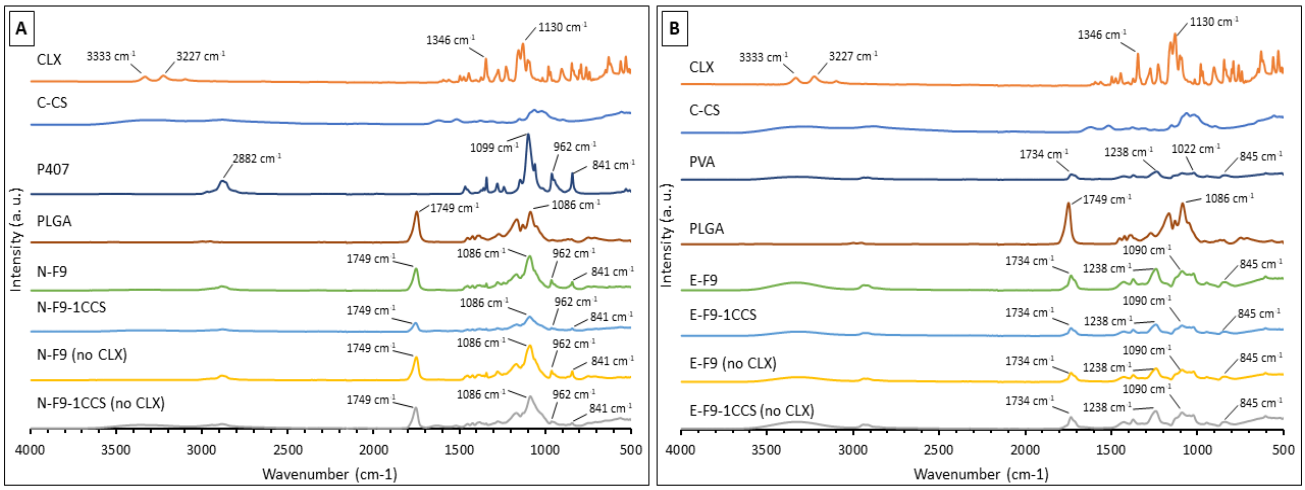


**Figure 5.7:** Fourier-transform infrared spectra of (A) raw materials and nanoparticles prepared by NPPT method, (B) raw materials and nanoparticles prepared by SE method. CLX = Celecoxib, C-CS = carboxymethyl chitosan, P407 = poloxamer P407, PVA = poly(vinyl alcohol), PLGA = poly(lactic-co-glycolic acid).

### 5.3.3. *In vitro* drug release

Differences in drug release profiles of CLX loaded PLGA nanoparticles, coated or uncoated with chitosan, were investigated. Additionally, changes in drug release profiles were expected due to different preparation method of nanoparticles used. PBS was chosen as the release buffer, however its pH was adjusted to 4.5 to mimic acidic environment. As discussed in **Chapter 4**, acidic pH is needed to enhance mucoadhesive properties of chitosan coated PLGA nanoparticle formulations [224]. Due to hydrophobicity of CLX and poor solubility in PBS pH = 4.5, surfactants are often added to the release medium to increase the drug solubility and maintain sink conditions, as it is often reported in the literature [255,389]. Therefore, 1% of Tween 80 was added to PBS (37 °C degrees, pH = 4.5) where CLX solubility was equal to 532.2 ± 34 µg/ml, compared to CLX solubility in PBS (37 °C degrees, pH = 4.5) alone, which was less than 0.5 µg/ml. Once release media composition was determined, free CLX release from dialysis bag was examined in order to compare release profiles of free CLX and CLX that is encapsulated into PLGA nanoparticles. CLX dissolved in EtOH showed 100% release from the dialysis bag within 1 to 2 hours of the assay, showing a fast drug release in sink conditions.

Results of drug release profiles of CLX loaded PLGA nanoparticles are shown in **Figure 5.8**. Biphasic release profile was seen in all formulations, with burst release of CLX observed within first 24 hours, followed by very slow increase documented up to 7 days (data not shown).

Interestingly, during the initial burst effect, N-F9 and N-F9-1CCS demonstrated approximately 58% of the drug released after 8 hours, while E-F9 and E-F9-1CCS showed approximately 45%, indicating that the release of CLX from nanoparticles prepared by SE was sustained more than from nanoparticles prepared by NPPT method. Similar findings were reported in the literature [410,411], with study by Wang et al., 2014 reporting that faster drug release of nanoparticles prepared by NPPT can be attributed to the smaller particle size. However, formulations N-F9 and N-F9-1CCS demonstrate the same drug release profiles, while their particle size is significantly different (**Table 5.13**), demonstrating that differences in particle size are unlikely to influence the drug release. A hypothesis was considered that different types and concentrations of surfactants used in these formulations (P407 was used in nanoparticles prepared by NPPT, while PVA was used in nanoparticles prepared by SE) influenced the rate of drug being released from PLGA nanoparticles. Prior research has showed that different surfactant coating of nanoparticles does influence initial burst release [410,412], therefore differences in nanoparticle preparation methods and surfactants used are likely to be the main reasons why E-F9 and E-F9-1CCS formulations demonstrated more sustained burst effect compared to N-F9 and N-F9-1CCS formulations. After the first 24 hours, all formulations continued to release from 4% to 10% of drug following the next 48 hours, after which the drug release reached a plateau. After 7 days of nanoparticle incubation in release medium, E-F9 and E-F9-1CCS formulations have released 99.9±10% and 84.1±1%, respectively, while formulations N-F9 and N-F9-1CCS released less of the CLX, totalling 82.5±3% and 77.6±2%, respectively.

Most of the studies report that CLX loaded PLGA formulations showed 100% release over time [255,387,388], however this was failed to achieve in present study, where formulations N-F9, N-F9-1CCS and E-F9-1CCS never reached a 100% release. It was observed by Alonso-González et al., 2022 that formulations with CLX showed a burst effect in the first 8 hours, then entered slower CLX release phase up to 7 days, finally reaching very slow release rate from day 7 to 28 [255]. Since the drug release assay was stopped at day 7 in the present study, it could be debated that release from formulations N-F9, N-F9-1CCS and E-F9-1CCS could have slowly continued up to a month. However, a slight decrease in CLX percentage was observed starting the day 5 (for nanoparticles prepared by NPPT) and day 6 (for nanoparticles prepared by SE) of the release assay, suggesting that all of the drug has been released, or that some drug degradation has occurred. Similarly to our study, Chu et al., 2023 reports only 82% of CLX released from PLGA nanoparticles after 7 days, with a plateau observed after 72 hours

of the release assay. Overall, conflicting results of CLX drug release rate are reported in the literature, with some reports indicating fast release within 1 to 2 days [386–388], and others demonstrating a prolonged sustained drug release of over a week, continuing for a month or more [255,389,402]. This can be attributed to the differences of parameters and chemicals used to prepare CLX loaded nanoparticles, as it has been shown that use of different organic solvents and surfactants used can reduce the burst drug release effect [386,387,410,412]. Additionally, the mechanism of drug entrapment can influence the rate of drug release, as nanoparticles with drug adsorbed onto the particle surface will demonstrate a burst effect, with drug dissolving immediately after being submerged into the media [413].

CLX location within the nanoparticle system could have a major impact on the release rate. For instance, CLX that is fully entrapped into nanoparticle core will demonstrate much slower release compared to nanoparticle system, which has CLX adsorbed onto the particle surface.

Formulations prepared by NPPT method demonstrated no difference in drug release profiles compared between nanoparticles with or without chitosan coating. In contrast, formulations prepared by SE method demonstrated lower overall CLX release when coated with chitosan compared to uncoated nanoparticles. It is important to note that no significant difference between E-F9 and F-F9-1CCS formulations was observed during the burst release of CLX during the first 8 hours of the assay. Additionally, due to large SD of E-F9 formulation, data of both formulations overlaps after the 48-hour timepoint. Hence, it is challenging to state whether chitosan coating had any significant difference to the release profiles of the CLX loaded PLGA nanoparticles prepared by SE method. Several publications demonstrated that PLGA nanoparticles showed sustained drug release when coated with chitosan [193,226,227]. Study by Lu et al, 2019 explained, that as chitosan coats the nanoparticle surface, it limits the drug adsorption onto the particle surface and consequently sustains drug release by reducing the initial burst effect [193]. However, no peaks indicating CLX adsorption on the nanoparticle surface were observed during PXRD and ATR-FTIR analysis in **section 5.3.2**. While this does not confirm there was no drug adsorption on the particle surface, in order to accurately report whether chitosan coating has a significant effect on CLX release profiles, more chitosan coated formulations would have to be studied, where release profiles of CLX loaded PLGA nanoparticles coated with different concentrations and types of chitosan would be investigated.

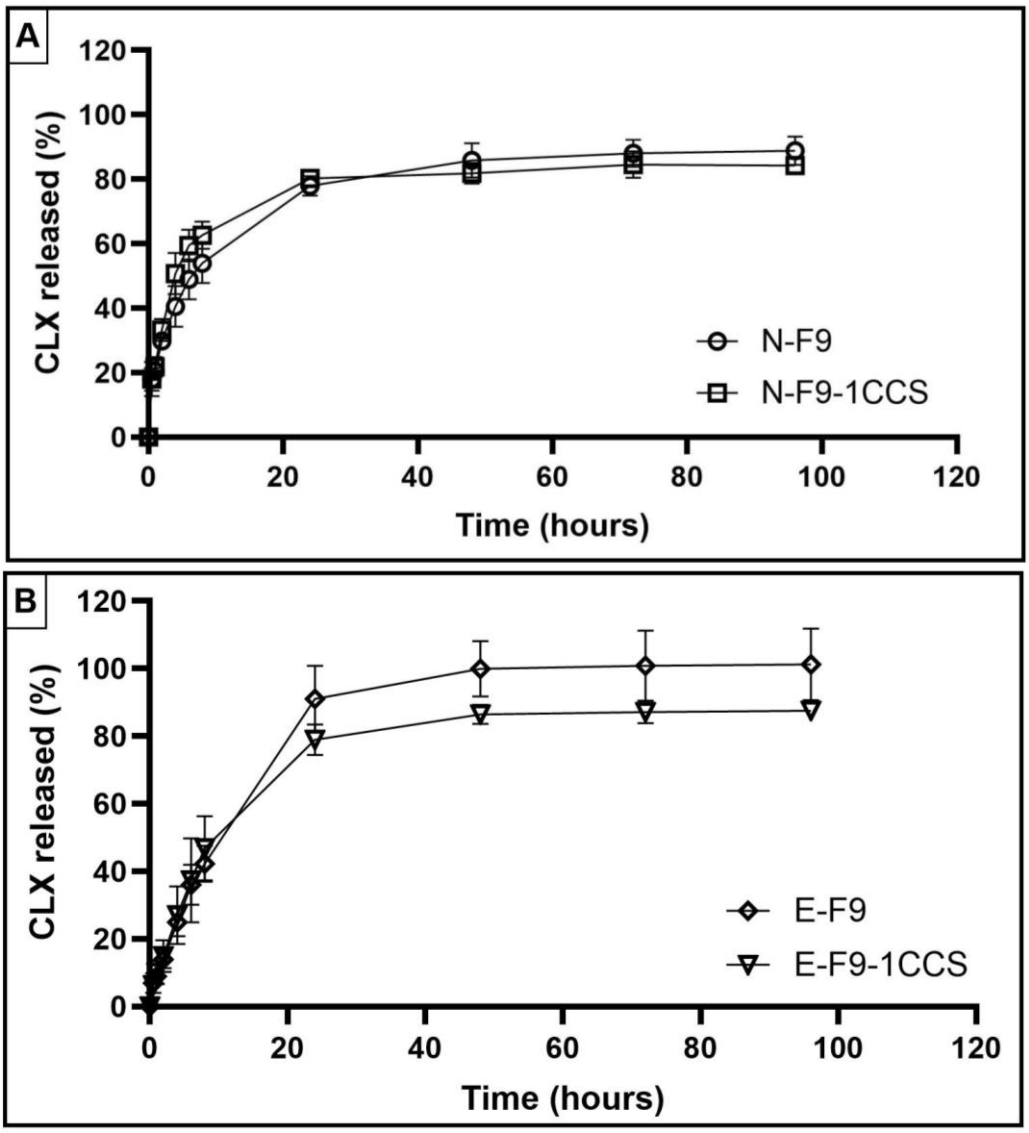


**Figure 5.8:** Cumulative *in vitro* CLX release from (A) formulations N-F9 and N-F9-1CCS, prepared by NPPT preparation method, (B) formulations E-F9 and E-F9-1CCS, prepared by SE preparation method. Formulations were incubated in PBS pH = 4.5 + 1% Tween 80 release medium, at 37 °C and 100 RPM shaking. Error bars represent the SD and n = 3.

## 5.3.4. Histology and histopathological evaluation

*Ex vivo* toxicity of mucoadhesive CLX loaded PLGA nanoparticles were examined on fresh porcine bladder tissues. After dissection of the bladder, 400 µl of each nanoparticle solution was pipetted onto the tissue, incubated for 1 hour, later fixed in formalin, embedded in paraffin, and finally sectioned. Following dehydration process and H&E staining, tissues were rehydrated and mounted onto the microscope slides. Images taken are presented in **Figure 5.9**.

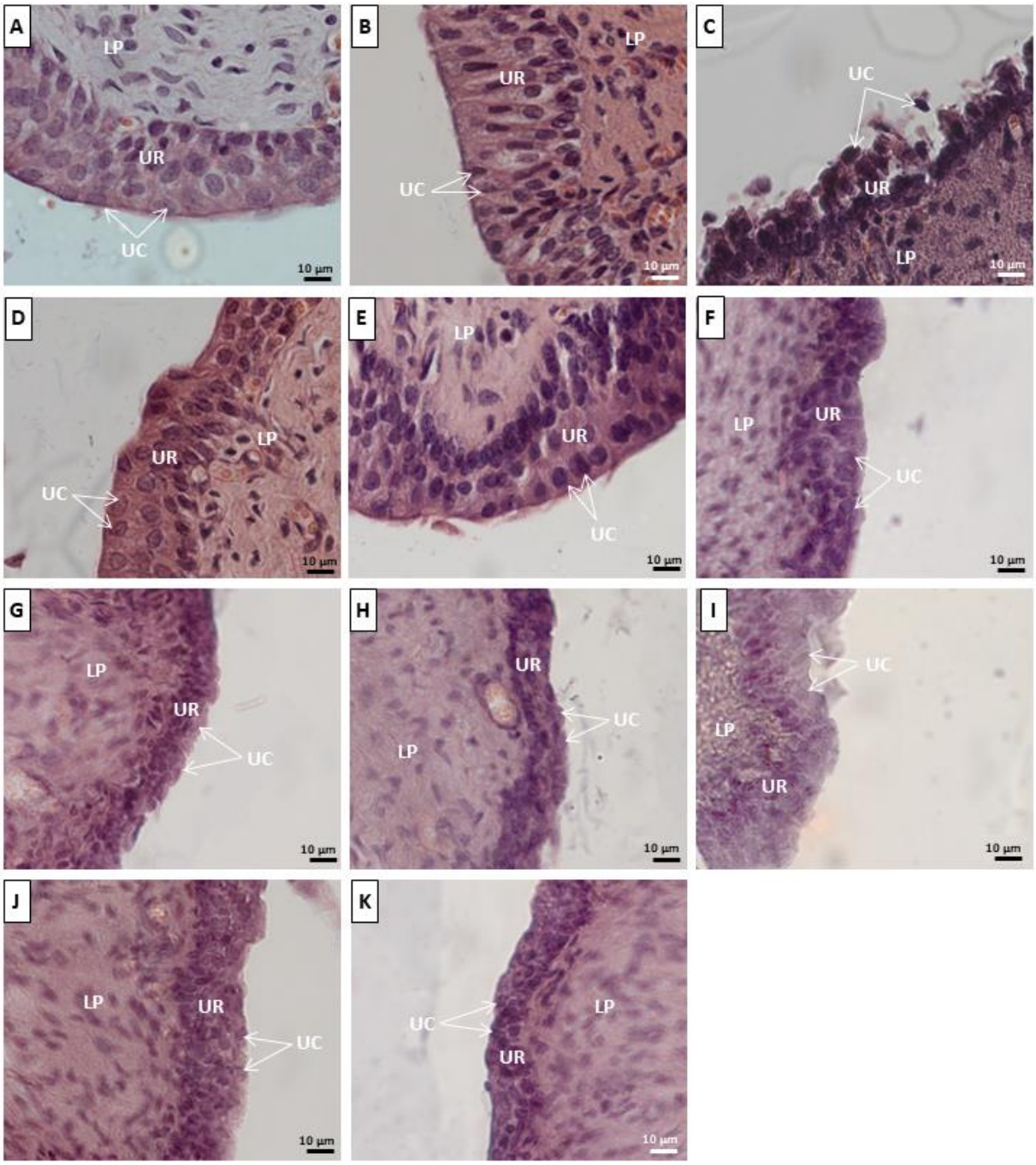


**Figure 5.9:** Microscopic images of H&E stained *ex vivo* porcine bladder tissue sections of 8 µm thickness. Images A-B demonstrate negative controls, in which tissues were kept on ice throughout transportation (A) and followed treatment procedure without administration of nanoparticle solutions (B). Positive control tissues were treated with 10 mg/ml PS for 1 hour at 37 °C (C). Images D-K demonstrate tissues incubated for 1 hour at 37 °C degrees with formulations N-F9 (no CLX) (D), N-F9-1CCS (no CLX) (E), E-F9 (no CLX) (F), E-F9-1CCS (no CLX) (G), N-F9 (H), N-F9-1CCS (I), E-F9 (J), E-F9-1CCS (K). Scale bar denotes 10µm, UC = umbrella cells, UR = urothelium, LP = lamina propria.

Obtained tissue sections were observed for any toxic effects caused by nanoparticles on urothelium layer of the bladder tissue. As observed in **Figure 5.9A-B**, healthy bladder tissues exhibit a tightly packed umbrella cell layer, which together with uroplakins forms an impermeable plaque that protects urothelium tissue from pathogens and controls water and ion exchange [4]. Based on these observations, transportation on ice and treatment process of washing and incubation at 37 °C did not cause any negative effects on the health of the tissue. In contrast, strong noxious effects can be observed in **Figure 5.9C**, as treatment with PS lead to disruption of tight and adherens junctions within urothelium layer, resulting in tissue desquamation and diminished intracellular matrix [333]. Compared to this, tissues treated with nanoparticle formulations for 1 hour showed no histopathological changes, therefore confirming the treatment to be safe. Some haziness can be observed around the urothelium barrier in **Figure 5.9**, specifically in images E, G, H and I, however it is likely to be artefacts, as umbrella cells of the urothelium demonstrate an intact barrier of bladder lining.

Short treatment time could be one of the reasons for no toxicity observed in mucoadhesive nanoparticles. Previous literature has demonstrated that increased incubation time of chitosan on bladder tissue increases damage caused to the urothelium, such as necrosis and desquamation of the umbrella cells [220,221]. Additionally, it was reported that increase in concentration of chitosan lead to more toxic effects caused, however concentration of chitosan used to coat nanoparticles in the present study was very low, ranging from 0.000005% to 0.00002% (w/v). Despite that, it has been shown that desquamation of bladder cells can occur within 10 minutes of the treatment with chitosan, after which a quick restoration and differentiation of the cells follows, concluding in restored urothelium layer within an hour from the treatment start [217,221]. Therefore, although chitosan coated nanoparticles could cause short term toxicity, regeneration of urothelium layer is fast and demonstrates no long-term toxicity effects [217,221].

PLGA nanoparticles have been deemed to be safe for use by drug delivery system in human body by Food and Drug Administration (FDA) [90]. During synthesis of nanoparticles by SE method, small concentration of PVA was used to stabilise the emulsion and prevent particle aggregation [136]. No toxicity was expected from PVA use in present study, as small concentrations of PVA were used, as well as intended intravesical application of the nanoparticle treatment. This was discussed in more detail in **section 3.3.6.**

CLX is a part of NSAID group, which are known to cause cardiovascular adverse effects, gastrointestinal bleeding, kidney injury, and hypertension [414]. However, CLX is selective COX-2 inhibitor drug, which demonstrates lower risk of toxicity compared to other NSAIDs [414]. Although there are no reports demonstrating instillation of CLX to the bladder, CLX was demonstrated as potential treatment of bladder cancer, as it suppresses tumour proliferation and invasion [415,416]. A recent study by Mohanty et al., 2023 demonstrated that inhibition of COX-2 leads to compromised innate immune system response, where production of antimicrobial peptides and pro-inflammatory cytokines, as well as integrity of the urothelium barrier is negatively affected [71]. However, more studies are needed to investigate and confirm these findings. Use of NSAIDs for UTI treatment is still a relatively novel therapy that lacks understanding in efficacy and how it compares with current therapeutic options. Despite this, current study demonstrates a promising CLX loaded nanoparticle system, that could be used as potential IDD facilitated treatment of other disorders.

## 5.4. Conclusion

CLX was successfully loaded into PLGA nanoparticles, which were prepared by using two conventional polymeric nanoparticle synthesis methods: NPPT and SE. DoE was used to analyse how the same parameters used in both preparation methods affected the physicochemical characteristics of the nanoparticles. Three parameters were chosen for this study: PLGA amount, CLX amount, and volume of the organic phase. Based on the screening test performed, the volume of the organic phase was the parameter that significantly impacted the characteristics of nanoparticles the most. Both particle size and PDI responses were significantly affected after different volumes of organic volume were used in preparation of PLGA nanoparticles by both NPPT and SE methods. Alternatively, change in CLX amount loaded significantly affected only EE% when nanoparticles were prepared by NPPT, and LC% when nanoparticles were prepared by SE method. Amount of PLGA was the parameter than significantly affected only one response, which was particle size, and only in nanoparticles prepared by NPPT method. The summary of DoE results is presented in **Table 5.15**, for nanoparticles synthesised by NPPT method, and **Table 5.16**, for nanoparticles prepared by SE method. Overall, this study demonstrates that depending on the nanoparticle preparation method, different nanoparticle physicochemical properties can be achieved. Smaller and more uniform nanoparticles can be achieved by using NPPT method, however more sustained drug release is achieved from nanoparticles prepared by SE. Up to 13% of CLX was loaded into

PLGA nanoparticles when SE method was used for nanoparticle synthesis, while only up to 6% of CLX loading was achieved in PLGA nanoparticles prepared by NPPT method.

**Table 5.15:** Summary of findings obtained from DoE study, showing significant effect of critical factors on the responses of CLX loaded PLGA nanoparticles prepared by NPPT method. Symbol "↑" demonstrates the increase, while symbol "↓" demonstrates decrease, "No effect" means no significant effect on the response.

| **Critical factors** | | | **Nanoparticles by NPPT** | | | |
|---|---|---|---|---|---|---|
| **Parameters tested** | **Levels of parameter** | | **Response in particle size** | **Response in PDI** | **Response in EE%** | **Response in LC%** |
| PLGA amount | ↑ | | ↑ | No effect | No effect | No effect |
| CLX amount | ↑ | | No effect | No effect | ↓ | No effect |
| Volume of organic solvent | ↑ | | ↓ | ↑ | No effect | No effect |

Further characterisation of the CLX loaded PLGA nanoparticles by PXRD and ATR-FTIR demonstrated no peaks of crystalline CLX in the formulation samples, suggesting that the drug was successfully loaded into the PLGA nanoparticles, with likely no drug adherence observed on the particle surface. Nanoparticles coated with chitosan were also fully characterised, demonstrating increased particle size and higher PDI. Additionally, chitosan coating increased particle charge from slightly negative to highly positive charge, suggesting enhanced mucoadhesive properties. Contrary to the findings reported in other studies, chitosan coating of CLX nanoparticles did not affect the drug release profiles of CLX loaded PLGA nanoparticles.

**Table 5.16:** Summary of findings obtained from DoE study, showing significant effect of critical factors on the responses of CLX loaded PLGA nanoparticles prepared by SE method. Symbol "↑" demonstrates the increase, while symbol "↓" demonstrates decrease, "No effect" means no significant effect on the response.

| **Critical factors** | | | **Nanoparticles by SE** | | | |
|---|---|---|---|---|---|---|
| **Parameters tested** | **Levels of parameter** | | **Response in particle size** | **Response in PDI** | **Response in EE%** | **Response in LC%** |
| PLGA amount | ↑ | | No effect | No effect | No effect | No effect |

| | | | | | | |
|---|---|---|---|---|---|---|
| CLX amount | ↑ | | No effect | No effect | No effect | ↑ |
| Volume of organic solvent | ↑ | | ↑ | ↑ | No effect | No effect |

In general, results obtained from this study demonstrates that use of different nanoparticle methods can significantly impact the physicochemical characteristics of the nanoparticles. Use of statistical models can predict the effect that changes of certain parameters will have on the characteristics of the nanoparticles, therefore shortening the optimisation process to achieve desired results.

# Chapter 6

## Conclusions and future outlook

## 6.1. General conclusions

The presented study demonstrates preparation, characterisation and optimisation of drug loaded polymeric nanoparticles that could be used as potential therapy for urinary tract infection (UTI) treatment and prophylaxis. Combined antibiotic and cyclooxygenase-2 (COX-2) inhibitor drug therapy was chosen as a novel therapeutic approach, with aims to reduce antibiotic treatment and enhance symptomatic treatment of UTIs. Current antibiotic use for treating bacterial infections have led to significant increase in antimicrobial resistance (AMR), therefore this study presents an alternative nanomedicine-based dual therapy which, along with inhibition of bacterial growth by using antimicrobial agents, would also involve symptomatic treatment of inflammation and pain associated with UTIs. Obtained drug loaded polymeric nanoparticle systems were tailored to enhance the loading of each drug, along with other physicochemical characteristics optimised for optimal drug delivery to the bladder. To avoid systemic drug exposure, intra-bladder drug delivery was proposed, however certain limitations were identified first. Direct to bladder drug instillation has been shown to suffer from urine dilution of drug therapeutic concentrations, as well as early drug expulsion from the bladder, hence demonstrating a need for improved drug delivery method to treat bladder disorders. Therefore, this study was also focused on attaining mucoadhesive properties of the drug loaded nanoparticles, which subsequently showed strong mucoadhesive interactions with *ex vivo* porcine bladder tissue, indicating promising results for prolonged particle retention time in the bladder. During the study, great importance was given to toxicology profiles of obtained nanoparticle formulations, to ensure that prolonged treatment of bladder tissues would not cause pathological events. No toxicity on *ex vivo* porcine tissue was observed after the tissues were treated with obtained nanoparticle formulations for 1 hour, demonstrating safe toxicology profiles.

### 6.1.1. Use of hydrophobic ion pairing (HIP) increases hydrophobicity of the hydrophilic antibiotic for improved encapsulation into polymeric nanoparticles

In **Chapter 3**, our focus was to obtain a robust biodegradable antibiotic loaded nanoparticle system for intravesical drug delivery (IDD). Antibiotic of choice was gentamicin (GEN), as it has shown great promise in effective and safe UTI treatment by IDD, however a major challenge associated with this drug was its hydrophilicity. After choosing polymeric

nanoparticles as the drug nanocarriers, we explored potential strategies in obtaining high drug loading of hydrophilic GEN into polymeric nanoparticles.

It has been demonstrated that hydrophilic drugs are particularly hard to encapsulate into nanoparticles, as they are likely to leach out into the aqueous phase during nanoparticle synthesis [182,280,281]. This leads to reduced mass entrapped into the particles, as well as burst release effects observed during *in vitro* drug release assays [182,280,281]. The study in **Chapter 3** demonstrates successful use of hydrophobic ion pairing (HIP) technique to reduce hydrophilicity of the drug. For this study, four different counterions were investigated based on their binding efficiency with the drug, as well as dissociation ability from the drug once therapeutic environment representing media is reached. Results showed that sodium oleate (OA) to be the superior counterion for binding with GEN, as it demonstrated roughly 90% of the drug complexed into ion paired GEN (GEN:HIP) complex, as well as high dissociation efficiency of 63% in acidic high-salt buffer. Although counterions docusate sodium salt (AOT) and sodium dodecyl sulphate (SDS) showed higher binding efficiency of > 96%, their dissociation in high salt buffers was around 50%. While high binding efficiency was an important factor to establish a strong GEN:HIP complex, the dissociation of the complex was essential for drug to achieve its therapeutic concentration within the target site. Therefore, this study demonstrated the importance of selecting a fitting counterion for ion pairing of the chosen drug, as interaction between the drug and HIP agent, as well as the composition of the physiological medium, can greatly impact the binding and dissociation of the obtained drug:HIP-agent complex.

GEN:HIP complex encapsulation into poly(lactic-co-glycolic acid) (PLGA) nanoparticles demonstrated high encapsulation efficiency (EE%) values of > 90%, compared to the un-paired free GEN (UNP-GEN), which demonstrates significantly lower entrapment of 33.1 ± 2%. However, some discrepancy was observed between EE% results and *in vitro* drug release results, which showed only 10% of GEN being released from the GEN:HIP loaded nanoparticles over the period of 6 months. Despite this, GEN demonstrated full 100% release from its GEN:HIP complex when incubated in medium representing physiological conditions, demonstrating full dissociation from the drug within 24 hours. This meant, that GEN release in the aqueous media was sustained by ~ 20 hours because of its complexation into the HIP complex. In comparison, UNP-GEN loaded PLGA nanoparticles showed burst release of GEN within the first 8 hours of the assay, demonstrating that drug entrapment into PLGA

nanoparticles sustained the release GEN for ~ 4 hours. These results showed a great potential of using the HIP technique to reduce hydrophilicity of water-soluble drugs, as ion paired GEN demonstrated greater sustained release profiles than GEN encapsulated into PLGA nanoparticles. Therefore, combining HIP with nanotechnology seems like a promising solution to achieve highly loaded hydrophilic drug nanoparticle systems, which could also demonstrate more than 20 hours of sustained drug release within the bladder. Although GEN loading into PLGA nanoparticles might appear redundant since GEN:HIP complex alone can demonstrate sustained drug release, GEN:HIP entrapment into nanoparticles is essential for effective IDD, as future formulations with mucoadhesive coating would also ensure prolonged retention time of the particles within the bladder.

Additionally, we found that GEN complexed in GEN:OA and GEN:SDS complexes demonstrated enhanced antimicrobial properties against *E. Coli*, compared to the non-ion paired free gentamicin (UNP-GEN) solution. This indicated, that use of HIP enhances antimicrobial properties of the antibiotics, which could suggest a lower dosage of the drug needed in order to treat UTIs in the future.

### 6.1.2. Preparation of mucoadhesive polymeric nanoparticles for direct to the bladder delivery

Addition of mucoadhesive agent to the drug loaded nanoparticle formulations was essential part of this study to ensure effectiveness of IDD to the bladder approach. Many different studies reported use of chitosan and its derivatives to obtain mucoadhesive nanocarriers. **Chapter 4** focused on using different types, molecular weights (MWs) and concentrations of chitosan to provide positive particle charge to usually negatively charged PLGA nanoparticles [119]. Positively charged nanoparticles could then form electrostatic interactions with negatively charged mucin layer of the bladder urothelium, therefore prolonging their retention time in the bladder and preventing washouts by urine voiding. For this study, chitosan of different MWs (low, medium, and high) and chitosan derivative carboxymethyl chitosan (C-CS) were used. We found that chitosan coating applied to PLGA nanoparticles significantly increased particle size, therefore addition of surfactants to the formulations was essential to ensure small particle size. Additionally, this study demonstrated that acidic environment enhanced positive charge of the particles. However, the pH of the nanoparticle solution had to be tailored to ensure no toxicity would be caused to the bladder during the future *in vivo* treatments, therefore lowest

possible acidity of pH = 4.5 was chosen, based on the reports in the literature [286,357]. These findings confirmed the need of improved urinary catheters, which could be used to safely drain urine from bladder lumen, followed by instillation of pre-treatment solution, which would ensure the correct bladder pH conditions to enhance the efficacy of the following mucoadhesive nanoparticle treatment.

*In vitro* and *ex vivo* mucoadhesion testing was conducted to examine mucoadhesive properties of chitosan coated PLGA formulations. Results showed that increase in MW or concentration of chitosan used in the nanoparticle formulations lead to stronger particle mucoadhesion to the bladder tissue. This also meant, that higher MW of chitosan used could compensate for lower concentrations of chitosan, which were needed for some formulations to ensure smaller particle size. Additionally, particle size was observed to be an important criterion for enhanced mucoadhesive properties. These results suggest that to achieve the most effective mucoadhesive coating, as well as preserve physicochemical properties of obtained drug loaded nanoparticle systems, chitosan coating likely needs to be specifically tailored to each nanoparticle formulation to enhance their performance in *in vivo* applications.

### 6.1.3. DoE study for encapsulation of celecoxib into mucoadhesive PLGA nanoparticles

As discussed in **Chapter** 1 of this study, UTI treatment with non-steroid anti-inflammatory drugs (NSAIDs) was reported as a potential alternative UTI treatment method to antibiotics, as it would reduce the risk of bacteria acquiring AMR form misuse and overuse of antibiotics [74–76]. Our study proposed the combined use of antibiotics and COX-2 inhibitor drug celecoxib (CLX) as a solution to reduce antibiotic use and enhance symptomatic treatment of inflammation and pain experienced during UTI. For this purpose, sustained release of CLX loaded PLGA nanoparticles was needed to reduce the need of frequent dosing. In addition, prolonged retention time in the bladder was essential, therefore mucoadhesive coating was added to the nanoparticles, as discussed in **Chapter 4**.

In **Chapter 5**, Design of Experiments (DoE) was used in order to obtain CLX loaded PLGA nanoparticles with small particle size and narrow size distribution, but high drug loading. CLX loaded PLGA nanoparticles were obtained by using two methods: nanoprecipitation (NPPT) and single emulsion – solvent evaporation (SE). The aim of this study was to compare how the

same parameters in both of those methods affect the physicochemical characteristics of CLX loaded PLGA nanoparticles. The selected parameters and outcomes of the screening DoE analysis are presented in **Figure 6.1**. Overall, smaller nanoparticles, with a narrow size distribution, were achieved by NPPT method, while higher drug loading was achieved in nanoparticles obtained through SE method.

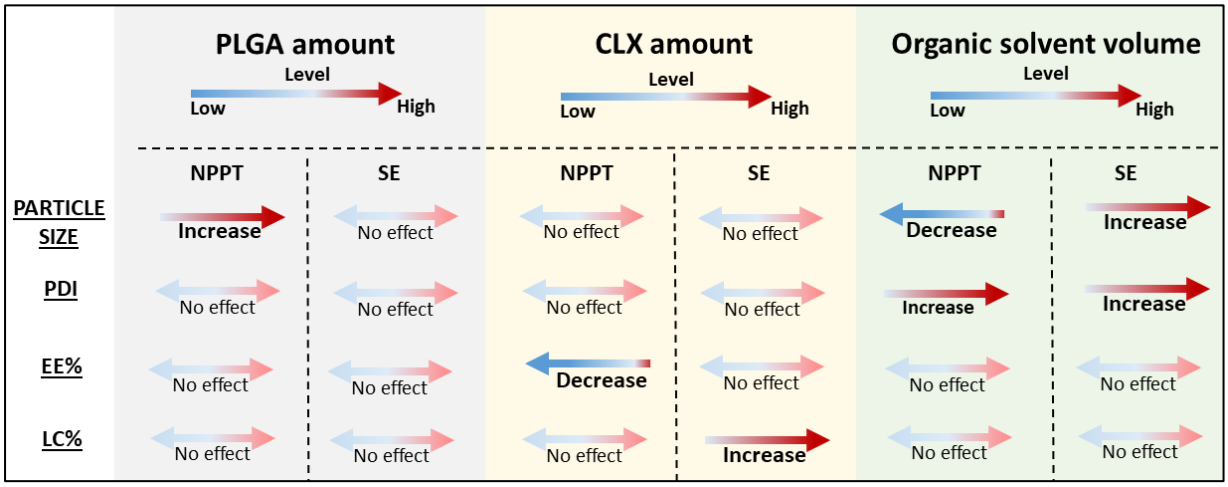


**Figure 6.1:** A summary illustration of DoE study outcomes: the significant impact on responses (on the left) observed after increase of the levels of critical factors (presented at the top). Responses of each critical factor are split between nanoparticles prepared by nanoprecipitation (NPPT) or single emulsion – solvent evaporation (SE) methods. PDI = polydispersity index, EE% = encapsulation efficiency, LC% = loading capacity.

Obtained formulations were then coated with different types of chitosan of varying concentrations, as optimised in **Chapter 4**, with final formulations demonstrating positive zeta potential of 14.3 ± 2 mV of nanoparticles prepared by SE method, and 32.9 ± 2 mV of nanoparticles synthesised by NPPT method. Based on the results obtained by *in vitro* and *ex vivo* mucoadhesion assays in **Chapter 4**, it is likely that nanoparticles synthesised by NPPT method would show stronger mucoadhesive interaction with bladder mucin layer due to two-fold higher zeta potential values, compared to nanoparticles prepared by SE method. Further characterisation by attenuated total reflectance – Fourier transform infra-red spectroscopy (ATR-FTIR) and powder X-ray diffraction (PXRD) indicated no particle adsorption on the particle surface, suggesting that CLX was successfully entrapped inside the PLGA nanoparticles.

*In vitro* drug release profiles of chitosan coated and non-coated nanoparticles obtained by different nanoparticle preparation methods were investigated. Results demonstrated that chitosan coating did not significantly affect the drug release rates. CLX loaded nanoparticles obtained through NPPT method demonstrated faster burst release of the drug, with over 60% of the drug released within 8 hours. In contrast, CLX loaded PLGA nanoparticles synthesised by SE method showed much slower release in the first 8 hours, with around 45% of the drug released. These results were likely to be the outcomes of certain parameters used within each method for synthesis of CLX loaded nanoparticles, such as surfactant type, surfactant concentration, and solvent type. Nevertheless, formulations obtained by both NPPT and SE methods demonstrated some desirable physicochemical properties or expected therapeutic behaviour, which demonstrate promising nanoparticle system for IDD to the bladder.

## 6.2. Future outlook

The work of this project aimed to develop an IDD therapy, facilitated with nanotechnology and dual pharmaceutical agent therapy for treatment and prophylaxis of UTIs. While IDD is currently used as off-label treatment for acute and complicated UTI cases [86], this route of drug administration to treat bladder disorders shows great potential. With progress of recent studies and this project in development of nanomedical therapies, improved medical devices for intra-bladder drug delivery are essential in order to safely and effectively deliver novel therapies. In addition to this, regulatory process of nanomedicine development, clinical testing and market approval needs to be re-evaluated and standardised. Currently many novel nanomedicine products demonstrate unexpected high toxicity profiles when tested in *in vivo* due to diversity of nanoparticle compositions, characteristics, surface coatings, and interactions with biological systems [172,174]. Despite these limitations, this study showed a proposed treatment of GEN and CLX loaded nanoparticle systems, exhibiting mucoadhesive properties for prolonged retention time on the bladder surface. However, the efficacy and compatibility of dual treatment has not yet been demonstrated *in vivo*. In addition, this study could benefit from some additional experiments to explore some areas of the study in even more detail. Thus, following experiments could provide further insight or offer novel ideas that can be investigated as next steps for this project.

The conducted studies in this project demonstrated that hydrophilic antibiotic complexation into a HIP complex can enhance hydrophobicity of the drug, which in turn can lead to sustained

drug release in aqueous media, as well as enhanced antimicrobial activity. However, some limitations were identified for HIP complex loading into PLGA nanoparticles as *in vitro* drug release assays showed only 10% of the drug being released after 6 months. Therefore, additional testing is needed to confirm that GEN:HIP complex is entrapped into the polymeric nanoparticles. This could include some improvements on the nanoparticle synthesis methods, to ensure that GEN:HIP complex precipitation due to hydrophobicity does not limit its encapsulation into PLGA during the nanoparticle preparation process.

Additionally, other nanocarrier systems might need to be evaluated for GEN:HIP complex delivery to the bladder. One of the biggest limitations of GEN entrapment into PLGA nanoparticles was the drug extraction from the nanoparticles in order to quantify the amount of GEN that was successfully encapsulated into the nanoparticles. The solvents used for extracting the drug from PLGA nanoparticles are not compatible with GEN solubility, meaning that fully dissolved system of both PLGA and GEN was not possible to achieve. This, therefore, resulted in use of indirect GEN quantification method, which does not provide insight into the actual quantity of GEN entrapped inside the nanoparticles. To ensure that GEN in quantified using direct method and therefore the amount of GEN entrapped into nanoparticles can be quantified, other materials might need to be used to encapsulate GEN into nano-sized delivery vehicles, as well as easily extract the drug out of them. As a drug delivery solution, we propose the use of lipid nanoparticles, or alternatively, mucoadhesive in-situ forming gels, that are discussed in later in this section, as well as in **Chapter 4**.

Chitosan and C-CS coatings optimised for mucoadhesive nanoparticle formulations in **Chapter 4** are among the promising findings of this study, however a few recent publications have demonstrated that the data obtained for this study could be used to further improve the drug delivery directly to bladder. Mucoadhesive in-situ forming hydrogels have been demonstrated to improve particle retention on the bladder lining, prolong sustained release, and showed no interference with the physiological function of bladder, nor any toxicity evidence [234–237]. Use of the in-situ mucoadhesive hydrogels to deliver obtained nanoparticle systems would negate the need for smaller particles, *in vitro* drug release profiles would likely demonstrate even more prolonged drug release than reported in **Chapters 3** and **5**, and finally, higher concentrations of chitosan could be used to enhance the mucoadhesive properties of the hydrogels without affecting physicochemical characteristics of the nanoparticles.

While obtained DoE study in **Chapter 5** provided a great insight into how the same parameters of different nanoparticle preparation methods affected the physicochemical characteristics of CLX loaded PLGA nanoparticles, additional DoE study could provide improvement on predicting dependent variables of the final formulations. After identifying significant variables in nanoparticles obtained by both NPPT and SE methods by screening DoE design, Response Surface Methodology (RSM) can be used to then point out the most critical levels of selected significant factors [390]. Results in **Chapter 5** demonstrated that predictions obtained by screening design have not been very accurate in predicting the experimental outcomes of final formulations. Therefore, by using RSM, non-significant variables would not be included in the design matrix, along with more levels chosen for the study [390]. Hence, use of RSM, such as Box-Behnken Design, could provide more precise models for this study, which could then be used to make accurate predictions of the parameters needed to achieve nanoparticles that have high EE% and loading capacity (LC%) values, small particle size, and narrow size distribution.

Finally, *in vivo* studies of obtained formulations would be beneficial to confirm that chitosan coated PLGA nanoparticles demonstrate short term toxicity and cell desquamation, followed by fast umbrella cell regeneration, therefore causing no long-term toxicity. Additionally, the dual treatment of antibiotic and COX-2 inhibitor drug, instilled intravesically could be assessed in treating UTIs in a mice or rat animal models, to ensure dual treatment efficacy, superiority compared to the antibiotic treatment, as well as safe toxicology profiles.

# References

[1] A. Mangera, N.I. Osman, C.R. Chapple. Anatomy of the lower urinary tract. *Surgery (United Kingdom)*. **31**, (2013), 319–325. https://doi.org/10.1016/j.mpsur.2013.04.013.

[2] M. Sarfraz, S. Qamar, M.U. Rehman, M.A. Tahir, M. Ijaz, A. Ahsan, M.H. Asim, I. Nazir. Nano-Formulation Based Intravesical Drug Delivery Systems: An Overview of Versatile Approaches to Improve Urinary Bladder Diseases. *Pharmaceutics*. **14**, (2022). https://doi.org/10.3390/pharmaceutics14091909.

[3] B.P. Livingston. Anatomy and neural control of the lower urinary tract and pelvic floor. *Top Geriatr Rehabil*. **32**, (2016), 280–294. https://doi.org/10.1097/TGR.0000000000000123.

[4] A.R. Jackson, C.B. Ching, K.M. McHugh, B. Becknell. Roles for urothelium in normal and aberrant urinary tract development. *Nat Rev Urol*. **17**, (2020), 459–468. https://doi.org/10.1038/s41585-020-0348-2.

[5] K.E. Andersson, K.D. McCloskey. Lamina propria: The functional center of the bladder? *Neurourol Urodyn*. **33**, (2014), 9–16. https://doi.org/10.1002/nau.22465.

[6] C. Tanabalan, A. Ballaro. The physiology and pharmacology of the lower urinary tract. *Surgery (Oxford)*. **37**, (2019), 365–371.

[7] D.A.W. Janssen, J.A. Schalken, J.P.F.A. Heesakkers. Urothelium update: how the bladder mucosa measures bladder filling. *Acta Physiologica*. **220**, (2017), 201–217. https://doi.org/10.1111/apha.12824.

[8] C.H. Fry, B. Vahabi. The Role of the Mucosa in Normal and Abnormal Bladder Function. *Basic Clin Pharmacol Toxicol*. **119**, (2016), 57–62. https://doi.org/10.1111/bcpt.12626.

[9] S. GuhaSarkar, R. Banerjee. Intravesical drug delivery: Challenges, current status, opportunities and novel strategies. *Journal of Controlled Release*. **148**, (2010), 147–157.

[10] M.G. Dalghi, N. Montalbetti, M.D. Carattino, G. Apodaca. The urothelium: Life in a liquid environment. *Physiol Rev*. **100**, (2020), 1621–1705. https://doi.org/10.1152/physrev.00041.2019.

[11] K.O. Tamadonfar, N.S. Omattage, C.N. Spaulding, S.J. Hultgren. Reaching the End of the Line: Urinary Tract Infections. *Microbiol Spectr*. **7**, (2019).

[12] J. Lojk, V.B. Bregar, K. Strojan, S. Hudoklin, P. Veranič, M. Pavlin, M.E. Kreft. Increased endocytosis of magnetic nanoparticles into cancerous urothelial cells versus normal urothelial cells. *Histochem Cell Biol*. **149**, (2018), 45–59. https://doi.org/10.1007/s00418-017-1605-1.

[13] E. Kamhi, E.J. Joo, J.S. Dordick, R.J. Linhardt. Glycosaminoglycans in infectious disease. *Biological Reviews*. **88**, (2013), 928–943. https://doi.org/10.1111/brv.12034.

[14] L.A. Birder. Urinary bladder, cystitis and nerve/urothelial interactions. *Autonomic Neuroscience*. **182**, (2014), 89–94. https://doi.org/10.1016/j.autneu.2013.12.005.

[15] A. Gomelsky, R.R. Dmochowski. GAG Layer Replenishment Therapy for Recurrent Infectious Bladder Dysfunction. *Curr Bladder Dysfunct Rep*. **7**, (2012), 113–119.

[16] C.H. Klingler. Glycosaminoglycans: how much do we know about their role in the bladder? *Urologia*. **83**, (2016), 11–14. https://doi.org/10.5301/uro.5000184.

[17] R. Damiano, G. Quarto, I. Bava, G. Ucciero, R. De Domenico, M.I. Palumbo, R. Autorino. Prevention of recurrent urinary tract infections by intravesical administration of hyaluronic acid and chondroitin sulphate: A placebo-controlled randomised trial. *Eur Urol*. **59**, (2011), 645–651. https://doi.org/10.1016/j.eururo.2010.12.039.

[18] A. Cicione, F. Cantiello, G. Ucciero, A. Salonia, I. Madeo, I. Bava, A. Aliberti, R. Damiano. Restoring the glycosaminoglycans layer in recurrent cystitis: Experimental and clinical foundations. *International Journal of Urology*. **21**, (2014), 763–768. https://doi.org/10.1111/iju.12430.

[19] L.A. Birder. More than just a barrier: Urothelium as a drug target for urinary bladder pain. *Am J Physiol Renal Physiol*. **289**, (2005), 489–495. https://doi.org/10.1152/ajprenal.00467.2004.

[20] I. Grabnar, M. Bogataj, A. Mrhar. Influence of chitosan and polycarbophil on permeation of a model hydrophilic drug into the urinary bladder wall. *Int J Pharm*. **256**, (2003), 167–173. https://doi.org/10.1016/S0378-5173(03)00074-7.

[21] P. Tyagi, S. Tyagi, L. Stewart, S. Glickman. SWOT and Root Cause Analyses of Antimicrobial Resistance to Oral Antimicrobial Treatment of Cystitis. *Antibiotics*. **12**, (2024). https://doi.org/10.3390/antibiotics13040328.

[22] M.S. Kumar, A.P. Das. Emerging nanotechnology based strategies for diagnosis and therapeutics of urinary tract infections: A review. *Adv Colloid Interface Sci*. **249**, (2017), 53–65. https://doi.org/10.1016/j.cis.2017.06.010.

[23] New awareness campaign to help reduce hospital admissions for urinary tract infections. (2023). https://www.england.nhs.uk/2023/10/new-awareness-campaign-to-help-reduce-hospital-admissions-for-urinary-tract-infections/ (accessed May 28, 2024).

[24] C.C. Butler, M.K.D. Hawking, A. Quigley, C.A.M. McNulty. Incidence, severity, help seeking, and management of uncomplicated urinary tract infection: A population-based

survey. *British Journal of General Practice*. **65**, (2015), e702–e707. https://doi.org/10.3399/bjgp15X686965.

[25] L.K. McLellan, D.A. Hunstad. Urinary Tract Infection: Pathogenesis and Outlook. *Trends Mol Med*. **22**, (2016), 946–957. https://doi.org/10.1016/j.molmed.2016.09.003.

[26] R. Mann, D.G. Mediati, I.G. Duggin, E.J. Harry, A.L. Bottomley. Metabolic adaptations of Uropathogenic E. coli in the urinary tract. *Front Cell Infect Microbiol*. **7**, (2017). https://doi.org/10.3389/fcimb.2017.00241.

[27] M.R. Asadi Karam, M. Habibi, S. Bouzari. Urinary tract infection: Pathogenicity, antibiotic resistance and development of effective vaccines against Uropathogenic Escherichia coli. *Mol Immunol*. **108**, (2019), 56–67. https://doi.org/10.1016/j.molimm.2019.02.007.

[28] A.L. Flores-Mireles, J.N. Walker, M. Caparon, S.J. Hultgren. Urinary tract infections: epidemiology, mechanisms of infection and treatment options. *Nat Rev Microbiol*. **13**, (2015), 269–284. https://doi.org/10.1038/nrmicro3432.

[29] M.E. Terlizzi, G. Gribaudo, M.E. Maffei. UroPathogenic Escherichia coli (UPEC) infections: Virulence factors, bladder responses, antibiotic, and non-antibiotic antimicrobial strategies. *Front Microbiol*. **8**, (2017). https://doi.org/10.3389/fmicb.2017.01566.

[30] M. Glover, C.G. Moreira, V. Sperandio, P. Zimmern. Recurrent urinary tract infections in healthy and nonpregnant women. *Urol Sci*. **25**, (2014), 1–8. https://doi.org/10.1016/j.urols.2013.11.007.

[31] M.G. Blango, E.M. Ott, A. Erman, P. Veranic, M.A. Mulvey. Forced Resurgence and Targeting of Intracellular Uropathogenic Escherichia coli Reservoirs. *PLoS One*. **9**, (2014), e93327. https://doi.org/10.1371/journal.pone.0093327.

[32] C. Spaulding, S. Hultgren. Adhesive Pili in UTI Pathogenesis and Drug Development. *Pathogens*. **30**, (2016). https://doi.org/10.3390/pathogens5010030.

[33] A.R. Eberly, K.A. Floyd, C.J. Beebout, S.J. Colling, M.J. Fitzgerald, C.W. Stratton, J.E. Schmitz, M. Hadjifrangiskou. Biofilm formation by uropathogenic escherichia coli is favored under oxygen conditions that mimic the bladder environment. *Int J Mol Sci*. **18**, (2017). https://doi.org/10.3390/ijms18102077.

[34] K.J. Wright, P.C. Seed, S.J. Hultgren. Uropathogenic Escherichia coli flagella aid in efficient urinary tract colonization. *Infect Immun*. **73**, (2005), 7657–7668. https://doi.org/10.1128/IAI.73.11.7657-7668.2005.

[35] G.G. Anderson, C.C. Goller, S. Justice, S.J. Hultgren, P.C. Seed. Polysaccharide capsule and sialic acid-mediated regulation promote biofilm-like intracellular bacterial communities during cystitis. *Infect Immun*. **78**, (2010), 963–975. https://doi.org/10.1128/IAI.00925-09.

[36] H.C. Flemming, J. Wingender. The biofilm matrix. *Nat Rev Microbiol*. **8**, (2010), 623–633. https://doi.org/10.1038/nrmicro2415.

[37] C. Delcaru, I. Alexandru, P. Podgoreanu, M. Grosu, E. Stavropoulos, M.C. Chifiriuc, V. Lazar. Microbial biofilms in urinary tract infections and prostatitis: Etiology, pathogenicity, and combating strategies. *Pathogens*. **5**, (2016). https://doi.org/10.3390/pathogens5040065.

[38] V. Smelov. Improved Classification of Urinary Tract Infection: Future Considerations. *European Urology Supplements*. **15**, (2016), 71–80.

[39] S. Lodhia, A. Sharaf, C. Foley. Management of recurrent urinary tract infections in adults. *Surgery (Oxford)*. **38**, (2020), 197–203. https://doi.org/10.1016/j.mpsur.2020.01.012.

[40] B. Foxman. Urinary Tract Infection Syndromes. *Infect Dis Clin North Am*. **28**, (2014), 1–13. https://doi.org/10.1016/j.idc.2013.09.003.

[41] A. Gomila, J. Carratalà, N. Eliakim-Raz, E. Shaw, I. Wiegand, L. Vallejo-Torres, A. Gorostiza, J.M. Vigo, S. Morris, M. Stoddart, S. Grier, C. Vank, N. Cuperus, L. Van den Heuvel, C. Vuong, A. Macgowan, L. Leibovici, I. Addy, M. Pujol. Risk factors and prognosis of complicated urinary tract infections caused by pseudomonas aeruginosa in hospitalized patients: A retrospective multicenter cohort study. *Infect Drug Resist*. **11**, (2018), 2571–2581. https://doi.org/10.2147/IDR.S185753.

[42] M. Negus, C. Phillips, R. Hindley. Recurrent urinary tract infections: a critical review of the currently available treatment options. *The Obstetrician & Gynaecologist*. **22**, (2020), 115–121. https://doi.org/10.1111/tog.12644.

[43] O. Storme, J.T. Saucedo, A. Garcia-Mora, M. Dehesa-Dávila, K.G. Naber. Risk factors and predisposing conditions for urinary tract infection. *Ther Adv Urol*. **11**, (2019), 19–28. https://doi.org/10.1177/1756287218814382.

[44] H. Alghoraibi, A. Asidan, R. Aljawaied, R. Almukhayzim, A. Alsaydan, E. Alamer, W. Baharoon, E. Masuadi, A. Al Shukairi, L. Layqah, S. Baharoon. Recurrent Urinary Tract Infection in Adult Patients, Risk Factors, and Efficacy of Low Dose Prophylactic Antibiotics Therapy. *J Epidemiol Glob Health*. **13**, (2023), 200–211. https://doi.org/10.1007/s44197-023-00105-4.

[45] M. Renko, J. Salo, M. Ekstrand, T. Pokka, O. Pieviläinen, M. Uhari, T. Tapiainen. Meta-analysis of the Risk Factors for Urinary Tract Infection in Children. *Pediatric Infectious Disease Journal*. **41**, (2022), 787–792. https://doi.org/10.1097/INF.0000000000003628.

[46] L. Kou, J. Sun, Y. Zhai, Z. He. The endocytosis and intracellular fate of nanomedicines: Implication for rational design. *Asian J Pharm Sci*. **8**, (2013), 1–10. https://doi.org/10.1016/j.ajps.2013.07.001.

[47] S. Von Vietinghoff, O. Shevchuk, U. Dobrindt, D.R. Engel, S.K. Jorch, C. Kurts, T. Miethke, F. Wagenlehner. The global burden of antimicrobial resistance – urinary tract infections. *Nephrology Dialysis Transplantation*. **39**, (2024), 581–588. https://doi.org/10.1093/ndt/gfad233.

[48] K.W.K. Tang, B.C. Millar, J.E. Moore. Antimicrobial Resistance (AMR). *Br J Biomed Sci*. **80**, (2023). https://doi.org/10.3389/bjbs.2023.11387.

[49] L.S.J. Roope, R.D. Smith, K.B. Pouwels, J. Buchanan, L. Abel, P. Eibich, C.C. Butler, P.S. Tan, A.S. Walker, J. V Robotham, S. Wordsworth. The challenge of antimicrobial resistance: What economics can contribute. *Science (1979)*. **364**, (2019), eaau4679. https://doi.org/10.1126/science.aau4679.

[50] P. Collignon, J.J. Beggs, T.R. Walsh, S. Gandra, R. Laxminarayan. Anthropological and socioeconomic factors contributing to global antimicrobial resistance: a univariate and multivariable analysis. *Lancet Planet Health*. **2**, (2018), e398–e405. https://doi.org/10.1016/S2542-5196(18)30186-4.

[51] M. Mohsenzadeh, S.-H. Abtahi-Eivary, A. Pirouzi, A. Khaledi, M. Rahimi. A systematic review and meta-analysis of urinary tract infection, frequency of IS elements and MDR isolates retrieved from adult patients. *Gene Rep*. **20**, (2020), 100707. https://doi.org/10.1016/j.genrep.2020.100707.

[52] A. Sorlozano, A. Jimenez-Pacheco, J. De Dios Luna Del Castillo, A. Sampedro, A. Martinez-Brocal, C. Miranda-Casas, J.M. Navarro-Marí, J. Gutiérrez-Fernández. Evolution of the resistance to antibiotics of bacteria involved in urinary tract infections: A 7-year surveillance study. *Am J Infect Control*. **42**, (2014), 1033–1038. https://doi.org/10.1016/j.ajic.2014.06.013.

[53] B. Yang, S. Foley, P. Toozs-Hobson. Urinary Tract Infections: Current and New Preventative Options. *SM Journal of Clinical Medicine*. **2**, (2016), 1018–1024.

[54] K. Claussen, E. Stocks, D. Bhat, J. Fish, C.D. Rubin. How Common Are Pulmonary and Hepatic Adverse Effects in Older Adults Prescribed Nitrofurantoin? *J Am Geriatr Soc*. **65**, (2017), 1316–1320. https://doi.org/10.1111/jgs.14796.

[55] A. Huttner, E.M. Verhaegh, S. Harbarth, A.E. Muller, U. Theuretzbacher, J.W. Mouton. Nitrofurantoin revisited: A systematic review and meta-analysis of controlled trials. *Journal of Antimicrobial Chemotherapy*. **70**, (2015), 2456–2464. https://doi.org/10.1093/jac/dkv147.

[56] A.M. Butler, M.J. Durkin, M.R. Keller, Y. Ma, W.G. Powderly, M.A. Olsen. Association of Adverse Events With Antibiotic Treatment for Urinary Tract Infection. *Clinical Infectious Diseases*. **74**, (2022), 1408–1418. https://doi.org/10.1093/cid/ciab637.

[57] E. Crellin, K.E. Mansfield, C. Leyrat, D. Nitsch, I.J. Douglas, A. Root, E. Williamson, L. Smeeth, L.A. Tomlinson. Trimethoprim use for urinary tract infection and risk of adverse outcomes in older patients: Cohort study. *BMJ (Online)*. **360**, (2018). https://doi.org/10.1136/bmj.k341.

[58] K.T. Elvers, V.J. Wilson, A. Hammond, L. Duncan, A.L. Huntley, A.D. Hay, E.T. van der Werf. Antibiotic-induced changes in the human gut microbiota for the most commonly prescribed antibiotics in primary care in the UK: a systematic review. *BMJ Open*. **10**, (2020), e035677. https://doi.org/10.1136/bmjopen-2019-035677.

[59] M.J. Blaser. Antibiotic use and its consequences for the normal microbiome. *Science (1979)*. **352**, (2016), 544–545. https://doi.org/10.1126/science.aad9358.

[60] M.M. Zacchè, I. Giarenis. Therapies in early development for the treatment of urinary tract inflammation. *Expert Opin Investig Drugs*. **25**, (2016), 531–540. https://doi.org/10.1517/13543784.2016.1161024.

[61] H. Wang, B.N. Palasik. Combating antimicrobial resistance with cefiderocol for complicated infections involving the urinary tract. *Ther Adv Urol*. **14**, (2022). https://doi.org/10.1177/17562872211065570.

[62] L.M. Avery, D.P. Nicolau. Investigational drugs for the treatment of infections caused by multidrug-resistant Gram-negative bacteria. *Expert Opin Investig Drugs*. **27**, (2018), 325–338. https://doi.org/10.1080/13543784.2018.1460354.

[63] S.S. Jean, I.M. Gould, W. Sen Lee, P.R. Hsueh. New Drugs for Multidrug-Resistant Gram-Negative Organisms: Time for Stewardship. *Drugs*. **79**, (2019), 705–714. https://doi.org/10.1007/s40265-019-01112-1.

[64] R. Bartoletti, T. Cai, G. Perletti, F. Me Wagenlehner, T.E. Bjerklund Johansen. Finafloxacin for the treatment of urinary tract infections. *Expert Opin Investig Drugs*. **24**, (2015), 957–963. https://doi.org/10.1517/13543784.2015.1052401.

[65] F. Wagenlehner, M. Nowicki, C. Bentley, M. Lückermann, S. Wohlert, C. Fischer, A. Vente, K. Naber, A. Dalhoff. Explorative Randomized Phase II Clinical Study of the

Efficacy and Safety of Finafloxacin versus Ciprofloxacin for Treatment of Complicated Urinary Tract Infections. *Antimicrob Agents Chemother*. **62**, (2018). https://doi.org/10.1128/AAC.02325-17.

[66] P. Loubet, J. Ranfaing, A. Dinh, C. Dunyach-Remy, L. Bernard, F. Bruyère, J.P. Lavigne, A. Sotto. Alternative Therapeutic Options to Antibiotics for the Treatment of Urinary Tract Infections. *Front Microbiol*. **11**, (2020), 1–18. https://doi.org/10.3389/fmicb.2020.01509.

[67] J. Curtis Nickel, S. Foley, B. Yang, M. Casanovas, R. Caballero, C.M. Diez-Rivero, M.F. Lorenzo-Gómez. Reducing Recurrent Urinary Tract Infections in Women with MV140 Impacts Personal Burden of Disease: Secondary Analyses of a Randomized Placebo-controlled Efficacy Study. *Eur Urol Open Sci*. **63**, (2024), 96–103. https://doi.org/10.1016/j.euros.2024.03.010.

[68] N. Aziminia, M. Hadjipavlou, Y. Philippou, S.S. Pandian, S. Malde, M.Y. Hammadeh. Vaccines for the prevention of recurrent urinary tract infections: a systematic review. *BJU Int*. **123**, (2019), 753–768. https://doi.org/10.1111/bju.14606.

[69] M.E. Falagas, G.I. Betsi, T. Tokas, S. Athanasiou. Probiotics for Prevention of Recurrent Urinary Tract Infections in Women A Review of the Evidence from Microbiological and Clinical Studies. *Drugs*. **66**, (2006), 1253–1261.

[70] V. Gupta, P. Mastromarino, R. Garg. Effectiveness of Prophylactic Oral and/or Vaginal Probiotic Supplementation in the Prevention of Recurrent Urinary Tract Infections: A Randomized, Double-Blind, Placebo-Controlled Trial. *Clinical Infectious Diseases*. **78**, (2024), 1154–1161. https://doi.org/10.1093/cid/ciad766.

[71] S. Mohanty, C. Lindelauf, J.K. White, A. Scheffschick, E. Ehrenborg, I. Demirel, H. Brauner, A. Brauner. Inhibition of COX-2 signaling favors E. coli during urinary tract infection. *Journal of Inflammation (United Kingdom)*. **20**, (2023). https://doi.org/10.1186/s12950-023-00356-9.

[72] N.-A. Mohsin, M. Irfan. Selective cyclooxygenase-2 inhibitors: A review of recent chemical scaffolds with promising anti-inflammatory and COX-2 inhibitory activities. *Medicinal Chemistry Research*. **29**, (2020), 809–830. https://doi.org/10.1007/s00044-020-02528-1.

[73] M. Arora, S. Choudhary, P.K. Singh, B. Sapra, O. Silakari. Structural investigation on the selective COX-2 inhibitors mediated cardiotoxicity: A review. *Life Sci*. **251**, (2020). https://doi.org/10.1016/j.lfs.2020.117631.

[74] J. Bleidorn, I. Gágyor, M.M. Kochen, K. Wegscheider, E. Hummers-Pradier. Symptomatic treatment (ibuprofen) or antibiotics (ciprofloxacin) for uncomplicated urinary tract infection? - Results of a randomized controlled pilot trial. *BMC Med*. **8**, (2010). https://doi.org/10.1186/1741-7015-8-30.

[75] I. Gágyor, J. Bleidorn, M.M. Kochen, G. Schmiemann, K. Wegscheider, E. Hummers-Pradier. Ibuprofen versus fosfomycin for uncomplicated urinary tract infection in women: Randomised controlled trial. *BMJ (Online)*. **351**, (2015). https://doi.org/10.1136/bmj.h6544.

[76] T.J. Hannan, P.L. Roberts, T.E. Riehl, S. van der Post, J.M. Binkley, D.J. Schwartz, H. Miyoshi, M. Mack, R.A. Schwendener, T.M. Hooton, T.S. Stappenbeck, G.C. Hansson, W.F. Stenson, M. Colonna, A.E. Stapleton, S.J. Hultgren. Inhibition of cyclooxygenase-2 prevents chronic and recurrent cystitis. *EBioMedicine*. **1**, (2014), 46–57. https://doi.org/10.1016/j.ebiom.2014.10.011.

[77] A.M. Kalle, A. Rizvi. Inhibition of bacterial multidrug resistance by celecoxib, a cyclooxygenase-2 inhibitor. *Antimicrob Agents Chemother*. **55**, (2011), 439–442. https://doi.org/10.1128/AAC.00735-10.

[78] M.P. Bilsen, J.I.M. van Uhm, J.E. Stalenhoef, C. van Nieuwkoop, R.H.H. Groenwold, L.G. Visser, M.M.C. Lambregts. Intravesical aminoglycoside instillations as prophylaxis for recurrent urinary tract infection: patient satisfaction, long-term safety and efficacy. *JAC Antimicrob Resist*. **5**, (2023). https://doi.org/10.1093/jacamr/dlad040.

[79] E. Andretta, R. Longo, M. Balladelli, C. Sgarabotto, D. Sgarabotto. Intravesical Gentamicin: An Option for Therapy and Prophylaxis against Recurrent UTIs and Resistant Bacteria in Neurogenic Bladder Patients on Intermittent Catheterization. *Antibiotics*. **11**, (2022). https://doi.org/10.3390/antibiotics11101335.

[80] M. Mouhssine, D. Al Ani, A. Al Shibli, G. Ghatasheh, A. Al Amri, H. Matta, R. Chedid, H. Narchi. Intravesical gentamicin instillation in the prevention of recurrent urinary tract infections in children with neurogenic bladder- a single-center retrospective observational study. *J Pediatr Urol*. **19**, (2023), 64.e1-64.e7. https://doi.org/10.1016/j.jpurol.2022.09.001.

[81] L. Cox, C. He, J. Bevins, J.Q. Clemens, J.T. Stoffel, A.P. Cameron. Gentamicin bladder instillations decrease symptomatic urinary tract infections in neurogenic bladder patients on intermittent catheterization. *Canadian Urological Association Journal*. **11**, (2017), E350–E354. https://doi.org/10.5489/cuaj.4434.

[82] P. Abrams, H. Hashim, C. Tomson, A. Macgowan, R. Skews, K. Warren. The use of intravesical gentamicin to treat recurrent urinary tract infections in lower urinary tract dysfunction. *Neurourol Urodyn*. **36**, (2017), 2109–2116. https://doi.org/10.1002/nau.23250.

[83] W. Defoor, D. Ferguson, S. Mashni, L. Creelman, D. Reeves, E. Minevich, P. Reddy, C. Sheldon. Safety of Gentamicin Bladder Irrigations in Complex Urological Cases. *Journal of Urology*. **175**, (2006), 1861–1864. https://doi.org/10.1016/S0022-5347(05)00928-6.

[84] M.M. Marei, R. Jackson, D.J.B. Keene. Intravesical gentamicin instillation for the treatment and prevention of urinary tract infections in complex paediatric urology patients: evidence for safety and efficacy. *J Pediatr Urol*. **17**, (2021), 65.e1-65.e11. https://doi.org/10.1016/j.jpurol.2020.08.007.

[85] C. van Nieuwkoop, P.L. den Exter, H.W. Elzevier, J. den Hartigh, J.T. van Dissel. Intravesical gentamicin for recurrent urinary tract infection in patients with intermittent bladder catheterisation. *Int J Antimicrob Agents*. **36**, (2010), 485–490. https://doi.org/10.1016/j.ijantimicag.2010.05.005.

[86] C.J. Morris, J.L. Rohn, S. Glickman, K.J. Mansfield. Effective Treatments of UTI—Is Intravesical Therapy the Future? *Pathogens*. **12**, (2023). https://doi.org/10.3390/pathogens12030417.

[87] A. Kakkar, G. Traverso, O.C. Farokhzad, R. Weissleder, R. Langer. Evolution of macromolecular complexity in drug delivery systems. *Nat Rev Chem*. **1**, (2017), 63. https://doi.org/10.1038/s41570-017-0063.

[88] C. Yu, S. Wang, W.F. Lai, D. Zhang. The Progress of Chitosan-Based Nanoparticles for Intravesical Bladder Cancer Treatment. *Pharmaceutics*. **15**, (2023). https://doi.org/10.3390/pharmaceutics15010211.

[89] R. Singh, J.W. Lillard Jr. Nanoparticle-based targeted drug delivery. *Exp Mol Pathol*. **86**, (2009), 215–223.

[90] D. Bobo, K.J. Robinson, J. Islam, K.J. Thurecht, S.R. Corrie. Nanoparticle-Based Medicines: A Review of FDA-Approved Materials and Clinical Trials to Date. *Pharm Res*. **33**, (2016), 2373–2387. https://doi.org/10.1007/s11095-016-1958-5.

[91] Y. Nakamura, A. Mochida, P.L. Choyke, H. Kobayashi. Nanodrug Delivery: Is the Enhanced Permeability and Retention Effect Sufficient for Curing Cancer? *Bioconjug Chem*. **27**, (2016), 2225–2238. https://doi.org/10.1021/acs.bioconjchem.6b00437.

[92] E. Ojewole, I. Mackraj, P. Naidoo, T. Govender. Exploring the use of novel drug delivery systems for antiretroviral drugs. *European Journal of Pharmaceutics and Biopharmaceutics*. **70**, (2008), 697–710. https://doi.org/10.1016/j.ejpb.2008.06.020.

[93] Z. Li, S. Tan, S. Li, Q. Shen, K. Wang. Cancer drug delivery in the nano era: An overview and perspectives. *Oncol Rep*. **38**, (2017), 611–624. https://doi.org/10.3892/or.2017.5718.

[94] C. Fornaguera, C. Castells-Sala, S. Borrós. Unraveling Polymeric Nanoparticles Cell Uptake Pathways: Two Decades Working to Understand Nanoparticles Journey to Improve Gene Therapy, in: Cell Biology and Translational Medicine, Volume 9, 2020: pp. 117–138. http://www.springer.com/series/15838.

[95] M. Barani, S.M. Hosseinikhah, A. Rahdar, L. Farhoudi, R. Arshad, M. Cucchiarini, S. Pandey. Nanotechnology in bladder cancer: Diagnosis and treatment. *Cancers (Basel)*. **13**, (2021), 1–29. https://doi.org/10.3390/cancers13092214.

[96] S.A.A. Rizvi, A.M. Saleh. Applications of nanoparticle systems in drug delivery technology. *Saudi Pharmaceutical Journal*. **26**, (2018), 64–70. https://doi.org/10.1016/j.jsps.2017.10.012.

[97] S. Onoue, S. Yamada, H.K. Chan. Nanodrugs: Pharmacokinetics and safety. *Int J Nanomedicine*. **9**, (2014), 1025–1037. https://doi.org/10.2147/IJN.S38378.

[98] B. Armendáriz-Barragán, N. Zafar, W. Badri, S.A. Galindo-Rodríguez, D. Kabbaj, H. Fessi, A. Elaissari. Plant extracts: from encapsulation to application. *Expert Opin Drug Deliv*. **13**, (2016), 1165–1175. https://doi.org/10.1080/17425247.2016.1182487.

[99] Z. Edis, J. Wang, M.K. Waqas, M. Ijaz, M. Ijaz. Nanocarriers-mediated drug delivery systems for anticancer agents: An overview and perspectives. *Int J Nanomedicine*. **16**, (2021), 1313–1330. https://doi.org/10.2147/IJN.S289443.

[100] K.M. El-Say, H.S. El-Sawy. Polymeric nanoparticles: Promising platform for drug delivery. *Int J Pharm*. **528**, (2017), 675–691. https://doi.org/10.1016/j.ijpharm.2017.06.052.

[101] J. Ahlawat, G. Henriquez, M. Narayan. Enhancing the Delivery of Chemotherapeutics: Role of Biodegradable Polymeric Nanoparticles. *Molecules*. **23**, (2018), 2157. https://doi.org/10.3390/molecules23092157.

[102] M. Iqbal, N. Zafar, H. Fessi, A. Elaissari. Double emulsion solvent evaporation techniques used for drug encapsulation. *Int J Pharm*. **496**, (2015), 173–190. https://doi.org/10.1016/j.ijpharm.2015.10.057.

[103] J.-M. Lü, X. Wang, C. Marin-Muller, H. Wang, P.H. Lin, Q. Yao, C. Chen. Current advances in research and clinical applications of PLGA-based nanotechnology. *Expert Rev Mol Diagn*. **9**, (2009), 325–341. https://doi.org/10.1586/erm.09.15.

[104] Q. Xu, L.M. Ensign, N.J. Boylan, A. Schön, X. Gong, J.-C. Yang, N.W. Lamb, S. Cai, T. Yu, E. Freire, J. Hanes. Impact of Surface Polyethylene Glycol (PEG) Density on Biodegradable Nanoparticle Transport in Mucus ex Vivo and Distribution in Vivo. *ACS Nano*. **9**, (2015), 9217–9227. https://doi.org/10.1021/acsnano.5b03876.

[105] R.H. Ansary, M.B. Awang, M.M. Rahman. Biodegradable Poly(D,L-lactic-co-glycolic acid)-Based Micro/Nanoparticles for Sustained Release of Protein Drugs - A Review. *Tropical Journal of Pharmaceutical Research*. **13**, (2014), 1179–1190. https://doi.org/10.4314/tjpr.v13i7.24.

[106] A.T.C.R. Silva, B.C.O. Cardoso, M.E.S.R. e Silva, R.F.S. Freitas, R.G. Sousa. Synthesis, Characterization, and Study of PLGA Copolymer in Vitro Degradation. *J Biomater Nanobiotechnol*. **06**, (2015), 8–19. https://doi.org/10.4236/jbnb.2015.61002.

[107] D.N. Kapoor, A. Bhatia, R. Kaur, R. Sharma, G. Kaur, S. Dhawan. PLGA: a unique polymer for drug delivery. *Ther Deliv*. **6**, (2015), 41–58. https://doi.org/10.4155/tde.14.91.

[108] M. Alvi, A. Yaqoob, K. Rehman, S.M. Shoaib, M.S.H. Akash. PLGA-based nanoparticles for the treatment of cancer: current strategies and perspectives. *AAPS Open*. **8**, (2022). https://doi.org/10.1186/s41120-022-00060-7.

[109] Y. Xu, C.S. Kim, D.M. Saylor, D. Koo. Polymer degradation and drug delivery in PLGA-based drug–polymer applications: A review of experiments and theories. *J Biomed Mater Res B Appl Biomater*. **105**, (2017), 1692–1716. https://doi.org/10.1002/jbm.b.33648.

[110] A. Budhian, S.J. Siegel, K.I. Winey. Production of haloperidol-loaded PLGA nanoparticles for extended controlled drug release of haloperidol. *J Microencapsul*. **22**, (2005), 773–785. https://doi.org/10.1080/02652040500273753.

[111] J.U. Menon, S. Kona, A.S. Wadajkar, F. Desai, A. Vadla, K.T. Nguyen. Effects of surfactants on the properties of PLGA nanoparticles. *J Biomed Mater Res A*. **100 A**, (2012), 1998–2005. https://doi.org/10.1002/jbm.a.34040.

[112] H. Cortés, H. Hernández-Parra, S.A. Bernal-Chávez, M.L. Del Prado-Audelo, I.H. Caballero-Florán, F. V. Borbolla-Jiménez, M. González-Torres, J.J. Magaña, G. Leyva-Gómez. Non-ionic surfactants for stabilization of polymeric nanoparticles for biomedical uses. *Materials*. **14**, (2021). https://doi.org/10.3390/ma14123197.

[113] B. Taghipour, M. Yakhchali, I. Haririan, A.M. Tamaddon, S.M. Samani. The effects of technical and compositional variables on the size and release profile of bovine serum albumin from PLGA based particulate systems. *Res Pharm Sci*. **9**, (2014), 407–420.

[114] R. Saadati, S. Dadashzadeh. Marked effects of combined TPGS and PVA emulsifiers in the fabrication of etoposide-loaded PLGA-PEG nanoparticles: In vitro and in vivo evaluation. *Int J Pharm*. **464**, (2014), 135–144. https://doi.org/10.1016/j.ijpharm.2014.01.014.

[115] A. Zielinska, F. Carreiró, A.M. Oliveira, A. Neves, B. Pires, D. Nagasamy Venkatesh, A. Durazzo, M. Lucarini, P. Eder, A.M. Silva, A. Santini, E.B. Souto. Polymeric Nanoparticles: Production, Characterization, Toxicology and Ecotoxicology. *Molecules*. **25**, (2020). https://doi.org/10.3390/molecules25163731.

[116] J.P. Rao, K.E. Geckeler. Polymer nanoparticles: Preparation techniques and size-control parameters. *Prog Polym Sci*. **36**, (2011), 887–913. https://doi.org/https://doi.org/10.1016/j.progpolymsci.2011.01.001.

[117] E. Cohen-Sela, M. Chorny, N. Koroukhov, H.D. Danenberg, G. Golomb. A new double emulsion solvent diffusion technique for encapsulating hydrophilic molecules in PLGA nanoparticles. *Journal of Controlled Release*. **133**, (2009), 90–95. https://doi.org/10.1016/j.jconrel.2008.09.073.

[118] P. Zakeri-Milani, B.D. Loveymi, M. Jelvehgari, H. Valizadeh. The characteristics and improved intestinal permeability of vancomycin PLGA-nanoparticles as colloidal drug delivery system. *Colloids Surf B Biointerfaces*. **103**, (2013), 174–181. https://doi.org/10.1016/j.colsurfb.2012.10.021.

[119] K.Y. Hernández-Giottonini, R.J. Rodríguez-Córdova, C.A. Gutiérrez-Valenzuela, O. Peñuñuri-Miranda, P. Zavala-Rivera, P. Guerrero-Germán, A. Lucero-Acuña. PLGA nanoparticle preparations by emulsification and nanoprecipitation techniques: Effects of formulation parameters. *RSC Adv*. **10**, (2020), 4218–4231. https://doi.org/10.1039/c9ra10857b.

[120] S. Sur, A. Rathore, V. Dave, K.R. Reddy, R.S. Chouhan, V. Sadhu. Recent developments in functionalized polymer nanoparticles for efficient drug delivery system. *Nano-Structures & Nano-Objects*. **20**, (2019), 100397. https://doi.org/10.1016/j.nanoso.2019.100397.

[121] S.M. Abdelghany, D.J. Quinn, R.J. Ingram, B.F. Gilmore, R.F. Donnelly, C.C. Taggart, C.J. Scott. Gentamicin-loaded nanoparticles show improved antimicrobial effects

towards Pseudomonas aeruginosa infection. *Int J Nanomedicine*. **7**, (2012), 4053–4063. https://doi.org/10.2147/IJN.S34341.

[122] S.I. Hamdallah, R. Zoqlam, B. Yang, A. Campbell, R. Booth, J. Booth, P. Belton, S. Qi. Using a systematic and quantitative approach to generate new insights into drug loading of PLGA nanoparticles using nanoprecipitation. *Nanoscale Adv*. (2024). https://doi.org/10.1039/d4na00087k.

[123] C.E. Astete, C.M. Sabliov. Synthesis and characterization of PLGA nanoparticles. *J Biomater Sci Polym Ed*. **17**, (2006), 247–289. https://doi.org/10.1163/156856206775997322.

[124] F. Madani, S.S. Esnaashari, B. Mujokoro, F. Dorkoosh, M. Khosravani, M. Adabi. Investigation of Effective Parameters on Size of Paclitaxel Loaded PLGA Nanoparticles. *Adv Pharm Bull*. **8**, (2018), 77–84. https://doi.org/10.15171/apb.2018.010.

[125] R.M. Mainardes, R.C. Evangelista. PLGA nanoparticles containing praziquantel: Effect of formulation variables on size distribution. *Int J Pharm*. **290**, (2005), 137–144. https://doi.org/10.1016/j.ijpharm.2004.11.027.

[126] S. Galindo-Rodriguez, E. Allé, H. Fessi, E. Doelker. Physicochemical Parameters Associated with Nanoparticle Formation in the Salting-out, Emulsification-Diffusion, and Nanoprecipitation Methods. *Pharm Res*. **21**, (2004), 1428–1439.

[127] Sonam, H. Chaudhary, V. Kumar. Taguchi design for optimization and development of antibacterial drug-loaded PLGA nanoparticles. *Int J Biol Macromol*. **64**, (2014), 99–105. https://doi.org/10.1016/j.ijbiomac.2013.11.032.

[128] O.A.A. Ahmed, S.M. Badr-Eldin. Biodegradable self-assembled nanoparticles of PEG-PLGA amphiphilic diblock copolymer as a promising stealth system for augmented vinpocetine brain delivery. *Int J Pharm*. **588**, (2020). https://doi.org/10.1016/j.ijpharm.2020.119778.

[129] C. Draheim, F. De Crécy, S. Hansen, E.M. Collnot, C.M. Lehr. A design of experiment study of nanoprecipitation and nano spray drying as processes to prepare PLGA nano- and microparticles with defined sizes and size distributions. *Pharm Res*. **32**, (2015), 2609–2624. https://doi.org/10.1007/s11095-015-1647-9.

[130] R. Bisht, I.D. Rupenthal. PLGA nanoparticles for intravitreal peptide delivery: statistical optimization, characterization and toxicity evaluation. *Pharm Dev Technol*. **23**, (2018), 324–333. https://doi.org/10.1080/10837450.2016.1240184.

[131] E. Lagreca, V. Onesto, C. Di Natale, S. La Manna, P.A. Netti, R. Vecchione. Recent advances in the formulation of PLGA microparticles for controlled drug delivery. *Prog Biomater*. **9**, (2020), 153–174. https://doi.org/10.1007/s40204-020-00139-y.

[132] M. Gümüşderelioğlu, G. Deniz. Sustained release of mitomycin-C from poly(DL-lactide)/ poly(DL-lactide-co-glycolide) films. *J Biomater Sci Polym Ed*. **11**, (2000), 1039–1050. https://doi.org/10.1163/156856200743562.

[133] K. Miladi, S. Sfar, H. Fessi, A. Elaissari. Encapsulation of alendronate sodium by nanoprecipitation and double emulsion: From preparation to in vitro studies. *Ind Crops Prod*. **72**, (2015), 24–33. https://doi.org/10.1016/j.indcrop.2015.01.079.

[134] E. dos-Santos-Silva, M.F. Alves-Silva, J.S. de Medeiros, R. dos Santos-Cavalcante, A.M. Cornélio, M.F. Fernandes-Pedrosa, E.S.T. do Egito, R.F. de Araújo-Júnior, A.A. da Silva-Júnior. Colloidal properties of self-assembled cationic hyperbranched-polyethyleneimine covered poly lactide-co-glycolide nanoparticles: Exploring modified release and cell delivery of methotrexate. *J Mol Liq*. **315**, (2020). https://doi.org/10.1016/j.molliq.2020.113721.

[135] H. Van De Ven, C. Paulussen, P.B. Feijens, A. Matheeussen, P. Rombaut, P. Kayaert, G. Van Den Mooter, W. Weyenberg, P. Cos, L. Maes, A. Ludwig. PLGA nanoparticles and nanosuspensions with amphotericin B: Potent in vitro and in vivo alternatives to Fungizone and AmBisome. *Journal of Controlled Release*. **161**, (2012), 795–803. https://doi.org/10.1016/j.jconrel.2012.05.037.

[136] Z.R. Stromberg, M. Lisa Phipps, H.D. Magurudeniya, C.A. Pedersen, T. Rajale, C.J. Sheehan, S.J. Courtney, S.B. Bradfute, P. Hraber, M.N. Rush, J.Z. Kubicek-Sutherland, J.S. Martinez. Formulation of stabilizer-free, nontoxic PLGA and elastin-PLGA nanoparticle delivery systems. *Int J Pharm*. **597**, (2021). https://doi.org/10.1016/j.ijpharm.2021.120340.

[137] S. Prabha, V. Labhasetwar. Critical Determinants in PLGA/PLA Nanoparticle-Mediated Gene Expression. *Pharm Res*. **21**, (2004), 354–365.

[138] H.M. Redhead, S.S. Davis, L. Illum. Drug delivery in poly(lactide-co-glycolide) nanoparticles surface modified with poloxamer 407 and poloxamine 908: in vitro characterisation and in vivo evaluation. *Journal of Controlled Release*. **70**, (2001), 353–363. www.elsevier.com/locate/jconrel.

[139] A. Lamprecht, N. Ubrich, H. Yamamoto, U. Schafer, H. Takeuchi, C.-M. Lehr, P. Maincent, Y. Kawashima. Design of rolipram-loaded nanoparticles: comparison of two

preparation methods. *Journal of Controlled Release*. **71**, (2001), 297–306. www.elsevier.com/locate/jconrel.

[140] F. Ito, H. Fujimori, H. Honnami, H. Kawakami, K. Kanamura, K. Makino. Study of types and mixture ratio of organic solvent used to dissolve polymers for preparation of drug-containing PLGA microspheres. *Eur Polym J*. **45**, (2009), 658–667. https://doi.org/https://doi.org/10.1016/j.eurpolymj.2008.12.037.

[141] A.F. Ribeiro, C.T.G. Ferreira, J.F. dos Santos, L.M. Cabral, V.P. de Sousa. Design of experiments for the development of poly(d,l-lactide-co-glycolide) nanoparticles loaded with Uncaria tomentosa. *Journal of Nanoparticle Research*. **17**, (2015). https://doi.org/10.1007/s11051-015-2883-y.

[142] S.A. Joshi, S.S. Chavhan, K.K. Sawant. Rivastigmine-loaded PLGA and PBCA nanoparticles: Preparation, optimization, characterization, in vitro and pharmacodynamic studies. *European Journal of Pharmaceutics and Biopharmaceutics*. **76**, (2010), 189–199. https://doi.org/10.1016/j.ejpb.2010.07.007.

[143] F. Yang, M.H. Cabe, S.D. Ogle, V. Sanchez, K.A. Langert. Optimization of critical parameters for coating of polymeric nanoparticles with plasma membrane vesicles by sonication. *Sci Rep*. **11**, (2021). https://doi.org/10.1038/s41598-021-03422-5.

[144] E. Ruiz, V.H. Orozco, L.M. Hoyos, L.F. Giraldo. Study of sonication parameters on PLA nanoparticles preparation by simple emulsion-evaporation solvent technique. *Eur Polym J*. **173**, (2022). https://doi.org/10.1016/j.eurpolymj.2022.111307.

[145] D.H. Jo, J.H. Kim, T.G. Lee, J.H. Kim. Size, surface charge, and shape determine therapeutic effects of nanoparticles on brain and retinal diseases. *Nanomedicine*. (2015), 1603–1611.

[146] D. Saha, S. Kumar, D. Ray, J. Mata, V.K. Aswal. Structure and stability of biodegradable polymer nanoparticles in electrolyte solution. *Materials Letters: X*. **10**, (2021). https://doi.org/10.1016/j.mlblux.2021.100066.

[147] B. Shkodra-Pula, C. Grune, A. Traeger, A. Vollrath, S. Schubert, D. Fischer, U.S. Schubert. Effect of surfactant on the size and stability of PLGA nanoparticles encapsulating a protein kinase C inhibitor. *Int J Pharm*. **566**, (2019), 756–764. https://doi.org/10.1016/j.ijpharm.2019.05.072.

[148] R. Seigneuric, L. Markey, D. S.A. Nuyten, C. Dubernet, C. T.A. Evelo, E. Finot, C. Garrido. From Nanotechnology to Nanomedicine: Applications to Cancer Research. *Curr Mol Med*. **10**, (2010), 640–652. https://doi.org/10.2174/156652410792630634.

[149] C. Kinnear, T.L. Moore, L. Rodriguez-Lorenzo, B. Rothen-Rutishauser, A. Petri-Fink. Form Follows Function: Nanoparticle Shape and Its Implications for Nanomedicine. *Chem Rev*. **117**, (2017), 11476–11521. https://doi.org/10.1021/acs.chemrev.7b00194.

[150] P. Decuzzi, B. Godin, T. Tanaka, S.-Y. Lee, C. Chiappini, X. Liu, M. Ferrari. Size and shape effects in the biodistribution of intravascularly injected particles. *Journal of Controlled Release*. **141**, (2010), 320–327. https://doi.org/10.1016/j.jconrel.2009.10.014.

[151] K. Murugan, Y.E. Choonara, P. Kumar, D. Bijukumar, L.C. du Toit, V. Pillay. Parameters and characteristics governing cellular internalization and trans-barrier trafficking nanostructures. *Int J Nanomedicine*. **10**, (2015), 2191–2206. https://doi.org/10.2147/IJN.S75615.

[152] D.M. Moss, M. Siccardi. Optimizing nanomedicine pharmacokinetics using physiologically based pharmacokinetics modelling. *Br J Pharmacol*. **171**, (2014), 3963–3979. https://doi.org/10.1111/bph.2014.171.issue-17.

[153] P.P. Karmali, D. Simberg. Interactions of nanoparticles with plasma proteins: implication on clearance and toxicity of drug delivery systems. *Expert Opin Drug Deliv*. **8**, (2011), 343–357. https://doi.org/10.1517/17425247.2011.554818.

[154] M.M. Zacchè, S. Srikrishna, L. Cardozo. Novel targeted bladder drug-delivery systems: A review. *Res Rep Urol*. **7**, (2015), 169–178. https://doi.org/10.2147/RRU.S56168.

[155] M.T. Oucif Khaled, A. Zaater, I. Ben Amor, S. Zeghoud, A. Ben Amor, H. Hemmami, A. Alnazza Alhamad. Drug delivery methods based on nanotechnology for the treatment of eye diseases. *Annals of Medicine & Surgery*. **85**, (2023), 6029–6040. https://doi.org/10.1097/ms9.0000000000001399.

[156] M.J. Mitchell, M.M. Billingsley, R.M. Haley, M.E. Wechsler, N.A. Peppas, R. Langer. Engineering precision nanoparticles for drug delivery. *Nat Rev Drug Discov*. **20**, (2021), 101–124. https://doi.org/10.1038/s41573-020-0090-8.

[157] A. Kumari, S.K. Yadav, S.C. Yadav. Biodegradable polymeric nanoparticles based drug delivery systems. *Colloids Surf B Biointerfaces*. **75**, (2010), 1–18. https://doi.org/10.1016/j.colsurfb.2009.09.001.

[158] H.I. Chiu, N.A. Samad, L. Fang, V. Lim. Cytotoxicity of targeted PLGA nanoparticles: a systematic review. *RSC Adv*. **11**, (2021), 9433–9449. https://doi.org/10.1039/d1ra00074h.

[159] Y. Cui, Q. Xu, P.K.H. Chow, D. Wang, C.H. Wang. Transferrin-conjugated magnetic silica PLGA nanoparticles loaded with doxorubicin and paclitaxel for brain glioma

treatment. *Biomaterials*. **34**, (2013), 8511–8520. https://doi.org/10.1016/j.biomaterials.2013.07.075.

[160] S. Di-Wen, G.Z. Pan, L. Hao, J. Zhang, Q.Z. Xue, P. Wang, Q.Z. Yuan. Improved antitumor activity of epirubicin-loaded CXCR4-targeted polymeric nanoparticles in liver cancers. *Int J Pharm*. **500**, (2016), 54–61. https://doi.org/10.1016/j.ijpharm.2015.12.066.

[161] A. Yusuf, A.R.Z. Almotairy, H. Henidi, O.Y. Alshehri, M.S. Aldughaim. Nanoparticles as Drug Delivery Systems: A Review of the Implication of Nanoparticles' Physicochemical Properties on Responses in Biological Systems. *Polymers (Basel)*. **15**, (2023). https://doi.org/10.3390/polym15071596.

[162] J. Ai, E. Biazar, M. Jafarpour, M. Montazeri, A. Majdi, S. Aminifard, M. Zafari, H.R. Akbari, H.G. Rad. Nanotoxicology and nanoparticle safety in biomedical designs. *Int J Nanomedicine*. (2011), 1117. https://doi.org/10.2147/IJN.S16603.

[163] N.M. Schaeublin, L.K. Braydich-Stolle, A.M. Schrand, J.M. Miller, J. Hutchison, J.J. Schlager, S.M. Hussain. Surface charge of gold nanoparticles mediates mechanism of toxicity. *Nanoscale*. **3**, (2011), 410–420. https://doi.org/10.1039/c0nr00478b.

[164] S. Jesus, M. Schmutz, C. Som, G. Borchard, P. Wick, O. Borges. Hazard Assessment of Polymeric Nanobiomaterials for Drug Delivery: What Can We Learn From Literature So Far. *Front Bioeng Biotechnol*. **7**, (2019). https://doi.org/10.3389/fbioe.2019.00261.

[165] J.S. Suk, Q. Xu, N. Kim, J. Hanes, L.M. Ensign. PEGylation as a strategy for improving nanoparticle-based drug and gene delivery. *Adv Drug Deliv Rev*. **99**, (2016), 28–51. https://doi.org/10.1016/j.addr.2015.09.012.

[166] Y.-Y. Wang, S.K. Lai, J.S. Suk, A. Pace, R. Cone, J. Hanes. Addressing the PEG Mucoadhesivity Paradox to Engineer Nanoparticles that "Slip" through the Human Mucus Barrier. *Angewandte Chemie International Edition*. **47**, (2008), 9726–9729. https://doi.org/10.1002/anie.200803526.

[167] E. Sánchez-López, M.A. Egea, A. Cano, M. Espina, A.C. Calpena, M. Ettcheto, A. Camins, E.B. Souto, A.M. Silva, M.L. García. PEGylated PLGA nanospheres optimized by design of experiments for ocular administration of dexibuprofen-in vitro, ex vivo and in vivo characterization. *Colloids Surf B Biointerfaces*. **145**, (2016), 241–250. https://doi.org/10.1016/j.colsurfb.2016.04.054.

[168] G. Dumortier, J.L. Grossiord, F. Agnely, J.C. Chaumeil. A review of poloxamer 407 pharmaceutical and pharmacological characteristics. *Pharm Res*. **23**, (2006), 2709–2728. https://doi.org/10.1007/s11095-006-9104-4.

[169] S. Mura, H. Hillaireau, J. Nicolas, B. Le Droumaguet, C. Gueutin, S. Zanna, N. Tsapis, E. Fattal. Influence of surface charge on the potential toxicity of PLGA nanoparticles towards Calu-3 cells. *Int J Nanomedicine*. **6**, (2011), 2591–2605. https://doi.org/10.2147/ijn.s24552.

[170] I. Takeuchi, Y. Kato, K. Makino. Effects of polyvinyl alcohol on drug release from nanocomposite particles using poly (L-lactide-co-glycolide). *J Oleo Sci*. **70**, (2021), 341–348. https://doi.org/10.5650/jos.ess20299.

[171] M. Chatterjee, N. Chanda. Formulation of PLGA nano-carriers: Specialized modification for cancer therapeutic applications. *Mater Adv*. **3**, (2022), 837–858. https://doi.org/10.1039/d1ma00600b.

[172] J.K. Patra, G. Das, L.F. Fraceto, E.V.R. Campos, M.D.P. Rodriguez-Torres, L.S. Acosta-Torres, L.A. Diaz-Torres, R. Grillo, M.K. Swamy, S. Sharma, S. Habtemariam, H.S. Shin. Nano based drug delivery systems: Recent developments and future prospects. *J Nanobiotechnology*. **16**, (2018). https://doi.org/10.1186/s12951-018-0392-8.

[173] K. Park, S. Skidmore, J. Hadar, J. Garner, H. Park, A. Otte, B.K. Soh, G. Yoon, D. Yu, Y. Yun, B.K. Lee, X. Jiang, Y. Wang. Injectable, long-acting PLGA formulations: Analyzing PLGA and understanding microparticle formation. *Journal of Controlled Release*. **304**, (2019), 125–134. https://doi.org/10.1016/j.jconrel.2019.05.003.

[174] V. Sainz, J. Conniot, A.I. Matos, C. Peres, E. Zupančič, L. Moura, L.C. Silva, H.F. Florindo, R.S. Gaspar. Regulatory aspects on nanomedicines. *Biochem Biophys Res Commun*. **468**, (2015), 504–510. https://doi.org/10.1016/j.bbrc.2015.08.023.

[175] E.D. Namiot, A. V. Sokolov, V.N. Chubarev, V. V. Tarasov, H.B. Schiöth. Nanoparticles in Clinical Trials: Analysis of Clinical Trials, FDA Approvals and Use for COVID-19 Vaccines. *Int J Mol Sci*. **24**, (2023). https://doi.org/10.3390/ijms24010787.

[176] H.O. Alsaab, F.D. Alharbi, A.S. Alhibs, N.B. Alanazi, B.Y. Alshehri, M.A. Saleh, F.S. Alshehri, M.A. Algarni, T. Almugaiteeb, M.N. Uddin, R.M. Alzhrani. PLGA-Based Nanomedicine: History of Advancement and Development in Clinical Applications of Multiple Diseases. *Pharmaceutics*. **14**, (2022). https://doi.org/10.3390/pharmaceutics14122728.

[177] H.Y. Yoon, H.M. Yang, C.H. Kim, Y.T. Goo, M.J. Kang, S. Lee, Y.W. Choi. Current status of the development of intravesical drug delivery systems for the treatment of bladder cancer. *Expert Opin Drug Deliv*. **17**, (2020), 1555–1572. https://doi.org/https://doi.org/10.1080/17425247.2020.1810016.

[178] E. Imbuluzqueta, C. Gamazo, H. Lana, M.Á. Campanero, D. Salas, A.G. Gil, E. Elizondo, N. Ventosa, J. Veciana, M.J. Blanco-Prieto. Hydrophobic gentamicin-loaded nanoparticles are effective against Brucella melitensis infection in mice. *Antimicrob Agents Chemother*. **57**, (2013), 3326–3333. https://doi.org/10.1128/AAC.00378-13.

[179] Y.-I. Jeong, H.-S. Na, D.-H. Seo, D.-G. Kim, H.-C. Lee, M.-K. Jang, S.-K. Na, S.-H. Roh, S.-I. Kim, J.-W. Nah. Ciprofloxacin-encapsulated poly(dl-lactide-co-glycolide) nanoparticles and its antibacterial activity. *Int J Pharm*. **352**, (2008), 317–323. https://doi.org/10.1016/j.ijpharm.2007.11.001.

[180] A. Kolate, G. Kore, P. Lesimple, D. Baradia, S. Patil, J.W. Hanrahan, A. Misra. Polymer assisted entrapment of netilmicin in PLGA nanoparticles for sustained antibacterial activity. *J Microencapsul*. **32**, (2015), 61–74. https://doi.org/10.3109/02652048.2014.944951.

[181] S. Taghavi, M. Ramezani, M. Alibolandi, K. Abnous, S.M. Taghdisi. Chitosan-modified PLGA nanoparticles tagged with 5TR1 aptamer for in vivo tumor-targeted drug delivery. *Cancer Lett*. **400**, (2017), 1–8. https://doi.org/10.1016/j.canlet.2017.04.008.

[182] R. Dorati, A. DeTrizio, M. Spalla, R. Migliavacca, L. Pagani, S. Pisani, E. Chiesa, B. Conti, T. Modena, I. Genta. Gentamicin Sulfate PEG-PLGA/PLGA-H nanoparticles: Screening design and antimicrobial effect evaluation toward clinic bacterial isolates. *Nanomaterials*. **8**, (2018). https://doi.org/10.3390/nano8010037.

[183] C. Dubernet, J.P. Benoit, G. Couarraze, D. Duchene. Microencapsulation of nitrofurantoin in poly(r-caprolactone): tableting and in vitro release studies. *Int J Pharm*. **35**, (1987), 12.

[184] J. Liu, S.Y. Chan, P.C. Ho. Polymer-coated microparticles for the sustained release of nitrofurantoin. *Journal of Pharmacy and Pharmacology*. **54**, (2002), 1205–1212. https://doi.org/10.1211/002235702320402044.

[185] W.K. Lau, D. Dharmasena, H. Horsley, N. V Jafari, J. Malone-Lee, E. Stride, M. Edirisinghe, J.L. Rohn. Novel antibiotic-loaded particles conferring eradication of deep tissue bacterial reservoirs for the treatment of chronic urinary tract infection. *Journal of Controlled Release*. **328**, (2020), 490–502. https://doi.org/10.1016/j.jconrel.2020.08.048.

[186] B. Brauner, J. Semmler. Trimethoprim-Loaded PLGA Nanoparticles Grafted with WGA as Potential Intravesical Therapy of Urinary Tract Infections - Studies on Adhesion to SV-HUCs Under Varying Time, pH, and Drug-Loading Conditions. *ACS Omega*. **5**, (2020), 17377–17384.

[187] B. Brauner, P. Schwarz, M. Wirth, F. Gabor. Micro vs. nano: PLGA particles loaded with trimethoprim for instillative treatment of urinary tract infections. *Int J Pharm*. **579**, (2020), 119158. https://doi.org/10.1016/j.ijpharm.2020.119158.

[188] B. Brauner, C. Schuster, M. Wirth, F. Gabor. Trimethoprim-Loaded Microspheres Prepared from Low-Molecular-Weight PLGA as a Potential Drug Delivery System for the Treatment of Urinary Tract Infections. *ACS Omega*. **5**, (2020), 9013–9022. https://doi.org/10.1021/acsomega.0c00981.

[189] K. Skoll, J. Palmetzhofer, M. Lummerstorfer, M. Anzengruber, F. Gabor, M. Wirth. Human serum albumin nanoparticles as a versatile vehicle for targeted delivery of antibiotics to combat bacterial infections. *Nanomedicine*. **50**, (2023). https://doi.org/10.1016/j.nano.2023.102685.

[190] M.M. Fernandes, K. Ivanova, A. Francesko, E. Mendoza, T. Tzanov. Immobilization of antimicrobial core-shell nanospheres onto silicone for prevention of Escherichia coli biofilm formation. *Process Biochemistry*. **59**, (2017), 116–122. https://doi.org/10.1016/j.procbio.2016.09.011.

[191] S. V. Sánchez, N. Navarro, J. Catalán-Figueroa, J.O. Morales. Nanoparticles as Potential Novel Therapies for Urinary Tract Infections. *Front Cell Infect Microbiol*. **11**, (2021). https://doi.org/10.3389/fcimb.2021.656496.

[192] A. Cano, M. Ettcheto, M. Espina, A. Lopez-Machado, Y. Cajal, F. Rabanal, E. Sanchez-Lopez, A. Camins, M.L. Garcia, E.B. Souto. State-of-the-art polymeric nanoparticles as promising therapeutic tools against human bacterial infections. *J Nanobiotechnology*. **18**, (2020). https://doi.org/https://doi.org/10.1186/s12951-020-00714-2.

[193] B. Lu, X. Lv, Y. Le. Chitosan-modified PLGA nanoparticles for control-released drug delivery. *Polymers (Basel)*. **11**, (2019). https://doi.org/10.3390/polym11020304.

[194] A. Crintea, R. Carpa, A.O. Mitre, R.I. Petho, V.F. Chelaru, S.M. Nădășan, L. Neamti, A.G. Dutu. Nanotechnology Involved in Treating Urinary Tract Infections: An Overview. *Nanomaterials*. **13**, (2023). https://doi.org/10.3390/nano13030555.

[195] M. Divya, G.S. Kiran, S. Hassan, J. Selvin. Biogenic synthesis and effect of silver nanoparticles (AgNPs) to combat catheter-related urinary tract infections. *Biocatal Agric Biotechnol*. **18**, (2019). https://doi.org/10.1016/j.bcab.2019.101037.

[196] M. Lopez-Carrizales, K.I. Velasco, C. Castillo, A. Flores, M. Magaña, G.A. Martinez-Castanon, F. Martinez-Gutierrez. In vitro synergism of silver nanoparticles with antibiotics as an alternative treatment in multiresistant uropathogens. *Antibiotics*. **7**, (2018). https://doi.org/10.3390/antibiotics7020050.

[197] M. Qindeel, M. Barani, A. Rahdar, R. Arshad, M. Cucchiarini. Nanomaterials for the Diagnosis and Treatment of Urinary Tract Infections. *Nanomaterials*. **11**, (2021). https://doi.org/10.3390/nano.

[198] A. Crane, S. Isharwal, H. Zhu. Current Therapeutic Strategies in Clinical Urology. *Mol Pharm*. **15**, (2018), 3010–3019. https://doi.org/10.1021/acs.molpharmaceut.8b00383.

[199] P. Tyagi, P.-C. Wu, M. Chancellor, N. Yoshimura, L. Huang. Recent Advances in Intravesical Drug/Gene Delivery. *Mol Pharm*. **3**, (2006), 369–379. https://doi.org/10.1021/mp060001j.

[200] E. Bilensoy, C. Sarisozen, G. Esendağlı, A.L. Doğan, Y. Aktaş, M. Şen, N.A. Mungan. Intravesical cationic nanoparticles of chitosan and polycaprolactone for the delivery of Mitomycin C to bladder tumors. *Int J Pharm*. **371**, (2009), 170–176. https://doi.org/10.1016/j.ijpharm.2008.12.015.

[201] S. Hashemi, A. Sahai, S. Malde. Applications of electromotive drug administration in urology. *Urol Ann*. **12**, (2020), 301–308. https://doi.org/10.4103/UA.UA_152_19.

[202] J.W.S. Min, N. Saeed, A. Coene, M. Adriaens, W. Ceelen. Electromotive Enhanced Drug Administration in Oncology: Principles, Evidence, Current and Emerging Applications. *Cancers (Basel)*. **14**, (2022). https://doi.org/10.3390/cancers14204980.

[203] B. Kos, J.L. Vásquez, D. Miklavčič, G.G.G. Hermann, J. Gehl. Investigation of the mechanisms of action behind Electromotive Drug Administration (EMDA). *PeerJ*. **4**, (2016), e2309. https://doi.org/10.7717/peerj.2309.

[204] M.T. Melgarejo-Segura, A. Morales-Martínez, Y. Yáñez-Castillo, M.Á. Arrabal-Polo, P. Gómez-Lechuga, M. Pareja-Vílchez, J.J. Jiménez-Moleón, M.A. Martín. A systematic review of the efficacy of intravesical electromotive drug administration therapy for non-muscle invasive bladder cancer. *Urologic Oncology: Seminars and Original Investigations*. **41**, (2023), 166–176. https://doi.org/10.1016/j.urolonc.2022.09.016.

[205] O.M. Kolawole, W.M. Lau, H. Mostafid, V. V. Khutoryanskiy. Advances in intravesical drug delivery systems to treat bladder cancer. *Int J Pharm*. **532**, (2017), 105–117. https://doi.org/10.1016/j.ijpharm.2017.08.120.

[206] P. Tyagi, M. Kashyap, H. Hensley, N. Yoshimura. Advances in intravesical therapy for urinary tract disorders. *Expert Opin Drug Deliv*. **13**, (2016), 71–84. https://doi.org/10.1517/17425247.2016.1100166.

[207] J.T. Hsieh, J. Zhou, C. Gore, P. Zimmern. R11, a novel cell-permeable peptide, as an intravesical delivery vehicle. *BJU Int*. **108**, (2011), 1666–1671. https://doi.org/10.1111/j.1464-410X.2011.10185.x.

[208] D. Araki, K. Takayama, M. Inoue, T. Watanabe, H. Kumon, S. Futaki, H. Matsui, K. Tomizawa. Cell-penetrating d-Isomer Peptides of p53 C-terminus: Long-term Inhibitory Effect on the Growth of Bladder Cancer. *Urology*. **75**, (2010), 813–819. https://doi.org/10.1016/j.urology.2009.10.002.

[209] P. Tyagi, R. Banerjee, S. Basu, N. Yoshimura, M. Chancellor, L. Huang. Intravesical antisense therapy for cystitis using TAT-peptide nucleic acid conjugates. *Mol Pharm*. **3**, (2006), 398–406. https://doi.org/10.1021/mp050093x.

[210] X.F. Gao, J.F. Feng, W. Wang, Z.H. Xiang, X.J. Liu, C. Zhu, Z.X. Tang, X.Z. Dong, C. He. Pirt reduces bladder overactivity by inhibiting purinergic receptor P2X3. *Nat Commun*. **6**, (2015). https://doi.org/10.1038/ncomms8650.

[211] J.I. Griffin, S.K. (Kevin) Cheng, T. Hayashi, D. Carson, M. Saraswathy, D.P. Nair, D. Simberg. Cell-penetrating peptide CGKRK mediates efficient and widespread targeting of bladder mucosa following focal injury. *Nanomedicine*. **13**, (2017), 1925–1932. https://doi.org/10.1016/j.nano.2017.04.004.

[212] J. Xie, Y. Bi, H. Zhang, S. Dong, L. Teng, R.J. Lee, Z. Yang. Cell-Penetrating Peptides in Diagnosis and Treatment of Human Diseases: From Preclinical Research to Clinical Application. *Front Pharmacol*. **11**, (2020). https://doi.org/10.3389/fphar.2020.00697.

[213] A. Erman, P. Veranič. The use of polymer chitosan in intravesical treatment of urinary bladder cancer and infections. *Polymers (Basel)*. **10**, (2018). https://doi.org/10.3390/polym10030265.

[214] M. Kerec, M. Bogataj, P. Veranič, A. Mrhar. Permeability of pig urinary bladder wall: The effect of chitosan and the role of calcium. *European Journal of Pharmaceutical Sciences*. **25**, (2005), 113–121. https://doi.org/10.1016/j.ejps.2005.02.003.

[215] T. Ahmed, B. Aljaeid. Preparation, characterization, and potential application of chitosan, chitosan derivatives, and chitosan metal nanoparticles in pharmaceutical drug delivery. *Drug Des Devel Ther*. (2016), 483. https://doi.org/10.2147/DDDT.S99651.

[216] T.M.M. Ways, W.M. Lau, V. V. Khutoryanskiy. Chitosan and its derivatives for application in mucoadhesive drug delivery systems. *Polymers (Basel)*. **10**, (2018). https://doi.org/10.3390/polym10030267.

[217] P. Veranič, A. Erman, M. Kerec-Kos, M. Bogataj, A. Mrhar, K. Jezernik. Rapid differentiation of superficial urothelial cells after chitosan-induced desquamation. *Histochem Cell Biol*. **131**, (2009), 129–139. https://doi.org/10.1007/s00418-008-0492-x.

[218] A. Erman, P. Veranič. Time- and temperature-dependent autolysis of urinary bladder epithelium during ex vivo preservation. *Protoplasma*. **248**, (2011), 541–550. https://doi.org/10.1007/s00709-010-0201-1.

[219] L.W. Hsu, Y.C. Ho, E.Y. Chuang, C.T. Chen, J.H. Juang, F.Y. Su, S.M. Hwang, H.W. Sung. Effects of pH on molecular mechanisms of chitosan-integrin interactions and resulting tight-junction disruptions. *Biomaterials*. **34**, (2013), 784–793. https://doi.org/10.1016/j.biomaterials.2012.09.082.

[220] M. Kos, M. Bogataj, P. Veranic, A. Mrhar. Chitosan is a linear copolymer of N-acetyl-D-glucosamine. *Biol Pharm Bull*. **29**, (2006), 1685–1691.

[221] A. Erman, V.K. Hergouth, M.G. Blango, M.K. Kos, M.A. Mulvey, P. Veranič. Repeated treatments with Chitosan in combination with antibiotics completely eradicate uropathogenic Escherichia coli from infected mouse urinary bladders. *Journal of Infectious Diseases*. **216**, (2017), 375–381. https://doi.org/10.1093/infdis/jix023.

[222] D.B. Kaldybekov, S.K. Filippov, A. Radulescu, V. V. Khutoryanskiy. Maleimide-functionalised PLGA-PEG nanoparticles as mucoadhesive carriers for intravesical drug delivery. *European Journal of Pharmaceutics and Biopharmaceutics*. **143**, (2019), 24–34. https://doi.org/10.1016/j.ejpb.2019.08.007.

[223] K. Netsomboon, A. Bernkop-Schnürch. Mucoadhesive vs. mucopenetrating particulate drug delivery. *European Journal of Pharmaceutics and Biopharmaceutics*. **98**, (2016), 76–89. https://doi.org/10.1016/j.ejpb.2015.11.003.

[224] H. Takeuchi, J. Thongborisute, Y. Matsui, H. Sugihara, H. Yamamoto, Y. Kawashima. Novel mucoadhesion tests for polymers and polymer-coated particles to design optimal mucoadhesive drug delivery systems. *Adv Drug Deliv Rev*. **57**, (2005), 1583–1594. https://doi.org/10.1016/j.addr.2005.07.008.

[225] N.K. Al-Nemrawi, A.R. Okour, R.H. Dave. Surface modification of PLGA nanoparticles using chitosan: Effect of molecular weight, concentration, and degree of deacetylation. *Advances in Polymer Technology*. **37**, (2018), 3066–3075. https://doi.org/10.1002/adv.22077.

[226] G.K. Jain, S.A. Pathan, S. Akhter, N. Ahmad, N. Jain, S. Talegaonkar, R.K. Khar, F.J. Ahmad. Mechanistic study of hydrolytic erosion and drug release behaviour of PLGA nanoparticles: Influence of chitosan. *Polym Degrad Stab*. **95**, (2010), 2360–2366. https://doi.org/10.1016/j.polymdegradstab.2010.08.015.

[227] H. Chen, L.Q. Xie, J. Qin, Y. Jia, X. Cai, W. Bin Nan, W. Yang, F. Lv, Q.Q. Zhang. Surface modification of PLGA nanoparticles with biotinylated chitosan for the sustained

in vitro release and the enhanced cytotoxicity of epirubicin. *Colloids Surf B Biointerfaces*. **138**, (2016), 1–9. https://doi.org/10.1016/j.colsurfb.2015.11.033.

[228] K.C. Hembram, S. Prabha, R. Chandra, B. Ahmed, S. Nimesh. Advances in preparation and characterization of chitosan nanoparticles for therapeutics. *Artif Cells Nanomed Biotechnol*. **44**, (2016), 305–314. https://doi.org/10.3109/21691401.2014.948548.

[229] J. Nilsen-Nygaard, S.P. Strand, K.M. Vårum, K.I. Draget, C.T. Nordgård. Chitosan: Gels and interfacial properties. *Polymers (Basel)*. **7**, (2015), 552–579. https://doi.org/10.3390/polym7030552.

[230] E.A. Mun, A.C. Williams, V. V. Khutoryanskiy. Adhesion of thiolated silica nanoparticles to urinary bladder mucosa: Effects of PEGylation, thiol content and particle size. *Int J Pharm*. **512**, (2016), 32–38. https://doi.org/10.1016/j.ijpharm.2016.08.026.

[231] J. Barthelmes, G. Perera, J. Hombach, S. Dünnhaupt, A. Bernkop-Schnürch. Development of a mucoadhesive nanoparticulate drug delivery system for a targeted drug release in the bladder. *Int J Pharm*. **416**, (2011), 339–345. https://doi.org/10.1016/j.ijpharm.2011.06.033.

[232] V.M. Leitner, G.F. Walker, A. Bernkop-Schnürch. Thiolated polymers: evidence for the formation of disulphide bonds with mucus glycoproteins. *European Journal of Pharmaceutics and Biopharmaceutics*. **56**, (2003), 207–214. https://doi.org/10.1016/S0939-6411(03)00061-4.

[233] O.M. Kolawole, W.M. Lau, V. V Khutoryanskiy. Methacrylated chitosan as a polymer with enhanced mucoadhesive properties for transmucosal drug delivery. *Int J Pharm*. **550**, (2018), 123–129. https://doi.org/10.1016/j.ijpharm.2018.08.034.

[234] S. Shawky, S. Makled, A. Awaad, N. Boraie. Quercetin Loaded Cationic Solid Lipid Nanoparticles in a Mucoadhesive In Situ Gel—A Novel Intravesical Therapy Tackling Bladder Cancer. *Pharmaceutics*. **14**, (2022). https://doi.org/10.3390/pharmaceutics14112527.

[235] F. Ricci, G.F. Racaniello, N. Denora, L. Gentile, A. Lopalco, A. Cutrignelli, M. Franco, R.M. Iacobazzi, V. Laquintana, A. Lopedota. Thermoresponsive mucoadhesive hydrogel based on Pluronic F127/thiolated glycol chitosan for intravesical administration of celecoxib/gemcitabine. *J Drug Deliv Sci Technol*. **86**, (2023). https://doi.org/10.1016/j.jddst.2023.104687.

[236] M. Hussain Asim, I. Nazir, A. Jalil, B. Matuszczak, A. Bernkop-Schnürch. Tetradeca-thiolated cyclodextrins: Highly mucoadhesive and in-situ gelling oligomers with

prolonged mucosal adhesion. *Int J Pharm*. **577**, (2020). https://doi.org/10.1016/j.ijpharm.2020.119040.

[237] O.M. Kolawole, W.M. Lau, V. V. Khutoryanskiy. Chitosan/β-glycerophosphate in situ gelling mucoadhesive systems for intravesical delivery of mitomycin-C. *Int J Pharm X*. **1**, (2019). https://doi.org/10.1016/j.ijpx.2019.100007.

[238] S.Y. Karavana, Z.A. Şenyiğit, Ç. Çalışkan, G. Sevin, D.İ. Özdemir, Y. Erzurumlu, S. Şen, E. Baloğlu. Gemcitabine hydrochloride microspheres used for intravesical treatment of superficial bladder cancer: A comprehensive in vitro/ex vivo/in vivo evaluation. *Drug Des Devel Ther*. **12**, (2018), 1959–1975. https://doi.org/10.2147/DDDT.S164704.

[239] A.Y. Sherif, G.M. Mahrous, F.K. Alanazi. Novel in-situ gel for intravesical administration of ketorolac. *Saudi Pharmaceutical Journal*. **26**, (2018), 845–851. https://doi.org/10.1016/j.jsps.2018.03.014.

[240] T. Lin, J. Wu, X. Zhao, H. Lian, A. Yuan, X. Tang, S. Zhao, H. Guo, Y. Hu. In situ floating hydrogel for intravesical delivery of adriamycin without blocking urinary tract. *J Pharm Sci*. **103**, (2014), 927–936. https://doi.org/10.1002/jps.23854.

[241] P. Gentile, V. Chiono, I. Carmagnola, P. V. Hatton. An overview of poly(lactic-co-glycolic) Acid (PLGA)-based biomaterials for bone tissue engineering. *Int J Mol Sci*. **15**, (2014), 3640–3659. https://doi.org/10.3390/ijms15033640.

[242] D.J. Hines, D.L. Kaplan. Poly (lactic-co-glycolic acid) controlled release systems: experimental and modeling insights. *Crit Rev Ther Drug Carrier Syst*. **30**, (2013), 257–276.

[243] C. Federer, M. Kurpiers, A. Bernkop-Schnürch. Thiolated Chitosans: A Multi-talented Class of Polymers for Various Applications. *Biomacromolecules*. **22**, (2021), 24–56. https://doi.org/10.1021/acs.biomac.0c00663.

[244] M.A.S. Abourehab, S. Pramanik, M.A. Abdelgawad, B.M. Abualsoud, A. Kadi, M.J. Ansari, A. Deepak. Recent Advances of Chitosan Formulations in Biomedical Applications. *Int J Mol Sci*. **23**, (2022). https://doi.org/10.3390/ijms231810975.

[245] W. Wang, Q. Meng, Q. Li, J. Liu, M. Zhou, Z. Jin, K. Zhao. Chitosan derivatives and their application in biomedicine. *Int J Mol Sci*. **21**, (2020). https://doi.org/10.3390/ijms21020487.

[246] B. Guan, A. Ali, H. Peng, W. Hu, L.R. Markely, S. Estes, S. Prajapati. Characterization of poloxamers by reversed-phase liquid chromatography. *Analytical Methods*. **8**, (2016), 2812–2819. https://doi.org/10.1039/c5ay03311j.

[247] Z.P. Bulman, R. Cirz, D. Hildebrandt, T. Kane, Z. Rosario, K. Wlasichuk, M. Park, L.D. Andrews. Unraveling the gentamicin drug product complexity reveals variation in microbiological activities and nephrotoxicity. *Antimicrob Agents Chemother*. **64**, (2020). https://doi.org/10.1128/AAC.00533-20.

[248] R.S. Hayward, J. Harding, R. Molloy, L. Land, K. Longcroft-Neal, D. Moore, J.D.C. Ross. Adverse effects of a single dose of gentamicin in adults: a systematic review. *Br J Clin Pharmacol*. **84**, (2018), 223–238. https://doi.org/10.1111/bcp.13439.

[249] Z. Wei, X. Shi, R. Lian, W. Wang, W. Hong, S. Guo. Exclusive production of gentamicin C1a from micromonospora purpurea by metabolic engineering. *Antibiotics*. **8**, (2019). https://doi.org/10.3390/antibiotics8040267.

[250] P. Saxena, P.K. Sharma, P. Purohit. A journey of celecoxib from pain to cancer. *Prostaglandins Other Lipid Mediat*. **147**, (2020). https://doi.org/10.1016/j.prostaglandins.2019.106379.

[251] N. Yamakawa, K. Suzuki, Y. Yamashita, T. Katsu, K. Hanaya, M. Shoji, T. Sugai, T. Mizushima. Structure-activity relationship of celecoxib and rofecoxib for the membrane permeabilizing activity. *Bioorg Med Chem*. **22**, (2014), 2529–2534. https://doi.org/10.1016/j.bmc.2014.02.032.

[252] U.S. Raikar, C.G. Renuka, Y.F. Nadaf, B.G. Mulimani, A.M. Karguppikar, M.K. Soudagar. Solvent effects on the absorption and fluorescence spectra of coumarins 6 and 7 molecules: Determination of ground and excited state dipole moment. *Spectrochim Acta A Mol Biomol Spectrosc*. **65**, (2006), 673–677. https://doi.org/10.1016/j.saa.2005.12.028.

[253] Y. Wang, P. Li, T.T.D. Tran, J. Zhang, L. Kong. Manufacturing techniques and surface engineering of polymer based nanoparticles for targeted drug delivery to cancer. *Nanomaterials*. **6**, (2016). https://doi.org/10.3390/nano6020026.

[254] R. Lancheros, C.A. Guerrero, R.D. Godoy-Silva. Improvement of N-Acetylcysteine Loaded in PLGA Nanoparticles by Nanoprecipitation Method. *J Nanotechnol*. **2018**, (2018). https://doi.org/10.1155/2018/3620373.

[255] M. Alonso-González, A. Fernández-Carballido, P. Quispe-Chauca, I. Lozza, C. Martín-Sabroso, A. Isabel Fraguas-Sánchez. DoE-based development of celecoxib loaded PLGA nanoparticles: In ovo assessment of its antiangiogenic effect. *European Journal of Pharmaceutics and Biopharmaceutics*. **180**, (2022), 149–160. https://doi.org/10.1016/j.ejpb.2022.09.022.

[256] M.R. Kim, T. Feng, Q. Zhang, H.Y.E. Chan, Y. Chau. Co-encapsulation and co-delivery of peptide drugs via polymeric nanoparticles. *Polymers (Basel)*. **11**, (2019). https://doi.org/10.3390/polym11020288.

[257] P. Senthil Kumar, K. Grace Pavithra, M. Naushad. Characterization techniques for nanomaterials, in: Nanomaterials for Solar Cell Applications, Elsevier, 2019: pp. 97–124 https://doi.org/10.1016/B978-0-12-813337-8.00004-7.

[258] N. Raval, R. Maheshwari, D. Kalyane, S.R. Youngren-Ortiz, M.B. Chougule, R.K. Tekade. Importance of physicochemical characterization of nanoparticles in pharmaceutical product development, in: Basic Fundamentals of Drug Delivery, Elsevier, 2018: pp. 369–400 https://doi.org/10.1016/B978-0-12-817909-3.00010-8.

[259] R. Shaw. Dynamic Light Scattering Training Achieving reliable nano particle sizing, 2014. https://www.chem.uci.edu/~dmitryf/manuals/Fundamentals/DLS%20concept.pdf (accessed May 13, 2024).

[260] J. Lim, S.P. Yeap, H.X. Che, S.C. Low. Characterization of magnetic nanoparticle by dynamic light scattering. *Nanoscale Res Lett*. **8**, (2013), 1–14. https://doi.org/10.1186/1556-276X-8-381.

[261] A. Paar. The principles of dynamic light scattering. (2024). https://wiki.anton-paar.com/uk-en/the-principles-of-dynamic-light-scattering/ (accessed May 17, 2024).

[262] J.D. Clogston, A.K. Patri. Zeta potential measurement, in: S. McNeil (Ed.), Characterization of Nanoparticles Intended for Drug Delivery, 2011: pp. 63–70. www.springer.com/series/7651.

[263] D. Hanaor, M. Michelazzi, C. Leonelli, C.C. Sorrell. The effects of carboxylic acids on the aqueous dispersion and electrophoretic deposition of ZrO2. *J Eur Ceram Soc*. **32**, (2012), 235–244. https://doi.org/10.1016/j.jeurceramsoc.2011.08.015.

[264] H. Tiernan, B. Byrne, S.G. Kazarian. ATR-FTIR spectroscopy and spectroscopic imaging for the analysis of biopharmaceuticals. *Spectrochim Acta A Mol Biomol Spectrosc*. **241**, (2020). https://doi.org/10.1016/j.saa.2020.118636.

[265] A.A. Bunaciu, H.Y. Aboul-Enein, S. Fleschin. Application of fourier transform infrared spectrophotometry in pharmaceutical drugs analysis. *Appl Spectrosc Rev*. **45**, (2010), 206–219. https://doi.org/10.1080/00387011003601044.

[266] S.E. Glassford, B. Byrne, S.G. Kazarian. Recent applications of ATR FTIR spectroscopy and imaging to proteins. *Biochim Biophys Acta Proteins Proteom*. **1834**, (2013), 2849–2858. https://doi.org/10.1016/j.bbapap.2013.07.015.

[267] S.G. Kazarian, K.L.A. Chan. ATR-FTIR spectroscopic imaging: Recent advances and applications to biological systems. *Analyst*. **138**, (2013), 1940–1951. https://doi.org/10.1039/c3an36865c.

[268] S. Tiquia-Arashiro, X. Li, K. Pokhrel, A. Kassem, L. Abbas, O. Coutinho, D. Kasperek, H. Najaf, S. Opara. Applications of Fourier Transform-Infrared spectroscopy in microbial cell biology and environmental microbiology: advances, challenges, and future perspectives. *Front Microbiol*. **14**, (2023). https://doi.org/10.3389/fmicb.2023.1304081.

[269] N.K. Thakral, R.L. Zanon, R.C. Kelly, S. Thakral. Applications of Powder X-Ray Diffraction in Small Molecule Pharmaceuticals: Achievements and Aspirations. *J Pharm Sci*. **107**, (2018), 2969–2982. https://doi.org/10.1016/j.xphs.2018.08.010.

[270] A.A. Bunaciu, E. gabriela Udriştioiu, H.Y. Aboul-Enein. X-Ray Diffraction: Instrumentation and Applications. *Crit Rev Anal Chem*. **45**, (2015), 289–299. https://doi.org/10.1080/10408347.2014.949616.

[271] G.F. Harrington, J. Santiso. Back-to-Basics tutorial: X-ray diffraction of thin films. *J Electroceram*. **47**, (2021), 141–163. https://doi.org/10.1007/s10832-021-00263-6.

[272] M. Malatesta. Transmission electron microscopy as a powerful tool to investigate the interaction of nanoparticles with subcellular structures. *Int J Mol Sci*. **22**, (2021). https://doi.org/10.3390/ijms222312789.

[273] J. Weng, H.H.Y. Tong, S.F. Chow. In vitro release study of the polymeric drug nanoparticles: Development and validation of a novel method. *Pharmaceutics*. **12**, (2020), 1–18. https://doi.org/10.3390/pharmaceutics12080732.

[274] G. Moreno-Bautista, K.C. Tam. Evaluation of dialysis membrane process for quantifying the in vitro drug-release from colloidal drug carriers. *Colloids Surf A Physicochem Eng Asp*. **389**, (2011), 299–303. https://doi.org/10.1016/j.colsurfa.2011.07.032.

[275] A. Bauer, P. Berben, S.S. Chakravarthi, S. Chattorraj, A. Garg, B. Gourdon, T. Heimbach, Y. Huang, C. Morrison, D. Mundhra, R. Palaparthy, P. Saha, M. Siemons, N.A. Shaik, Y. Shi, S. Shum, N.K. Thakral, S. Urva, R. Vargo, V.R. Koganti, S.E. Barrett. Current State and Opportunities with Long-acting Injectables: Industry Perspectives from the Innovation and Quality Consortium "Long-Acting Injectables" Working Group. *Pharm Res*. **40**, (2023), 1601–1631. https://doi.org/10.1007/s11095-022-03391-y.

[276] H.A. Alturkistani, F.M. Tashkandi, Z.M. Mohammedsaleh. Histological Stains: A Literature Review and Case Study. *Glob J Health Sci*. **8**, (2015), 72–79. https://doi.org/10.5539/gjhs.v8n3p72.

[277] N. Schmitz, S. Laverty, V.B. Kraus, T. Aigner. Basic methods in histopathology of joint tissues. *Osteoarthritis Cartilage*. **18**, (2010). https://doi.org/10.1016/j.joca.2010.05.026.

[278] D.B. Kaldybekov, P. Tonglairoum, P. Opanasopit, V. V. Khutoryanskiy. Mucoadhesive maleimide-functionalised liposomes for drug delivery to urinary bladder. *European Journal of Pharmaceutical Sciences*. **111**, (2018), 83–90. https://doi.org/10.1016/j.ejps.2017.09.039.

[279] P. Dadgostar. Antimicrobial resistance: implications and costs. *Infect Drug Resist*. **12**, (2019), 3903–3910. https://doi.org/10.2147/IDR.S234610.

[280] E. Imbuluzqueta, E. Elizondo, C. Gamazo, E. Moreno-Calvo, J. Veciana, N. Ventosa, M.J. Blanco-Prieto. Novel bioactive hydrophobic gentamicin carriers for the treatment of intracellular bacterial infections. *Acta Biomater*. **7**, (2011), 1599–1608. https://doi.org/10.1016/j.actbio.2010.11.031.

[281] H.D. Lu, P. Rummaneethorn, K.D. Ristroph, R.K. Prud'Homme. Hydrophobic Ion Pairing of Peptide Antibiotics for Processing into Controlled Release Nanocarrier Formulations. *Mol Pharm*. **15**, (2018), 216–225. https://doi.org/10.1021/acs.molpharmaceut.7b00824.

[282] K.D. Ristroph, R.K. Prud'homme. Hydrophobic ion pairing: Encapsulating small molecules, peptides, and proteins into nanocarriers. *Nanoscale Adv*. **1**, (2019), 4207–4237. https://doi.org/10.1039/c9na00308h.

[283] G. Noh, T. Keum, S. Bashyal, J.E. Seo, L. Shrawani, J.H. Kim, S. Lee. Recent progress in hydrophobic ion-pairing and lipid-based drug delivery systems for enhanced oral delivery of biopharmaceuticals. *J Pharm Investig*. **52**, (2022), 75–93. https://doi.org/10.1007/s40005-021-00549-5.

[284] A. Gamboa, N. Schüßler, E. Soto-Bustamante, P. Romero-Hasler, L. Meinel, J.O. Morales. Delivery of ionizable hydrophilic drugs based on pharmaceutical formulation of ion pairs and ionic liquids. *European Journal of Pharmaceutics and Biopharmaceutics*. **156**, (2020), 203–218. https://doi.org/10.1016/j.ejpb.2020.09.007.

[285] A. Patel, R. Gaudana, A.K. Mitra. A novel approach for antibody nanocarriers development through hydrophobic ion-pairing complexation. *J Microencapsul*. **31**, (2014), 542–550. https://doi.org/10.3109/02652048.2014.885606.

[286] I.N. Tahtali, T. Yildiz, M.M. Dincer. The new therapeutic option for female stress and stress-predominant mixed urinary incontinence: Periurethral hypertonic saline (10%) injection. *LUTS: Lower Urinary Tract Symptoms*. **14**, (2022), 186–192. https://doi.org/10.1111/luts.12422.

[287] P.J. Kuehl, S. De, B. Eppler, J. Marsters, L. Matthews, M.D. Reed, J.D. Talton. Development and Validation of an HPLC Assay For Dual Detection of Gentamicin Sulfate and Leucine From a Novel Dry Powder For Inhalation. *J Anal Bioanal Tech*. **03**, (2012). https://doi.org/10.4172/2155-9872.1000152.

[288] A. Joseph, A. Rustum. Development and validation of a RP-HPLC method for the determination of gentamicin sulfate and its related substances in a pharmaceutical cream using a short pentafluorophenyl column and a Charged Aerosol Detector. *J Pharm Biomed Anal*. **51**, (2010), 521–531. https://doi.org/10.1016/j.jpba.2009.09.002.

[289] J.H. Lim, Y.G. Na, H.K. Lee, S.J. Kim, H.J. Lee, K.H. Bang, M. Wang, Y.C. Pyo, H.W. Huh, C.W. Cho. Effect of surfactant on the preparation and characterization of gemcitabine-loaded particles. *J Pharm Investig*. **49**, (2019), 271–278. https://doi.org/10.1007/s40005-018-0402-8.

[290] Determination of minimum inhibitory concentrations (MICs) of antibacterial agents by broth dilution. *Clinical Microbiology and Infection*. **9**, (2003), ix–xv. https://doi.org/10.1046/j.1469-0691.2003.00790.x.

[291] I.T. Somé, R. Semde, O. Moustapha, K. Amighi, P.I. Guissou, P. Duez, J. Dubois. Validation of gentamicin congeners using HPLC with electrochemical detection: Comparison with fluorimetric detection. *Comptes Rendus Chimie*. **7**, (2004), 1087–1093. https://doi.org/10.1016/j.crci.2003.12.037.

[292] H. Brozmanova, R. Urinovska, K. Safarcik, F. Vsiansky, I. Kacirova, M. Grundmann. Liquid chromatography-tandem mass spectrometry method for quantification of gentamicin and its individual congeners in serum and comparison results with two immunoanalytical methods (fluorescence polarization immunoassay and chemiluminiscent microparticle immunoassay). *Clinica Chimica Acta*. **521**, (2021), 191–198. https://doi.org/10.1016/j.cca.2021.07.014.

[293] C. Lecároz, M.A. Campanero, C. Gamazo, M.J. Blanco-Prieto. Determination of gentamicin in different matrices by a new sensitive high-performance liquid chromatography-mass spectrometric method. *Journal of Antimicrobial Chemotherapy*. **58**, (2006), 557–563. https://doi.org/10.1093/jac/dkl258.

[294] I. Clarot, P. Chaimbault, F. Hasdenteufel, P. Netter, A. Nicolas. Determination of gentamicin sulfate and related compounds by high-performance liquid chromatography with evaporative light scattering detection. *J Chromatogr A*. **1031**, (2004), 281–287. https://doi.org/10.1016/j.chroma.2003.12.032.

[295] A.F.H. Ismail, F. Mohamed, L.M.M. Rosli, M.A.M. Shafri, M.S. Haris, A.B. Adina. Spectrophotometric determination of gentamicin loaded PLGA microparticles and method validation via ninhydrin-gentamicin complex as a rapid quantification approach. *J Appl Pharm Sci*. **6**, (2016), 007–014. https://doi.org/10.7324/JAPS.2016.600102.

[296] C. Dhal, R. Mishra. Formulation development and in vitro evaluation of gentamicin sulfate-loaded PLGA nanoparticles based film for the treatment of surgical site infection by Box–Behnken design. *Drug Dev Ind Pharm*. **45**, (2019), 805–818. https://doi.org/10.1080/03639045.2019.1576719.

[297] U. Posadowska, M. Brzychczy-Włoch, E. Pamuła. Gentamicin loaded PLGA nanoparticles as local drug delivery system for the osteomyelitis treatment. *Acta Bioeng Biomech*. **17**, (2015), 41–47. https://doi.org/10.5277/ABB-00188-2014-02.

[298] K. Stypulkowska, A. Blazewicz, Z. Fijalek, K. Sarna. Determination of gentamicin sulphate composition and related substances in pharmaceutical preparations by LC with charged aerosol detection. *Chromatographia*. **72**, (2010), 1225–1229. https://doi.org/10.1365/s10337-010-1763-y.

[299] V. Claus, M. Sandmeier, N. Hock, H. Spleis, S. Lindner, M. Kalb, A. Bernkop-Schnürch. Counterion optimization for hydrophobic ion pairing (HIP): Unraveling the key factors. *Int J Pharm*. **647**, (2023). https://doi.org/10.1016/j.ijpharm.2023.123507.

[300] N. Dharaiya, U. Patel, D. Ray, V.K. Aswal, N. V. Sastry, P. Bahadur. Different pH triggered aggregate morphologies in sodium oleate-cationic surfactants mixed systems. *New Journal of Chemistry*. **41**, (2017), 9142–9151. https://doi.org/10.1039/c6nj03871a.

[301] J. Liu, Y. Xu, Z. Liu, H. Ren, Z. Meng, K. Liu, Z. Liu, J. Yong, Y. Wang, X. Li. A modified hydrophobic ion-pairing complex strategy for long-term peptide delivery with high drug encapsulation and reduced burst release from PLGA microspheres. *European Journal of Pharmaceutics and Biopharmaceutics*. **144**, (2019), 217–229. https://doi.org/10.1016/j.ejpb.2019.09.022.

[302] K. Kwiecień, M. Brzychczy-Włoch, E. Pamuła. Antibiotics modified by hydrophobic ion-pairing – A solution world's problems with resistant bacteria? *Sustainable Materials and Technologies*. **37**, (2023). https://doi.org/10.1016/j.susmat.2023.e00662.

[303] D.J. Kozuch, K. Ristroph, R.K. Prud'Homme, P.G. Debenedetti. Insights into Hydrophobic Ion Pairing from Molecular Simulation and Experiment. *ACS Nano*. **14**, (2020), 6097–6106. https://doi.org/10.1021/acsnano.0c01835.

[304] D. Modi, S. Jonnalagadda, G.A. Campbell, G. Dalwadi. Enhancing Oil Solubility of BCS Class II Drug Phenytoin Through Hydrophobic Ion Pairing to Enable High Drug Load in Injectable Nanoemulsion to Prevent Precipitation at Physiological pH With a Potential to Prevent Phlebitis. *J Pharm Sci*. **112**, (2023), 2427–2443. https://doi.org/10.1016/j.xphs.2023.03.012.

[305] S. Li, J. Guo, A. Reva, F. Huang, B. Xiong, Y. Liu, Z. Deng, P.F. Leadlay, Y. Sun. Methyltransferases of gentamicin biosynthesis. *Proc Natl Acad Sci U S A*. **115**, (2018), 1340–1345. https://doi.org/10.1073/pnas.1711603115.

[306] M. Asad, A. Rasul, G. Abbas, M.A. Shah, I. Nazir. Self-emulsifying drug delivery systems: A versatile approach to enhance the oral delivery of BCS class III drug via hydrophobic ion pairing. *PLoS One*. **18**, (2023). https://doi.org/10.1371/journal.pone.0286668.

[307] J. Griesser, G. Hetényi, M. Moser, F. Demarne, V. Jannin, A. Bernkop-Schnürch. Hydrophobic ion pairing: Key to highly payloaded self-emulsifying peptide drug delivery systems. *Int J Pharm*. **520**, (2017), 267–274. https://doi.org/10.1016/j.ijpharm.2017.02.019.

[308] M. Yu, H.A. Every, W. Jiskoot, G.J. Witkamp, W. Buijs. Molecular structure of dextran sulphate sodium in aqueous environment. *J Mol Struct*. **1156**, (2018), 320–329. https://doi.org/10.1016/j.molstruc.2017.11.090.

[309] A.S. Torky, M.S. Freag, M.M.A. Nasra, O.Y. Abdallah. Novel skin penetrating berberine oleate complex capitalizing on hydrophobic ion pairing approach. *Int J Pharm*. **549**, (2018), 76–86. https://doi.org/10.1016/j.ijpharm.2018.07.051.

[310] B. Hammouda. Temperature Effect on the Nanostructure of SDS Micelles in Water. *J Res Natl Inst Stand Technol*. **118**, (2013), 151. https://doi.org/10.6028/jres.118.008.

[311] W.G. Chambliss, R.W. Cleary, R. Fischer, A.B. Jones, P. Skierkowski, W. Nicholes, A.H. Kibbex. Effect of Docusate Sodium on Drug Release from a Controlled-Release Dosage Form. *J Pharm Sci*. **70**, (1981), 1248–1251.

[312] S. Llanos, L.J. Giraldo, O. Santamaria, C.A. Franco, F.B. Cortés. Effect of Sodium Oleate Surfactant Concentration Grafted onto SiO2 Nanoparticles in Polymer Flooding Processes. *ACS Omega*. **3**, (2018), 18673–18684. https://doi.org/10.1021/acsomega.8b02944.

[313] R. Batul, M. Bhave, P.J. Mahon, A. Yu. Polydopamine nanosphere with in-situ loaded gentamicin and its antimicrobial activity. *Molecules*. **25**, (2020). https://doi.org/10.3390/molecules25092090.

[314] S. Cavalu, G. Roiu, O. Pop, D.A.P. Heredea, T.O. Costea, C.F. Costea. Nano-scale modifications of amniotic membrane induced by UV and antibiotic treatment: Histological, AFM and FTIR spectroscopy evidence. *Materials*. **14**, (2021), 1–19. https://doi.org/10.3390/ma14040863.

[315] W.G. Dai, L.C. Dong. Characterization of physiochemical and biological properties of an insulin/lauryl sulfate complex formed by hydrophobic ion pairing. *Int J Pharm*. **336**, (2007), 58–66. https://doi.org/10.1016/j.ijpharm.2006.11.035.

[316] J. Cai, J. Deng, S. Wen, Y. Zhang, D. Wu, H. Luo, G. Cheng. Surface modification and flotation improvement of ilmenite by using sodium hypochlorite as oxidant and activator. *Journal of Materials Research and Technology*. **9**, (2020), 3368–3377. https://doi.org/10.1016/j.jmrt.2020.01.031.

[317] L. Casettari, D. Vllasaliu, E. Castagnino, S. Stolnik, S. Howdle, L. Illum. PEGylated chitosan derivatives: Synthesis, characterizations and pharmaceutical applications. *Prog Polym Sci*. **37**, (2012), 659–685. https://doi.org/10.1016/j.progpolymsci.2011.10.001.

[318] M. Surendranath, M.R. Rekha, R. Parameswaran. Recent advances in functionally modified polymers for mucoadhesive drug delivery. *J Mater Chem B*. **10**, (2022), 5913–5924. https://doi.org/10.1039/d2tb00856d.

[319] S.I. Abd-El Hafeez, N.E. Eleraky, E. Hafez, S.A. Abouelmagd. Design and optimization of metformin hydrophobic ion pairs for efficient encapsulation in polymeric drug carriers. *Sci Rep*. **12**, (2022). https://doi.org/10.1038/s41598-022-09384-6.

[320] J. Mudassir, A. Raza, M.A. Khan, H. Hameed, G.A. Shazly, A. Irfan, S.J. Rana, K. Abbas, M.S. Arshad, S. Muhammad, Y.A. Bin Jardan. Design and Evaluation of Hydrophobic Ion Paired Insulin Loaded Self Micro-Emulsifying Drug Delivery System for Oral Delivery. *Pharmaceutics*. **15**, (2023). https://doi.org/10.3390/pharmaceutics15071973.

[321] K. Kwiecień, I. Pudełko, K. Knap, K. Reczyńska-Kolman, M. Krok-Borkowicz, D. Ochońska, M. Brzychczy-Włoch, E. Pamuła. Insight in Superiority of the Hydrophobized Gentamycin in Terms of Antibiotics Delivery to Bone Tissue. *Int J Mol Sci*. **23**, (2022). https://doi.org/10.3390/ijms232012077.

[322] C. Tang, E. Zhang, Y. Li, L. Yang. An innovative method for preparation of hydrophobic ion-pairing colistin entrapped poly(lactic acid) nanoparticles: Loading and release

mechanism study. *European Journal of Pharmaceutical Sciences*. **102**, (2017), 63–70. https://doi.org/10.1016/j.ejps.2017.02.036.

[323] C. Lecaroz, C. Gamazo, M.J. Renedo, M.J. Blanco-Prieto. Biodegradable micro- and nanoparticles as long-term delivery vehicles for gentamicin. *J Microencapsul*. **23**, (2006), 782–792. https://doi.org/10.1080/02652040600946886.

[324] D. Panigrahi, P.K. Sahu, S. Swain, R.K. Verma. Quality by design prospects of pharmaceuticals application of double emulsion method for PLGA loaded nanoparticles. *SN Appl Sci*. **3**, (2021). https://doi.org/10.1007/s42452-021-04609-1.

[325] Y. Zambito, E. Pedreschi, G. Di Colo. Is dialysis a reliable method for studying drug release from nanoparticulate systems? - A case study. *Int J Pharm*. **434**, (2012), 28–34. https://doi.org/10.1016/j.ijpharm.2012.05.020.

[326] M. Alkholief, M.A. Kalam, M.K. Anwer, A. Alshamsan. Effect of Solvents, Stabilizers and the Concentration of Stabilizers on the Physical Properties of Poly(D,L-lactide-co-glycolide) Nanoparticles: Encapsulation, In Vitro Release of Indomethacin and Cytotoxicity against HepG2-Cell. *Pharmaceutics*. **14**, (2022). https://doi.org/10.3390/pharmaceutics14040870.

[327] A.K. Mohammad, J.J. Reineke. Quantitative detection of PLGA nanoparticle degradation in tissues following intravenous administration. *Mol Pharm*. **10**, (2013), 2183–2189. https://doi.org/10.1021/mp300559v.

[328] A.S. Hussein, N. Abdullah, F.R. Ahmadun. In vitro degradation of poly (D, L-lactide-co-glycolide) nanoparticles loaded with linamarin. *IET Nanobiotechnol*. **7**, (2013), 33–41. https://doi.org/10.1049/iet-nbt.2012.0012.

[329] S.G. Rotman, K. Thompson, D.W. Grijpma, R.G. Richards, T.F. Moriarty, D. Eglin, O. Guillaume. Development of bone seeker–functionalised microspheres as a targeted local antibiotic delivery system for bone infections. *J Orthop Translat*. **21**, (2020), 136–145. https://doi.org/10.1016/j.jot.2019.07.006.

[330] Y. Sun, A. Bhattacharjee, M. Reynolds, Y.V. Li. Synthesis and characterizations of gentamicin-loaded poly-lactic-co-glycolic (PLGA) nanoparticles. *Journal of Nanoparticle Research*. **23**, (2021). https://doi.org/10.1007/s11051-021-05293-3.

[331] G.A. Ter Boo, D.W. Grijpma, R.G. Richards, T.F. Moriarty, D. Eglin. Preparation of gentamicin dioctyl sulfosuccinate loaded poly(trimethylene carbonate) matrices intended for the treatment of orthopaedic infections. *Clin Hemorheol Microcirc*. **60**, (2015), 89–98. https://doi.org/10.3233/CH-151935.

[332] R. Dave, P. Jayaraj, P.K. Ajikumar, H. Joshi, T. Mathews, V.P. Venugopalan. Endogenously triggered electrospun fibres for tailored and controlled antibiotic release. *J Biomater Sci Polym Ed*. **24**, (2013), 1305–1319. https://doi.org/10.1080/09205063.2012.757725.

[333] N. V. Jafari, J.L. Rohn. The urothelium: a multi-faceted barrier against a harsh environment. *Mucosal Immunol*. **15**, (2022), 1127–1142. https://doi.org/10.1038/s41385-022-00565-0.

[334] G. Rutherford, L.J. Tan, O. Aboumarzouk, J. de Souza, R. Khan, B. Somani, T. Amer. Intravesical gentamicin treatment for recurrent urinary tract infections: A systematic review over the last two decades. *J Clin Urol*. (2022). https://doi.org/10.1177/20514158221138845.

[335] S. Sun, F. Cui, Y. Kawashima, N. Liang, L. Zhang, K. Shi, Y. Yu. A novel insulin-sodium oleate complex for oral administration: preparation, characterization and in vivo evaluation. *Journal of Drug Delivery Science and Technology*. **18**, (2008), 239–243.

[336] D. Tatini, M. Raudino, M. Ambrosi, E. Carretti, I. Davidovich, Y. Talmon, B.W. Ninham, P. Lo Nostro. Physicochemical characterization of green sodium oleate-based formulations. Part 1. Structure and rheology. *J Colloid Interface Sci*. **590**, (2021), 238–248. https://doi.org/10.1016/j.jcis.2021.01.040.

[337] A. Schoubben, P. Blasi, M.L. Marenzoni, L. Barberini, S. Giovagnoli, C. Cirotto, M. Ricci. Capreomycin supergenerics for pulmonary tuberculosis treatment: Preparation, in vitro, and in vivo characterization. *European Journal of Pharmaceutics and Biopharmaceutics*. **83**, (2013), 388–395. https://doi.org/10.1016/j.ejpb.2012.11.005.

[338] R. Ismail, T.N.Q. Phan, F. Laffleur, I. Csóka, A. Bernkop-Schnürch. Hydrophobic ion pairing of a GLP-1 analogue for incorporating into lipid nanocarriers designed for oral delivery. *European Journal of Pharmaceutics and Biopharmaceutics*. **152**, (2020), 10–17. https://doi.org/10.1016/j.ejpb.2020.04.025.

[339] J. Welch, J. Wallace, A.B. Lansley, C. Roper. Evaluation of the toxicity of sodium dodecyl sulphate (SDS) in the MucilAir$^{TM}$ human airway model in vitro. *Regulatory Toxicology and Pharmacology*. **125**, (2021). https://doi.org/10.1016/j.yrtph.2021.105022.

[340] M.K. Marwah, S. Shehzad, H. Shokr, J. Sacharczuk, K. Wang, S. Ahmad, L. Sanchez-Aranguren. Novel controlled-release polylactic-co-glycolic acid (PLGA) nanoparticles for sodium thiosulphate, a hydrogen sulphide donor, retains pro-angiogenic potential of

hydrogen sulphide. *J Exp Nanosci*. **17**, (2022), 197–213. https://doi.org/10.1080/17458080.2022.2060963.

[341] M. Ekinci, G. Yeğen, B. Aksu, D. İlem-Özdemir. Preparation and Evaluation of Poly(lactic acid)/Poly(vinyl alcohol) Nanoparticles Using the Quality by Design Approach. *ACS Omega*. **7**, (2022), 33793–33807. https://doi.org/10.1021/acsomega.2c02141.

[342] J. Barthelmes, S. Dünnhaupt, S. Unterhofer, G. Perera, W. Schlocker, A. Bernkop-Schnürch. Thiolated particles as effective intravesical drug delivery systems for treatment of bladder-related diseases. *Nanomedicine*. **8**, (2013), 65–75. https://doi.org/10.2217/nnm.12.76.

[343] O.M. Kolawole, W.M. Lau, V. V. Khutoryanskiy. Synthesis and Evaluation of Boronated Chitosan as a Mucoadhesive Polymer for Intravesical Drug Delivery. *J Pharm Sci*. **108**, (2019), 3046–3053. https://doi.org/10.1016/j.xphs.2019.05.006.

[344] N.K. Al-Nemrawi, R.M. Altawabeyeh, R.S. Darweesh. Preparation and Characterization of Docetaxel-PLGA Nanoparticles Coated with Folic Acid-chitosan Conjugate for Cancer Treatment. *J Pharm Sci*. **111**, (2022), 485–494. https://doi.org/10.1016/j.xphs.2021.10.034.

[345] P. Zhang, G. Wu, D. Zhang, W.F. Lai. Mechanisms and strategies to enhance penetration during intravesical drug therapy for bladder cancer. *Journal of Controlled Release*. **354**, (2023), 69–79. https://doi.org/10.1016/j.jconrel.2023.01.001.

[346] A.M. De Campos, Y. Diebold, E.L.S. Carvalho, A. Sánchez, M.J. Alonso. Chitosan Nanoparticles as New Ocular Drug Delivery Systems: in Vitro Stability, in Vivo Fate, and Cellular Toxicity. *Pharm Res*. **21**, (2004), 803–810.

[347] G.F. Tong, N. Qin, L.W. Sun. Development and evaluation of Desvenlafaxine loaded PLGA-chitosan nanoparticles for brain delivery. *Saudi Pharmaceutical Journal*. **25**, (2017), 844–851. https://doi.org/10.1016/j.jsps.2016.12.003.

[348] B.S. Kang, J.S. Choi, S.E. Lee, J.K. Lee, T.H. Kim, W.S. Jang, A. Tunsirikongkon, J.K. Kim, J.S. Park. Enhancing the in vitro anticancer activity of albendazole incorporated into chitosan-coated PLGA nanoparticles. *Carbohydr Polym*. **159**, (2017), 39–47. https://doi.org/10.1016/j.carbpol.2016.12.009.

[349] I.A. de Lima, N.M. Khalil, T.T. Tominaga, A. Lechanteur, B. Sarmento, R.M. Mainardes. Mucoadhesive chitosan-coated PLGA nanoparticles for oral delivery of ferulic acid. *Artif Cells Nanomed Biotechnol*. **46**, (2018), 993–1002. https://doi.org/10.1080/21691401.2018.1477788.

[350] R. Yang, W.S. Shim, F. De Cui, G. Cheng, X. Han, Q.R. Jin, D.D. Kim, S.J. Chung, C.K. Shim. Enhanced electrostatic interaction between chitosan-modified PLGA nanoparticle and tumor. *Int J Pharm*. **371**, (2009), 142–147. https://doi.org/10.1016/j.ijpharm.2008.12.007.

[351] J. Zhang, P. Liu, Z. Zhang, J. Han, X. Yang, A. Wang, X. Zhang. Apatinib-loaded nanoparticles inhibit tumor growth and angiogenesis in a model of melanoma. *Biochem Biophys Res Commun*. **521**, (2020), 296–302. https://doi.org/10.1016/j.bbrc.2019.10.084.

[352] T. Silvestri, L. Grumetto, I. Neri, M. De Falco, S.F. Graziano, S. Damiano, D. Giaquinto, L. Maruccio, P. de Girolamo, F. Villapiano, R. Ciarcia, L. Mayol, M. Biondi. Investigating the Effect of Surface Hydrophilicity on the Destiny of PLGA-Poloxamer Nanoparticles in an In Vivo Animal Model. *Int J Mol Sci*. **24**, (2023). https://doi.org/10.3390/ijms241914523.

[353] B.P. Panda, R. Krishnamoorthy, N.K.H. Shivashekaregowda, S. Patnaik. Influence of poloxamer 188 on design and development of second generation PLGA nanocrystals of metformin hydrochloride. *Nano Biomed Eng*. **10**, (2018), 334–343. https://doi.org/10.5101/nbe.v10i4.p334-343.

[354] A.O. Kamel, G.A.S. Awad, A.S. Geneidi, N.D. Mortada. Preparation of intravenous stealthy acyclovir nanoparticles with increased mean residence time. *AAPS PharmSciTech*. **10**, (2009), 1427–1436. https://doi.org/10.1208/s12249-009-9342-y.

[355] F. Esmaeili, M.H. Ghahremani, B. Esmaeili, M.R. Khoshayand, F. Atyabi, R. Dinarvand. PLGA nanoparticles of different surface properties: Preparation and evaluation of their body distribution. *Int J Pharm*. **349**, (2008), 249–255. https://doi.org/10.1016/j.ijpharm.2007.07.038.

[356] İ. Yıldırım, H. Koçan. The pH of Drinking Water and Its Effect on the pH of Urine. *Cureus*. **15**, (2023). https://doi.org/10.7759/cureus.47437.

[357] H.C. Lai, S.N. Chang, H.C. Lin, Y.L. Hsu, H.M. Wei, C.C. Kuo, K.P. Hwang, H.Y. Chiang. Association between urine pH and common uropathogens in children with urinary tract infections. *Journal of Microbiology, Immunology and Infection*. **54**, (2021), 290–298. https://doi.org/10.1016/j.jmii.2019.08.002.

[358] S. Kalliola, E. Repo, V. Srivastava, F. Zhao, J.P. Heiskanen, J.A. Sirviö, H. Liimatainen, M. Sillanpää. Carboxymethyl Chitosan and Its Hydrophobically Modified Derivative as pH-Switchable Emulsifiers. *Langmuir*. **34**, (2018), 2800–2806. https://doi.org/10.1021/acs.langmuir.7b03959.

[359] G. Jiang, S. Tang, X. Chen, F. Ding. Enhancing the receptor-mediated cell uptake of PLGA nanoparticle for targeted drug delivery by incorporation chitosan onto the particle surface. *Journal of Nanoparticle Research*. **16**, (2014). https://doi.org/10.1007/s11051-014-2453-8.

[360] C.C. Pola, A.R.F. Moraes, E.A.A. Medeiros, R.F. Teófilo, N.F.F. Soares, C.L. Gomes. Development and optimization of pH-responsive PLGA-chitosan nanoparticles for triggered release of antimicrobials. *Food Chem*. **295**, (2019), 671–679. https://doi.org/10.1016/j.foodchem.2019.05.165.

[361] D. Pawar, S. Mangal, R. Goswami, K.S. Jaganathan. Development and characterization of surface modified PLGA nanoparticles for nasal vaccine delivery: Effect of mucoadhesive coating on antigen uptake and immune adjuvant activity. *European Journal of Pharmaceutics and Biopharmaceutics*. **85**, (2013), 550–559. https://doi.org/10.1016/j.ejpb.2013.06.017.

[362] D.T. Martin, C.J. Hoimes, H.Z. Kaimakliotis, C.J. Cheng, K. Zhang, J. Liu, M.A. Wheeler, W.K. Kelly, G.N. Tew, W.M. Saltzman, R.M. Weiss. Nanoparticles for urothelium penetration and delivery of the histone deacetylase inhibitor belinostat for treatment of bladder cancer. *Nanomedicine*. **9**, (2013), 1124–1134. https://doi.org/10.1016/j.nano.2013.05.017.

[363] I. V. Marchenko, D.B. Trushina. Local Drug Delivery in Bladder Cancer: Advances of Nano/Micro/Macro-Scale Drug Delivery Systems. *Pharmaceutics*. **15**, (2023). https://doi.org/10.3390/pharmaceutics15122724.

[364] F. Yang, M. Cabe, H.A. Nowak, K.A. Langert. Chitosan/poly(lactic-co-glycolic)acid Nanoparticle Formulations with Finely-Tuned Size Distributions for Enhanced Mucoadhesion. *Pharmaceutics*. **14**, (2022). https://doi.org/10.3390/pharmaceutics14010095.

[365] H.M. Aldawsari, N.A. Alhakamy, R. Padder, M. Husain, S. Md. Preparation and characterization of chitosan coated PLGA nanoparticles of resveratrol: Improved stability, antioxidant and apoptotic activities in H1299 lung cancer cells. *Coatings*. **10**, (2020). https://doi.org/10.3390/COATINGS10050439.

[366] U.A. Shinde, P.N. Joshi, D.D. Jain, K. Singh. Preparation and Evaluation of N-Trimethyl Chitosan Nanoparticles of Flurbiprofen for Ocular Delivery. *Curr Eye Res*. **44**, (2019), 575–582. https://doi.org/10.1080/02713683.2019.1567793.

[367] R.S. Bhatta, H. Chandasana, Y.S. Chhonker, C. Rathi, D. Kumar, K. Mitra, P.K. Shukla. Mucoadhesive nanoparticles for prolonged ocular delivery of natamycin: In vitro and

pharmacokinetics studies. *Int J Pharm*. **432**, (2012), 105–112. https://doi.org/10.1016/j.ijpharm.2012.04.060.

[368] R.M. Aman, R.A. Zaghloul, M.S. El-Dahhan. Formulation, optimization and characterization of allantoin-loaded chitosan nanoparticles to alleviate ethanol-induced gastric ulcer: in-vitro and in-vivo studies. *Sci Rep*. **11**, (2021). https://doi.org/10.1038/s41598-021-81183-x.

[369] S.K. Linden, P. Sutton, N.G. Karlsson, V. Korolik, M.A. McGuckin. Mucins in the mucosal barrier to infection. *Mucosal Immunol*. **1**, (2008), 183–197. https://doi.org/10.1038/mi.2008.5.

[370] R.B. Qaqish, M.M. Amiji. Synthesis of a fluorescent chitosan derivative and its application for the study of chitosan-mucin interactions. *Carbohydr Polym*. **38**, (1999), 99–107.

[371] F. Bigucci, B. Luppi, T. Cerchiara, M. Sorrenti, G. Bettinetti, L. Rodriguez, V. Zecchi. Chitosan/pectin polyelectrolyte complexes: Selection of suitable preparative conditions for colon-specific delivery of vancomycin. *European Journal of Pharmaceutical Sciences*. **35**, (2008), 435–441. https://doi.org/10.1016/j.ejps.2008.09.004.

[372] I.S. Bayer. Recent Advances in Mucoadhesive Interface Materials, Mucoadhesion Characterization, and Technologies. *Adv Mater Interfaces*. **9**, (2022). https://doi.org/10.1002/admi.202200211.

[373] M. Fu, S.K. Filippov, A.C. Williams, V. V. Khutoryanskiy. On the mucoadhesive properties of synthetic and natural polyampholytes. *J Colloid Interface Sci*. **659**, (2024), 849–858. https://doi.org/10.1016/j.jcis.2023.12.176.

[374] S.E. Kudaibergenov, N. Nuraje. Intra- and interpolyelectrolyte complexes of polyampholytes. *Polymers (Basel)*. **10**, (2018). https://doi.org/10.3390/polym10101146.

[375] G. Sandri, S. Rossi, M. Bonferoni, F. Ferrari, M. Mori, C. Caramella. The role of chitosan as a mucoadhesive agent in mucosal drug delivery. *J Drug Deliv Sci Technol*. **22**, (2012), 275–284.

[376] W.G. Hill. Control of urinary drainage and voiding. *Clinical Journal of the American Society of Nephrology*. **10**, (2015), 480–492. https://doi.org/10.2215/CJN.04520413.

[377] M.H. Elkomy, A.A. Ali, H.M. Eid. Chitosan on the surface of nanoparticles for enhanced drug delivery: A comprehensive review. *Journal of Controlled Release*. **351**, (2022), 923–940. https://doi.org/10.1016/j.jconrel.2022.10.005.

[378] J.C. Mathai, E.H. Zhou, W. Yu, J.H. Kim, G. Zhou, Y. Liao, T.T. Sun, J.J. Fredberg, M.L. Zeidel. Hypercompliant apical membranes of bladder umbrella cells. *Biophys J*. **107**, (2014), 1273–1279. https://doi.org/10.1016/j.bpj.2014.07.047.

[379] N.A. Williams, J.L. Bowen, G. Al-Jayyoussi, M. Gumbleton, C.J. Allender, J. Li, T. Harrah, A. Raja, H.B. Joshi. An ex vivo investigation into the transurothelial permeability and bladder wall distribution of the nonsteroidal anti-inflammatory ketorolac. *Mol Pharm*. **11**, (2014), 673–682. https://doi.org/10.1021/mp400274z.

[380] J. Lavelle, S. Meyers, R. Ramage, S. Bastacky, D. Doty, G. Apodaca, M.L. Zeidel, S.-D. Bastacky. Bladder permeability barrier: recovery from selective injury of surface epithelial cells. *Am J Physiol Renal Physiol*. **283**, (2002), 242–253. https://doi.org/10.1152/ajprenal.00307.2001.

[381] A. Kumar, A. Kumar. Chitosan-Based Drug Conjugated Nanocomposites: Advances and Innovation in Cancer Therapy. *Regen Eng Transl Med*. **10**, (2023), 1–8. https://doi.org/10.1007/s40883-023-00310-4.

[382] C. Marques, C. Som, M. Schmutz, O. Borges, G. Borchard. How the Lack of Chitosan Characterization Precludes Implementation of the Safe-by-Design Concept. *Front Bioeng Biotechnol*. **8**, (2020). https://doi.org/10.3389/fbioe.2020.00165.

[383] D.T. Martin, J.M. Steinbach, J. Liu, S. Shimizu, H.Z. Kaimakliotis, M.A. Wheeler, A.B. Hittelman, W. Mark Saltzman, R.M. Weiss. Surface-modified nanoparticles enhance transurothelial penetration and delivery of survivin siRNA in treating bladder cancer. *Mol Cancer Ther*. **13**, (2013), 71–81. https://doi.org/10.1158/1535-7163.MCT-13-0502.

[384] T. Hoffmann, R. Peiris, C. Del Mar, G. Cleo, P. Glasziou. Natural history of uncomplicated urinary tract infection without antibiotics: A systematic review. *British Journal of General Practice*. **70**, (2020), E714–E722. https://doi.org/10.3399/bjgp20X712781.

[385] N. Sihra, A. Goodman, R. Zakri, A. Sahai, S. Malde. Nonantibiotic prevention and management of recurrent urinary tract infection. *Nat Rev Urol*. **15**, (2018), 750–776. https://doi.org/10.1038/s41585-018-0106-x.

[386] P.A. McCarron, R.F. Donnelly, W. Marouf. Celecoxib-loaded poly(D,L-lactide-co-glycolide) nanoparticles prepared using a novel and controllable combination of diffusion and emulsification steps as part of the salting-out procedure. *J Microencapsul*. **23**, (2006), 480–498. https://doi.org/10.1080/02652040600682390.

[387] T.H. Kim, Y. Il Jeong, S.G. Jin, J. Pei, T.Y. Jung, K.S. Moon, I.Y. Kim, S.S. Kang, S. Jung. Preparation of polylactide-co-glycolide nanoparticles incorporating celecoxib and

their antitumor activity against brain tumor cells. *Int J Nanomedicine*. **6**, (2011), 2621–2631. https://doi.org/10.2147/ijn.s19497.

[388] J. Emami, A. Pourmashhadi, H. Sadeghi, J. Varshosaz, H. Hamishehkar. Formulation and optimization of celecoxib-loaded PLGA nanoparticles by the Taguchi design and their in vitro cytotoxicity for lung cancer therapy. *Pharm Dev Technol*. **20**, (2015), 791–800. https://doi.org/10.3109/10837450.2014.920360.

[389] K. Chu, Y. Zhu, G. Lu, S. Huang, C. Yang, J. Zheng, J. Chen, J. Ban, H. Jia, Z. Lu. Formation of Hydrophilic Nanofibers from Nanostructural Design in the Co-Encapsulation of Celecoxib through Electrospinning. *Pharmaceutics*. **15**, (2023). https://doi.org/10.3390/pharmaceutics15030730.

[390] M. Tavares Luiz, J. Santos Rosa Viegas, J. Palma Abriata, F. Viegas, F. Testa Moura de Carvalho Vicentini, M.V. Lopes Badra Bentley, M. Chorilli, J. Maldonado Marchetti, D.R. Tapia-Blácido. Design of experiments (DoE) to develop and to optimize nanoparticles as drug delivery systems. *European Journal of Pharmaceutics and Biopharmaceutics*. **165**, (2021), 127–148. https://doi.org/10.1016/j.ejpb.2021.05.011.

[391] W.H. Song, J.H. Park, D.W. Yeom, B.K. Ahn, K.M. Lee, S.G. Lee, H.S. Woo, Y.W. Choi. Enhanced dissolution of celecoxib by supersaturating self-emulsifying drug delivery system (S-SEDDS) formulation. *Arch Pharm Res*. **36**, (2013), 69–78. https://doi.org/10.1007/s12272-013-0011-z.

[392] H. Cai, Z. Liang, W. Huang, L. Wen, G. Chen. Engineering PLGA nano-based systems through understanding the influence of nanoparticle properties and cell-penetrating peptides for cochlear drug delivery. *Int J Pharm*. **532**, (2017), 55–65. https://doi.org/10.1016/j.ijpharm.2017.08.084.

[393] M.E. Machado, P. de Souza Furtado, C. da Costa Bernardes Araújo, A. Simon, M.C. de Moraes, L.C.R.P. da Silva, F.A. do Carmo, L.M. Cabral, P.C. Sathler. Novel rivaroxaban-loaded poly(lactic-co-glycolic acid)/poloxamer nanoparticles: Preparation, physicochemical characterization, in vitro evaluation of time-dependent anticoagulant activity and toxicological profile. *Nanotechnology*. **32**, (2021). https://doi.org/10.1088/1361-6528/abd0b5.

[394] E.M. Williamson, Z. Sun, L. Mora-Tamez, R.L. Brutchey. Design of Experiments for Nanocrystal Syntheses: A How-To Guide for Proper Implementation. *Chemistry of Materials*. **34**, (2022), 9823–9835. https://doi.org/10.1021/acs.chemmater.2c02924.

[395] H. Vardhan, P. Mittal, S.K.R. Adena, B. Mishra. Long-circulating polyhydroxybutyrate-co-hydroxyvalerate nanoparticles for tumor targeted docetaxel delivery: Formulation,

optimization and in vitro characterization. *European Journal of Pharmaceutical Sciences*. **99**, (2017), 85–94. https://doi.org/10.1016/j.ejps.2016.12.007.

[396] N. Cheraga, N.C. Sun, X.X. Huang, Z. Ye, Q.R. Xiao, N.P. Huang. Optimized rapamycin-loaded PEGylated PLGA nanoparticles: Preparation, characterization and pharmacokinetics study. *J Drug Deliv Sci Technol*. **61**, (2021). https://doi.org/10.1016/j.jddst.2020.102144.

[397] M.K. Anwer, M. Mohammad, M. Iqbal, M.N. Ansari, E. Ezzeldin, F. Fatima, S.M. Alshahrani, M.F. Aldawsari, A. Alalaiwe, A.A. Alzahrani, A.M. Aldayel. Sustained release and enhanced oral bioavailability of rivaroxaban by PLGA nanoparticles with no food effect. *J Thromb Thrombolysis*. **49**, (2020), 404–412. https://doi.org/10.1007/s11239-019-02022-5.

[398] D. Sharma, D. Maheshwari, G. Philip, R. Rana, S. Bhatia, M. Singh, R. Gabrani, S.K. Sharma, J. Ali, R.K. Sharma, S. Dang. Formulation and optimization of polymeric nanoparticles for intranasal delivery of lorazepam using Box-Behnken design: In vitro and in vivo evaluation. *Biomed Res Int*. **2014**, (2014). https://doi.org/10.1155/2014/156010.

[399] A. Khedr, A. Striolo. Quantification of Ostwald Ripening in Emulsions via Coarse-Grained Simulations. *J Chem Theory Comput*. **15**, (2019), 5058–5068. https://doi.org/10.1021/acs.jctc.9b00296.

[400] J. Das Neves, B. Sarmento. Precise engineering of dapivirine-loaded nanoparticles for the development of anti-HIV vaginal microbicides. *Acta Biomater*. **18**, (2015), 77–87. https://doi.org/10.1016/j.actbio.2015.02.007.

[401] N. Ahmad, M.J.A. Al-Ghamdi, H.S.M. Alnajjad, B.B.A. Al Omar, M.F. Khan, Z.S. Almalki, A.A. Albassam, Z. Ullah, M.S. Khalid, K. Ashraf. A comparative brain Toxico-Pharmacokinetics study of a developed tannic acid nanoparticles in the treatment of epilepsy. *J Drug Deliv Sci Technol*. **76**, (2022). https://doi.org/10.1016/j.jddst.2022.103772.

[402] S.P. Ayalasomayajula, U.B. Kompella. Subconjunctivally administered celecoxib-PLGA microparticles sustain retinal drug levels and alleviate diabetes-induced oxidative stress in a rat model. *Eur J Pharmacol*. **511**, (2005), 191–198. https://doi.org/10.1016/j.ejphar.2005.02.019.

[403] Q. Meng, A. Wang, H. Hua, Y. Jiang, Y. Wang, H. Mu, Z. Wu, K. Sun. Intranasal delivery of Huperzine A to the brain using lactoferrin-conjugated N-trimethylated chitosan

surface-modified PLGA nanoparticles for treatment of Alzheimer's disease. *Int J Nanomedicine*. **13**, (2018), 705–718. https://doi.org/10.2147/IJN.S151474.

[404] M.J. Ramalho, J.A. Loureiro, M.A.N. Coelho, M.C. Pereira. Factorial design as a tool for the optimization of PLGA nanoparticles for the co-delivery of temozolomide and O6-benzylguanine. *Pharmaceutics*. **11**, (2019). https://doi.org/10.3390/pharmaceutics11080401.

[405] A. Abbas, N.G. Eissa, H.M. El-Bassossy, M.M. Ghorab, H.M. El-Nahas. Polymeric linagliptin nanoparticles as a sustained release treatment for type 2 diabetes. *J Drug Deliv Sci Technol*. **93**, (2024). https://doi.org/10.1016/j.jddst.2024.105438.

[406] Y. Guo, X. Li, R.B. Macgregor, H. Yan, R.X. Zhang. Microfluidics-based PLGA nanoparticles of ratiometric multidrug: From encapsulation and release rates to cytotoxicity in human lens epithelial cells. *Heliyon*. **9**, (2023). https://doi.org/10.1016/j.heliyon.2023.e18318.

[407] S. Ray, S. Ghosh (Ray), S. Mandal. Development of bicalutamide-loaded PLGA nanoparticles: preparation, characterization and in-vitro evaluation for the treatment of prostate cancer. *Artif Cells Nanomed Biotechnol*. **45**, (2017), 944–954. https://doi.org/10.1080/21691401.2016.1196457.

[408] A. Homayouni, F. Sadeghi, A. Nokhodchi, J. Varshosaz, H.A. Garekani. Preparation and Characterization of Celecoxib Dispersions in Soluplus ® : Comparison of Spray Drying and Conventional Methods. *Iranian Journal of Pharmaceutical Research*. **14**, (2015), 35–50.

[409] G.S. El Bahy, E.-S.M. El-Sayed, A.A. Mahmoud, N.M. Gweily. Preparation and Characterization of Poly Vinyl Alcohol /Gelatin Blends. *J Appl Sci Res*. **8**, (2012), 3544–3551.

[410] B. Karolewicz, M. Gajda, A. Górniak, A. Owczarek, I. Mucha. Pluronic F127 as a suitable carrier for preparing the imatinib base solid dispersions and its potential in development of a modified release dosage forms: Thermal, spectroscopic, microscopic, and dissolution studies. *J Therm Anal Calorim*. **130**, (2017), 383–390. https://doi.org/10.1007/s10973-017-6139-1.

[411] Q. Wang, P. Wu, W. Ren, K. Xin, Y. Yang, C. Xie, C. Yang, Q. Liu, L. Yu, X. Jiang, B. Liu, R. Li, L. Wang. Comparative studies of salinomycin-loaded nanoparticles prepared by nanoprecipitation and single emulsion method. *Nanoscale Res Lett*. **9**, (2014). https://doi.org/10.1186/1556-276X-9-351.

[412] C. Shi, S. Ahmad Khan, K. Wang, M. Schneider. Improved delivery of the natural anticancer drug tetrandrine. *Int J Pharm*. **479**, (2015), 41–51. https://doi.org/10.1016/j.ijpharm.2014.12.022.

[413] Y. Herdiana, N. Wathoni, S. Shamsuddin, M. Muchtaridi. Drug release study of the chitosan-based nanoparticles. *Heliyon*. **8**, (2022). https://doi.org/10.1016/j.heliyon.2021.e08674.

[414] D.H. Solomon, M.E. Husni, P.A. Libby, N.D. Yeomans, A.M. Lincoff, T.F. Lüscher, V. Menon, D.M. Brennan, L.M. Wisniewski, S.E. Nissen, J.S. Borer. The Risk of Major NSAID Toxicity with Celecoxib, Ibuprofen, or Naproxen: A Secondary Analysis of the PRECISION Trial. *American Journal of Medicine*. **130**, (2017), 1415-1422.e4. https://doi.org/10.1016/j.amjmed.2017.06.028.

[415] X. Liu, Y. Wu, Z. Zhou, M. Huang, W. Deng, Y. Wang, X. Zhou, L. Chen, Y. Li, T. Zeng, G. Wang, B. Fu. Celecoxib inhibits the epithelial-to-mesenchymal transition in bladder cancer via the miRNA-145/TGFBR2/Smad3 axis. *Int J Mol Med*. **44**, (2019), 683–693. https://doi.org/10.3892/ijmm.2019.4241.

[416] V. Pagliarulo, P. Ancona, I. Martines, R. Spadavecchia, S. di Stasi, S. Alba, L. Cormio, C. Fanizza, A. Salerno, G. Carrieri, A. Pagliarulo. Celecoxib for the prevention of nonmuscle invasive bladder cancer: Results from a matched control study. *Ther Adv Urol*. **7**, (2015), 303–311. https://doi.org/10.1177/1756287215599695.